Understanding structure/function relationships between polylactide microstructure, macromolecular mobility and barrier properties for the creation of tomorrows biobased packaging materials

Samira Fernandes Nassar

Thèse de doctorat
de
L'Université Paris-Saclay
préparée à
"AGROPARISTECH"

Ecole Doctorale n° 581 ABIES
Agriculture, alimentation, biologie, environnement et santé

Spécialité de doctorat
Génie des procédés

Par

Mademoiselle Samira FERNANDES NASSAR

Compréhension de la relation entre la microstructure du Polylactide, sa mobilité macromoléculaire et ses propriétés barrière pour la création des emballages issus de ressources renouvelables de demain

Thèse présentée et soutenue à Paris, le 22 février 2017

Composition du Jury :

M. Dantras, Eric	Maître de Conférences HDR, Université Paul Sabatier	Rapporteur
Mme Gaucher, Valérie	Professeur, Université des sciences et Technologie de Lille	Rapporteur
M. Roger, Philippe	Professeur, Université Paris Saclay	Examinateur
M. Haudin, Jean-Marc	Professeur émérite, CEMEF-MINES ParisTech	Examinateur
M. Bruzaud, Stéphane	Professeur, Université de Bretagne-Sud	Président du jury
Mme Domenek, Sandra	Maître de Conférences HDR, AgroParisTech – Paris Saclay	Directeur de thèse
M. Sollogoub, Cyrille	Maître de Conférences HDR, Arts et Métiers ParisTech – CNAM	Co-encadrant de thèse
M. Delpouve, Nicolas	Maître de Conférences, Université de Rouen	Co-encadrant de thèse
M. Guinault, Alain	Ingénieur de Recherche, Arts et Métiers ParisTech - CNAM	Invité
M. Sobral, Paulo	Professeur, Université de Sao Paulo - FZEA	Invité

université PARIS-SACLAY
ÉCOLE DOCTORALE
Agriculture, alimentation, biologie, environnement, santé (ABIES)

Titre : Compréhension de la relation entre la microstructure du polylacide, sa mobilité macromoléculaire et ses propriétés barrières pour la création des emballages issues de ressources renouvelables de demain

Mots clés : Polylactide, cristallisation, mobilité macromoléculaire, confinement, propriétés barrières

Résumé : Ces dernières années, une attention particulière a été portée aux polymères biodégradables et biocompatibles, notamment du point de vue écologique. Le développement de biopolymères pour des applications d'emballage alimentaire implique des exigences industrielles spécifiques telles qu'un bas prix ainsi que de bonnes propriétés mécaniques, thermiques et barrières. Le Polylactide (PLA) a attiré beaucoup d'attention car il est produit à partir de ressources naturelles renouvelables, et en raison de sa capacité de mise en œuvre et de ses bonnes propriétés mécaniques. Pour que le PLA puisse être développé à grande échelle pour des applications industrielles dans le domaine de l'emballage, ses propriétés barrières doivent être améliorées. La cristallisation est une méthode très utilisée pour améliorer les propriétés barrières mais n'est pas suffisante dans le cas du PLA. De nouvelles stratégies sont étudiées pour obtenir des effets plus importants. L'une d'entre elles consiste à confiner géométriquement le polymère jusqu'à l'échelle nano en utilisant le procédé de co-extrusion multicouche combiné éventuellement avec un recuit. Cette technologie respecte l'environnement et a déjà prouvé son efficacité pour améliorer les propriétés barrières aux gaz dans le cas d'autres polymères. Cette étude propose d'abord le développement de films PLA avec des structures cristallines différentes dans le but d'optimiser les conditions de cristallisation pour obtenir de meilleures propriétés barrières à l'oxygène. Parmi les différentes structures cristallines obtenues, la perméabilité est la meilleure lorsque le PLA a été cristallisé rapidement à partir de l'état vitreux pour atteindre un degré de cristallinité élevé et un bon découplage de la phase amorphe et cristalline. Ensuite, le PLLA a été confiné par deux polymères amorphes, le Polystyrène et le Polycarbonate. Nous avons montré que le polymère confineur peut influencer la structure cristalline et la mobilité de la phase amorphe du PLLA, influençant ainsi sa perméabilité.

Université Paris-Saclay

Espace Technologique / Immeuble Discovery

Route de l'Orme aux Merisiers RD 128 / 91190 Saint-Aubin, France

Title : Understanding structure/function relationships between polylactide microstructure, macromolecular mobility and barrier properties for the creation of tomorrows biobased packaging materials

Keywords : Polylactide, crystallization, molecular mobility, confinement, barrier properties

Abstract : In recent years, much attention has been focused on biodegradable and biocompatible polymers, particularly from an ecological viewpoint. The development of biopolymers for food-packaging applications implies ecofriendly character to specific industrial requirements as low-cost and good mechanical, thermal and barrier properties. Polylactide (PLA) has been attracting great attention, because it can be obtained from renewable sources, and due to its good process ability and mechanical properties. As one of the major challenges for high performance PLA packaging at a large scale is the improvement of its gas barrier properties, the tailoring of the PLA microstructure. Crystallization is a method used to improve barrier properties but is not sufficient in the case of PLA. New strategies are actually studied to obtained stronger effects. One of them consists in the geometrical confinement of the polymer at the molecular scale using the layer-multiplying co-extrusion process combined eventually with annealing processes to create nanometric thickness layers. This technology is environmentally friendly and has already proved its efficiency to improve the gas barrier properties in case of other polymers. This study first proposes the development of PLA films with different structures crystalline with the aim of optimize the crystallization conditions to get better oxygen barrier properties. Among the different crystalline structures obtained, permeability was better when PLA was rapidly crystallized from glass to reach a high crystallinity degree and decoupling of the amorphous and crystalline phase. Then, PLLA was confined by two amorphous polymers, polystyrene and polycarbonate, and its crystals structure and amorphous mobility was changed. We showed that the confiner polymer could influence PLLA confinement, both in the crystalline phase and in the amorphous phase, thus influencing its permeability.

Université Paris-Saclay

Espace Technologique / Immeuble Discovery

Route de l'Orme aux Merisiers RD 128 / 91190 Saint-Aubin, France

REMERCIEMENTS

En premier lieu, je tiens à remercier ma directrice de thèse, Sandra Domenek, pour la confiance qu'elle m'a accordée en acceptant d'encadrer ce travail doctoral.

Mes remerciements vont également à Cyrille Sollogoub pour avoir accepté de participer à l'encadrement de cette thèse et pour sa bonne humeur infatigable.

Merci à Alain Guinault qui a eu beaucoup de patience avec moi, surtout chaque fois que je frappais à sa porte avec mes questions. J'aimerais également lui dire à quel point j'ai apprécié sa grande disponibilité et son respect sans faille des délais serrés de relecture des documents que je lui ai adressé.

Merci à Nicolas Delpouve qui m'a énormément appris en termes scientifiques, qui a partagé toute sa connaissance avec moi. Sa compétence, sa rigueur scientifique et sa clairvoyance m'ont beaucoup fait progresser. Cela a été à de nombreuses reprises un moteur dans mon travail de chercheur.

Je tiens à remercier toutes les personnes du PIMM qui de par leur bonne humeur ont fait que venir au laboratoire a toujours été un plaisir.

Ces remerciements seraient incomplets si je n'en adressais pas à l'ensemble des doctorants des laboratoires PIMM, AgroParisTech et LECAP pour leur soutien moral ainsi que pour la très bonne ambiance que j'ai toujours trouvée dans tous les laboratoires où j'ai pu travailler.

Je remercie mon cher copain Tanguy pour son soutien quotidien indéfectible et son enthousiasme contagieux à l'égard de mes travaux comme de la vie en général.

Enfin, ces remerciements ne peuvent s'achever, sans une pensée pour mes premiers fans : mes parents. Obrigada pai e mãe pelo apoio incondicional, sem vocês nada disso seria possivel. Eu amo vocês mais que tudo ! Malgré mon éloignement depuis de (trop) nombreuses années, leur confiance, leur tendresse, leur amour me portent et me guident tous les jours. Merci pour avoir fait de moi ce que je suis aujourd'hui. Est-ce un bon endroit pour dire ce genre de choses ? Je n'en connais en tous cas pas de mauvais. Je vous aime.

ABBREVIATIONS

AFM	Atomic force microscopy
C’	In-phase component of the complex heat capacity (ΔC_p)
C’’	Out-of-phase component of the complex heat capacity (ΔC_p)
CED	Cohesive energy density
CRR	Cooperative rearranging region
D	Diffusion
DSC	Differential scanning calorimetry
d-sp	d-spacing
FFV	Free volume fraction
K	Crystallization rate constant
k_B	Boltzmann constant
L/l	Thickness
L_Z	Long period
m	Mass
MAF	Mobile amorphous phase
MFI	Melt flow index
MT-DSC	Modulated-temperature differential scanning calorimetry
n	Avrami exponent
OTR	Oxygen transmission rate
P	Permeability
PC	Polycarbonate
PET	Poly(ethylene terephthalate)

PLA	Polylactide
PLLA	Poly(L-lactide)
$P(O_2)$	Oxygen permeability
POM	Polarizing optical microscopy
PS	Poly(styrene)
q+	Heating rate
RAF	Rigid amorphous fraction
RH	Relative humidity
S	Solubility
SAXS	Small-angle x-ray scattering
SEM	Scanning electron microscopy
$t_{1/2}$	Crystallization half-time
T_α	Dynamic glass transition temperature
T_g	Glass transition temperature
t_{lag}/θ	Time lag
X_c	Crystallinity degree
X_{MA}	Content of MAF
X_{RA}	Content of RAF
XRD	X-ray diffraction
X_t	Relative crystallinity
WAXS	Wide-angle x-ray diffraction
α (t)	Relative crystallinity fraction from Avrami equation
ΔC_p	Heat capacity
ΔC_p^0	Heat capacity of the fully amorphous sample

ΔH_f	Enthalpy of fusion or melting
ΔHF	Heat flow difference
ΔH_{cc}	Enthalpy of cold crystallization
ΔH_f^0	Enthalpy of the melting of the perfect crystal of infinite size
ρ	Density
$\xi_{T\alpha}$	Size of cooperative rearranging region
δT	Average temperature fluctuation
η	Viscosity

TABLE DE MATIERES

Introduction **1**

1. Literature Review **7**

1.1. Characterization of PLA **8**

1.1.1. Synthesis of PLA **8**

1.1.2. Crystalline morphology of PLA **9**

1.1.3. Amorphous phase dynamics of PLA **10**

1.2. Formation of the Rigid Amorphous Fraction in semicrystalline polymers **13**

1.2.1. Properties of the Rigid Amorphous Fraction in PET **14**

1.2.2. Properties of the Rigid Amorphous Fraction in PLA **15**

1.3. Gas barrier properties of PLA **19**

1.4. Confinement of polymers **26**

1.4.1. Different methods of confinement of polymers **26**

1.4.2. Crystallization of polymers under confinement **27**

1.4.3. Amorphous phase relaxation in confined polymers **30**

1.4.4. Gas barrier properties of confined polymers using the nanolayer-multiplying system **31**

1.5. Conclusion **33**

1.6. References **35**

2. Matériaux et méthodes **51**

2.1. Matériaux **51**

2.1.1. Choix des polymères **51**

2.2. Méthodes expérimentales **51**

2.2.1. Caractérisation des granulés **51**

2.2.1.1. Séchage des granulés de PLA, et PC **51**

2.2.1.1.1. Description des sécheurs à granulés **52**

2.2.1.1.2. Protocole expérimental de séchage de granulés **52**

2.2.2. Rhéologie **52**

2.2.3. Mise en œuvre des films **55**

2.2.3.1. Mise en œuvre des films monocouche **55**

2.2.3.2. Mise en œuvre de films multicouches (PLLA/PS et PLLA/PC) 55
2.2.4. Caractérisation des films 59
2.2.4.1. Perméabilité à l'oxygène 59
2.2.4.2. Perméabilité à l'hélium 62
2.2.4.3. Analyse thermique par MT-DSC 63
2.2.4.3.1. Protocoles expérimentaux 63
2.2.4.3.2. Quantification des phases 64
2.2.4.3.3. Longueur de coopérativité 67
2.2.4.4. Diffractions des rayons x 68
2.2.4.5. Recuit des films monocouche 69
2.2.4.5.1. Cinétique de cristallisation 70
2.2.4.6. Recuit des films multicouches 70
2.2.4.6.1. Recuit des films PS/PLLA 70
2.2.4.6.1.1. . Cinétique de cristallisation des films PS/PLLA 70
2.2.4.6.2. Recuit des films PC/PLLA 73
2.2.4.6.2.1. Cinétique de cristallisation des films PC/PLLA 73
2.2.4.7. Observation des structures cristallines 74
2.2.4.8. Digestion enzymatique et Microscopie électronique à balayage 75
2.2.4.9. Observation des couches 75
2.2.4.9.1. Analyse des images AFM 76
2.2.4.9.1.1. Mesure des épaisseurs des couches et vérification de la proportion de chaque polymère dans les films 76
2.2.4.10. Caractérisation du vieillissement physique des films multicouches PLLA/PS 78
2.3. Bibliographie 80

3. Multi-scale analysis of the impact of polylactide morphology on gas barrier properties 85
3.1. Abstract 86
3.2. Introduction 87
3.3. Material and Methods 89
3.3.1. Sample preparation 89
3.3.2. Sample characterization 90
3.4. Results and Discussion 92

3.4.1. PLA crystallization kinetics 92
3.4.2. Crystalline structure and space filling 93
3.4.3. Crystalline morphology 96
3.4.4. Structural description of the amorphous phase and its cooperativity at the glass transition 99
3.4.5. Oxygen permeability study 103
3.5. Conclusion 106
3.6. References 107

4. Structural and dynamic heterogeneity in the amorphous phase of PLLA confined at the nanoscale by co-extrusion process 115
4.1. Abstract 117
4.2. Introduction 118
4.3. Experimental 120
4.3.1. Process and crystallization parameters 120
4.3.2. Characterization 122
4.4. Results and discussion 123
4.4.1. Optimization of the layer multiplying co-extrusion process 123
4.4.2. Crystallization of PLLA under confinement 125
4.4.3. Dynamic heterogeneity of confined PLLA 130
4.5. Conclusion 134
4.6. References 136
4.7. Supplementary information 145

5. The impact of nanoconfinement on PLLA crystallization and gas barrier properties 149
5.1. Abstract 151
5.2. Introduction 152
5.3. Materials and methods 154
5.3.1. Materials and processing 154
5.3.2. Methods 155
5.4. Results and discussion 156
5.4.1. Optimization of the layer multiplying co-extrusion process 156

5.4.2. Crystallization kinetics and crystalline lamellae orientation of confined PLLA layers 158
5.4.3. Impact of the layer multiplying co-extrusion on the confining polymer PC 162
5.4.4. Maximum crystallinity degree and amorphous phase dynamics and of confined PLLA 164
5.4.5. Impact of PLLA microstructure on helium and oxygen permeability 167
5.5. Conclusion 169
5.6. References 171

---

6. Physical aging in PLLA confined at the nanoscale by multilayer coextrusion 179
6.1. Introduction 180
6.2. Materials and methods 181
6.2.1. Characterization of physical aging 181
6.3. Results and discussion 184
6.4. Conclusion 190
6.5. References 191

Conclusions générales et perspectives 197

Introduction

Introduction

Bioplastics are of strong interest to the plastics industry, as they are a means to, decrease its environmental footprint by the replacement of fossil by renewable sources for the production of polymers. Furthermore, the use of such novel resins can increase consumer acceptance of plastics and help converters to diversify their polymer sources. Today, roughly 40% of the annually produced volume of plastics is used in packaging applications. Meanwhile, only a very limited number of polymers (polyolefin, poly(ethylene terephthalate), polystyrene, poly(vinyl chloride)) is used for the large majority of commodity applications. The tailoring and diversification of the desired use properties of those resins is principally achieved through the polymer processing. Plastics processers are combining polymers and realizing controlled assemblies by blending, co-extrusion or complexing or use the inherent properties of different chemical structures in optimizing the microstructure by controlling crystallization via annealing and/or introducing constraints in the amorphous phase by bi-axial stretching. Common plastics processing controls the material morphology on a macroscopic or, at best, a mesoscopic scale. The resulting effects on the mechanical behaviour or barrier properties are therefore often limited. In the aim to open the door to commodity applications for novel biobased and biodegradable polymers larger property improvements are required, though.

Among the different biobased matrices, the semicrystalline polyester polylactide (PLA) is already readily available on the market. PLA is produced from renewable natural sources, such as corn, wheat, sugar beet. Moreover it has been attracting great attention in industry as a good candidate for food packaging, because it can be converted by conventional polymer processes and it possesses satisfying stiffness and high transparence. Nevertheless, although the PLA possesses many of the necessary requirements for the thermoplastic packaging, this polymer suffers also drawbacks such as poor barrier properties. A huge research and industrial effort has been concentrated on this polymer during the last two decades for optimizing its properties (mechanical properties, barrier properties, heat stability, crystallization kinetics…). Improvements were often achieved by compounding and blending with technological additives, the elaboration of nanocomposites or by chemical modifications of the material. Many of these routes are however not viable from an applicative point of view as they imply important cost overruns, increase safety requirements and are not environmentally suitable, as they require the use of supplementary chemicals.

An alternative strategy is to modify the macroscopic properties of a polymer is to change the length scale attained by plastics processing to the macromolecular scale. Confinement of the polymers can create new amorphous and/or crystalline microstructures, which can lead to a significant improvement of properties.

Generally speaking, confining a system to a scale comparable to its characteristic length (for macromolecules, gyration radius for example), and the increase surface-to-volume ratios multiplying interface effects between confined polymer layers and surroundings, results in significant deviations of the structural and dynamical properties with respect to the bulk. In the case of semicrystalline polymers, the amorphous phase gets confined between lamella crystallites, and differences in the macromolecular behavior of intra-spherulitic phases and bulk phases were already evidenced. Confinement of polymers can be furthermore achieved by different technologies, such as spin-coating, layer-by-layer superposition techniques and layer-multiplying co-extrusion. This latter process allows combining two polymers in an alternating layered structure of thousands of single polymer layers, creating thereby films with continuous and regular layers down to 10 nm thickness. This process appears as an efficient tool to create confined polymer structures by forced assembly, with the huge advantage of being able to produce objects at large scale.

Many studies were already conducted to improve PLA properties, where crystallization is one of the most commonly used ways. In the literature, this step is performed by different ways, as add nucleation agents or bi-axial drawing. However, the use of these techniques did not result in a sufficient gain in properties, and in particular in barrier properties for the use of PLA in most packaging applications. It appeared furthermore, that the structure/function relationships of barrier properties and crystallinity degree were not completely understood.

Nanolayered confined systems appear as ideal model systems to get new insights in relationships between polymer structure on the macromolecular length scale and the macroscopic properties, such as barrier properties. Those systems allow producing different degrees of confinement by varying the layer thickness and different types of interactions between the confined polymer layers and the confiner polymer by changing the chemistry of the latter. Besides the interest of testing a novel technology on a biobased and biodegradable polymer, PLA presents also several advantages as a model system in this study, because it has rather slow crystallization kinetics, which can moreover be adapted by a proper choice of the stereo-chemistry of the macromolecular chain.

The aim of the thesis is gaining insight in process/structure/function relationships of confined PLA, for underpinning the development of an innovative extrusion methodology aiming to improve macroscopic polymer properties, in particular barrier properties.

This thesis is organized in 6 chapters and a final chapter to conclude and project some perspectives.

- The literature review presented in chapter 1 is focused on characterization of PLA (amorphous and crystalline phase), the impact of a third phase existing in many semi crystalline polymers, called rigid amorphous phase, gas barrier properties of PLA and a review about confinement.

- The second chapter presents the materials, the stages of the process of bulk and multilayers films and the description of all methods used during the project.

The experimental results are presented in 4 chapters

- The third chapter aims to optimize the crystallization conditions of PLA to get better oxygen barrier properties by investigating the impact of the crystalline morphology, structure and the amorphous phase dynamics.

- The fourth chapter is focused in the study of amorphous and crystallized PLLA confined by polystyrene using multi nanolayered process in order to understand the macromolecular mobility in the amorphous phase and the coupling between the amorphous and crystalline phases in PLLA when it is geometrically restricted.

- The fifth chapter is dedicated to understand the changes in microstructure of confined PLLA by two different polymers, polystyrene (PS) and polycarbonate (PC) and the impact on its macroscopic gas barrier properties.

- The sixty chapter is dedicated to the study of physical aging of PLLA confined by PS using a flash DSC.

This thesis was part of three research teams:

- The “polymer and composites” team, in the laboratory of process and engineering in mechanics and materials (PIMM), Arts et métiers Paristech in the center of Paris whose the research focus is to understand the relationship between processes, microstructure, polymer properties and their durability (amorphous, semi-crystalline and elastomers) and multiphase polymers materials (composites, micro (or nano) charged polymers, etc.). Thus, it has in particular the main processing equipment found in polymer industry (extrusion, injection, compression of thermoplastics, etc.).

- The “Interaction Matériaux Milieu au Contact (I2MC)” team, in the UMR 1145 GENIAL, AgroParisTech, which the objectives are to understand the mechanisms that control the barrier properties or selectivity of materials in contact with food products. For this, the team has many means of physico-chemical characterization (TMDSC, ATG, permeability equipment, etc.) and analytic chemistry (SEC, GC, GC-MS, ATR-IR, etc.).

- The laboratory for the study and characterization of amorphous and polymeric materials (LECAP) in Normandie university, which the research is focus mostly in relationship between microstructure and properties of materials, aging and properties dependency of time, molecular mobility, physical properties. For this, it has many equipment as TMDSC, Flash-DSC, DMA, and broadband dielectric spectroscopy.

Chapter 1 – Literature Review

Les polylactide (PLA) est bien connu pour sa biodégradabilité et surtout parce qu'il est fabriqué à partir de ressources renouvelables comme l'amidon de maïs ou la pomme de terre, ce qui en fait un polymère «vert». Plusieurs études ont montré que le PLA est potentiellement utilisable dans certains secteurs d'emballage et les problématiques environnementales ont suscité l'intérêt pour le développement de nouveaux matériaux d'emballage biodégradables pour remplacer les emballages plastiques issus de l'industrie pétrochimique.

Les matériaux utilisés dans les emballages doivent avoir de bonnes propriétés barrière aux gaz pour augmenter leurs domaines d'utilisation, en particulier dans les aliments, les cosmétiques et les médicaments. Grâce au recyclage, au marketing et aux coûts, les emballages en métal et en verre ont été remplacés par des polymères dont les propriétés barrière ne sont pas bien connues ce qui explique notre intérêt pour les améliorer. Les propriétés barrière aux gaz d'un polymère ne sont pas seulement liées à la phase cristalline (contenu, orientation) mais aussi à la mobilité de la phase amorphe. Une autre stratégie pour modifier les propriétés des polymères, principalement la perméabilité, consiste à modifier l'échelle de longueur atteinte par le traitement des plastiques à l'échelle macromoléculaire. Le confinement des polymères peut créer de nouvelles microstructures amorphes et / ou cristallines, ce qui peut conduire à une amélioration significative des propriétés. Dans ce chapitre, nous aborderons tout d'abord l'influence de la cristallinité et de la phase amorphe sur les propriétés barrière du PLA, la relation structure/fonction de la microstructure du PLA et les propriétés de transport, puis l'impact des structures confinées par la cristallinité, la mobilité de la phase amorphe et par conséquent l'impact sur la perméabilité.

1. Literature Review

Poly(lactide) (PLA) polymers are well known for their biodegradability and especially by the fact that they are made from renewable resources as corn starch or potato which makes them "green" polymers. Several studies have showed that PLA is potentially usable in some packaging sectors [1,2] and the concern with the environment has increased the interest in the development of biodegradable packaging materials to replace plastic packaging coming from the petrochemical industry. The materials used in packaging must have good gas barrier properties to increase their ranges of use, particularly in the food, cosmetics and medicine. Through recycling, marketing and costs, metal and glass packaging were replaced by polymers,

whose barrier properties are not well known and hence the interest from the study in order to improve it. The gas barrier properties of a polymer are not only linked to the crystalline phase (content, orientation) but also to the mobility of the amorphous phase. An alternative strategy to change properties of polymers, mainly permeability, is to change the length scale attained by plastics processing to the macromolecular scale. Confinement of the polymers can create new amorphous and/or crystalline microstructures, which can lead to a significant improvement of properties

In this chapter, we will first of all discuss about the influence of crystallinity and amorphous phase on barrier properties of bulk PLA, the structure/function relationship between PLA microstructure and transport properties and then the impact of confined structures on crystallinity, amorphous phase mobility and consequently on permeability.

1.1. Characterization of PLA

1.1.1. Synthesis of PLA

PLA can be synthesized by different routes, including two paths which allow to obtain high molecular weight polymers: the polycondensation of lactic acid (often using coupling agents for increasing the molecular weight) and polymerization by opening the lactide ring, obtained by condensation of two lactic acids [3]. The latter process is used in majority to produce commercially available PLA. Lactic acid (2-hydroxypropanoic acid) is obtained by fermentation of glucose coming from vegetal sources. It has a chiral carbon atom and exists in two enantiomeric forms called L-lactic acid and D-lactic acid as shown in *Figure 1.1*. L-lactic acid is preferentially produced by bacterial fermentation. The content of D-lactic in the macromolecular chain and the molecular weight determine polymer properties such as the maximum achievable crystallinity [4]. PLA containing more than 93% of L-lactic is semi-crystalline contrary to PLA with L-lactic between 50 and 93% which is amorphous [1]. PLLA can reach 65% of crystallinity degree (Xc) [5] while a PLA with L-lactic content of 96% can crystallize only up to 40% Xc [6].

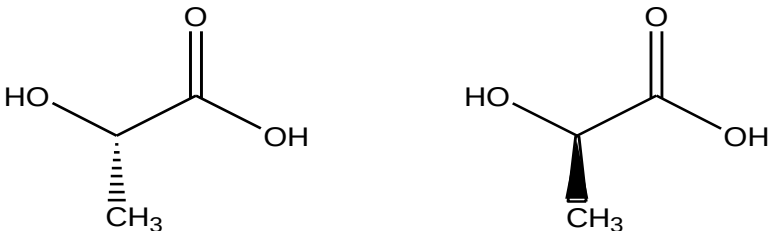

Acid L-lactic Acid D-lactic

Figure 1.1. Two enantiomeric forms of 2-hydroxypropanoic acid (lactic acid).

1.1.2. Crystalline morphology of PLA

PLA, like many semi-crystalline polymers, is polymorphic. It crystallizes under three main forms, dependent on the preparation conditions: α, α' (or the newly termed "δ") [7], β, and γ. The β and γ forms are obtained in specific conditions and therefore not found in packaging applications. The β-polymorph is obtained by stretching PLLA fibers at high temperatures [8],[9]. The γ form is obtained with an epitaxial crystallization of PLLA chains [10]. PLLA and PDLA homopolymers can also crystallize under the form of a stereo-complex with distinct properties. It has triclinic geometry with lattice parameters equal to a = b = 0.916 nm and c = 0.87 nm [11]. The particularity of this phase is its high melting point (230 °C), attributed to the presence of hydrogen links in the lattice.

Based on a conformational analysis of the PLA, De Santis and Kovacs were the first to give a representation of the α crystal conformation [12], which its geometry is orthorhombic with lattice parameters equal to a = 1.06 nm, b = 0.61 nm and c = 2.88 nm. Zhang et al. [13] showed the existence of a α'-phase (or δ phase) considered as a distorted α-phase. This phase has a pseudo hexagonal geometry with lattice parameters equal to a = b = 0.62 nm and c = 2.88 nm [14]. It is obtained during thermal crystallization at low temperatures, i.e. below 100°C and it converts into α when its thermal crystallized above 120°C. In the calorimetric analysis of PLA this conversion causes of an exothermic peak just before a multiple melting endotherm [15–17] [18]. Crystallization between 100 and 120°C gives rise to the coexistence of α and α' crystal structures [13,14]. The WAXS patterns of the α and α' forms of PLA are very similar, with small differences in 2θ values for the two strongest reflections ((110/200) and (203)) and the apparition of a characteristic peak of α'form at 2θ≈24.5° [18,19] (*Figure 1.2*).

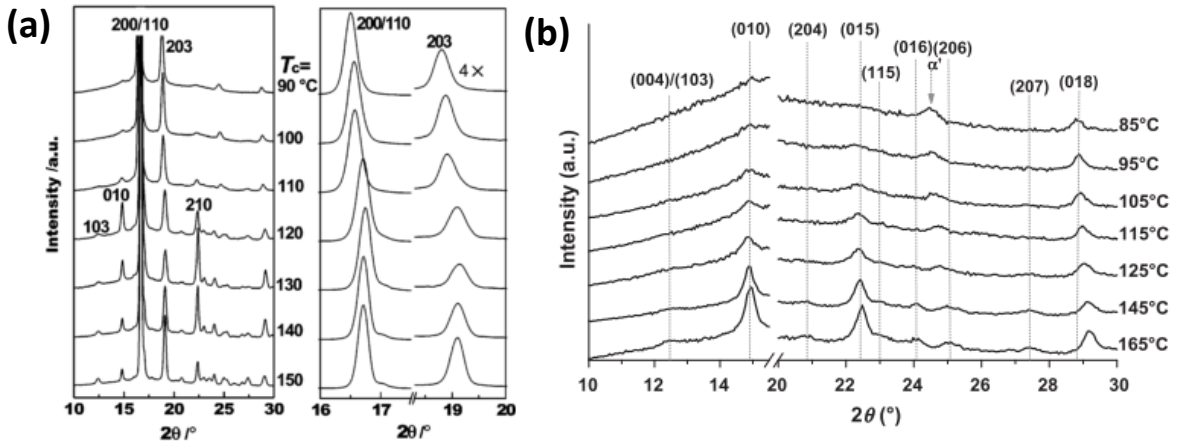

Figure 1.2. (a) PLLA intensity profile of α and α' crystalline forms (Reproduced from Zhang et al.[13]) and (b) WAXS profile of PLLA samples crystallized at different temperatures. At 24,5° the apparition of a characteristic peak of α' (Reproduced from Di Lorenzo et al.[18]).

Because of the different structures of PLLA α' and α crystals, it is considered that the mechanical, thermal properties and biodegradability of PLLA crystallized at different crystallization temperature are different [20]. As a consequence of the disordered structure, Cocca et al showed that the α' crystal leads to a lower modulus and barrier properties and to higher elongation at break compared to α crystal [19].

The values of enthalpy of 100% crystalline polylactide found in literature can vary from 82 to 203 J/g [21–25]. However, the most used value for enthalpy of 100% crystalline polylactide in literature is 93.1 J/g. Due to the polymorphic nature of PLA leading to a melt recrystallization process and to its complex stereo-chemistry, this value may reasonably be debated.

1.1.3. Amorphous phase dynamics of PLA

The amorphous phase, contrary to the crystalline phase, is a disordered phase, which is studied considering its dynamic. The amorphous phase of polymers, like all liquids which are glass-forming, undergoes a slow-down of its relaxation dynamics at temperatures close to the glass transition temperature. Many studies [26–28] link this behavior to the increase in the energy barrier that a structural unit must pass for relaxation.

The description of the cooperative movement of structural units in a polymer at the glass transition introduced by Adam and Gibbs [29] giving rise to the Cooperative Rearranging Regions (CRRs) concept. The hypothesis is that molecules do not relax independently which

means that the movement of a molecule depends on its close neighbours and it is only possible if a given number of adjacent structural units are also moving. The glass-forming liquid can therefore be divided into independent sub-systems (CRRs). These structural units are the smallest amorphous domain where a conformational rearrangement may occur without causing structural change at its boundary. Each CRR has its own glass transition and relaxation time. The average size of CRR is the cooperativity length (ξ) and can be estimated from the heterogeneity of the relaxation times related to the distribution of the glass transitions around the conventional glass transition of the polymer. Donth proposed a calorimetric method for the determination of the CRR size and formulated the following equation [30]:

$$\xi_{T\alpha}^{3} = \frac{\Delta(1/C_p)}{\rho(\delta T^2)} k_B T_\alpha^2 ,$$

where,

δT is the mean temperature fluctuation related to the dynamic glass transition of one CRR, kB the Boltzmann constant, ρ the polymer density, $\Delta(1/C_p)$ is equal to $(1/C_p)_{glass} - (1/C_p)_{liquid}$ and C_p is the heat capacity and T_α the dynamic glass transition.

The mean value of CRR size for an amorphous sample of PLA at dynamic glass transition temperature is 3 nm [6]. There are same causes referenced in literature inducing changes in CRR size. For example, when polymer undergoes structural constraints such as confinement [31,32] or when it is plasticized [33].

Many works using the CRR concept to describe the amorphous phase dynamics in semi-crystalline polymers were published [6,34–36]. Schick and Donth [37] demonstrated that the CRR length of poly(ethylene terephthalate) (PET) is proportional to the thickness of self-organized the amorphous phase layers and it decreases when the crystalline fraction increases. Codou et al. [38] found the same behavior for poly(ethylene 2,5-furandicarboxylate) (PEF) and PET. The increase of the crystallinity degree decreased the CRR length (*Figure 1.3*). Other authors have also seen the same behavior, as Lixon et al. [35] for PET, Delpouve et al. [36,39] and Saiter et al. [34] for PLLA. Furushima et al. [40] studied the characteristic lenght of CRR for uniaxial drawn PET films and they observed that CRR size increases linearly with increasing MAF. However, a non linear behavior was observed between crystallinity and CRR size.

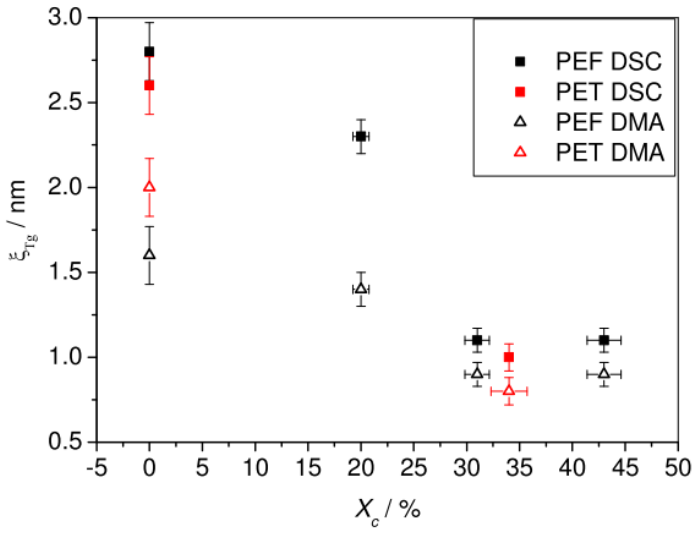

Figure 1.3. Variation of CRR length as function of crystallinity fraction for PEF (black points) and PET (red points). Reproduced from Codou et al. [38]

Delpouve et al. [36] studied the cooperativity length in drawn PLA. The macromolecular orientation generated by the drawing process above Tg led to the generation of oriented crystals and geometric restrictions in the amorphous phase. A decrease in the cooperativity length with increasing degree of crystallinity was observed. This was attributed to the geometric restrictions of the amorphous fraction between crystallites, which induced a geometrical confinement of the macromolecular chains (*Figure 1.4*).

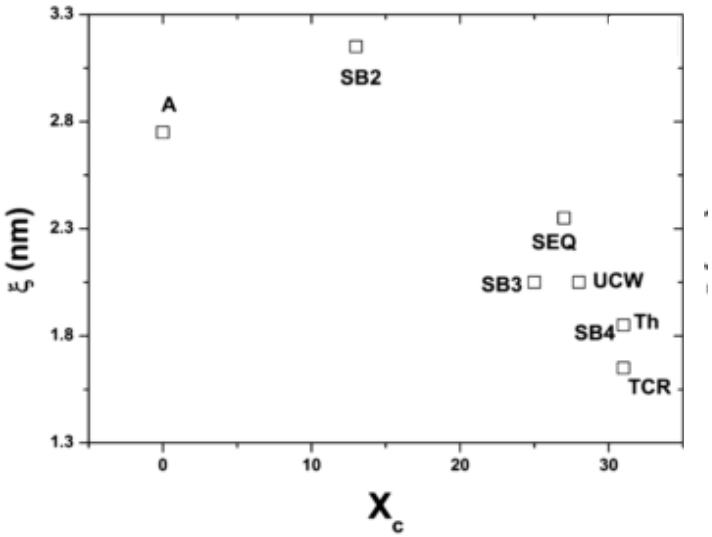

Figure 1.4. Cooperativity length versus degree of crystallinity. Reproduced from Delpouve et al.[36]

1.2. Formation of the Rigid Amorphous Fraction in semicrystalline polymers

In semicrystalline polymers, such as PET or PLA, a three-phase model, introduced by Wunderlich et al. [41], is used to describe the organization of the material at the nanometric scale. This concept was introduced to explain the deviation between crystallinity and heat capacity in the glass transition for several polymers [42]. In the three phase model (sketched in *Figure 1.5*), next to the crystalline phase, two fractions can be distinguished in the amorphous phase. The mobile amorphous fraction (MAF), which relaxes at the glass transition and the rigid fraction (RAF), which devitrifies a higher temperature. The RAF is the intermediate phase connecting the crystalline phase to the mobile amorphous fraction (MAF) [43] as we can see in the scheme in *Figure 1.5*. It constitutes moreover a dedensified amorphous phase [44] because of the geometrical constraints preventing structure relaxation. Because it requires more energy for relaxation, the RAF does not participate of the glass transition. Wunderlich [45] showed that the RAF does not stay rigid up to the melting, it disappears progressively above Tg. Depending on the polymer and the conditions of crystallization, the RAF can devitrify in a very wide temperature range, even above the melting temperature of the crystals [46].

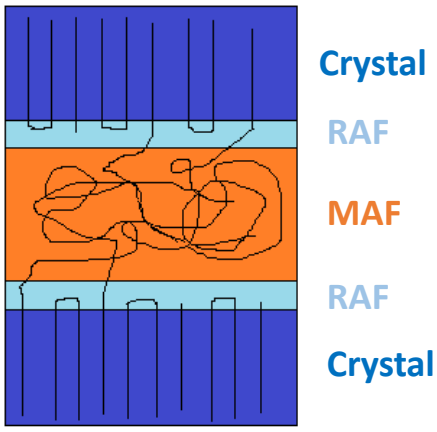

Figure 1.5. Schema of a three-phase model with a crystalline fraction, a mobile amorphous fraction (MAF) and a rigid amorphous fraction (RAF)

The presence of RAF have been reported in many semi crystalline polymers, for example in poly(phenylene sulphide) (PPS) [47], poly(ether ether ketone) (PEEK) [48], syndiotactic polystyrene (sPS) [49], poly(ethylene terephtalate) (PET) [50]. It was also studied for biodegradable polyesters. For example, Esposito et al. [51] studied poly(3-hydroxy butyrate-co-valerate) (PHBV). They showed that crystallization from the melt at high temperature

favored the decoupling of amorphous and crystalline phase, but also of MAF and RAF. Crystallization from the glassy state at low temperature favored in contrary the coupling between amorphous and crystalline phase. In that case, the RAF and the MAF could be hardly distinguished and the 3-phase model could be better described by a "continuum of mobility". They affirmed that this could be extended to a wide range of semicrystalline polymers. A thorough study of the literature on the results about RAF in PET and PLA is presented below.

1.2.1. Properties of the Rigid Amorphous Fraction in PET

The properties of the RAF of PET have received most academic interest. Androsch and Wunderlich [50] studied the link between crystallinity and RAF in PET. They observed an increase of the RAF with increasing Xc during cold-crystallization (maximum of 44% RAF at 24% Xc). Interestingly, further increase of Xc by subsequent annealing at elevated temperature resulted in a reduction of the RAF. Indeed, the ratio between RAF and Xc decreased from 1.8 at 24% Xc to 0.7 at 44% Xc. Androsch and Wunderlich [50] attributed this decrease to perfection of the crystalline morphology during annealing, which reduces the coupling between amorphous and crystalline phase and thereby the strain put on the latter. The analysis of the heat capacity of the annealed samples showed furthermore that at annealing temperature the RAF was still vitrified.

Lin et al. [42] crystallized PET from the glass at 110°C and from the melt at 210°C. They observed an increase in the RAF content with increasing crystallinity. However, a difference was found comparing cold and melt crystallization. In the case of cold crystallization, they observed 37% RAF and in case of melt crystallization 14% RAF, although the Xc of both samples types was equal (25 %). The larger amount of RAF in cold crystallized PET was attributed to the lower crystallization temperature which induced the formation of thinner lamellas and resulted in an increase of the lamellas in the lamella stacks. The higher number of lamellas led to a larger amount of constrained amorphous phase thin layers between the crystalline lamellas (*Figure 1.6*).

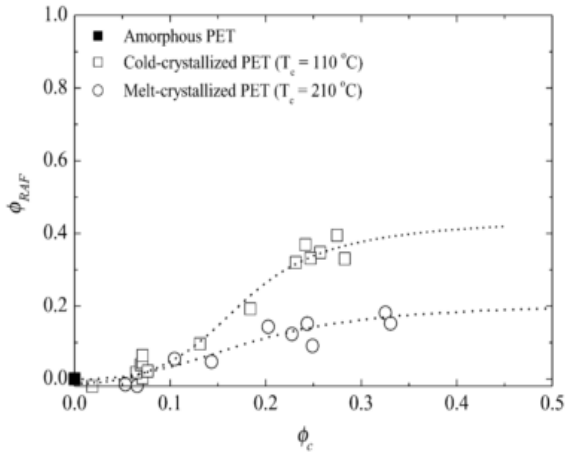

Figure 1.6. Volume portions of RAF versus volume portion of crystallinity for cold crystallization at 110°C and melt crystallization at 210°C. reproduced from Lin et al.[42]

Codou et al. [38] compared an amorphous PET with a PET crystallized at 130°C during 30 minutes (34% of crystallinity). They found a three-phase model with 25% of RAF. The behavior observed is a shift of Tg to higher temperature (around 8°C).

1.2.2. Properties of the Rigid Amorphous Fraction in PLA

The analysis of the PLA microstructure with the help of the 3-phase model was already studied in detail. The devitrification domain of the RAF in PLA is close to its formation temperature (i.e. the temperature of crystallization) [52] and according to del Rio et al. [44], the RAF fraction increases with the annealing time. It can reach a total content of almost 50% (*Figure 1.7*). Righetti and Tombari [52] evidenced that the development of the RAF in PLLA depends on the macromolecular chain mobility. At lower crystallization temperatures, the mobility is lower and the RAF develops easier, and it is created preferentially during the first phase of crystallization. Conversely, at high crystallization temperatures and high chain mobility, the RAF is generated in a lesser amount and only after spherulite impingement in the later phase of crystallization. Zuza et al [53]. showed the creation of the RAF after isothermal crystallization at a temperature above Tg.

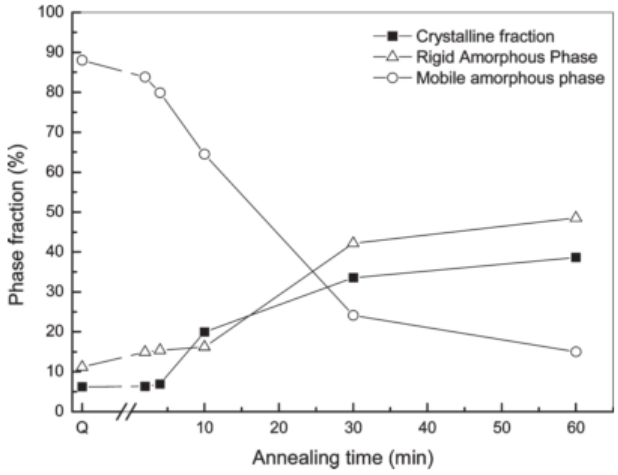

Figure 1.7. Xc, RAF and MAF versus annealing time at 100°C in PLLA. Reproduced from del Rio et al. [44]

Arnoult et al. [54] compared the results of the 3-phase model of PLLA and PET (*Figure 1.8*). They showed that in PET, RAF increases quasi-linearly with Xc and reaches 50% of the material (30% Xc). In PLLA, the percentage of RAF remained small up to 40% Xc but it increased up to 25% of the material as the crystallization time increased. The authors explained this behavior by a better chain flexibility of PLLA compared to PET due to the absence of any aromatic cycle [54]. In a study on PLLA/PET blends, Chen et al. [55] showed that the amount of RAF in PET was much bigger than in PLLA with the same crystallinity degree, which corroborates the results of Arnoult et al. [54].

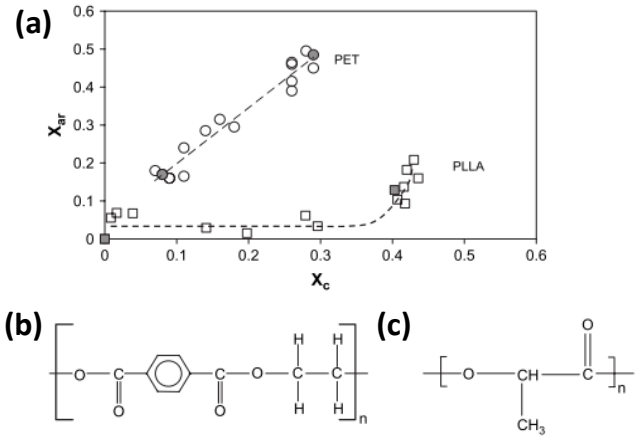

Figure 1.8. (a) Degree of crystallinity dependence of RAF for PET and PLLA (b) PET and (c) PLA constitutive units. Reproduced from Arnoult et al.[54]

Delpouve et al. [6] studied the effects of the stereoregularity and the crystallization process on the amorphous phase dynamics of PLA. An isothermal crystallization from the melt at 150°C and a cold crystallization at 80°C was carried out. The cold crystallization led to the generation of 35% RAF, but only 10% of RAF were generated by sample annealing from the melt. Delpouve et al. [36] also investigated the link between the occurrence of the RAF and the CRR length (*Figure 1.9*). The RAF added to the limitation of the chain rearrangement caused by the geometric restrictions (geometrical confinement) in semicristalline samples. Therefore it caused a further decrease in the cooperativity length of the MAF in addition to Xc (*Figure 1.9*) and a mesophase caused by chain orientation of drawn PLA.

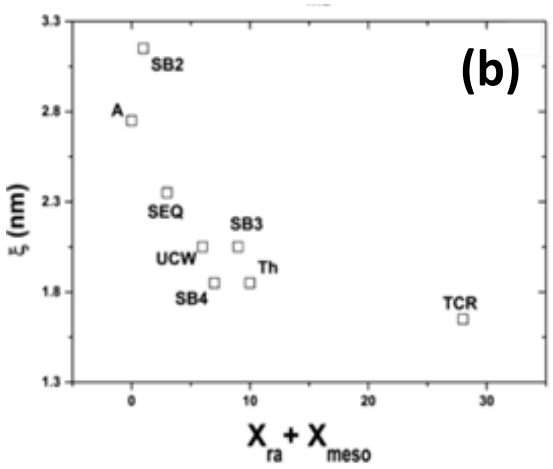

Figure 1.9. Cooperativity length ξ versus rigid amorphous phase fraction (XRA) and mesophase (XRA + Xmeso). Reproduced from Delpouve et al. [36]

Wang et al. [56] crystallized PLLA from the melt and the glass. They observed an increase in Tg of annealed samples. The Tg increase was higher for samples crystallized from the melt. The layer thickness of the RAF was higher at lower Tg (*Figure 1.10*). The authors proposed that a thicker RAF might reduce the constraints imposed by the crystalline lamellae on the amorphous chain motions in the glass transition.

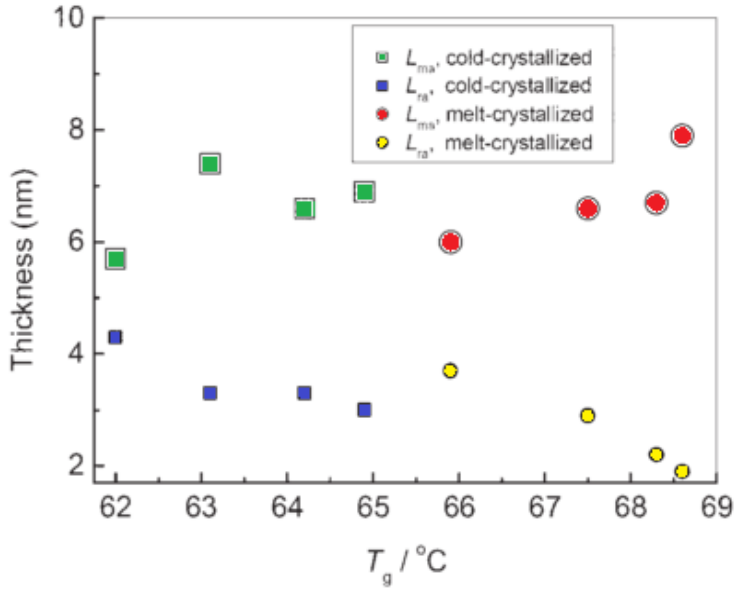

Figure 1.10. Plot of thickness of (green) MAF at cold crystallization (red) MAF at melt crystallization (blue) RAF at cold crystallization and (yellow) RAF at melt crystallization. Modified and reproduced from Wang et al. [56]

An isothermal melt crystallization of PLLA was studied in the temperature range of 90 to 135°C by Iannace and Nicolais [57]. They analyzed the presence of RAF in as a function of the crystallization temperature. A significant decrease of the RAF was observed in samples crystallized over 40% (*Figure 1.11*).

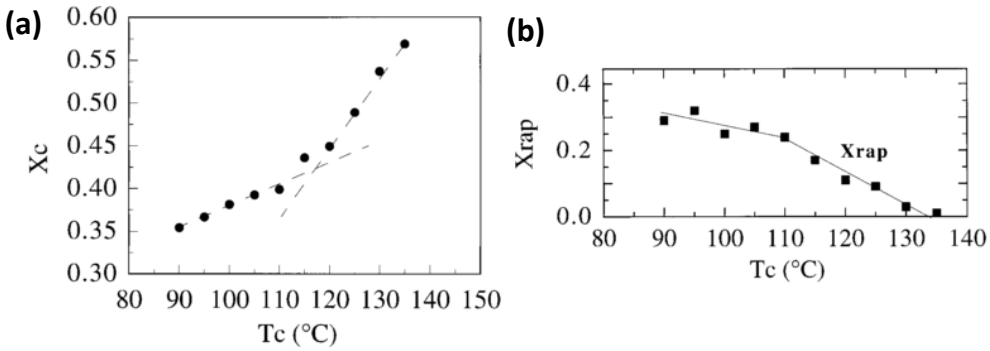

Figure 1.11. (a) Degree of crystallinity versus crystallization temperature (b) RAF as a function of crystallization temperature. Reproduced and modified from Iannace and Nicolais [57].

The crystal polymorphism in PLA can also influence the amount of RAF. Di Lorenzo et al. [18] analyzed the RAF content of semicrystalline PLA as a function of the crystalline form. They

showed that the content of RAF decreased when PLA was annealed at high temperatures in the α-polymorph. If the crystallization temperature was chosen between 95°C and 125°C to yield the α' polymorph, a smaller coupling of the amorphous and crystalline chain segments was obtained and less RAF (*Figure 1.12*).

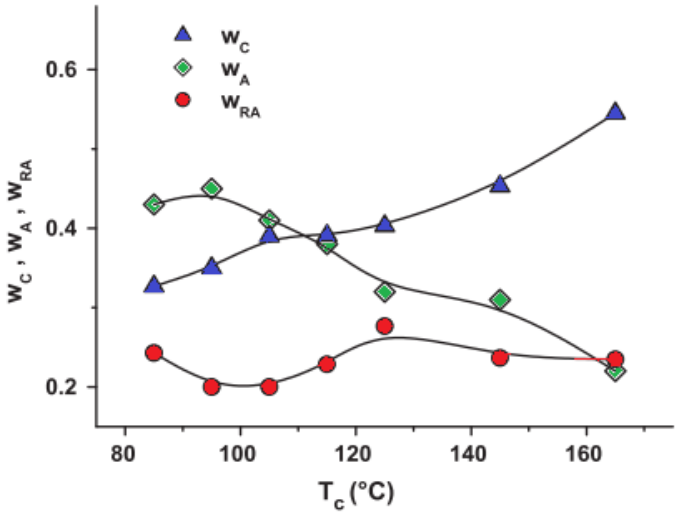

Figure 1.12. (blue) crystalline fraction, (green) MAF and (red) RAF of PLLA after isothermal cold crystallization at various crystallization temperature. Reproduced from Di Lorenzo et al.[18]

The opposite behavior was observed by Guinault et al .[58]. They studied the impact of crystallinity in gas barrier properties and they showed a higher content of RAF in the presence of the α' polymorph. Drieskens et al. [59] studied the effect of crystallinity on barrier properties of PLA, and they found an increase in solubility of PLA with increasing crystallinity and explained it by the presence of the RAF.

1.3. Gas barrier properties of PLA

This part of the chapter is part of a book published in Advances in Polymer Science.

S. DOMENEK, S. FERNANDES NASSAR, V. DUCRUET, Rheology, mechanical properties, barrier properties of poly(lactic acid), in Synthesis, Structure and Properties of Poly(lactic acid) in Advances in Polymer Science, Springer Handbook., M.L. Di Lorenzo, R. Androsch, 2016. https://hal.archives-ouvertes.fr/hal-01417723

One of the major hurdles for using PLA in commodity applications (food packaging for example) is its insufficient barrier properties. Permeability is therefore influenced by different intrinsic factors of a given polymer, such as the free volume fraction (FFV) of the polymer, the glass transition temperature, the Cohesive Energy Density (CED), the degree of crystallinity, the molecular orientation, the copolymerization. At macroscopic length scale, the design of global material architecture (blend structures, multilayers) influences the barrier properties. At the smaller length scale, the morphology of a given polymer and, in particular, the presence of impermeable obstacles in the pathway of diffusion changes the transport properties. Those obstacles are creating a more tortuous, longer, pathway for the diffusive transport of solutes and, as a result, decrease the macroscopic diffusion coefficient. On the molecular scale, diffusion proceeds by successive hops of the permeant from one void in the polymer matrix to another.

In semi-crystalline polymers, the diffusion takes place exclusively in the amorphous phase. Crystallites force tortuosity of the diffusive pathway of penetrants, which yields macroscopically lower diffusion coefficients. The increase of the tortuous pathway of diffusion inside PLA has been pursued by two different approaches: (i) increasing the polymer crystallinity, since the crystallites are impermeable to small molecules, and (ii) adding fillers or nanofillers [60].

Among the different gases, oxygen has high applicative importance and, not surprisingly, most literature studies on gas barrier properties are concerning the oxygen permeability of PLA. *Table 1.1* sums up some experimental data of the PLA oxygen permeability ($P(O_2)$) in comparison to petrochemical polymers. The PLA performance is similar to PS and below the performance of PET.

The $P(O_2)$ of amorphous PLA has been reported between 1.3 and 2.0 $\times 10^{-18}$ ($m^3.m/m^2.s.Pa$) at 30°C depending on the L/D ratio [61]. The oxygen transport coefficients of PLA, whatever the L/D ratio, are sensitive to the measurement temperature and Relative Humidity (RH). Auras et al. [62] showed that at 0 % RH, the oxygen permeability and solubility coefficients increased with temperature. Mensitieri et al. [63] investigated coupled effects of water vapor and $P(O_2)$ and showed that PLA, like other biopolymers, had lower oxygen barrier performances than petrochemical polymers, and that its performance was negatively influenced by its moisture susceptibility. The addition of plasticizers for the improvement of mechanical properties lead to an increase in the $P(O_2)$ due to the higher mobility of the polymer chain and higher free

volume brought by the plasticizer to the polymer matrix [64,65]. In some cases, the low molecular weight molecules can also fill in free volume, in which case they are positive for the barrier properties. This was demonstrated by the use of low molecular weight lactic acid oligomers. The blending of PLA with 25 wt% of lactic acid oligomers reduced the $P(O_2)$ by 22 % [66].

Table 1.1. Oxygen, permeability of petrochemical polymers and biopolyesters [61,67–70].

Polymer	$P(O_2) \times 10^{20}$ at 23°C/50 % or 0 % RH ($m^3.m/m^2.s.Pa$)
Polylactide (PLA)	130-300
Poly(3-hydroxy butyrate valerate) (PHBV)	50-157 (0 % RH)
Polycaprolactone (PCL)	430 (0 % RH)
Low density polyethylene (LDPE)	2200
High density polyethylene (HDPE)	300
Polypropylene (PP)	550-1100
Polystyrene (PS)	2000
Polycarbonate (PC)	1050
Poly(vinyl acetate) (PVA)	310
Poly(vinyl chloride) (PVC)	30
Poly(ethylene terephthalate) (PET)	10-60
Poly(ethylene naphthalate) (PEN)	5.7
Cellophane	1.6
Polyamide 6 (PA6)	1-30
Polyamide MXD6 (PA MXD6)	0.6
Liquid crystal polymer (LCP)	0.3
Poly(acrylonitrile) (PAN)	0.15-5
Poly(vinyl alcohol) (PVOH)	0.2-6.65 (0%RH)
Poly(vinylidene chloride) (PVDC)	0.1-3
Ethylene vinyl alcohol (EVOH)	0.002-1 (0 % RH)

The tailoring of the PLA microstructure for the increase of its barrier properties has been largely investigated in the recent years [70,69]. Dong et al. [71] reported a small increase of the oxygen barrier properties of bi-axially stretched and annealed PLA. The initial $P(O_2)$ was 2.03×10^{-18} ($m^3.m/m^2.s.Pa$). After drawing with a stretching ratio of 3.5, the $P(O_2)$ decreased to 1.53×10^{-18} ($m^3.m/m^2.s.Pa$). In the case of stretched and annealed samples, the $P(O_2)$ decreased from 1.83×10^{-18} ($m^3.m/m^2.s.Pa$) (stretching ratio 1 and annealed) to 1.31×10^{-18} ($m^3.m/m^2.s.Pa$) (stretching ratio 3.5 and annealed) [71].

The effect of crystallinity on PLA oxygen barrier properties was studied by a number of authors [58,59,72–74]. However, there were a number of conflicting results, for which no clear relationship between PLA crystallinity degree and barrier properties could be shaped. This situation was encountered in the case of several glassy polymers, as shown by Kanehasi et al. [75]. Guinault et al. [58] did a systematic study of the PLA barrier properties in function of the crystallinity degree. Their main results are shown in *Figure 1.13*. The $P(O_2)$ of PLA was either stable or even increased with increasing crystallinity degree (*Figure 1.13*). Guinault et al. [58] showed, that in the case of crystallization of PLA in α'(δ)-form high percentages of dedensified rigid amorphous fraction were created in the amorphous phase. This produced a pathway of accelerated gas transport around the crystalline lamellae. The oxygen permeability coefficient of PLA containing α-form was lower than that of containing α'(δ)- form [59], because the crystallization from the melt produced less dedensified amorphous phase [58]. For increasing PLA gas barrier properties high tortuosity needs to be achieved and formation of dedensified amorphous phases has to be avoided.

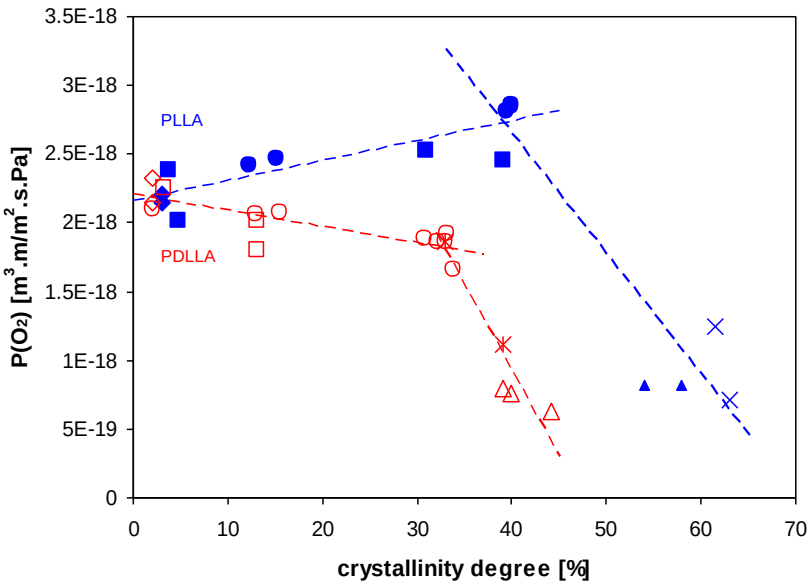

Figure 1.13. Impact of thermal crystallization on the oxygen permeability ($P(O_2)$) of PLA with two different %D (PLLA = 1% D, PDLLA = 4.3 % D). Reproduced from Guinault et al. [58], European Polymer Journal, with permission from Elsevier.

Bai et al [76] studied the $P(O_2)$ of PLA with an original crystalline morphology, described as parallel-aligned shish-kebab-like crystals with the aid of N,N′,N″-Tricyclohexyl-1,3,5-benzene-tricarboxylamide (trade name TMC-328), a highly active nucleating agent. As shown in the *Figure 1.14*, the oxygen barrier performance of PLA with such parallel-aligned shish-kebab-like crystals was more than 2 orders of magnitude higher than that of PLA with spherulitic crystals. The growing crystalline lamellae interlocked at the boundary regions and thereby formed a very densely packed structure, which decreased the gas permeability. The concentration of nucleating agent from 0.2 to 0.5 wt % impacted the oxygen permeability. The PLA with 0.5 wt% TMC sheet had a $P(O_2)$ of 1.989×10^{-20} $m^3 \cdot m/m^2 \cdot s \cdot Pa$, about 500 times lower than the amorphous PLA sheets (9.692×10^{-18} $m^3 \cdot m/m^2 \cdot s \cdot Pa$) [76].

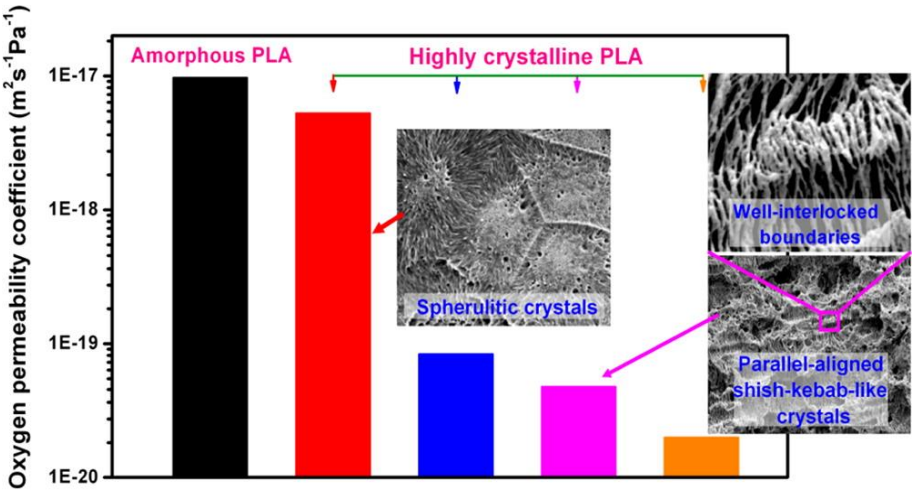

Figure 1.14.Improvement of PLA oxygen barrier properties by the formation of shish-kebab-like crystals. Reprinted with permission from Bai et al. [76], Biomacromolecules. Copyright 2016 American Chemical Society.

The second option to improve PLA barrier properties which was largely studies it the increase of the tortuosity in the permeant pathway by the incorporation of inert, nano-scale fillers in PLA [77–81]. The nano-scale particles need to have at least one dimension that is smaller than 100 nm, which yields a high aspect ratio (length/diameter = 100 to 500). The most widely used nano-fillers are Montmorillonites (MMT). MMT are hydrated alumina-silicate layered clays with a high surface area and large aspect ratio (50-1000). Exfoliation of clay minerals in the polymer is of high importance to obtain the desired high aspect ratio and a positive impact on the barrier properties. Furthermore, at a constant clay content, the permeability coefficient was reported to decrease as the length of the clay particles increased [78,82]. Using nanoclays, the permeability coefficient was globally divided by a factor 2 or 3, depending on the type of the nanoclays (e.g. organo-modified MMT, Cloisite 25A (quaternary ammonium salt modified MMT) or 30B (alkyl quaternary ammonium salt bentonite), organo-modified synthetic fluorine mica) and the efficiency of the exfoliation [83–85].

Guo et al [86] studied the $P(O_2)$ of PLA and different nanocomposites using MMT, organo-modified MMT, halloysite nanotubes and organo-modified halloysite nanotubes. They showed that the largest decrease in $P(O_2)$ was obtained by organomodified MMT. The halloysite nanotubes had no impact on the $P(O_2)$ of PLA [86]. Picard et al. [78] reported a decrease in $P(O_2)$ of annealed crystalline films containing 4 wt% of MMT with respect to the amorphous reference PLA film. They evidenced that the organo-modified clays had a tortuosity effect in the matrix. The more important role of the nano-fillers was however their effect as nucleating

agents, which helped to achieve a high crystallinity degree of PLA and thereby to decrease the $P(O_2)$ [78]. PLA blended with 1 wt% of surface-modified nanoparticles by in situ polymerization of L-lactide using two different nanoparticles (nanosilica and an organo-modified MMT (Cloisite R 15A)) showed an increase both in crystallinity (up to 70 %) and in barrier properties [87]. $P(O_2)$ was reduced by 80%, carbon dioxide and water vapor permeability were reduced by 50% and 45% respectively in comparison to pure PLA [87].

One of the most recent inorganic nano-fillers used in PLA is graphene and graphene oxide. To achieve a good dispersion of these nano-fillers, a pre-incorporation of graphene sheets by in situ melt polycondensation with lactic acid oligomers was tested by Ambrosio-Martin [66]. This procedure enhanced the barrier properties. A reduction of up to 45 % and 41 % in oxygen and water permeability, respectively, was reported. Graphene oxide is similar to graphene but the presence of some oxide groups allows a better compatibility with the polar polymer matrix. Pinto et al. [88] reported that $P(O_2)$ decreased from $3.76.10^{-18}$ ($m^3.m/m^2.s.Pa$) for pristine PLA to $1.34 - 1.49.10^{-18}$ ($m^3.m/m^2.s.Pa$) for PLA with 0.2-0.6 wt% of graphene oxide. These authors obtained the same results for PLA loaded with 0.2-0.6 wt% of graphene nanoplatelets.

In the framework of biobased and biodegradable materials, the increase of PLA barrier properties was also attempted using organic and biobased materials. Tripathi and Katiyar [89] studied biocomposites obtained with microspheres composed of arabic gum (LA-g-GA) grafted with lactic acid. A decrease of $P(O_2)$ by a factor 10 was achieved independently of the amount of the LA-g-GA (3, 5, 8 and 10%). Bionanocomposites of PLA were also developed using cellulose nanostructures. Cellulose microfibrils (MFC) have nanosized diameters (2-20 nm depending on the origin) and lengths in the micrometer range. The crystalline parts of the MFC can be isolated by several mechanical and chemical treatments, in the aim to obtain cellulose nanocrystals (CNC) or nanowhiskers. The lengths of CNC nanostructures range from 200 nm up to 1-2 µm and about 8-50 nm or less in diameter, which results in high aspect ratios [90–92]. Sanchez-Garcia et al. [93,94] compared the effect of the same content of MFC and CNC. The addition of 5 wt% of MFC had no effect on the gas barrier properties of PLA bionanocomposites while 5 wt % of CNC decreased slightly (factor 2) the $P(O_2)$. This result was also shown by Espino et al. [90].

Furthermore, different strategies for the fabrication of multilayer materials with improved barrier properties were investigated. A bi-layer sample composed of filtered 2,2,6,6-tetramethylpiperidine-1-oxyl (TEMPO)-radical oxidized cellulose nanofibers and PLA was studied by Fukuzumi et al. [95]. Under dry conditions, the $P(O_2)$ of the multilayer system

decreased by two orders of magnitude. Martucci and Ruseckaite [96] proposed three-layer sheets based on glycerol-plasticized gelatin as the inner layer and PLA as the outer layers. A decrease of $P(O_2)$ from 1.24 10^{-18} ($m^3.m/m^2.s.Pa$) for neat PLA to 0.81 ($m^3.m/m^2.s.Pa$) for the three layers was reported. Svagan et al. [97] used a layer-by-layer approach by electrostatic forces to assemble alternating layers of MMT and chitosan on extruded PLA film surfaces. When 70 MMT/chitosan bilayers were applied, the oxygen permeability was reduced by 99 and 96%, respectively, at 20 and 50% RH [97]. The novel processing techniques, such as layer-by-layer fabrication or the layer-multiplying co-extrusion process, permit to fabricate materials with large numbers of layers having nanometer thickness (often between 20 and 100 nm). In that case, the interface area in the multilayer material is very large and interface effects or inter-diffusion of polymers at the interface have an effect on the material properties. Liu et al. [98] showed the potential of such materials to improve barrier properties. Boufarguine et al. [99] produced PLA-PHBV multilayer films (129 layers) by layer-multiplying co-extrusion. They showed that the multiplication of the layer number had a positive effect on the helium permeability, compared to the 3-layer PLA-PHBV-PLA configuration. The helium permeability decreased from 120 $\times 10^{-18}$ ($m^3.m/m^2.s.Pa$) to 77.6 and 74.3 $\times 10^{-18}$ ($m^3.m/m^2.s.Pa$) for materials having 129 and 3 layers, respectively.

1.4. Confinement of polymers

Confinement of polymers occurs when geometric constraints are imposed on the macromolecular chain and it is constrained in a volume comparable to the size of macromolecules. Confining a system to a scale comparable to its characteristic length (gyration radius, for example) results in significant deviations of the structural and dynamical properties with respect to the bulk. Much research is done in the area of nano-science to improve and to achieve innovation in polymer thin films [100,101]. In particular, the interest in the area of nanoconfinement where the reduction of critical dimensions to the nano-scale can yield novel structures that impact bulk properties [102].

1.4.1. Different methods of confinement of polymers

The properties of polymer films are highly dependent on the processing conditions used to produce the final product. There are many techniques used to confine polymers at the nanoscale

including spin coating thin films onto a substrate [103–106], block copolymers containing a crystallizing block [107–109], layer-by-layer depositing [110,111] and more recently (nano)layer multiplying co-extrusion [99,112]. The layer multiplying co-extrusion offers the huge advantage of being able to produce objects at large scale and to be transferable to the industry for the fabrication of commodity materials.

This process combines two or three polymers into a continuous alternating layered structure with hundreds or thousands of layers. This can decrease the layer thickness of each individual layer to about 10 nm. However, the confinement effect in the whole volume of the material can only be reached when perfectly continuous multi-nanolayer structures are created with a homogenous layer thickness.

1.4.2. Crystallization of polymers under confinement

The macromolecular organization of polymers confined in the nanometer space, such as ultrathin films, can result in unique crystalline morphologies [102]. For semi crystalline polymers, we have to consider that the crystalline morphology changes from three-dimensional spherulites to lamellar morphology as the thickness decreases from the micrometer scale to nanometer scale (see example in *Figure 1.15*). Therefore, the processes of nucleation and growth that control the crystallization kinetics can be profoundly affected by nanoscale confinement [113].

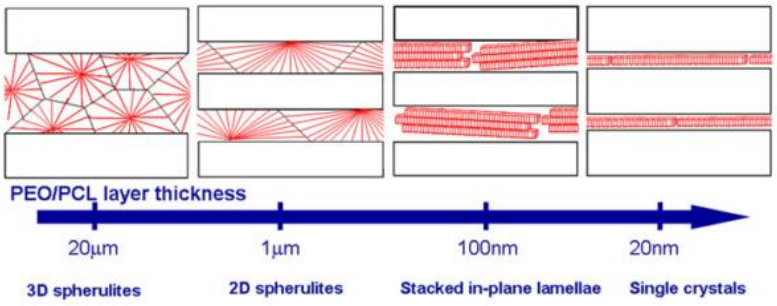

Figure 1.15. Structure evolution of a polymer in confined layers as the thickness is reduced from the microscale to the nanoscale. Reproduced from Carr et al.[112]

The thickness of ultrathin polymer layers is comparable to a small multiple of the lamellar crystal thickness. Hence, the isotropic growth of lamellar crystals is greatly hampered, and

crystallization under confinement can produce a specific lamellar crystal orientation. We will discuss preferentially results obtained on samples produced by the layer-multiplying coextrusion process. The orientation of the crystalline lamellas can be vertical to the layer (on-edge) [114–118] or, at the other extreme, it can be parallel to the layer (in-plane) [102,119–121] (*Figure 1.16*). Depending on the polymer, the literature describes the preferred orientation as either on-edge or in-plane. For example, PE [122] and isotactic PP [115] are reported to form on-edge crystals and isotactic PS [123], PLLA [119] and syndiotactic PP [124] form in-plane crystals.

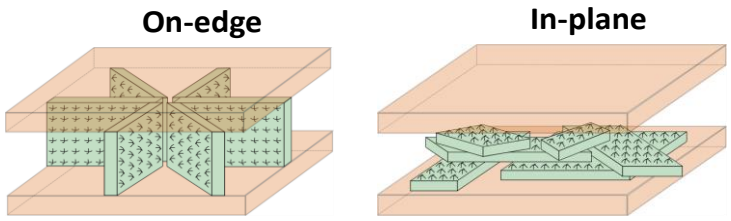

Figure 1.16. Two types of lamellar crystal orientation in confined system, on-edge and in-plane.

Furthermore the crystallization conditions can have an impact on the lamella orientation. Wang et al. [125] found an abrupt transition from in-plane to on-edge lamellar orientation of POE crystallites upon increase of the quenching temperature of 5°C. They suggest that this is due to a transition from heterogeneous nucleation to homogeneous nucleation. The AFM images clearly shows the in-plane and on-edge lamellae (*Figure 1.17*).

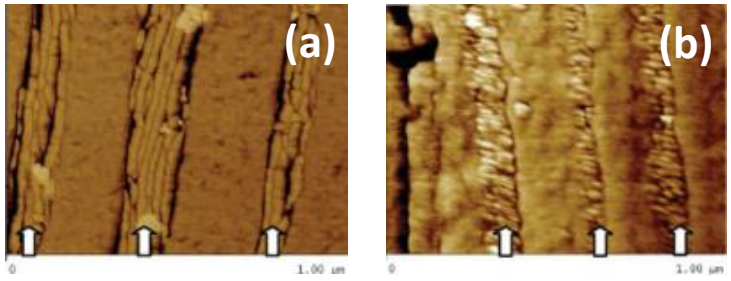

Figure 1.17. AFM images of 75 nm thickness of PEO layers (a) in-plane lamellae (b) on-edge lamellae. Reproduced from Wang et al.[125]

The crystallization kinetics under confinement was also investigated. Generally, the crystallization rate decreased [126] as shown by Wang et al in a study about PEO [127] (*Figure 1.18*).

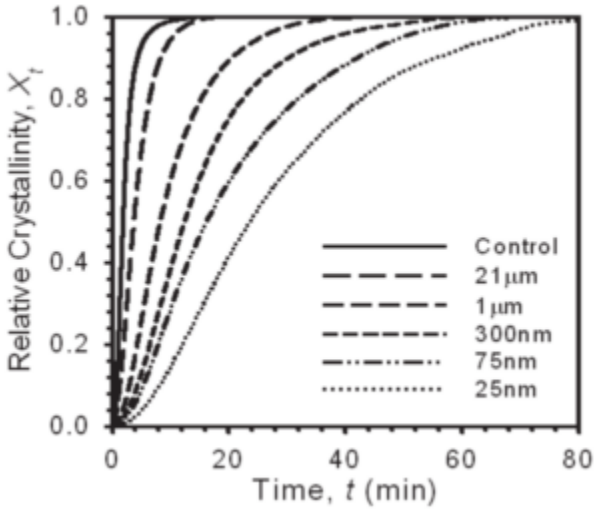

Figure 1.18. Relative crystallinity of PEO layers versus time for isothermal crystallization at 53°C. Reproduced from Wang et al.[127]

No studies on confinement of PLA by the layer-multiplying co-extrusion process were published today. There are however studies on confined PLA using the "hard confinement" methodology, i.e. confinement between two solid layers. In opposite, "soft confinement" means that the ultrathin film is bordered by a support and air (coated films) or by materials with lower modulus than the confined layer. PLLA was confined by PS in a diblock copolymer and then crystallized at a temperature lower than the Tg of PS (hard confinement conditions, *Figure 1.19*a) [119]. Using this methodology, the PLLA crystalline chains oriented perpendicular to the lamellae (i.e., in-plane). On the contrary, when PLLA was crystallized at a temperature higher than the Tg of PS (soft confinement conditions, *Figure 1.19b*), an undulated crystalline morphology was observed *(Figure 1.19*b). Ho et al. [119] attributed this behavior to the change from homogeneous nucleation (hard confinement) to heterogeneous nucleation (soft confinement). In the case of crystallization under hard confinement, the stress build up by PLLA could not move the barriers of glass PS, which left the original morphology unchanged.

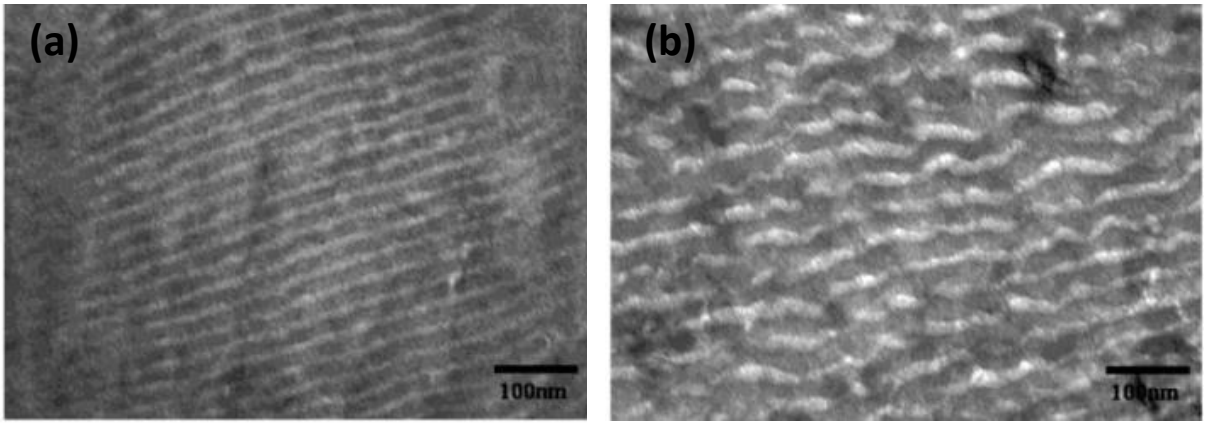

Figure 1.19. TEM micrographs of PS-PLLA samples (a) crystallized at 70°C (under hard confinement) (b) crystallized at 100°C (under soft confinement). Reproduced from Ho et al. [119]

1.4.3. Amorphous phase relaxation in confined polymers

The length scale of the glass transition in confined systems has been extensively studied to gain understanding of their deviation from the polymer bulk properties. For example, in a study where PS was confined by the spin coating method, Fukao and Miyamoto [128] observed a decrease in Tg with decreasing film thickness. In another study, Fukao et al. [31] investigated the relaxation at Tg of poly(vinyl acetate) (PVAc) and PMMA in spin-coated thin films. For PVAc, the Tg decreased gradually with decreasing film thickness and for PMMA, the Tg remained almost constant as the thickness decreased. In polyisoprene (PI) thin films, Serghei and Kremer [129] observed constant Tg despite the pronounced chain confinement effect.

There are a few studies about the impact of confinement on the amorphous phase dynamics fabricated by the nanolayer-multiplying system. In PC/PMMA multilayer films, Arabeche et al. [32] studied the influence of thickness reduction on the cooperativity at the glass transition of each polymeric component. They observed a decrease in the dynamic glass transition temperature for PC, while it remained constant for PMMA. For PC, a significant reduction in the CRR size could be correlated to the effect of confinement and associated to conformational changes in the macromolecular chains. PMMA has weaker intermolecular interactions between chains, which resulted in weaker confinement effects. Therefore, a very weak evolution of CRR size was observed.

Casalini et al. [130] studied the dynamics of PMMA in multilayer films with polycarbonate and compared bulk films to films having layer thickness of 25 nm, 8 nm and 4 nm. They observed

a small effect on the amorphous phase dynamics comparing bulk PMMA with confined PMMA layers of 25 nm thickness. Interestingly, the showed absence of confinement effects on the cooperativity length comparing the most confined PMMA (8 nm and 4 nm) to the bulk properties. Indeed, the values of ξ were equal to or smaller than the layer thickness of PMMA. Thus, they concluded that the dynamic correlation length did not appear to be limited by the geometrical confinement. Another interesting aspect of this study is the increase in Tg when thickness layers decreases, which was explained by interfacial interactions between PMMA and PC.

1.4.4. Gas barrier properties of confined polymers using the nanolayer-multiplying system

The interface area in the multilayer material where a single layer has nanometer thickness is huge and interface effects have significant importance for the material properties. The orientation of the crystals induced by confinement is a key parameter regarding the barrier properties. Several studies of gas transport in multilayer materials were undertaken in the area of barrier materials [99,113,126,131–133]. The formation of this confined morphology in nanolayered films had a dramatic impact on the gas transport and in some cases can reduce permeability in 100 times comparing to bulk permeability [134].

Liu et al. [98] showed the potential of the nanolayer-multiplying coextrusion for the improvement of the gas barrier properties of PC using PMMA. The fabrication of PMMA nanolayers allowed obtaining a high aspect ratio of the PMMA phase in PC. Under conditions which avainded the break up of the PMMA layers (layer thickness higher than 5 nm) a gain of 35% of oxygen barrier could be obtained by the use of only 2.5% of PMMA in the PC films [98].

Zhang et al [133] showed for HDPE confined by a PC that, thanks to the confinement obtained by the nanolayer-multiplying process and after recrystallization at high temperatures (25°C higher than HDPE's melting temperature and 20°C lower than PC's glass transition temperature), HDPE is fully melted when the confining layer of PC remain solid and hard allowing a twisted behavior in HDPE lamellas. The change in the lamellar morphology has improved the oxygen permeability of the multilayer films by 2 times.

Carr et al. [135] studied the confinement of poly(vinylidene fluoride-co-tetrafluoroethylene) (P(VDF-TFE)) by PET and its crystallization from the melt state. The resulting oxygen

permeability was about 400 times lower than that of extruded P(VDF-TFE)/PET films. They explain this spectacular improvement of oxygen barrier properties improvement by the orientation of the crystals in plane, i.e. parallel to the layer direction. Those crystals act as a barrier for oxygen by an important increase of the tortuosity of the diffusive pathway of oxygen through the film.

The group of Pr. Eric Baer did also numerous studies on the effect of Polyethylene oxide (PEO) confinement by nanolayer-multiplying co-extrusion of barrier properties. PEO layers down to at 25 nanometers produced a gradual decrease of the oxygen permeability. The maximum decrease was about 150 times compared to properties bulk of PEO. The large improvement in confined PEO layer oxygen barrier was attributed to single crystal in-plane lamellae induced through nano- layer confinement [136].

Wang et al. [113] studied the effect of crystallization under confinement of PEO coextruded with polyethylene-co-acrylic acid) (EAA) on the oxygen permeability. They observed a steady decrease in the oxygen permeability as the EAA and PEO layers became thinner. Again the POE crystals having in plane orientations were on the orgin of the improved barrier properties (factor 100) (crystals in-plane) (*Figure 1.20*).

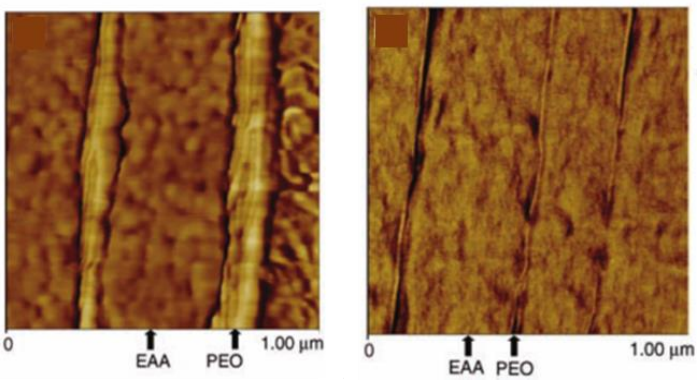

Figure 1.20. AFM images of EAA/PEO films with PEO layers of 110 nm and 20 nm of thickness. Reproduced from Wang et al.[113].

In another study, Wang et al. [126] studied the crystallization of PEO confined in microlayers and nanolayers by PS. The oxygen permeability of PS/PEO layered films dramatically decreased as the layers became thinner. Crystallization with in plane lamellas reduced 2 orders of magnitude in oxygen permeability.

This approach was also explored for polycaprolactone (PCL) [137]. Confinement of PCL led to the same morphology and improvements in barrier properties than PEO. Permeability decreased with decreasing layer thickness, as we can see in *Figure 1.21*.

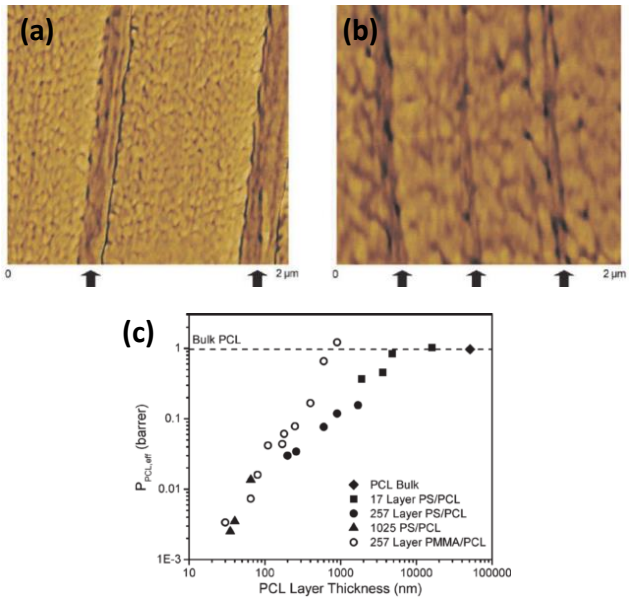

Figure 1.21. AFM images of PS/PCL films with PCL layers of (a) 250 nm, (b) 25 nm and (c) effect of layer thickness on the permeability of PCL layers. Reproduced from [137].

The bibliography about gas barrier properties using this process for PLA is virtually non-existent, except studies carried out by the UMR PIMM and already mentioned in the sub-chapter "Barrier properties of PLA". Boufarguine et al. [99] produced PLA-PHBV multilayer films (129 layers) by nanolayer-multiplying co-extrusion. They showed that the multiplication of the number of crystallized PHBV layers had a positive effect on the helium permeability, compared to the dry blend. The helium permeability decreased from 100 ×10-18 (m^3.m/m^2.s.Pa) to 77.6 and 74.3 ×10-18 (m^3.m/m^2.s.Pa) for materials having 129 and 3 layers, respectively.

1.5. Conclusion

PLA is today one of the most promising novel biobased and biodegradable resins for the fabrication of commodity materials. Because it has received large academic and industrial interest in the last 20 years, much of its properties on the macromolecular scale, such as amorphous phase dynamics and crystallization properties are today already satisfyingly understood. PLA processing is mastered in a number of plastics converting processing and

processing aids and blending strategies exist for adapting use properties, such as ductility and stiffness. One of the open questions is the improvement of the PLA gas barrier properties, in the aim to widen its application spectrum in the packaging industry. Gas transport through polymers takes place in the amorphous phase, but the relationship between those dynamics and molecular transport are still open. Next to that, the literature shows that the confinement of polymers by other polymers, using in particular the nanolayer multiplying coextrusion process, and the crystallization of such confined layers might be a way for large barrier properties improvements. The use of PLA in this processing technology needs to be investigated, yet. Moreover, the amorphous phase dynamics and crystallization of PLA under such confinement are unexplored and, as a consequence, understanding of the impact of such dynamics on the macroscopic properties of the confined PLA is missing. Using PLA in the nanolayer multiplying coextrusion process and investigating the structure/function relationships of confined PLA are the objectives of this thesis.

1.6. References

[1] R. Auras, B. Harte, S. Selke, An overview of polylactides as packaging materials, Macromol. Biosci. 4 (2004) 835–864. doi:10.1002/mabi.200400043.

[2] R. a. Auras, S.P. Singh, J.J. Singh, Evaluation of oriented poly(lactide) polymers vs. existing PET and oriented PS for fresh food service containers, Packag. Technol. Sci. 18 (2005) 207–216. doi:10.1002/pts.692.

[3] D. Garlotta, A Literature Review of Poly (Lactic Acid), J. Polym. Environ. 9 (2002) 63–84. doi:10.1023/A:1020200822435.

[4] S. Saeidlou, M.A. Huneault, H. Li, C.B. Park, Poly(lactic acid) crystallization, Prog. Polym. Sci. 37 (2012) 1657–1677. doi:10.1016/j.progpolymsci.2012.07.005.

[5] M.L. Di Lorenzo, The crystallization and melting processes of poly(L-lactic acid), Macromol. Symp. 234 (2006) 176–183. doi:10.1002/masy.200650223.

[6] N. Delpouve, a. Saiter, E. Dargent, Cooperativity length evolution during crystallization of poly(lactic acid), Eur. Polym. J. 47 (2011) 2414–2423. doi:10.1016/j.eurpolymj.2011.09.027.

[7] K. Wasanasuk, K. Tashiro, Crystal structure and disorder in Poly(l-lactic acid) δ form (α' form) and the phase transition mechanism to the ordered α form, Polymer. 52 (2011) 6097–6109. doi:10.1016/j.polymer.2011.10.046.

[8] B. Eling, S. Gogolewski, a. J. Pennings, Biodegradable materials of poly (L-lactic acid):, Polymer. 23 (1982) 1587–1593.

[9] W. Hoogsteen, A.R. Postema, A.J. Pennings, G. Brinke, Crystal Structure, Conformation, and Morphology of Solution-Spun Poly(L-lactide) Fibers, Macromolecules. (1990) 634–642.

[10] L. Cartier, T. Okihara, Y. Ikada, H. Tsuji, J. Puiggali, B. Lotz, Epitaxial crystallization and crystalline polymorphism of polylactides, Polymer. 41 (2000) 8909–8919. doi:10.1016/0032-3861(94)90933-4.

[11] T. Okihara, M. Tsuji, A. Kawaguchi, K. Katayama, Crystal structure of stereocomplex of poly (L- lactide) and poly (D-lactide), (1991) 119–140.

[12] P. De Santis, J. Kovacs, Molecular conformation of poly (S-lactic acid), Biopolymers. 6 (1968) 299–306. doi:10.1002/bip.36.v6.

[13] J. Zhang, K. Tashiro, H. Tsuji, A.J. Domb, Disorder-to-order phase transition and multiple melting behavior of poly(L-lactide) investigated by simultaneous measurements of WAXD and DSC, Macromolecules. 41 (2008) 1352–1357. doi:10.1021/ma0706071.

[14] T. Kawai, N. Rahman, G. Matsuba, K. Nishida, T. Kanaya, M. Nakano, H. Okamoto, J. Kawada, A. Usuki, N. Honma, K. Nakajima, M. Matsuda, Crystallization and Melting Behavior of Poly (L-lactic Acid), Macromolecules. 40 (2007) 9463–9469.

[15] J. Zhang, Y. Duan, H. Sato, H. Tsuji, I. Noda, S. Yan, Y. Ozaki, Crystal Modifications and Thermal Behavior of Poly (L -lactic acid) Revealed by Infrared Spectroscopy, (2005) 8012–8021.

[16] P. Pan, B. Zhu, W. Kai, T. Dong, Y. Inoue, Polymorphic transition in disordered poly(L-lactide) crystals induced by annealing at elevated temperatures, Macromolecules. 41 (2008) 4296–4304. doi:10.1021/ma800343g.

[17] P. Pan, W. Kai, B. Zhu, T. Dong, Y. Inoue, Polymorphous Crystallization and Multiple Melting Behavior of Poly(l -lactide): Molecular Weight Dependence, Macromolecules. 40 (2007) 6898–6905. doi:10.1021/ma071258d.

[18] M.L. Di Lorenzo, M. Cocca, M. Malinconico, Crystal polymorphism of poly(l-lactic acid) and its influence on thermal properties, Thermochim. Acta. 522 (2011) 110–117. doi:10.1016/j.tca.2010.12.027.

[19] M. Cocca, M.L. Di Lorenzo, M. Malinconico, V. Frezza, Influence of crystal polymorphism on mechanical and barrier properties of poly(l-lactic acid), Eur. Polym. J. 47 (2011) 1073–1080. doi:10.1016/j.eurpolymj.2011.02.009.

[20] P. Pan, B. Zhu, W. Kai, T. Dong, Y. Inoue, Effect of crystallization temperature on crystal modifications and crystallization kinetics of poly(L-lactide), J. Appl. Polym. Sci. 107 (2008) 54–62. doi:10.1002/app.27102.

[21] H. Tsuji, Y. Ikada, Blends of isotactic and atactic poly(lactide)s: 2. Molecular-weight effects of atactic component on crystallization and morphology of equimolar blends from the melt, Polymer. 37 (1996) 595–602. doi:10.1016/0032-3861(96)83146-6.

[22] B.E.W. Fischer, H.J. Sterzel, G. Wegner, Investigation of the structure of solution grown crystals of lactide copolymers by means of chemical reactions by means of chemical reactions, Kolloid-Z. U. Z. Polym. 251 (1973) 980–990.

[23] J.P. Kalish, K. Aou, X. Yang, S.L. Hsu, Spectroscopic and thermal analyses of a and a' crystalline forms of poly(l-lactic acid), Polymer. 52 (2011) 814–821. doi:10.1016/j.polymer.2010.12.042.

[24] M. Pyda, R.C. Bopp, B. Wunderlich, Heat capacity of poly(lactic acid), J. Chem. Thermodyn. 36 (2004) 731–742. doi:10.1016/j.jct.2004.05.003.

[25] J.-R. Sarasua, R.E. Prud'homme, M. Wisniewski, A. Le Borgne, N. Spassky, Crystallization and Melting Behavior of Polylactides, Macromolecules. 31 (1998) 3895–3905. doi:10.1021/ma971545p.

[26] A. Saiter, N. Delpouve, E. Dargent, W. Oberhauser, L. Conzatti, F. Cicogna, E. Passaglia, Probing the chain segment mobility at the interface of semi-crystalline polylactide/clay nanocomposites, Eur. Polym. J. 78 (2016) 274–289. doi:10.1016/j.eurpolymj.2016.03.040.

[27] T.A. Tran, S. Saïd, Y. Grohens, Nanoscale characteristic length at the glass transition in confined syndiotactic poly(methyl methacrylate), Macromolecules. 38 (2005) 3867–3871. doi:10.1021/ma0487296.

[28] C. Lixon, N. Delpouve, a. Saiter, E. Dargent, Y. Grohens, Evidence of Cooperative Rearranging Region size anisotropy for drawn PET, Eur. Polym. J. 44 (2008) 3377–3384. doi:10.1016/j.eurpolymj.2008.08.001.

[29] G. Adam, J.H. Gibbs, On the Temperature Dependence of Cooperative Relaxation Properties in Glass-Forming Liquids, J. Chem. Phys. 43 (1965) 139–146. doi:10.1063/1.1696442.

[30] E. Donth, The size of cooperatively rearranging regions at the glass transition, J. Non. Cryst. Solids. 53 (1982) 325–330. doi:10.1016/0022-3093(82)90089-8.

[31] K. Fukao, S. Uno, Y. Miyamoto, A. Hoshino, H. Miyaji, Dynamics of α and β processes in thin polymer films: Poly(vinyl acetate) and poly(methyl methacrylate), Phys. Rev. E. 64 (2001) 051807. doi:10.1103/PhysRevE.64.051807.

[32] K. Arabeche, L. Delbreilh, R. Adhikari, G.H. Michler, A. Hiltner, E. Baer, J.M. Saiter, Study of the cooperativity at the glass transition temperature in PC/PMMA multilayered films: Influence of thickness reduction from macro- to nanoscale, Polymer . 53 (2012) 1355–1361. doi:10.1016/j.polymer.2012.01.045.

[33] X. Monnier, N. Delpouve, N. Basson, a. Guinault, S. Domenek, a. Saiter, P.E. Mallon, E. Dargent, Molecular dynamics in electrospun amorphous plasticized polylactide fibers, Polym. (United Kingdom). 73 (2015) 68–78. doi:10.1016/j.polymer.2015.07.047.

[34] A. Saiter, N. Delpouve, E. Dargent, J.M. Saiter, Cooperative rearranging region size determination by temperature modulated DSC in semi-crystalline poly(l-lactide acid), Eur. Polym. J. 43 (2007) 4675–4682. doi:10.1016/j.eurpolymj.2007.07.039.

[35] Y. Lixon, C., Delpouve, N., Saiter, A., Dargent, E., Grohens, Evidence of cooperative Rearranging Region Size anisotropy for drawn PET, Eur. Polym. J. 44 (2008) 3377–3384.

[36] N. Delpouve, L. Delbreilh, G. Stoclet, A. Saiter, E. Dargent, Structural dependence of the molecular mobility in the amorphous fractions of polylactide, Macromolecules. 47 (2014) 5186–5197. doi:10.1021/ma500839p.

[37] C. Schick, E. Donth, Characteristic length of glass transition: experimental evidence Characteristic Length of G lass Transition : Experimenta I Evidence, Phys. Scr. 43 (1991) 423–429.

[38] A. Codou, M. Moncel, J. Van Berkel, N. Guigo, N. Sbirrazzuoli, Glass Transition Dynamics and Cooperativity Length of Poly(ethylene 2,5-furandicarboxylate) compared to Poly(ethylene terephthalate), Phys. Chem. Chem. Phys. (2016). doi:10.1039/C6CP01227B.

[39] N. Delpouve, A. Saiter, J.F. Mano, E. Dargent, Cooperative rearranging region size in semi-crystalline poly(L-lactic acid), Polymer. 49 (2008) 3130–3135. doi:10.1016/j.polymer.2008.04.045.

[40] Y. Furushima, K. Ishikiriyama, T. Higashioji, The characteristic length of cooperative rearranging region for uniaxial drawn poly(ethylene terephthalate) films, Polym. (United Kingdom). 54 (2013) 4078–4084. doi:10.1016/j.polymer.2013.06.030.

[41] B. Wunderlich, Effect of decoupling of molecular segments, microscopic stress-transfer and confinement of the nanophases in semicrystalline polymers, Macromol. Rapid Commun. 26 (2005) 1521–1531. doi:10.1002/marc.200500488.

[42] J. Lin, S. Shenogin, S. Nazarenko, Oxygen solubility and specific volume of rigid amorphous fraction in semicrystalline poly(ethylene terephthalate), Polymer. 43 (2002) 4733–4743. doi:10.1016/S0032-3861(02)00278-1.

[43] B. Wunderlich, Reversible crystallization and the rigid amorphous phase in semicrys-talline macromolecules, Prog. Polym. Sci. 28 (2003) 408–409.

[44] J. Del Rıó, A. Etxeberria, N.L. Lopez-Rodrıuez, E. Lizundia, J.R. Sarasua, A PALS Contribution to the Supramolecular Structure of Poly(L-lactide), Macromolecules. 43 (2010) 4698–4707. doi:10.1021/ma902247y.

[45] B. Wunderlich, Reversible crystallization and the rigid-amorphous phase in semicrystalline macromolecules, Prog. Polym. Sci. 28 (2003) 383–450. doi:10.1016/S0079-6700(02)00085-0.

[46] A. Sargsyan, A. Tonoyan, S. Davtyan, C. Schick, The amount of immobilized polymer in PMMA SiO2 nanocomposites determined from calorimetric data, Eur. Polym. J. 43 (2007) 3113–3127. doi:10.1016/j.eurpolymj.2007.05.011.

[47] S.X. Lu, P. Cebe, Effects of annealing on the disappearance and creation of constrained amorphous phase, Polymer. 37 (1996) 4857–4863. doi:10.1016/S0032-3861(96)00376-X.

[48] A. Nogales, T. Ezquerra, F. Batallan, B. Frick, E. Lopez-Cabarcos, F. Balta-Calleja, Restricted dynamics in poly (ether ether ketone) as revealed by incoherent quasielastic neutron scattering and broad-band dielectric spectroscopy, Macromolecules. 32 (1999) 2301–2308.

[49] H. Xu, P. Cebe, Transitions from solid to liquid in isotactic polystyrene studied by thermal analysis and X-ray scattering, Polymer. 46 (2005) 8734–8744. doi:10.1016/j.polymer.2005.01.105.

[50] R. Androsch, B. Wunderlich, The link between rigid amorphous fraction and crystal perfection in cold-crystallized poly(ethylene terephthalate), Polymer. 46 (2005) 12556–12566. doi:10.1016/j.polymer.2005.10.099.

[51] A. Esposito, N. Delpouve, V. Causin, A. Dhotel, L. Delbreilh, E. Dargent, From a Three-Phase Model to a Continuous Description of Molecular Mobility in Semicrystalline Poly(hydroxybutyrate- *co* -hydroxyvalerate), Macromolecules. (2016). doi:10.1021/acs.macromol.6b00384.

[52] M.C. Righetti, E. Tombari, Crystalline, mobile amorphous and rigid amorphous fractions in poly(L-lactic acid) by TMDSC, Thermochim. Acta. 522 (2011) 118–127. doi:10.1016/j.tca.2010.12.024.

[53] E. Zuza, J.M. Ugartemendia, A. Lopez, E. Meaurio, A. Lejardi, J.R. Sarasua, Glass transition behavior and dynamic fragility in polylactides containing mobile and rigid amorphous fractions, Polymer. 49 (2008) 4427–4432. doi:10.1016/j.polymer.2008.08.012.

[54] M. Arnoult, E. Dargent, J.F. Mano, Mobile amorphous phase fragility in semi-crystalline polymers: Comparison of PET and PLLA, Polymer. 48 (2007) 1012–1019. doi:10.1016/j.polymer.2006.12.053.

[55] H. Chen, M. Pyda, P. Cebe, Non-isothermal crystallization of PET/PLA blends, Thermochim. Acta. 492 (2009) 61–66. doi:10.1016/j.tca.2009.04.023.

[56] Y. Wang, S.S. Funari, J.F. Mano, Influence of semicrystalline morphology on the glass transition of poly(L-lactic acid), Macromol. Chem. Phys. 207 (2006) 1262–1271. doi:10.1002/macp.200600114.

[57] S. Iannace, L. Nicolais, Isothermal Crystallization and Chain Mobility of Poly (L - lactide), J. Appl. Polym. Sci. (1997) 911–919.

[58] A. Guinault, C. Sollogoub, V. Ducruet, S. Domenek, Impact of crystallinity of poly(lactide) on helium and oxygen barrier properties, Eur. Polym. J. 48 (2012) 779–788. doi:10.1016/j.eurpolymj.2012.01.014.

[59] M. Drieskens, R. Peeters, J. Mullens, D. Franco, P. Lemstra, D. Hristova-Bogaerds, Structure Versus Properties Relationship of Poly(lactic acid). I. Effect of Crystallinity on Barrier Properties, J. Polym. Sci. Part B Polym. Phys. 47 (2009) 2247–2258. doi:10.1002/polb.21822.

[60] I. Armentano, N. Bitinis, E. Fortunati, S. Mattioli, N. Rescignano, R. Verdejo, M. a. Lopez-Manchado, J.M. Kenny, Multifunctional nanostructured PLA materials for packaging and tissue engineering, Prog. Polym. Sci. 38 (2013) 1720–1747. doi:10.1016/j.progpolymsci.2013.05.010.

[61] J. Lange, W. Yves, Recent innovations in barrier technologies for plastic packaging - a review, Packag. Technol. Sci. 16 (2003) 149–158. http://dx.doi.org/10.1002/pts.621.

[62] R. a Auras, B. Harte, S. Selke, R. Hernandez, Mechanical, Physical, and Barrier Properties of Poly(Lactide) Films, J. Plast. Film Sheeting. 19 (2003) 123–135. doi:10.1177/8756087903039702.

[63] G. Mensitieri, E. Di Maio, G.G. Buonocore, I. Nedi, M. Oliviero, L. Sansone, S. Iannace, Processing and shelf life issues of selected food packaging materials and structures from renewable resources, Trends Food Sci. Technol. 22 (2011) 72–80. doi:10.1016/j.tifs.2010.10.001.

[64] V.P. Martino, A. Jimenez, R.A. Ruseckaite, Processing and Characterization of Poly(lactic acid) Films Plasticized with Commercial Adipates, J. Appl. Polym. Sci. 112 (2009) 2010–2018. doi:10.1002/app.

[65] C. Courgneau, S. Domenek, R. Lebossé, A. Guinault, L. Avérous, V. Ducruet, Effect of crystallization on barrier properties of formulated polylactide, Polym. Int. 61 (2012) 180–189. doi:10.1002/pi.3167.

[66] A. Ambrosio-Martın, Jesus Lopez-Rubio, M.J. Fabra, M.A. Lopez-Manchado, A. Sorrentino, G. Gorrasi, J.M. Lagaron, On1, Synergistic effect of lactic acid oligomers

and laminar graphene sheets on the barrier properties of polylactide nanocomposites obtained by the in situ polymerization pre-incorporation method, J. Appl. Polym. Sci. 133 (2016) 42661–42672. doi:10.1002/app.42971.

[67] M.D. Sanchez-Garcia, E. Gimenez, J.M. Lagaron, Novel PET Nanocomposites of Interest in Food Packaging Applications and Comparative Barrier Performance With Biopolyester Nanocomposites, J. Plast. Film Sheeting. 23 (2007) 133–148. doi:10.1177/8756087907083590.

[68] L. Bélard, F. Poncin-Epaillard, P. Dole, L. Avérous, Plasma-polymer coatings onto different biodegradable polyesters surfaces, Eur. Polym. J. 49 (2013) 882–892. doi:10.1016/j.eurpolymj.2012.11.022.

[69] S. Pauly, Permeability and diffusion data. In: Brandrup J, Immergut EH, Grulke EA (eds) Polymer Handbook, vol 2. John Wiley & Sons, Inc., New York, 1999.

[70] S. Domenek, C. Courgneau, V. Ducruet, Characteristics and applications of PLA In: Kalia S, Averous L (eds) Biopolymers: Biomedical and Environmental Applications. John Wiley & Scrivener Pub, 2011.

[71] T. Dong, Z. Yu, J. Wu, Z. Zhao, X. Yun, Y. Wang, Y. Jin, J. Yang, Thermal and barrier properties of stretched and annealed polylactide films, Polym. Sci. Ser. A. 57 (2015) 738–746. doi:10.1134/S0965545X15060073.

[72] Z. Kulinski, E. Piorkowska, K. Gadzinowska, M. Stasiak, Plasticization of Poly (l-lactide) with Poly (propylene glycol), Biomacromolecules. 7 (2006) 2128–2135. doi:10.1021/bm060089m.

[73] G. Colomines, V. Ducruet, Ć. Courgneau, A. Guinault, S. Domenek, Barrier properties of poly(lactic acid) and its morphological changes induced by aroma compound sorption, Polym. Int. 59 (2010) 818–826. doi:10.1002/pi.2793.

[74] H. Sawada, Y. Takahashi, S. Miyata, S. Kanehashi, S. Sato, K. Nagai, Gas Transport Properties and Crystalline Structures of Poly(lactic acid) Membranes, Trans. Mater. Res. Soc. Japan. 35 (2010) 241–246. doi:10.14723/tmrsj.35.241.

[75] S. Kanehashi, A. Kusakabe, S. Sato, K. Nagai, Analysis of permeability; solubility and diffusivity of carbon dioxide; oxygen; and nitrogen in crystalline and liquid crystalline polymers, J. Memb. Sci. 365 (2010) 40–51. doi:10.1016/j.memsci.2010.08.035.

[76] H. Bai, C. Huang, H. Xiu, Q. Zhang, H. Deng, K. Wang, F. Chen, Q. Fu, Significantly improving oxygen barrier properties of polylactide via constructing parallel-aligned

shish-kebab-like crystals with well-interlocked boundaries, Biomacromolecules. 15 (2014) 1507–1514. doi:10.1021/bm500167u.

[77] X. Wen, K. Zhang, Y. Wang, L. Han, C. Han, H. Zhang, S. Chen, L. Dong, Study of the thermal stabilization mechanism of biodegradable poly(L-lactide)/silica nanocomposites, Polym. Int. 60 (2011) 202–210. doi:10.1002/pi.2927.

[78] E. Picard, E. Espuche, R. Fulchiron, Effect of an organo-modified montmorillonite on PLA crystallization and gas barrier properties, Appl. Clay Sci. 53 (2011) 58–65. doi:10.1016/j.clay.2011.04.023.

[79] H. Li, M. a. Huneault, Effect of nucleation and plasticization on the crystallization of poly(lactic acid), Polymer. 48 (2007) 6855–6866. doi:10.1016/j.polymer.2007.09.020.

[80] J.G. Wijmans, R.W. Baker, The solution-diffusion model: a review, J. Memb. Sci. 107 (1995) 1–21. doi:10.1016/0376-7388(95)00102-I.

[81] G. Choudalakis, a. D. Gotsis, Permeability of polymer/clay nanocomposites: A review, Eur. Polym. J. 45 (2009) 967–984. doi:10.1016/j.eurpolymj.2009.01.027.

[82] M. a. Paul, M. Alexandre, P. Degee, C. Henrist, a., Dubois and, R. P., New Nanocomposites Materials Based on Plasticized Poly (L-lactide) and Organo-modified Montmorillonites: Thermal and Morphological Study, Polymer. 44 (2003) 443–450. doi:10.1016/S0032-3861(02)00778-4.

[83] J. Chang, Y.U. An, G.S. Sur, Poly(Lactic Acid) Nanocomposites with Various Organoclays. I.Thermomechanical Properties, Morphology, and Gas Permeability, J. Polym. Sci. Part B Polym. Phys. 41 (2003) 94–103. doi:10.1002/polb.10349.

[84] S.S. Ray, P. Maiti, M. Okamoto, K. Yamada, K. Ueda, New Polylactide / Layered Silicate Nanocomposites . 1 . Preparation , Characterization , and Properties, 35 (2002) 3104–3110.

[85] M. Zenkiewicz, J. Richert, Permeability of polylactide nanocomposite films for water vapour, oxygen and carbon dioxide, Polym. Test. 27 (2008) 835–840. doi:10.1016/j.polymertesting.2008.06.005.

[86] Y. Guo, K. Yang, X. Zuo, Y. Xue, C. Marmorat, Y. Liu, C.-C. Chang, M.H. Rafailovich, Effects of clay platelets and natural nanotubes on mechanical properties and gas permeability of Poly (lactic acid) nanocomposites, Polymer. 83 (2016) 246–259. doi:10.1016/j.polymer.2015.12.012.

[87] M. a. Ortenzi, L. Basilissi, H. Farina, G. Di Silvestro, L. Piergiovanni, E. Mascheroni, Evaluation of crystallinity and gas barrier properties of films obtained from PLA

nanocomposites synthesized via “in situ” polymerization of L-lactide with silane-modified nanosilica and montmorillonite, Eur. Polym. J. 66 (2015) 478–491. doi:10.1016/j.eurpolymj.2015.03.006.

[88] A.M. Pinto, J. Cabral, D. a P. Tanaka, A.M. Mendes, F.D. Magalhães, Effect of incorporation of graphene oxide and graphene nanoplatelets on mechanical and gas permeability properties of poly(lactic acid) films, Polym. Int. 62 (2013) 33–40. doi:10.1002/pi.4290.

[89] N. Tripathi, V. Katiyar, PLA/functionalized-gum arabic based bionanocomposite films for high gas barrier applications, J. Appl. Polym. Sci. 133 (2016) n/a–n/a. doi:10.1002/app.43458.

[90] E. Espino-Pérez, J. Bras, V. Ducruet, A. Guinault, A. Dufresne, S. Domenek, Influence of chemical surface modification of cellulose nanowhiskers on thermal, mechanical, and barrier properties of poly(lactide) based bionanocomposites, Eur. Polym. J. 49 (2013) 3144–3154. doi:10.1016/j.eurpolymj.2013.07.017.

[91] E. Espino-Pérez, S. Domenek, N. Belgacem, C. Sillard, J. Bras, Green process for chemical functionalization of nanocellulose with carboxylic acids, Biomacromolecules. 15 (2014) 4551–4560. doi:10.1021/bm5013458.

[92] E. Espino-Perez, R.G. Gilbert, S. Domenek, M.C. Brochier-Salon, M.N. Belgacem, J. Bras, Nanocomposites with functionalised polysaccharide nanocrystals through aqueous free radical polymerisation promoted by ozonolysis, Carbohydr. Polym. 135 (2016) 256–266. doi:10.1016/j.carbpol.2015.09.005.

[93] M.D. Sanchez-Garcia, J.M. Lagaron, On the use of plant cellulose nanowhiskers to enhance the barrier properties of polylactic acid, Cellulose. 17 (2010) 987–1004. doi:10.1007/s10570-010-9430-x.

[94] M.D. Sanchez-Garcia, E. Gimenez, J.M. Lagaron, Morphology and barrier properties of solvent cast composites of thermoplastic biopolymers and purified cellulose fibers, Carbohydr. Polym. 71 (2008) 235–244. doi:10.1016/j.carbpol.2007.05.041.

[95] H. Fukuzumi, T. Saito, T. Iwata, Y. Kumamoto, A. Isogai, Transparent and High Gas Barrier Films of Cellulose Nanofibers Prepared by TEMPO-Mediated Oxidation Transparent and High Gas Barrier Films of Cellulose Nanofibers Prepared by TEMPO-Mediated Oxidation, (2009) 162–165. doi:10.1021/bm801065u.

[96] J.F. Martucci, R.A. Ruseckaite, Three-Layer Sheets Based on Gelatin and Poly(lactic acid), Part 1: Preparation and Properties, J. ofAppliedPolymer Sci. 118 (2010) 3102–3110. doi:10.1002/app.

[97] A.J. Svagan, A. Åkesson, M. Cárdenas, S. Bulut, J.C. Knudsen, J. Risbo, D. Plackett, Transparent films based on PLA and montmorillonite with tunable oxygen barrier properties, Biomacromolecules. 13 (2012) 397–405. doi:10.1021/bm201438m.

[98] R.Y.F. Liu, a. P. Ranade, H.P. Wang, T.E. Bernal-Lara, a. Hiltner, E. Baer, Forced assembly of polymer nanolayers thinner than the interphase, Macromolecules. 38 (2005) 10721–10727. doi:10.1021/ma051649x.

[99] M. Boufarguine, A. Guinault, G. Miquelard-Garnier, C. Sollogoub, PLA/PHBV films with improved mechanical and gas barrier properties, Macromol. Mater. Eng. 298 (2013) 1065–1073. doi:10.1002/mame.201200285.

[100] W. Li, H.; Huck, Polymers in Nanotechnology, Curr. Opin. Solid State Mater. Sci. 6 (2002) 3–8.

[101] M.R. Bockstaller, R. a. Mickiewicz, E.L. Thomas, Block copolymer nanocomposites: Perspectives for tailored functional materials, Adv. Mater. 17 (2005) 1331–1349. doi:10.1002/adma.200500167.

[102] M. Reiter, G; Botiz, I; Graveleau, L; Grozev, N; Albrecht, K; Mourran, A; Moller, Morphologies of Polymer Crystals in Thin Films, in: Notes, 2007: pp. 179–200. doi:10.1007/3-540-47307-6.

[103] D. Guo, N. Setter, Impact of confinement-induced cooperative molecular orientation change on the ferroelectric size effect in ultrathin P(VDF-TrFE) films, Macromolecules. 46 (2013) 1883–1889. doi:10.1021/ma302377q.

[104] N. Bhandaru, A. Das, R. Mukherjee, Confinement Induced Ordering in Dewetting of Ultra Thin Polymer Bilayers on Nano Patterned Substrates, Nanoscale. (2015) 1073–1087. doi:10.1039/C5NR06690E.

[105] S. Askar, C.M. Evans, J.M. Torkelson, Residual stress relaxation and stiffness in spin-coated polymer films: Characterization by ellipsometry and fluorescence, Polym. (United Kingdom). 76 (2015) 113–122. doi:10.1016/j.polymer.2015.08.036.

[106] M.K. Mundra, C.J. Ellison, R.E. Behling, J.M. Torkelson, Confinement, composition, and spin-coating effects on the glass transition and stress relaxation of thin films of polystyrene and styrene-containing random copolymers: Sensing by intrinsic fluorescence, Polymer. 47 (2006) 7747–7759. doi:10.1016/j.polymer.2006.08.064.

[107] T.M. Burt, S. Monemian, a M. Jordan, L.T.J. Korley, Thin film confinement of a spherical block copolymer via forced assembly co-extrusion, Soft Matter. 9 (2013) 4381–4385. doi:Doi 10.1039/C3sm27797f.

[108] T.M. Burt, J. Keum, A. Hiltner, E. Baer, L.T.J. Korley, Confinement of elastomeric block copolymers via forced assembly coextrusion, ACS Appl. Mater. Interfaces. 3 (2011) 4804–4811. doi:10.1021/am201297f.

[109] L. Zhu, S.Z.D. Cheng, B.H. Calhoun, Q. Ge, R.P. Quirk, E.L. Thomas, B.S. Hsiao, F. Yeh, B. Lotz, Crystallization temperature-dependent crystal orientations within nanoscale confined lamellae of a self-assembled crystalline - Amorphous diblock copolymer, J. Am. Chem. Soc. 122 (2000) 5957–5967. doi:10.1021/ja000275e.

[110] W. Xu, Z. Wang, L. Shi, Y. Ma, S. Yuan, L. Sun, Y. Zhao, M. Zhang, J. Zhu, Layer-by-Layer Deposition of Organic-Inorganic Hybrid Multilayer on Microporous Polyethylene Separator to Enhance the Electrochemical Performance of Lithium-Ion Battery, ACS Appl. Mater. Interfaces. 7 (2015) 20678–20686. doi:10.1021/acsami.5b05457.

[111] J.J. Richardson, M. Bjornmalm, F. Caruso, Technology-driven layer-by-layer assembly of nanofilms, Science. 348 (2015) 2491–2491. doi:10.1126/science.aaa2491.

[112] J.M. Carr, D.S. Langhe, M.T. Ponting, A. Hiltner, E. Baer, Confined crystallization in polymer nanolayered films: A review, J. Mater. Res. 27 (2012) 1326–1350. doi:10.1557/jmr.2012.17.

[113] H. Wang, J.K. Keum, A. Hiltner, E. Baer, B. Freeman, A. Rozanski, A. Galeski, Confined crystallization of polyethylene oxide in nanolayer assemblies., Science. 323 (2009) 757–760. doi:10.1126/science.1164601.

[114] T.E. Bernal-Lara, R.Y.F. Liu, a. Hiltner, E. Baer, Structure and thermal stability of polyethylene nanolayers, Polymer. 46 (2005) 3043–3055. doi:10.1016/j.polymer.2005.01.055.

[115] Y. Jin, M. Rogunova, a. Hiltner, E. Baer, R. Nowacki, a. Galeski, E. Piorkowska, Structure of polypropylene crystallized in confined nanolayers, J. Polym. Sci. Part B Polym. Phys. 42 (2004) 3380–3396. doi:10.1002/polb.20211.

[116] F. Ania, F.J. Baltá-Calleja, a. Flores, G.H. Michler, S. Scholtyssek, D. Khariwala, a. Hiltner, E. Baer, L. Rong, B.S. Hsiao, Nanostructure and crystallization phenomena in multilayered films of alternating iPP and PA6 semicrystalline polymers, Eur. Polym. J. 48 (2012) 86–96. doi:10.1016/j.eurpolymj.2011.10.003.

[117] Y. Lin, A. Hiltner, E. Baer, Nanolayer enhancement of biaxially oriented polypropylene film for increased gas barrier, Polymer. 51 (2010) 5807–5814. doi:10.1016/j.polymer.2010.09.070.

[118] G. Zhang, H. Xu, K. MacInnis, E. Baer, Crystallization of linear low density polyethylene under two-dimensional confinement in high barrier blend systems, Polymer. 55 (2014) 6853–6860. doi:10.1016/j.polymer.2014.10.040.

[119] R.-M. Ho, F.-H. Lin, C.-C. Tsai, C.-C. Lin, B.-T. Ko, B.S. Hsiao, I. Sics, Crystallization-Induced Undulated Morphology in Polystyrene-b-Poly(L-lactide) Block Copolymer, Macromolecules. 37 (2004) 5985–5994. doi:10.1021/ma0492869.

[120] Y. Sen Sun, T.M. Chung, Y.J. Li, R.M. Ho, B.T. Ko, U.S. Jeng, B. Lotz, Crystalline polymers in nanoscale 1D spatial confinement, Macromolecules. 39 (2006) 5782–5788. doi:10.1021/ma0608121.

[121] M. Hsiao, J.X. Zheng, S. Leng, R.M. Van Horn, R.P. Quirk, E. L, H. Chen, B.S. Hsiao, L. Rong, B. Lotz, S.Z.D. Cheng, E.L. Thomas, Crystal Orientation Change and Its Origin in One-Dimensional Nanoconfinement Constructed by Polystyrene-block-poly (ethylene oxide) Single Crystal Mats Crystal Orientation Change and Its Origin in One-Dimensional Nanoconfinement Constructed by Polystyre, Macromolecules. 41 (2008) 8114–8123. doi:10.1021/ma801641w.

[122] Z. Bartczak, a. S. Argon, R.E. Cohen, T. Kowalewski, The morphology and orientation of polyethylene in films of sub-micron thickness crystallized in contact with calcite and rubber substrates, Polymer. 40 (1999) 2367–2380. doi:10.1016/S0032-3861(98)00443-1.

[123] S. Sutton, K. Izumi, H. Miyaji, Y. Miyamoto, The morphology of isotactic polystyrene crystals grown in thin films: the effect of substrate material, J. Mater. Sci. 32 (1997) 5621–5627.

[124] Z. Bu, Y. Yoon, R. Ho, W. Zhou, I. Jangchud, R.K. Eby, S.Z.D. Cheng, E.T. Hsieh, T.W. Johnson, R.G. Geerts, S.J. Palackal, G.R. Hawley, M. Bruce Welch, Crystallization, melting, and morphology of syndiotactic polypropylene fractions. 3. Lamellar single crystals and chain folding, Macromolecules. 29 (1996) 6575–6581.

[125] H. Wang, J.K. Keum, A. Hiltner, E. Baer, Impact of nanoscale confinement on crystal orientation of poly(ethylene oxide), Macromol. Rapid Commun. 31 (2010) 356–361. doi:10.1002/marc.200900653.

[126] H. Wang, J.K. Keum, A. Hiltner, E. Baer, Confined crystallization of peo in nanolayered films impacting structure and oxygen permeability, Macromolecules. 42 (2009) 7055–7066. doi:10.1021/ma901379f.

[127] H. Wang, J.K. Keum, A. Hiltner, E. Baer, Crystallization kinetics of poly(ethylene oxide) in confined nanolayers, Macromolecules. 43 (2010) 3359–3364. doi:10.1021/ma902780p.

[128] K. Fukao, Y. Miyamoto, Glass transitions and dynamics in thin polymer films: Dielectric relaxation of thin films of polystyrene, Phys. Rev. E. 61 (2000) 1743–1754. doi:10.1103/PhysRevE.61.1743.

[129] a Serghei, F. Kremer, Confinement-induced relaxation process in thin films of cis-polyisoprene., Phys. Rev. Lett. 91 (2003) 165702. doi:10.1103/PhysRevLett.91.165702.

[130] R. Casalini, L. Zhu, E. Baer, C.M. Roland, Segmental dynamics and the correlation length in nanoconfined PMMA, Polym. (United Kingdom). 88 (2016) 133–136. doi:10.1016/j.polymer.2016.02.030.

[131] R. Huang, P. Chari, J.-K. Tseng, G. Zhang, M. Cox, J.M. Maia, Microconfinement effect on gas barrier and mechanical properties of multilayer rigid/soft thermoplastic polyurethane films, J. Appl. Polym. Sci. 132 (2015) n/a–n/a. doi:10.1002/app.41849.

[132] G.T. Offord, S.R. Armstrong, B.D. Freeman, E. Baer, A. Hiltner, D.R. Paul, Gas transport in coextruded multilayered membranes with alternating dense and porous polymeric layers, Polym. (United Kingdom). 55 (2014) 1259–1266. doi:10.1016/j.polymer.2014.01.030.

[133] G. Zhang, P.C. Lee, S. Jenkins, J. Dooley, E. Baer, The effect of confined crystallization on high-density poly(ethylene) lamellar morphology, Polym. (United Kingdom). 55 (2014) 663–672. doi:10.1016/j.polymer.2013.12.027.

[134] M. MacKey, L. Flandin, A. Hiltner, E. Baer, Confined crystallization of PVDF and a PVDF-TFE copolymer in nanolayered films, J. Polym. Sci. Part B Polym. Phys. 49 (2011) 1750–1761. doi:10.1002/polb.22375.

[135] J.M. Carr, M. Mackey, L. Flandin, A. Hiltner, E. Baer, Structure and transport properties of polyethylene terephthalate and poly(vinylidene fluoride-co-tetrafluoroethylene) multilayer films, Polymer. 54 (2013) 1679–1690. doi:10.1016/j.polymer.2013.01.037.

[136] M. Ponting, A. Hiltner, E. Baer, Polymer nanostructures by forced assembly: Process, structure, and properties, Macromol. Symp. 294 (2010) 19–32. doi:10.1002/masy.201050803.

[137] M. Ponting, Y. Lin, J.K. Keum, A. Hiltner, E. Baer, Effect of substrate on the isothermal crystallization kinetics of confined poly(ε-caprolactone) nanolayers, Macromolecules. 43 (2010) 8619–8627. doi:10.1021/ma101625h.

Chapter 2 – Matériaux et méthodes

2. Matériaux et méthodes

2.1. Matériaux

2.1.1. Choix des polymères

Les Polylactides de référence PLA4042D et PLA REVODE190 (L175) étudiés lors de cette thèse ont été fournis respectivement par Resinex (granulés NatureWorks) et Corbion Purac sous forme de granulés. La teneur en acide lactique de forme L de ces 2 polymères est respectivement de 96 ± 0,5% et supérieure à 99% selon les fiches techniques. Ils sont notés respectivement PDLLA et PLLA dans la suite.

Deux groupes de films ont été étudies lors de ce travail :

- Films monocouches fabriqués avec le PLA4042D (PDLLA),
- Films multicouches fabriqués avec le PLA REVODE190 (L175) (PLLA).

Le polystyrène (PS) de référence PS1340 a été fourni par Schulman (granulés Total Petrochemicals) et le polycarbonate (PC) de référence PC121R a été fourni par gazechim (granulés Sabic). Les deux polymères (PS et PC) utilisés comme polymères confineurs sont amorphes, pour faciliter, en particulier, les analyses de cristallinité des PLA.

Les grades de PS et de PC ont été choisis pour leur viscosité de façon à ce qu'ils aient la même viscosité que le PLLA aux températures d'extrusion et aux taux de cisaillement imposés par l'extrusion. Toutefois, les seules données disponibles sont les MFI (Melt flow index ou indice de fluidité à chaud (IFC)). Des mesures de rhéologie sont nécessaires pour confirmer le choix des polymères.

2.2. Méthodes expérimentales

2.2.1. Caractérisation des granulés

2.2.1.1.Séchage des granulés de PLA et de PC

Le PLA est sensible à la dégradation hydrolytique, il est essentiel de le sécher avant toute transformation afin d'en minimiser l'effet [1]. Le séchage du PC avant son passage dans

l'extrudeuse a été réalisé pour éviter la formation de bulles d'air dans les films, préjudiciable aux propriétés mécaniques et aux propriétés barrières.

2.2.1.1.1. Description des sécheurs à granulés

Le sécheur utilisé de marque Somos du laboratoire PIMM possède une capacité de 60 L. Il dispose d'un dispositif de dessiccation permettant d'assurer le séchage des granulés sous air sec et ainsi atteindre de basses teneurs en humidité résiduelle. La température et le temps de séchage, paramètres dépendant du polymère, doivent faire l'objet d'une étude tant ce critère est crucial pour la qualité finale du film de polylactide. Cette humidité résiduelle après séchage est contrôlée par dosage chimique lors du chauffage d'une quantité déterminée de granulés. Cette analyse est réalisée grâce à l'utilisation d'un Hydrotracer ABONI FMX™ (*Figure 2.1*).

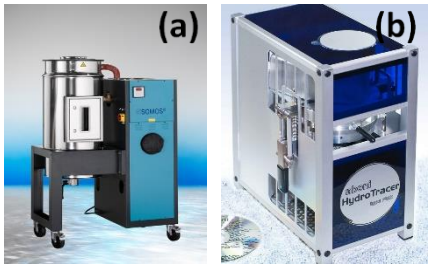

Figure 2.1. (a) Sécheur Somos 60 L et (b) Hydrotracer Aboni FMX™

2.2.1.1.2. Protocole expérimental de séchage de granulés

Les polylactides utilisés dans la thèse sont des grades semi-cristallins. Nous avons fixé la consigne à 80°C pour l'étape de séchage. Apres vérification grâce à l'Hydrotracer ABONI FMX™, le temps de séchage a été fixé à 12 heures pour atteindre des taux d'humidité de 250 à 300 ppm, tel que préconisé par Natureworks.
Le PS n'a pas été séché et le PC a été séché à 120°C pendant 12 heures pour atteindre la valeur préconisée de 150 à 250 ppm.

2.2.2. Rhéologie

Deux différents grades de PS et de PC ont été analysés par rhéologie dans le but de trouver le grade ayant un rapport de viscosité avec le PLLA le plus proche de 1 à 200°C pour le PS et

240°C pour le PC (températures choisies en fonction des températures utilisées lors de l'extrusion). L'uniformité et la continuité des couches dépendent fortement du rapport de viscosité. Un mauvais rapport de viscosité peut se traduire par des phénomènes d'encapsulation du polymère de faible viscosité par le polymère de viscosité supérieure [2]. Le rapport de viscosité *p* entre les deux polymères peut être déterminé, avec $\eta_{confiné}$ et $\eta_{confineur}$ la viscosité du polymère confiné et confineur respectivement, avec l'équation suivante :

$$p = \frac{\eta_{confiné}}{\eta_{confineur}} \qquad \text{Équation 2.1}$$

Les courbes de viscosité de chaque polymère ont été déterminées à l'aide d'un rhéomètre ANTON PAAR de référence MCR 502. Les mesures ont été réalisées en mode oscillatoire entre 0,01 et 100 rad/s. La déformation a été préalablement déterminée en réalisant des balayages en déformation, et a été fixée à 1% pour les trois polymères.
Le taux de cisaillement rencontré dans le procédé de coextrusion a été calculé avec l'équation suivante en considérant que le cisaillement le plus important dans le procédé se passe au niveau de la filière :

$$\dot{\gamma} = \frac{6 \cdot Q}{L \cdot e^2} \qquad \text{Équation 2.2}$$

où Q est le débit (de 0,67 cm^3/s soit 2,4 kg/heure), L est la largeur de la filière (de 200 mm) et e est l'ouverture de la filière au niveau de ses lèvres (de 2 mm). On obtient donc un taux de cisaillement de 5 s^{-1} d'après le calcul présenté ci-dessous.

$$\dot{\gamma} = \frac{6 \cdot Q}{L \cdot e^2} \Rightarrow \frac{6 \cdot 0{,}67}{20 \cdot 0{,}2^2} \Rightarrow \dot{\gamma} = 5s^{-1}$$

La *Figure 2.2* représente les courbes de rapport de viscosité sur le domaine de fréquence angulaire déterminé à l'aide du rhéomètre.

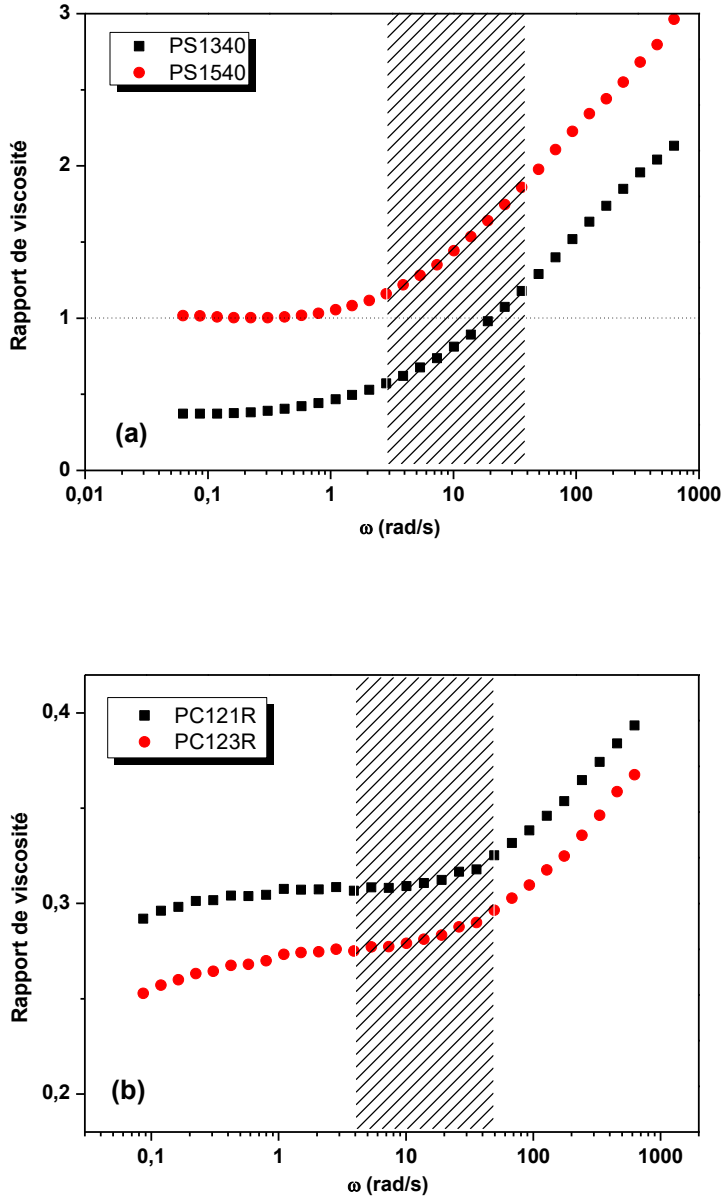

Figure 2.2. Rapport de viscosité pour (a) les couples PLLA/PS à 200°C, (b) les couples PLLA/PC à 240°C ; en considérant dans les deux cas le PLLA comme matrice. La zone hachurée correspond aux taux de cisaillement rencontrés dans le procédé de co-extrusion en considérant la loi de Cox Merz ($\eta(\omega) = \eta(\dot{\gamma})$).

Considérant la loi de Cox Merz et d'après les résultats de rhéologie, le PS (PC) donnant lieu au rapport de viscosité le plus proche de 1 est le grade PS1340 (le grade PC121R). Néanmoins, pour le PC, le rapport de viscosité obtenu est autour de 0,4, en sachant que le grade PC121R est le grade le plus fluide de la gamme. De plus, sa faible viscosité va permettre de le mettre en

œuvre à de températures plus basses et donc plus compatibles avec le PLLA (autour de 240 °C), alors que le PC est normalement extrudé à de températures autour de 350°C.

2.2.3. Mise en œuvre des films

2.2.3.1.Mise en œuvre des films monocouches

Apres séchage des granulés, le PDLLA a été extrudé à l'aide d'une extrudeuse monovis MAPRE de 30 mm de diamètre et une vis à trois sections sans élément de mélange. La vitesse de la vis de l'extrudeuse a été réglée à 40 tr/min. Le profil de température des six zones de l'extrudeuse est présenté dans la *Figure 2.3.* et était 180-180-180-185-190-190°C. La température du dispositif mélangeur (4 Sulzer SMX) et de la filière a été fixée à 200°C. Une filière plate de 200 mm de largeur et un rouleau froid (T = 20°C) ont été utilisés pour fabriquer des films d'environ 300 μm d'épaisseur en jouant sur la vitesse de tirage du rouleau de refroidissement (chill roll).

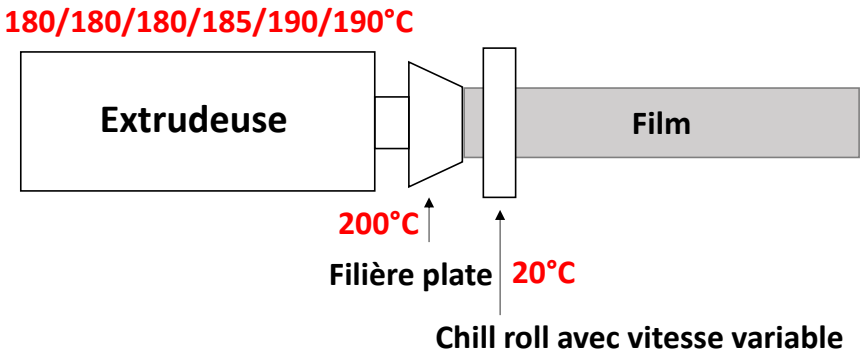

Figure 2.3. Représentation schématique de la préparation de l'échantillon comprenant des procédures d'extrusion.

2.2.3.2.Mise en œuvre de films multicouches (PLLA/PS et PLLA/PC)

Les films multicouches après séchage des granulés, ont été fabriqués en utilisant un procédé de co-extrusion multi-nanocouche. Ce procédé est constitué de deux extrudeuses monovis de 20 mm avec des doseurs (cas du PS/PLLA) ou des pompes à engrenages (cas du PC/PLLA), permettant un réglage précis du débit de chaque matière, un bloc d'alimentation à trois couches

(A-B-A), une série de blocs multiplicateurs de couches, une filière plate et des rouleaux de refroidissement en sortie comme illustré sur la *Figure 2.4*.

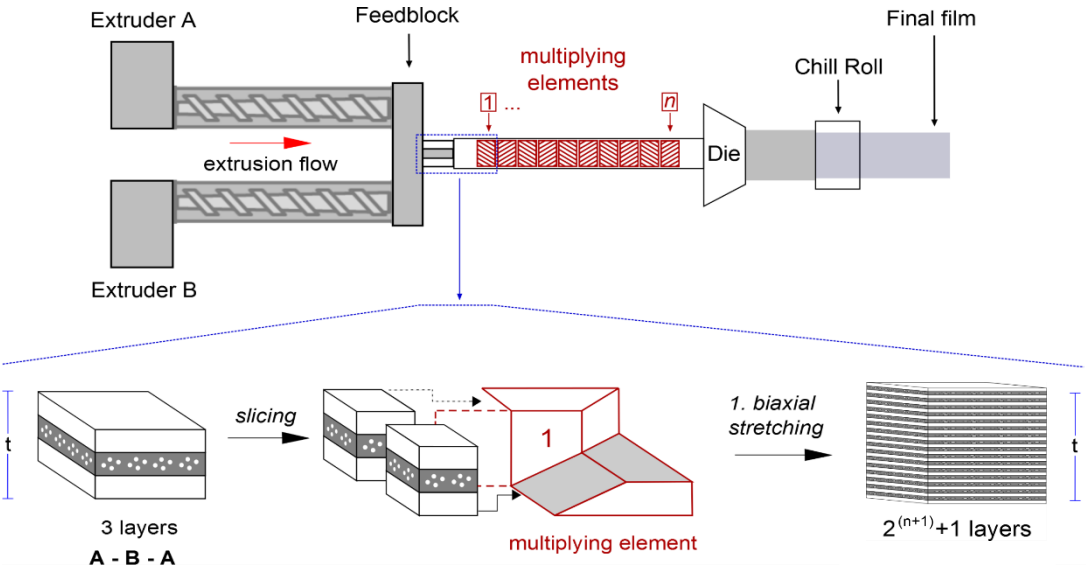

Figure 2.4. Principe du procédé de co-extrusion multi-nano-couches pour la fabrication des films.

Les conditions d'extrusion de chaque couple de polymères (PLLA/PS et PLLA/PC) sont données dans les *Tableau 2.1* et *Tableau 2.2*.

Tableau 2.1. Conditions pour le procédé d'extrusion selon les matériaux utilisés (PS/PLLA)

(en °C)	**Extrudeuses**	**Pompes + Bloc de répartition**	**Eléments multiplicateurs**	**Filière**
PLLA	190/200/200/200	200	200	200
PS 1340	200/200/200/210			

Température matière (°C)	200
Température rouleau (°C)	70
Vitesse Vis PLLA (tr/min)	22
Vitesse Vis PS (tr/min)	57
Vitesse pompe (tr/min)	-
Débit PLLA (g/h)	600
Débit PS (g/h)	1800

Tableau 2.2. Conditions pour le procédé d'extrusion selon les matériaux utilisés (PC/PLLA)

(en °C)	**Extrudeuses**	**Pompes + Bloc de répartition**	**Eléments multiplicateurs**	**Filière**
PLLA	230/220/210/210	240	240	220
PC 121R	280/260/260/260			

Température matière (°C)	210
Température rouleau (°C)	120
Vitesse Vis PLLA (tr/min)	15
Vitesse Vis PC (tr/min)	34
Vitesse pompe PC (tr/min)	49
Débit PLLA (g/h)	600
Débit PC (g/h)	1800

Le PLLA a été extrudé pour former la couche interne des films et le PS (ou le PC) les couches externes. L'introduction des pompes à engrenages ou des doseurs dans le système de co-extrusion permet un contrôle supplémentaire sur le rapport relatif de l'épaisseur, lorsque les polymères entrent dans le bloc d'alimentation A-B-A. La fraction massique du polymère B dans le film a été fixée et maintenue constante en ajustant le débit en fonction de la vitesse des pompes à engrenages ou des doseurs. Le système initial à trois couches pénètre dans la section

de mélange, composée d'une séquence d'éléments multiplicateurs. La masse fondue est initialement coupée en deux verticalement, puis chaque moitié est comprimée puis étirée à sa largeur d'origine, pour doubler le nombre de couches à chaque passage dans un élément multiplicateur. Une série de n éléments avec la configuration tricouche initiale produit ainsi $2^{n+1}+1$ couches alternées, comme le montre la *Figure 2.4*.

Les films ont été réalisés avec 0, 8 et 10 multiplicateurs de couches (0M, 8M et 10M), donnant respectivement 3, 512 et 2049 couches. Dans tous les films, la composition massique des polymères est 25% en masse de polylactide (ω_{PLLA}) et 75% en masse de polystyrène ou polycarbonate. Le calcul de l'épaisseur théorique (ou épaisseur nominale) du PLLA a été fait à l'aide de l'équation suivante :

$$e_{PLLA} = \frac{\omega_{PLLA} \cdot e_{film}}{n_{PLLA}} \qquad \text{Équation 2.3}$$

où ω_{PLLA} est la fraction massique du PLLA, e_{film} est l'épaisseur totale du film et n_{PLLA} est le nombre de couches de PLLA dans le film. n_{PLLA} est déterminé par l'équation $n_{PLLA}=2^n$ où n est le nombre de multiplicateurs. Les informations concernant les films fabriqués et permettant le calcul des épaisseurs individuelles de couche sont données dans les *Tableau 2.3* et *Tableau 2.4*.

Tableau 2.3. Informations sur les films de PLLA/PS

PLLA/PS	Vitesse d'étirage (cm/min)	Epaisseur du film (μm) (e_{film})	Nombre de couche de PLLA (n_{PLLA})	Epaisseur d'une couche de PLLA (nm) (e_{PLLA})
0M	60	120	1	30000
8M	60	300	256	293
10M	180	80	1024	20

Tableau 2.4. Informations sur les films de PLLA/PC

PLLA/PC	Vitesse d'étirage (cm/min)	Epaisseur du film (μm) (e_{film})	Nombre de couche de PLLA (n_{PLLA})	Epaisseur d'une couche de PLLA (nm) (e_{PLLA})
8M	60	330	256	330
10M	180	90	1024	22

2.2.4. Caractérisation des films

2.2.4.1.Perméabilité à l'oxygène

La mesure directe de la perméabilité à l'oxygène est réalisée selon la norme ASTMD 3985 grâce à un détecteur coulométrique. La vitesse de transmission de l'oxygène (ou OTR, oxygen transmission rate) est mesurée en mode dynamique à 23 °C et 0 % de humidité relative à l'aide d'un appareil Systech 8001. Son principe de fonctionnement est montré sur la *Figure 2.5*. De l'oxygène pur (99,9%) est débité dans la chambre supérieure, tandis qu'un gaz vecteur exempt d'oxygène (N_2 à 99,9% pur), débite dans la chambre inférieure. Les molécules d'oxygène diffusent à travers le film vers la chambre inférieure et le gaz vecteur entraine l'oxygène vers la cellule de mesure d'oxygène. Cela permet une mesure directe d'oxygène.

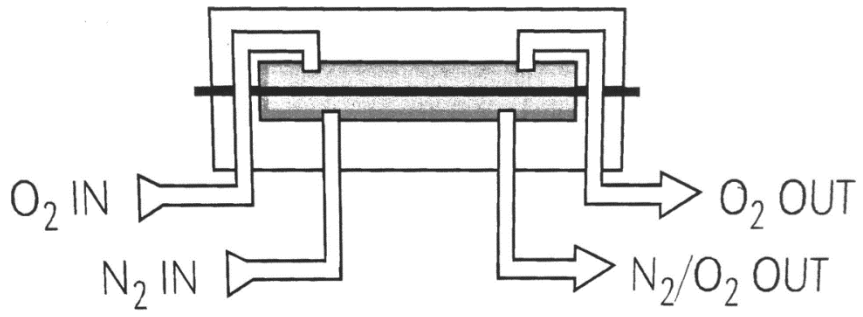

Figure 2.5. Principe du fonctionnement de l'appareil Systech 8001 pour la mesure de la perméabilité à l'oxygène.

La mesure de la quantité d'oxygène traversant le film est réalisée jusqu'à l'obtention du régime stationnaire. La valeur de perméabilité est alors donnée par :

$$P = \frac{J \times l}{S \times (p_1 - p_2)} \qquad \text{Équation 2.4}$$

Avec J, la densité de flux ($m^3.s^{-1}$), l (m), l'épaisseur de film, S (m^2) la surface d'échange et p_1 et p_2 (Pa) la pression dans les compartiments amont et aval, respectivement. J/S correspondant à la vitesse de transmission de l'oxygène ($cc.m^{-2}.j^{-1}$) et la différence de pression entre les deux compartiments étant de 1 bar lors des mesures, la perméabilité peut s'écrire :

$$P = OTR \times l = \frac{J}{S} \times l$$ Équation 2.5

La valeur de perméabilité ainsi obtenue est en $m^3.m.m^{-2}.s^{-1}.Pa^{-1}$ dans le système SI. La valeur retenue lors de nos mesures est la valeur lue à l'équilibre (*Figure 2.6*). A partir de la courbe de l'OTR en fonction du temps, moyennent une purge totale, il est possible d'accéder à la mesure du coefficient de diffusion D et du coefficient de solubilité S.

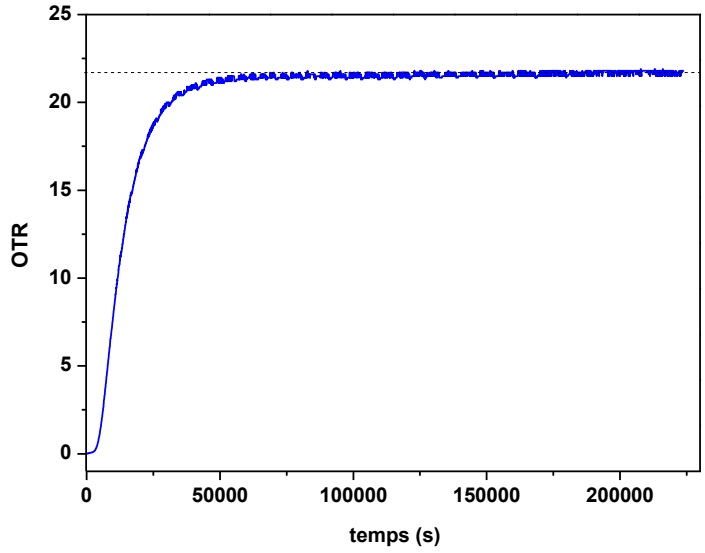

Figure 2.6. Exemple d'une courbe de perméabilité (OTR en fonction du temps)

Le coefficient de diffusion du gaz (oxygène) est calculé par la méthode du time lag (θ ou temps de retard) (*Figure 2.7*), c'est-à-dire le temps nécessaire à l'obtention du régime stationnaire. Pour cela, la courbe de la *Figure 2.6* est intégrée pour obtenir la courbe de la *Figure 2.7*, sur laquelle l'axe des ordonnées correspond à la somme des OTR.
D est déterminé par l'Equation 2.6 :

$$D = \frac{l^2}{6 \times \theta}$$ Équation 2.6

où l est l'épaisseur du film en mètre, θ est le time lag en seconde et D est le coefficient de diffusion en $m^2.s^{-1}$.

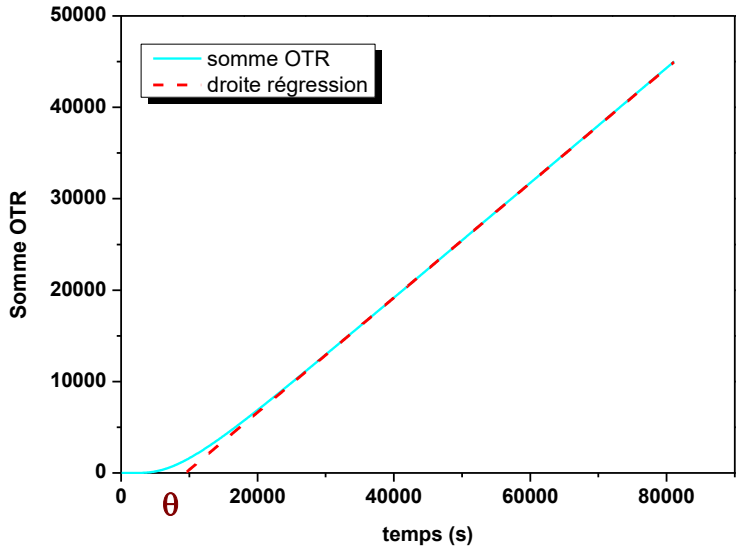

Figure 2.7. Exemple de la méthode du time lag

Les coefficients de solubilité ont été calculés en utilisant l'Equation 2.7 :

$$P = D \times S \qquad \text{Équation 2.7}$$

Les mesures sont préférentiellement réalisées sur des échantillons de surface 50 cm^2. Dans le cas où les échantillons sont plus petits, un masque de surface 5 cm^2 est utilisé. Les mesures sont réalisées uniquement à température ambiante et 0% RH.
Pour les échantillons multicouches, la perméabilité du PLLA est calculé en utilisant l'équation ci-dessous. Dans cette équation on considère 75% de PS ou PC et 25 de PLLA.

$$\frac{1}{P_{film}} = \frac{0{,}25}{\rho_{PLLA} \cdot P_{PLLA}} + \frac{0{,}75}{\rho_{confineur} \cdot P_{confineur}} \qquad \text{Équation 2.8}$$

où ρ_{PLLA} est la masse volumique du PLLA (1,25 g/cm^3), ρ_{PS} est la masse volumique du PS (1,05 g/cm^3) et ρ_{PC} celle du PC (1,2 g/cm^3).

2.2.4.2.Perméabilité à l'hélium

La perméabilité à l'hélium est mesurée à température et humidité relative ambiante. Le système utilisé a été développé par le Laboratoire P-2AM (Propriétés Architectures des Alliages et Mélanges) du CNAM et est basé sur la norme ISO 15105-2 :2003. La mesure directe est réalisée grâce à un spectromètre de masse Adixen ASM 142 utilisé comme détecteur jusqu'à l'obtention du régime stationnaire. Ce spectromètre de masse à déflexion magnétique est réglé sur la masse de l'hélium (m/e = 4) de manière à ne mesurer que le flux d'hélium. La mesure réalisée par le spectromètre de masse est en mode reniflage. Comme pour la mesure de perméabilité à l'oxygène, le système utilisé est composé de deux cellules : en amont, la cellule est balayée par un flux d'hélium qui traverse le film tandis qu'en aval, la cellule est balayée par un flux d'azote qui maintient une pression transmembranaire constante et induit ainsi un delta de pression nu et véhicule l'hélium ayant traversé le film vers la cellule de mesure. Des joints toriques assurent l'étanchéité du système. Les analyses ont été au minimum dupliquées. La valeur de perméabilité est exprimée en fonction du débit volumique Q (mbar.L.s^{-1}) donnée par le spectromètre de masse, de la différence de pression entre les compartiments amont (p_1) et aval (p_2), de l'épaisseur l (m) et de la surface de film (S = 23,7.10^{-4} m²) :

$$P = \frac{Q \times l}{S \times (p_2 - p_1)} \qquad \text{Équation 2.9}$$

Le delta de pression étant de 1 bar, la valeur de perméabilité est calculée grâce à la relation ci-dessous :

$$P = \frac{Q \times l}{S} \qquad \text{Équation 2.10}$$

La valeur de perméabilité, mesurée à l'équilibre comme pour l'oxygène, ainsi obtenue est exprimée en m^3.m.m^{-2}.s^{-1}.Pa^{-1}.
La mesure du coefficient de diffusion (D) et de solubilité (S) n'est pas possible compte tenu des « time lag » très courts.

2.2.4.3.Analyse thermique par MT-DSC

Les analyses thermiques ont été faites à l'aide d'une DSC (TA DSC Q1000). L'azote a été utilisé comme gaz de purge (50 ml/min). Les échantillons utilisés pour faire les analyses pesés autour de 5-10 mg, placés d'une façon à avoir le meilleur contact thermique possible dans les creusets d'aluminium hermétiques Tzero. La calibration en température a été effectuée en utilisant des valeurs standard d'indium et la capacité calorifique spécifique pour chaque échantillon a été mesurée en utilisant le saphir comme référence.

2.2.4.3.1. Protocoles expérimentaux

La quantité de fraction amorphe rigide (Xra), fraction amorphe mobile (Xma), taux de cristallinité (Xc) et la longueur de coopérativité à la transition vitreuse ont été étudiés par calorimétrie différentielle à balayage à modulation de température (MT-DSC). Deux calibrations ont été faites : une en mode heat-only (amplitude d'oscillation de 0.318°C, période d'oscillation de 60 s et vitesse de chauffe de 2°C min^{-1} de -20°C à 200°C et amplitude d'oscillation de 0.318°C, la période d'oscillation de 60 s et la vitesse de chauffe de 2°C min^{-1} de 20°C à 220°C) et une autre calibration en mode heat-cool (l'amplitude d'oscillation de 2,5°C, période d'oscillation de 100 s et vitesse de chauffage de 1°C min^{-1} de -20°C à 70°C et l'amplitude d'oscillation de 3°C, la période d'oscillation de 120 s et la vitesse de chauffage de 1°C min^{-1} de -20°C à 100°C), procédures décrites par Saiter et al. [3].

Le mode « heat-cool » consiste à chauffer l'échantillon tout en modulant la température avec une alternance de vitesses de chauffage instantanées positives et négatives. Chaque modulation inclut donc un refroidissement ponctuel. Ce mode de chauffage est recommandé pour une mesure de la transition vitreuse [4].
En revanche, lorsque nous souhaitons analyser des événements thermiques tels que la fusion de polymères semi-cristallins, il est nécessaire d'éviter tout refroidissement dans la période de modulation afin d'éviter la recristallisation [5]. Pour pallier ce problème, il est possible d'effectuer des analyses en mode « heat-only », pour lequel la vitesse de chauffage instantanée ne descend jamais sous zéro. Ce mode est recommandé lorsque l'on souhaite analyser les phénomènes de cristallisation et de fusion.

2.2.4.3.2. Quantification des phases

Le taux de phase amorphe qui relaxe au passage de la transition vitreuse, nommé aussi taux de phase amorphe mobile et noté X_{am}, est calculé en utilisant le signal du flux de chaleur moyen comme présenté en *Figure 2.8*, et en utilisant l'Equation 2.11 et l'Equation 2.12.

$$\Delta C_p = \frac{\Delta HF}{m \cdot q^+} \qquad \text{Équation 2.11}$$

où ΔHF est la différence de flux de chaleur caractéristique du passage de la transition vitreuse, ΔC_p le saut de chaleur spécifique à pression constante, m la masse de l'échantillon et q+ la vitesse de chauffage. Le saut de C_p à T_g est proportionnel à la quantité de phase amorphe qui relaxe à T_g d'où :

$$X_{am} = \frac{\Delta C_p}{\Delta C_p^0} \qquad \text{Équation 2.12}$$

où ΔC_p^0 est le saut de chaleur spécifique à pression constante pour un polymère 100% amorphe.

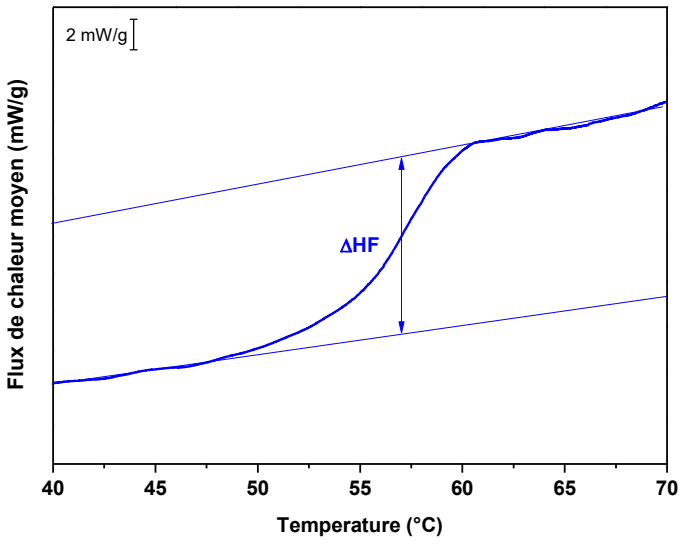

Figure 2.8. Flux de chaleur moyen d'un PLA 4042D cristallisé à 85°C pendant 60 min au passage de la transition vitreuse.

Le taux de cristallinité (X_c) de nos matériaux a été calculé comme indiqué sur la *Figure 2.9*, d'après l'Equation 2.13 [6]

$$X_c = \frac{\Delta H_f - \sum \Delta H_c}{\Delta H_f^0} \qquad \text{Équation 2.13}$$

avec

ΔH_f l'enthalpie de fusion du matériau, $\Sigma\Delta H_c$ la somme des enthalpies des pics exothermiques, et en admettant que l'enthalpie de fusion d'un PLA 100% cristallin ($\Delta H_f°$) est de 93 J g^{-1} [7].

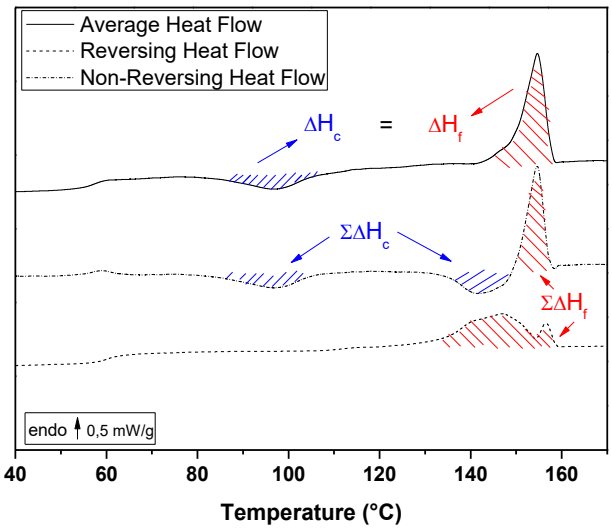

Figure 2.9. Exemple de calcul du taux de cristallinité sur un PLA.

Et donc, le taux de phase amorphe rigide (X_{ra}) est obtenu par l'Equation 2.14

$$X_{ma} + X_{ra} + X_c = 100\% \qquad \text{Équation 2.14}$$

Pour les échantillons multicouches PS/PLLA qui n'ont pas été cristallisés sous presse, la détermination du taux de cristallinité n'était pas possible par la méthode décrite avant (*Figure 2.9*) car, comme expliqué dans le paragraphe de cinétique de cristallisation, la cristallisation froide du PLLA se superpose à la Tg du PS. La détermination du caractère amorphe ou cristallin de ces échantillons s'est effectuée à partir de la quantification du saut de chaleur spécifique

(ΔC_p). Les courbes qui montrent la superposition de la Tg du PS avec le pic de cristallisation froide du PLLA ont été faites par MT-DSC en mode « heat only » (*Figure 2.10*), et les courbes utilisées pour la détermination précise du ΔC_p ont été réalisées par MT-DSC en mode « heat cool » (*Figure 2.11*).

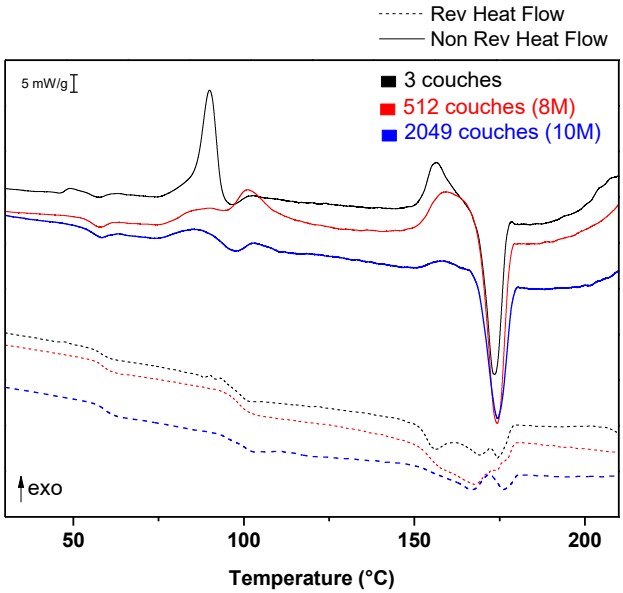

Figure 2.10. MT-DSC en mode « heat only » des échantillons PS/PLLA amorphes.

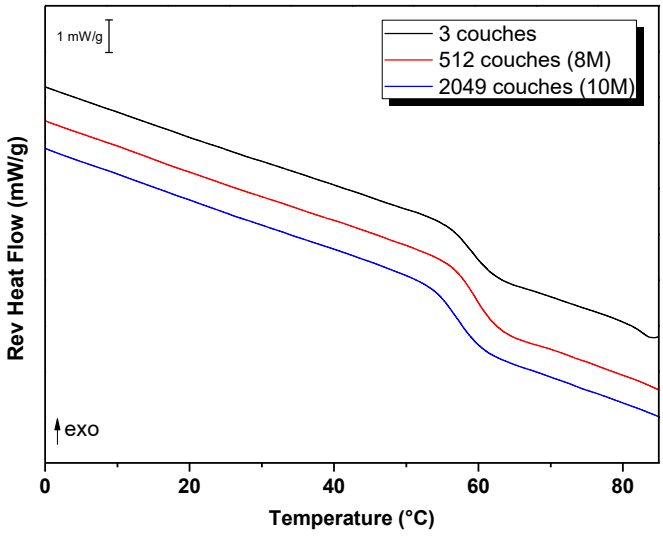

Figure 2.11. MT-DSC en mode « heat cool » des échantillons PS/PLLA amorphes.

Pour les échantillons multicouches PS/PLLA cristallisés sous presse, la cristallisation froide n'est pas présente (*Figure 2.12*), donc la détermination du taux de cristallinité peut être effectuée par MT-DSC en mode « heat only » en utilisant la méthode décrite dans la *Figure 2.9*.

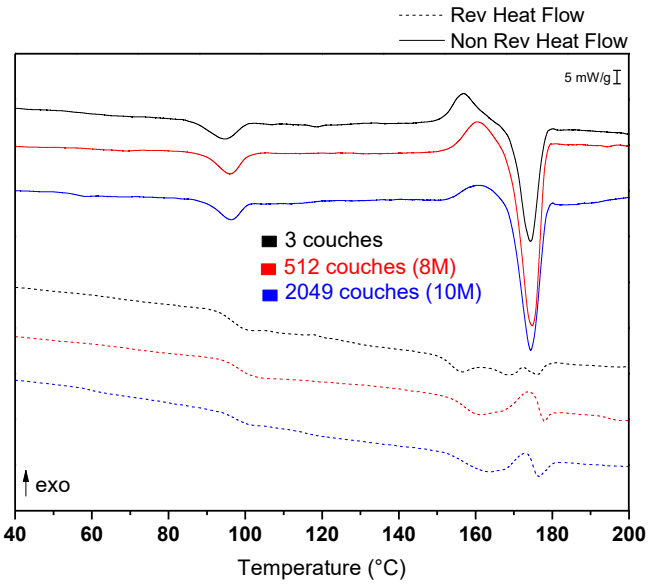

Figure 2.12. MT-DSC en mode « heat only » des échantillons PS/PLLA cristallisés.

2.2.4.3.3. Longueur de coopérativité

Le concept de Région de Réarrangement Coopérative (CRR) est défini comme étant le plus petit domaine amorphe où un réarrangement conformationnel peut se produire sans provoquer de réarrangements dans les régions adjacentes [8].

Cette approche fournit une image du temps de relaxation à la transition vitreuse qui est directement observable par des mesures colorimétriques [9]. Selon cette approche [10], le $\xi T\alpha^3$, volume de coopérativité à la température de transition vitreuse dynamique $T\alpha$, peut être estimé à partir de l'Equation 2.15 :

$$\xi_{T\alpha}^3 = \frac{\left(1/C_p\right)_{verre} - \left(1/C_p\right)_{Liquide}}{\rho\left(\delta T\right)^2} k_B T_\alpha^2 \qquad \text{Équation 2.15}$$

où k_B est la constante de Boltzmann ($1{,}38.10^{-23}$ J K^{-1}), δT la fluctuation moyenne de température dans une CRR, ρ la masse volumique de la phase amorphe du PLA (1250 kg m^{-3}),

$\Delta C_{p_{verre}}$ et $\Delta C_{p_{liquide}}$ respectivement les capacités thermiques massiques à pression constante du verre et du liquide.

Un exemple d'un protocole pour obtenir tous les paramètres nécessaires pour le calcul du volume de coopérativité ξT_α^3 à la température de transition vitreuse dynamique Tα est donné sur la *Figure 2.13*.

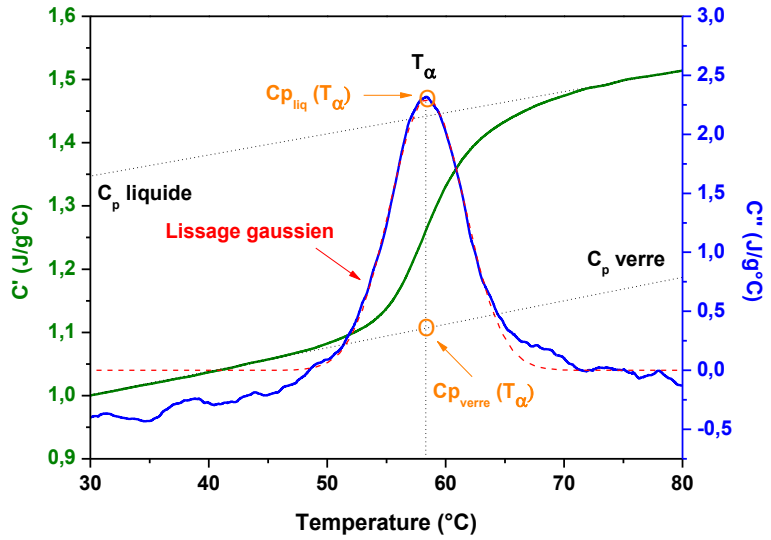

Figure 2.13. Composantes en phase C' (en ligne continue verte) et hors phase C'' (en ligne continue bleue) du module de la capacité thermique complexe C* obtenues sur un PLA 4042D cristallisé à 85°C pendant 60 minutes. Les lignes pointillés rouges correspondent au lissage gaussien du pic du C''. Les droites du verre et du liquide sur le signal du C' sont indiquées en pointillés noirs. La prolongation de ces droites jusqu'au maximum du pic du C'' représentant Tα permet d'obtenir les paramètres $Cp_{verreT\alpha}$ et $Cp_{liquideT\alpha}$.

2.2.4.4.Diffractions des rayons x

La structure cristalline des échantillons a été étudiée par diffraction des rayons X aux grands et petits angles (WAXS et SAXS) en utilisant la ligne Soleil du synchrotron et une ligne PANanalytical de laboratoire (UMET à Lille). Les paramètres de la ligne du synchrotron étaient : le faisceau incident, d'énergie 12 keV (1,03 Å), avait une dimension de 30 µm de

hauteur et 300 µm de large. La distance entre l'échantillon et la caméra est de 1555 mm pour les mesures SAXS et 555,5 mm pour les mesures WAXS.

Pour la PANanalytical, le faisceau produit à partir d'une source de radiation CuKa (λ=1,54Å) a été filtré à l'aide d'un filtre nickel. Les diffractrogrammes WAXS ont été enregistrés par une CDD camera (Photonic Science) en 2-D. Afin de déterminer la structure des échantillons, une analyse semi-quantitative a été réalisée en intégrant les profils azimutaux de 180° et en utilisant le logiciel FIT2D.

2.2.4.5.Recuit des films monocouches

Afin d'obtenir des échantillons ayant une microstructure définie [11], deux procédés de recuit ont été effectués sur des films de PLA préalablement conservés en dessiccateur pour éviter la reprise en humidité. Pour les recuits à partir de l'état vitreux, les films ont été placés entre deux feuilles de téflon dans un four à la température de recuit (85°C ou 130°C). Pour les recuits à partir de l'état fondu, les échantillons ont été pris en sandwich entre deux feuilles de Téflon et deux plaques d'acier inoxydable, le sandwich ensuite a été thermocompressé au-dessus de la température de fusion (210°C pendant 10 minutes) à 5 x 10^6 Pa à l'aide d'une thermopresse (Darragon, France) avant d'être placé dans un four à la température de recuit (85°C ou 130°C) le plus rapidement possible (*Figure 2.14*). La procédure de cristallisation isotherme dans le four a été choisie en raison de la contrainte pour produire de grands échantillons (diamètre = 10 cm) compatibles avec les mesures de perméabilité. Une fois le processus réalisé, le sandwich a été rapidement ouvert et les films ont été placés à la température ambiante sur une surface froide, puis ont été stockés à température ambiante dans des sacs hermétiques.

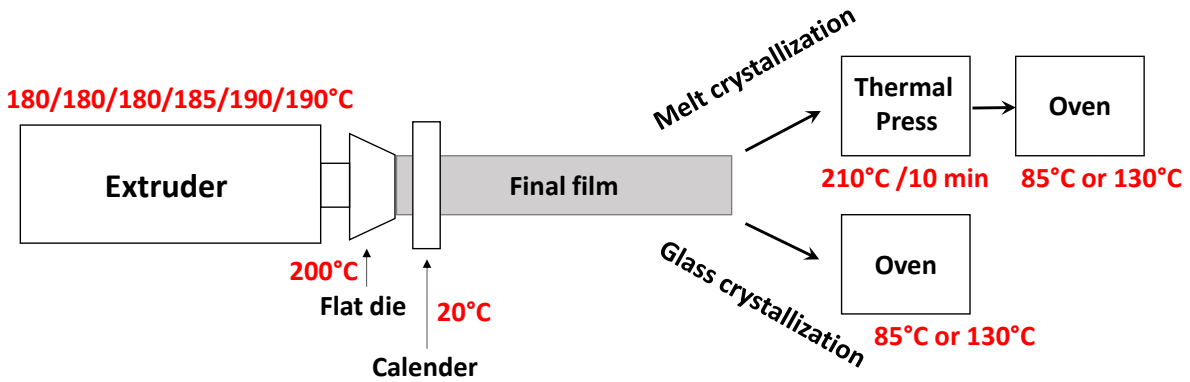

Figure 2.14. Représentation schématique de la préparation de l'échantillon comprenant des procédures d'extrusion et recuit.

2.2.4.5.1. Cinétique de cristallisation

La cinétique de cristallisation des films a été étudiée par calorimétrie différentielle à balayage classique dans une DSC Q100 (TA Instruments), équipée d'un Intracooler. Les calibrations en température et en énergie ont été réalisées à l'aide d'un étalon d'indium et de zinc et la calibration de la capacité thermique a été effectuée à l'aide d'un étalon de saphir. Le saphir est utilisé comme échantillon étalon car il ne subit pas de transition dans la gamme de température utilisée pour étudier la plupart des polymères. La capacité thermique du saphir en fonction de la température est très précisément connue [12]. Le gaz de purge est l'azote et son débit est de 50 mL min^{-1}. Les échantillons (5-8 mg, placés dans des creusets d'aluminium Tzero) ont été chauffés à une vitesse de chauffage constante de 10°C min^{-1} de 20 à 200°C.

2.2.4.6.Recuit des films multicouches

2.2.4.6.1. Recuit des films PS/PLLA

Les films PS/PLLA, découpés pour éviter les effets de bords (os de chien), ont été mis en sandwich entre deux feuilles de Téflon et deux plaques d'acier inoxydable. Ensuite le sandwich a été thermocompressé au-dessus de la température de transition vitreuse du PLLA (85°C) à 5 x 10^6 Pa à l'aide d'une thermopresse (Darragon, France). Les températures de recuit ont été choisies par rapport à la température de transition vitreuse du polymère confineur. Le PS ayant une Tg de 100°C, une température de recuit de 85°C a été choisie afin de préserver l'intégrité des couches et imposer un confinement fort (« hard confinement »). Le temps de recuit a fait l'objet d'une optimisation par DSC et WAXS.

2.2.4.6.1.1. Cinétique de cristallisation des films PS/PLLA

Pour pouvoir définir le temps de recuit pour lequel le PLLA est totalement cristallisé, nous avons d'abord fait une isotherme à partir du film multicouche de PLLA avec une DSC en mode

classique (chauffage à 10°C/min) (*Figure 2.15*). Cependant, avec cette méthode, aucun pic de cristallisation n'a été observé sur une durée d'isotherme de plus de 1 heure.

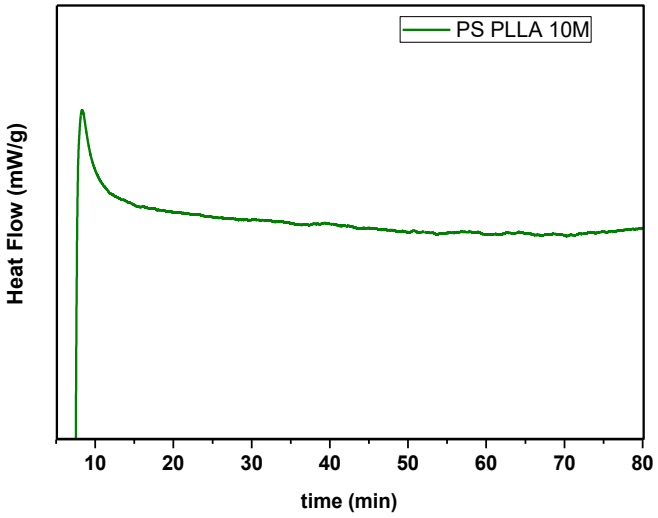

Figure 2.15. Isotherme d'un échantillon amorphe PS/PLLA avec 2049 couches.

Nous avons cristallisé les échantillons *in situ* dans la DSC à différents temps de cristallisation et nous avons ensuite fait une analyse thermique en MT-DSC pour pouvoir comparer leur saut de chaleur spécifique (ΔC_p). Le principe de la MT-DSC est de séparer la contribution dépendant de la température de celle dépendant de la vitesse de changement de la température dans la réponse de l'échantillon. Des évènements thermiques peuvent se superposer lors d'une analyse en DSC classique rendant celle-ci difficile à interpréter. La MT-DSC peut permettre de pallier ces difficultés. Cette méthode a été choisie car dans le cas où les échantillons ne sont pas cristallisés à leur maximum possible, la cristallisation froide du PLLA se superpose à la transition vitreuse du PS, empêchant le calcul du taux de cristallinité. Un exemple de cette courbe est donné en *Figure 2.16*.

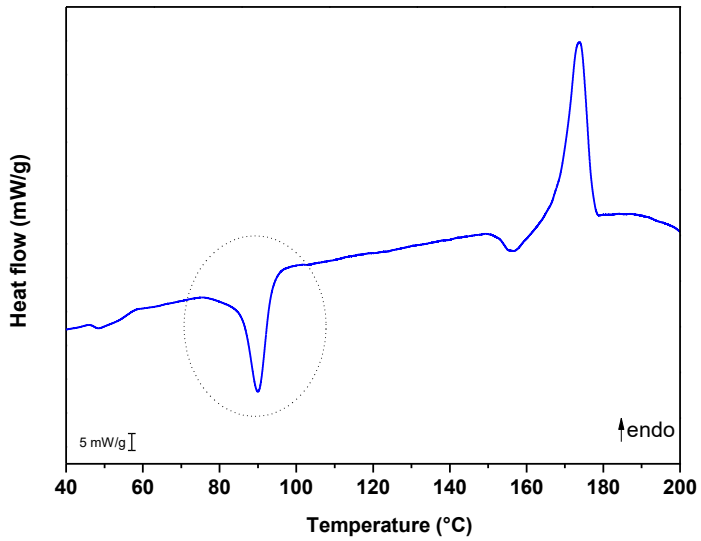

Figure 2.16. Analyse en MT-DSC d'un échantillon 3 couches PLLA/PS amorphe. La zone entourée est la superposition de la température de transition vitreuse du PS avec la cristallisation froide du PLLA.

Des analyses de la cinétique de cristallisation isotherme ont été faites à l'aide de diffractions de rayons X. Les échantillons ont été cristallisés *in situ* dans une platine chauffante disposé dans un dispositif de diffraction de rayons X (*Figure 2.17*). On suit alors l'évolution de la cristallinité relative en fonction du temps, et on observe que, à 3 heures de recuit, le PLLA est complètement cristallisé sauf pour l'échantillon 10M. Nous avons choisi 3 heures (180 minutes) pour faire le recuit des échantillons. En *Figure 2.17* on observe que, à 3 heures de recuit, l'échantillon 10M n'avait pas encore atteint la cristallinité maximale. En revanche, sur les analyses en MT-DSC des échantillons recuits pendant 180 minutes, aucun pic de cristallisation froide n'a été observé, nous permettant de conclure que cet échantillon était cristallisé au maximum.

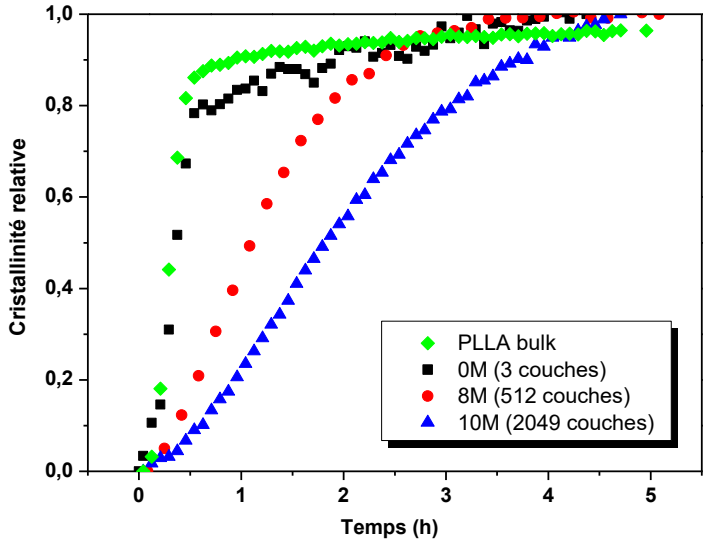

Figure 2.17. Cristallisation in situ des échantillons PS/PLLA (Diffractions de rayons x)

2.2.4.6.2. Recuit des films PC/PLLA

Les films PC/PLLA ont été recuits en utilisant la même technique que celle utilisée pour les films PS/PLLA. Cependant nous avons choisi deux températures, 85°C et 120°C étant donnée que la Tg du PC est de 150°C. Nous avons ainsi pu étudier les différentes formes cristallines obtenues à partir de la cristallisation à basse et haute température étant donné l'importance de ce paramètre comme montré dans la publication de Guinault et al., 2012 [11]. Le temps de cristallisation est déterminé par la méthode utilisée pour le PS et les résultats sont montrés dans la suite.

2.2.4.6.2.1.Cinétique de cristallisation des films PC/PLLA

Des analyses de la cinétique de cristallisation isotherme ont aussi été faites à l'aide des diffractions de rayons X pour les échantillons PC/PLLA (*Figure 2.18*). Comme pour le PS, le temps de 3 heures a été choisi pour faire les recuits.

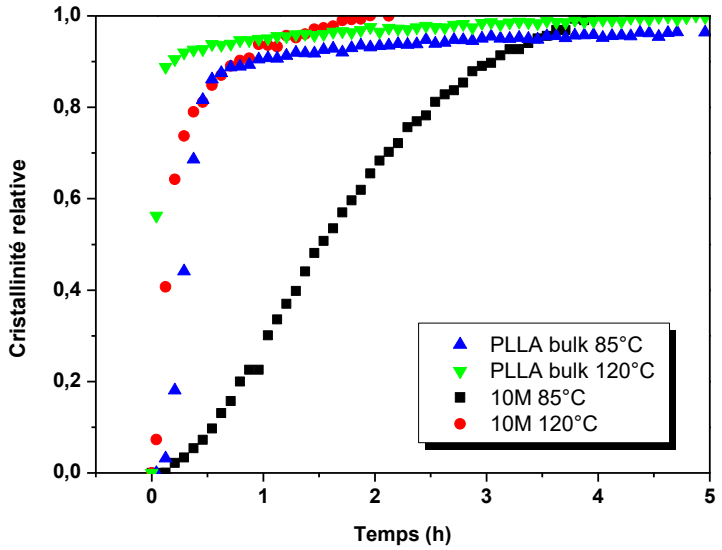

Figure 2.18. Cristallisation in situ des échantillons PC/PLLA (Diffractions de rayons X)

2.2.4.7.Observation des structures cristallines

Les échantillons ont été observés en utilisant un microscope optique à transmission (Nachet, France) sous lumière polarisée en utilisant une caméra (Leica DFC 320). Les échantillons ont été préparés à l'aide d'un microtome (Leica, France) (*Figure 2.19*) pour produire des échantillons minces de 5 à 10 µm d'épaisseur. Ils sont, après découpes, placés entre 2 lames de verre et collés avec de l'essence de cèdre qui a la particularité d'être neutre vis-à-vis de la polarisation.

Figure 2.19. Microtome Leica, France.

2.2.4.8.Digestion enzymatique et Microscopie électronique à balayage

Une méthode utilisée pour observer plus finement les structures semi-cristallines consiste à réaliser une digestion enzymatique lors de laquelle les enzymes ne vont attaquer que la partie amorphe des échantillons (à condition que les conditions de digestion soient optimisées). La digestion enzymatique a été réalisée avec des échantillons immergés dans une solution de Tris (0,05 M) contenant 800 μg/ml de protéinase K pendant 5 heures à 37°C. Les échantillons ont ensuite été rincés avec de l'eau distillée et séchés à la température ambiante.
Apres digestion enzymatique, les échantillons sont recouverts d'une pellicule d'or afin de les métalliser à l'aide de l'appareil à dépôt sous vide Edward S50B Sputter Coater. Ensuite les échantillons sont introduits dans le MEB (EVO MA 10 Zeiss à électrode de tungstène) sous vide afin d'être observés. Nous avons observé préférentiellement les échantillons sur leur tranche pour éviter les effets de peaux.

2.2.4.9.Observation des couches

Les échantillons multinanocouches ont été observés par microscopie à force atomique (AFM). Les images AFM ont été obtenues en mode tapping à l'aide d'un microscope commandé par un contrôleur Nanoscope V (Veeco), fonctionnant sous atmosphère ambiante. La pointe (silicium, ressort constant de 40 N / m, la fréquence d'oscillation environ 300 kHz) a été fournie par BudgetSensors. Le rayon de courbure de la pointe est inférieur à 10 nm. Les images de phase, de hauteur et d'amplitude ont été acquises simultanément. Les échantillons ont été découpés à partir du centre des films extrudés et sectionnés perpendiculairement à leur surface avec un ultramicrotome UltrotomeV 2088 (LKB) à une vitesse de coupe de 1mm/s. Les images ont été enregistrées en pleine résolution (4096 × 4096 pixels), avec une vitesse de balayage de 0,9 Hz. Les images AFM ont été prises à partir de la direction d'extrusion. Le signal de phase a été décrit comme étant une mesure de la dissipation d'énergie impliquée dans le contact entre la pointe et l'échantillon, qui dépend d'un certain nombre de facteurs, y compris la viscoélasticité, l'adhérence et la topographie. Etant donné que ces facteurs sont différents entre les polymères que nous avons étudiés, l'épaisseur des couches a été mesurée à partir des images de phase, qui ont révélé le plus clairement la structure des couches des films.

2.2.4.9.1. Analyse des images AFM

2.2.4.9.1.1. Mesure des épaisseurs des couches et vérification de la proportion de chaque polymère dans les films

Sur le film PS/PLLA 8M (composé de 513 couches au total avec 256 de PLLA), dix images réparties sur la tranche du film comportant chacune 40 couches ont été analysées. On en analyse 12 pour l'échantillon PS/PLLA à 10 multiplicateurs de couches, qui comporte 2049 couches au total dont 1024 de PLLA. Le nombre d'image acquise et analysée a été choisi en utilisant l'Equation 2.16 [13].

$$L = \left(\frac{4K}{\in_{rel}^2 \overline{Z^2 n}} \right)^{\frac{1}{\gamma}} \qquad \text{Équation 2.16}$$

Où L est la taille d'image, $\in_{rel}$ est le pourcentage d'erreur, Z est l'épaisseur théorique du polymère, n est le nombre d'image, γ et K sont des constantes.

Les images de phase obtenues révèlent clairement la structure multicouche des films. Les variations en hauteur de la pointe correspondent au relief de l'échantillon. Elles servent donc à la construction de l'image topographique.

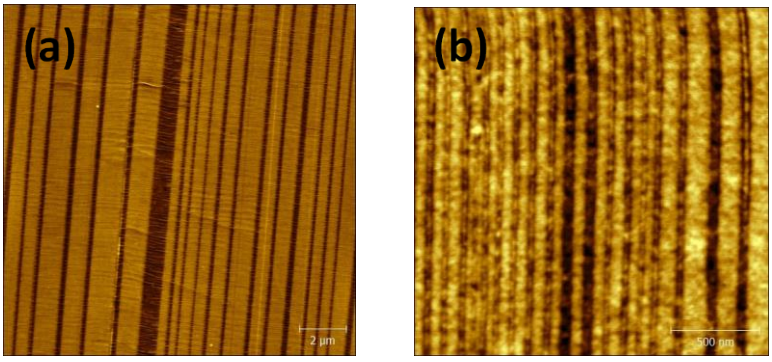

Figure 2.20. (a) Image AFM de la hauteur PS/PLLA 8M (b) Image AFM de la phase PS/PLLA 10M.

On observe sur la *Figure 2.20* les couches de PLLA (25%) en brun et celles du PS (75%) en dorée. Les lignes horizontales représentent les traces de compressions causées par l'ultra-

microtome et les traits non parallèles aux couches de PLLA correspondent aux traits de coupe causés par le couteau de diamant.

Les épaisseurs des couches ont été mesurées à l'aide du logiciel Gwiddion. Grâce au logiciel, un profil de phase peut être extrait montrant la variation du degré de phase, comme le montre la *Figure 2.21*. Dans le profil de phase, chaque couche est caractérisée par son pic et par convention, on place deux curseurs à mi-hauteur de chaque pic. L'intervalle entre les deux curseurs nous donne la valeur de l'épaisseur de la couche de grandeur nanométrique. Ces mesures incluent plusieurs sources d'erreurs telles que la pointe de l'AFM ou encore la position des curseurs de mesure, entre autres.

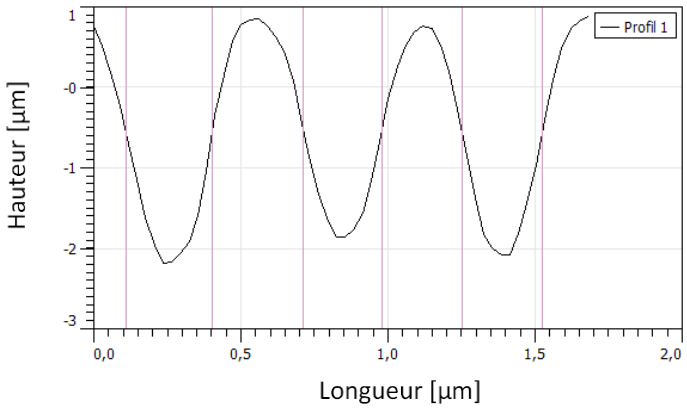

Figure 2.21. Exemple d'un profil de phase sur Gwyddion.

A l'aide d'un logiciel d'analyse d'image appelé imageJ, nous avons pu vérifier les proportions de chacun des polymères qui, rappelons-le, doivent être de 25% pour le PLLA et 75% pour le PS. Pour cela, nous avons binarisé l'image (*Figure 2.22*) ainsi, le logiciel nous mesure automatiquement la quantité de partie blanche et de partie noire.

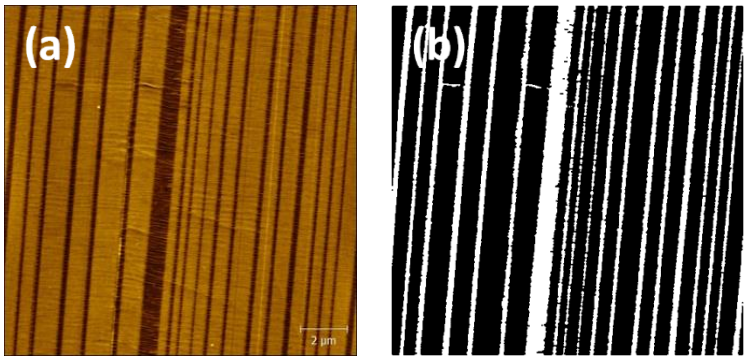

Figure 2.22. (a) Image AFM utilisé pour l'étude des proportions (b) l'image binaire pour le calcul des proportions

2.2.4.10. Caractérisation du vieillissement physique des films multicouches PLLA/PS

Les expériences ont été effectuées en utilisant un calorimètre Flash DSC (Mettler-Toledo). Les échantillons ont été placés sur les capteurs MultiSTAR UFS1 MEMS (*Figure 2.23*). L'aire disponible pour placer les échantillons est de 180 x 180 μm. Un bloc de refroidissement Intracooler Huber TC100 a été utilisé pour refroidir les échantillons jusqu'à 178 K et exploiter des vitesses de refroidissement élevées. Le gaz de purge utilisé était l'azote pour éviter la condensation de l'eau provenant de l'environnement. Un flux de 20 mL min^{-1} a été choisi pour optimiser la performance de la machine [14].

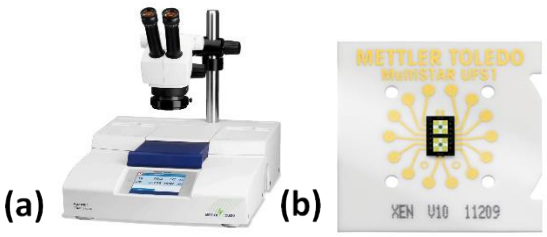

Figure 2.23. (a) Flash DSC (Mettler-Toledo) (b) Capteur MultiSTAR UFS1.

Le programme de température utilisé pour faire le vieillissement physique du PLLA à l'aide de la Flash DSC est montré dans la *Figure 2.24*. La vitesse de chauffe utilisée c'était 1000 K s^{-1}. La température de vieillissement a été estimée 15°C en-dessous de la température de transition vitreuse estimée au refroidissement des échantillons en Flash DSC.

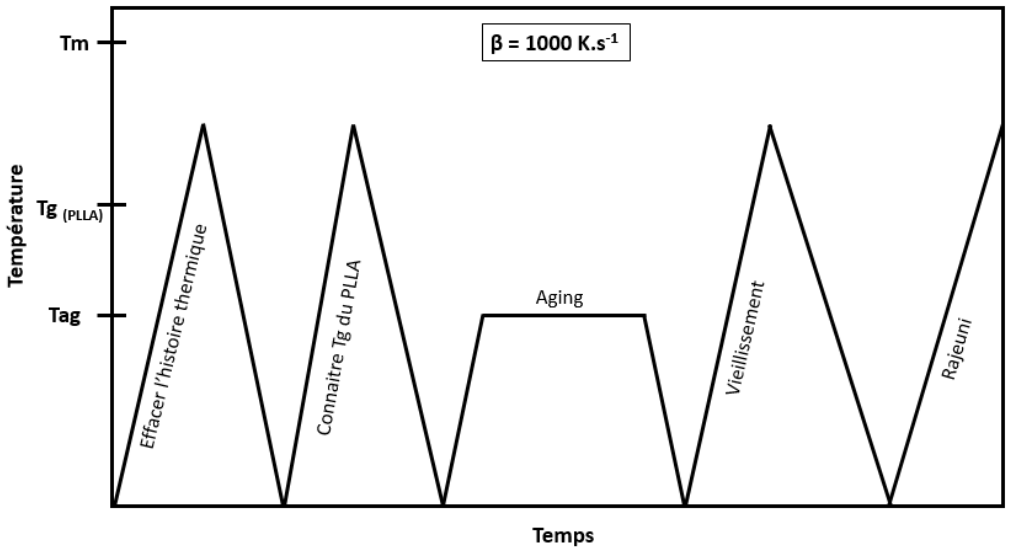

Figure 2.24. Programme de température pour le vieillissement physique du PLLA en Flash DSC.

2.3. Bibliographie

[1] F. Peurton, Nanocomposites à matrices thermoplastique et renforts plaquettaires : relation élaboration-structure-propriétés, 2008.

[2] M. Ponting, A. Hiltner, E. Baer, Polymer nanostructures by forced assembly: Process, structure, and properties, Macromol. Symp. 294 (2010) 19–32. doi:10.1002/masy.201050803.

[3] A. Saiter, N. Delpouve, E. Dargent, W. Oberhauser, L. Conzatti, F. Cicogna, E. Passaglia, Probing the chain segment mobility at the interface of semi-crystalline polylactide/clay nanocomposites, Eur. Polym. J. 78 (2016) 274–289. doi:10.1016/j.eurpolymj.2016.03.040.

[4] J.M. Hutchinson, Studying the glass transition by DSC and TMDSC, J. Therm. Anal. Calorim. 72 (2003) 619–629. doi:10.1023/A:1024542103314.

[5] D.J. Reading, M.; Hourston, Modulated temperature differential scanning calorimetry: theoretical and practical applications in polymer characterisation, Springer, 2006.

[6] H. Tsuji, Y. Ikada, Blends of isotactic and atactic poly(lactide)s: 2. Molecular-weight effects of atactic component on crystallization and morphology of equimolar blends from the melt, Polymer. 37 (1996) 595–602. doi:10.1016/0032-3861(96)83146-6.

[7] B.E.W. Fischer, H.J. Sterzel, G. Wegner, Investigation of the structure of solution grown crystals of lactide copolymers by means of chemical reactions by means of chemical reactions, Kolloid-Z. U. Z. Polym. 251 (1973) 980–990.

[8] G. Adam, J.H. Gibbs, On the Temperature Dependence of Cooperative Relaxation Properties in Glass-Forming Liquids, J. Chem. Phys. 43 (1965) 139–146. doi:10.1063/1.1696442.

[9] E. Hempel, G. Hempel, a. Hensel, C. Schick, E. Donth, Characteristic Length of Dynamic Glass Transition near T g for a Wide Assortment of Glass-Forming Substances, J. Phys. Chem. B. 104 (2000) 2460–2466. doi:10.1021/jp991153f.

[10] E. Donth, The size of cooperatively rearranging regions at the glass transition, J. Non. Cryst. Solids. 53 (1982) 325–330. doi:10.1016/0022-3093(82)90089-8.

[11] A. Guinault, C. Sollogoub, V. Ducruet, S. Domenek, Impact of crystallinity of poly(lactide) on helium and oxygen barrier properties, Eur. Polym. J. 48 (2012) 779–788. doi:10.1016/j.eurpolymj.2012.01.014.

[12] S.M. Sarge, E. Gmelin, G.W.H. Höhne, H.K. Cammenga, W. Hemminger, W. Eysel, The caloric calibration of scanning calorimeters, Thermochim. Acta. 247 (1994) 129–168. doi:10.1016/0040-6031(94)80118-5.

[13] a Bironeau, J. Dirrenberger, C. Sollogoub, G. Miquelard-Garnier, S. Roland, Evaluation of morphologically representative sample sizes for nanolayered polymer blends, J. Microsc. 00 (2016) 1–11. doi:10.1111/jmi.12415.

[14] G. Vanden Poel, D. Istrate, A. Magon, V. Mathot, Performance and calibration of the Flash DSC 1, a new, MEMS-based fast scanning calorimeter, J. Therm. Anal. Calorim. 110 (2012) 1533–1546. doi:10.1007/s10973-012-2722-7.

Chapter 3 – Multi-scale analysis of the impact of polylactide morphology on gas barrier properties

Des films de polylactide semi-cristallins (PLA) avec une morphologie contrôlée ont été produits par cristallisation thermique pour optimiser les propriétés barrière à l'oxygène. La morphologie cristalline du PLA à l'échelle de la lamelle et sphérolitique a été étudiée ainsi que la dynamique de la phase amorphe mobile. La morphologie cristalline a un impact négligeable sur le coefficient de diffusion à l'oxygène. L'apparition d'une fraction amorphe rigide (RAF) dans la phase amorphe en raison de son découplage insuffisant avec la phase cristalline a fourni une voie accélérée pour la diffusion. Pour conclure, pour atteindre des propriétés barrière optimales, le PLA semi-cristallin doit être pré-nucléé et cristallisé rapidement à partir du verre dans la forme α-polymorphe dans le but d'atteindre un degré de cristallinité élevé et un découplage total de la phase amorphe et cristalline. Ces recommandations peuvent profiter à l'industrie pour l'optimisation des traitements de recuit du PLA.

3. Multi-scale analysis of the impact of polylactide morphology on gas barrier properties

Samira Fernandes Nassar[a], Alain Guinault[b], Nicolas Delpouve[c], Véronique Divry[a], Violette Ducruet[a], Cyrille Sollogoub[b], Sandra Domenek[a,*]

[a]UMR Ingénierie Procédés Aliments, AgroParisTech, INRA, Université Paris-Saclay, 1 avenue des Olympiades, F-91300 Massy, France

[b]PIMM, Arts et Métiers ParisTech/CNRS/CNAM, 151 Bd de l'Hôpital, F-75013 Paris Cedex, France

[c]Normandie Univ, UNIROUEN, LECAP, 76000 Rouen, France

Corresponding author: Sandra Domenek, UMR Ingénierie Procédés Aliments, 1 avenue des Olympiades, F-91300 Massy, France

email: sandra.domenek@agroparistech.fr

3.1.Abstract

Semicrystalline polylactide (PLA) films with controlled morphology were produced by thermal crystallization to optimize the oxygen barrier properties. The crystalline morphology of PLA at the scales of the lamella and the spherulite was investigated and the mobile amorphous phase dynamics were studied. The crystalline morphology had a negligible impact on the oxygen diffusion coefficient. The occurrence of a rigid amorphous fraction (RAF) in the amorphous phase due to its insufficient decoupling from the crystalline phase provided an accelerated pathway for diffusion, though. As a conclusion, for reaching optimal barrier properties, semicrystalline PLA should be pre-nucleated and rapidly crystallized from the glass in the α-polymorph in the aim to reach a high crystallinity degree and decoupling of the amorphous and the crystalline phase. These recommendations can benefit to industry for the optimization of PLA annealing treatments.

Key words: PLA, poly(lactic acid), crystallization, amorphous phase, permeability, rigid amorphous fraction, cooperative rearranging region, PLA polymorphism

3.2.Introduction

Poly(lactide), PLA, is today one of the most produced bioplastics. Although there is a growing interest for the use of PLA in durable applications (textile, automotive, printing), rigid and flexible packaging is still its major use. In particular, in short-lived packaging applications, the biodegradable and biobased character of PLA is of environmental advantage. The low gas barrier properties of PLA are, however, a major hurdle to broaden the applications spectrum in this field. For example, PLA is today suitable to pack fresh fruits and vegetables, cheeses or oil containing food but not for contents with long shelf-life, such as infant foods or prepared meals. For that, the oxygen permeability of PLA needs to be decreased by one order of magnitude in the aim of approaching the one of poly(ethylene terephthalate), PET [1,2].

PLA is a semicrystalline polymer, and there has been and is a great research effort for increasing its crystallization kinetics and tailoring its crystallization to specific applications [3]. Crystallization is a means for increasing the gas barrier properties as it acts theoretically on both components of the permeability. Crystallites are excluded volume for the permeants, they bring thus tortuosity to their pathway, which decreases the diffusion coefficient. Furthermore, penetrants cannot sorb into crystalline structures, which decreases the solubility coefficient [4]. From an applied point of view, property improvement by crystallization is advantageous for applications such as packaging, as the process technology is already mastered and it does not need sophisticated addition of processing aids.

However, a number of results in the literature show that the structure/function relationship between PLA morphology and gas barrier properties is not completely understood yet [5–9]. In some cases, constancy or even an increase in the oxygen permeability with an increasing crystallinity degree of PLA was found [6,9]. A similar result was also observed in the case of the water vapour permeability of crystallized PLA [10,11]. Kanehashi et al. [12] did an impressive review on approximately 300 studies concerning the relationship between gas permeability and crystallinity of various polymers. They demonstrated, that the diffusion coefficient and the permeability were constant at low degrees of crystallization, regardless the polymer. Drieskens et al. [13] and Guinault et al. [14] analysed more precisely the change of the oxygen barrier properties upon the crystallization of PLA. Both authors showed the decrease of the PLA oxygen permeability at high crystallinity degrees (approximately > 30 %). However, there was as difference in behaviour occasioned by the crystalline polymorph of PLA [14]. In case of crystallization in α'-form (also named δ-form by some authors), which is a structurally

less ordered crystalline form of PLA [15] obtained at crystallization temperatures lower than 100 °C [16,17], no reduction of the gas permeability was be obtained, even if the crystallization was carried out up to the maximum crystallinity degree [14]. When the PLA crystallization was carried out at high temperatures (> 100 °C) to obtain the α-polymorph, the oxygen permeability could be decreased by a factor of approximately 4 [13,14]. Much better results were obtained, when the crystalline morphology was designed by arrangements of parallel lamellae perpendicular to the permeation direction. This was achieved with "shish-kebab like" structures by Bai et al [18].

The transport properties in PLA are also strongly linked to the nature of the amorphous phase, which includes its content, its dynamics, and its degree of coupling with the crystalline phase. The morphology of semicrystalline PLA and its amorphous phase dynamics were described with the help of the three-phase model, including the crystalline phase, and two fractions of the amorphous phase, *i.e.* the mobile amorphous fraction (MAF) and the rigid amorphous fraction (RAF) [19–22]. The RAF is the intermediate phase connecting the crystalline phase to the mobile amorphous fraction (MAF) [23]. The RAF constitutes a dedensified amorphous phase [24] because of geometrical constraints preventing structure relaxation. Guinault et al. [14] showed that the formation of RAF was favoured when PLA was crystallized from the glassy state in α'-form. They suggested that it constituted therefore an accelerated pathway for transport of penetrants around crystalline lamellae, counteracting the tortuosity increase occasioned by the same lamellae. Delpouve et al. [25] worked on the cooperativity length and the fragility index of semicrystalline bi-axially stretched and post-stretching annealed PLA samples. They showed that the amorphous phase of the annealed samples had accelerated segmental motions, which would be beneficial for the gas permeability and not for the barrier properties.

The objective of this study is to optimize the crystallization conditions of PLA to get better oxygen barrier properties by investigating the impact of the crystalline morphology, structure and space filling as well as the amorphous phase dynamics. For that, a set of samples with different size of spherulites and PLA polymorph was prepared. The experimental conditions were chosen to either favour the formation of RAF or not. The amorphous phase dynamics were analysed by modulated-temperature differential scanning calorimetry (MT-DSC) and the crystalline structure by X-ray diffraction and electron microscopy. These data were linked to the oxygen permeability parameters.

3.3.Material and Methods

3.3.1. Sample preparation

Poly(lactide) 4042D was purchased from NatureWorks LLC (USA) and has a percentage of D-lactide acid units of 4.3%. The PLA pellets were dried under low pressure (10^4 Pa) for 4 h at 90°C and subsequently extruded by single screw extrusion with a 30 mm diameter extruder (with a 33 L/D (length on diameter) barrel) and a three sections screw without mixing elements. The extruder screw speed was set to 40 rpm. The temperature profile of the barrel for the six zones, as presented in the *Figure 3.1*, was 180-180-180-185-190-190°C. The temperature of the mixer device (4 Sulzer SMX®) and the die was 200°C. A flat die of 200 mm width and a chill roll equipment were used to manufacture films of approximately 300 µm thickness. The roll temperature was fixed at 20°C to cool down the films. In order to obtain samples with defined microstructure, two procedures of annealing were performed on PLA films. For annealing from the glassy state, the films were sandwiched between two Teflon sheets and two stainless steel plates and placed directly in an oven at the temperature of annealing (85°C or 130°C). They were pressed by a weight of 10 kg. For annealing from the melted state, the samples were sandwiched between two Teflon sheets and two stainless steel plates then pressed above the fusion temperature (210°C during 10 minutes) at 5 x 10^6 Pa with the help of a thermal press (Darragon, France). After that time, they were taken out quickly and placed in the oven at the temperature of annealing (85°C or 130°C), where they were maintained under a weight of 10 kg. The procedure of isothermal crystallization in the oven was chosen because of the constraint to produce large samples (diameter = 10 cm) compatible with permeability measurements. After the process, the sandwich was quickly opened and the films were quenched to room temperature at a cold surface. Then they were stored at room temperature. Samples studied in this work were chosen by visual inspection, i.e. only samples that appeared to be homogeneous across the surface were selected and analysed.

Sample codes contain the way of crystallizing from the melt, coded with “M”, and from the glass, coded with “G”, followed by a number denoting the annealing temperature, then a number indicating the duration of annealing and a number giving the crystallinity degree. For example “G85_1200_39” means crystallized from the glass at 85 °C during 1200 minutes and having a crystallinity degree of 39%.

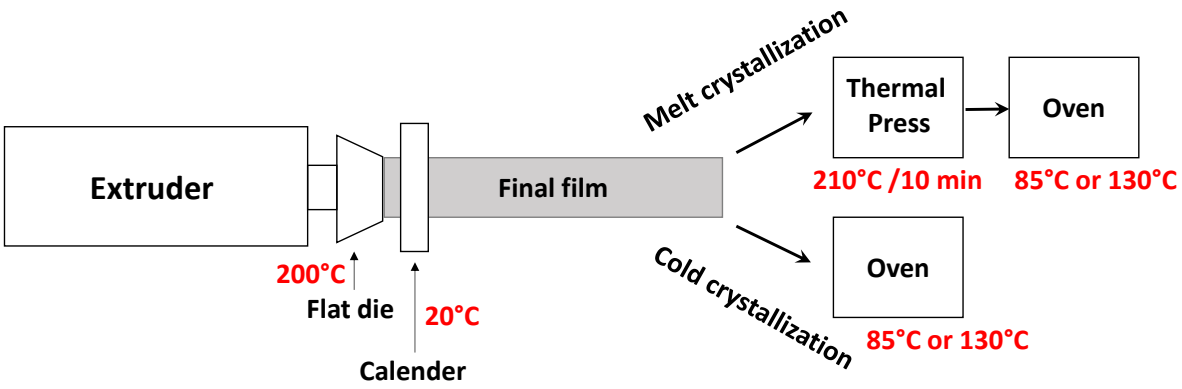

Figure 3.1. Schematic representation of the sample preparation process including the extrusion and the annealing procedure.

3.3.2. Sample characterization

To choose representative samples for investigating the barrier properties in relation with the microstructure, the crystallization kinetics in the oven were recorded for each annealing treatment. The thermal features of the samples were analysed by means of differential scanning calorimetry in a Q100 DSC (TA Instruments) apparatus, equipped with an intracooler. The temperature calibration was performed with the help of indium and zinc standards and the calibration of the heat capacity was done with the help of a sapphire standard. The purge gas flow was 50 $mL \cdot min^{-1}$ N_2. The samples (5-8 mg, loaded in aluminium Tzero crucibles) were heated at a constant heating rate of $10°C \cdot min^{-1}$ from 20 to 200°C.

The crystalline morphology of the films was investigated with microscopy techniques. The samples were observed by using an optical transmission microscope (Nachet, France) under polarized light. The samples were prepared using a microtome (Leica, France) to yield thin samples of 5-10 µm thickness. Enzymatic digestion was carried out on samples by immersion in a solution of Tris (tris hydroxymethyl aminomethane, 0.05M) with pH 8 containing 800 $\mu m \cdot mL^{-1}$ of proteinase K during 5 h at 37 °C. Then, the samples were coated with a thin gold film and observed in a scanning electron microscopy (EVO MA 10 Zeiss with tungsten electrode).

The crystalline structure of the films samples was investigated by wide-angle and small-angle X-ray scattering (WAXS and SAXS) using the SWING beamline of Soleil (St. Aubin, France). The beam had 12 KeV (1.03 Å) of energy and was formatted at 30 µm in height and 300 µm in

width. The distance between sample and camera was 1555 mm for the SAXS measurements and 555.5 mm for the WAXS measurements.

The content of each amorphous phase fraction and the cooperativity length at the glass transition were investigated by modulated-temperature differential scanning calorimetry (MT-DSC, Q100, TA Instruments) using the heat-only (oscillation amplitude of 0.318 °C, oscillation period of 60 s and heating rate of 2°C min^{-1} from -20 °C to 200°C) and the heat-cool (oscillation amplitude of 2.5 °C, oscillation period of 100 s and heating rate of 1 °C min^{-1} from -20 °C to 70°C) procedure as recommended in ref [26]. For the analysis of thermal transitions, a minimum of five modulation steps during the transition is required. In the heat-only mode the instant heating rate never drops below zero. This mode is recommended for the analysis of crystallization and melting, because this analysis is not perturbed by the reversible crystallization. The heat-cool mode consists in heating the sample while modulating the temperature with alternating positive and negative instantaneous heating rates. This mode is adapted for the measurement of the glass transition [27].

The oxygen permeability was measured with a Systech analyser 8001 at 23°C and 0% relative humidity. The oxygen permeability was calculated from the measured oxygen transmission rate (OTR) by multiplying it by the sample thickness (measured with a micrometer on 9 points). For assessing reproducibility, the permeability measurements were carried out on at least two different samples obtained by the same temperature protocol. The measurement variability of the permeability was ± 10 %. The Diffusion (D) and the Sorption (S) coefficient were calculated with the help of the time-lag method. The time lag (t_{lag}) was obtained by calculating the intercept on the abscissa of the cumulated flux curve, and D was found by evaluating

$$t_{lag} = \frac{L^2}{6D} \qquad \text{Equation 3.1}$$

where L is the sample thickness. S was obtained with the help of the general relationship, $P = D \cdot S$, where P denotes the permeability.

3.4.Results and Discussion

3.4.1. PLA crystallization kinetics

In the aim of choosing annealed PLA samples with controlled morphology and structure, the crystallization kinetics under the annealing conditions in the oven were recorded. We recall that the crystallization kinetics, which are shown in the *Figure 3.2*, were measured on large samples obtained by annealing between metal plates in an oven. The degree of crystallinity (X_c) of the PLA samples was calculated from

$$X_c = \frac{\Delta H_f - \Delta H_{cc}}{\Delta H_f^0} \qquad \text{Equation 3.2}$$

where ΔH_f is the enthalpy of fusion or melting after subtraction of the small exothermal event at the beginning of the melting peak, ΔH_{cc} is the enthalpy of the cold crystallization, and $\Delta H_f°$ is the enthalpy of the melting of the perfect crystal of infinite size, *i.e*. the totally crystalline polymer (93.1 J/g [28]). Due to the polymorphic nature of PLA leading to a melt recrystallization process and to its complex stereo-chemistry, this value may reasonably be debated [29]. The crystallization kinetics are plotted in the *Figure 3.2*. The path of crystallization discriminated the overall crystallization kinetics. The change in the crystallization rate due to the annealing temperatures could not be discriminated in the present experimental set-up. We think that the procedure in the annealing oven involved non isothermal nucleation, because of the time necessary for the oven to adjust and stabilize the temperature (approximately 10 min) after opening of the door for putting in the sample. The crystallization rate was faster from the glass than from the melt. When its thermal history was erased by melting, PLA was shown to crystallize slower at low temperatures because of the low amount of energy provided to the system, which delayed the nucleation process [30]. In the present study the samples crystallized from the glass were annealed just after the extrusion process, *i.e*., in experimental conditions strongly favouring the nucleation. This apparently accelerated the crystallization kinetics, while the samples crystallized from the melt were of course melted before annealing. This processing effect on polymer crystallization kinetics has already been evidenced for isotactic polypropylene [31,32].

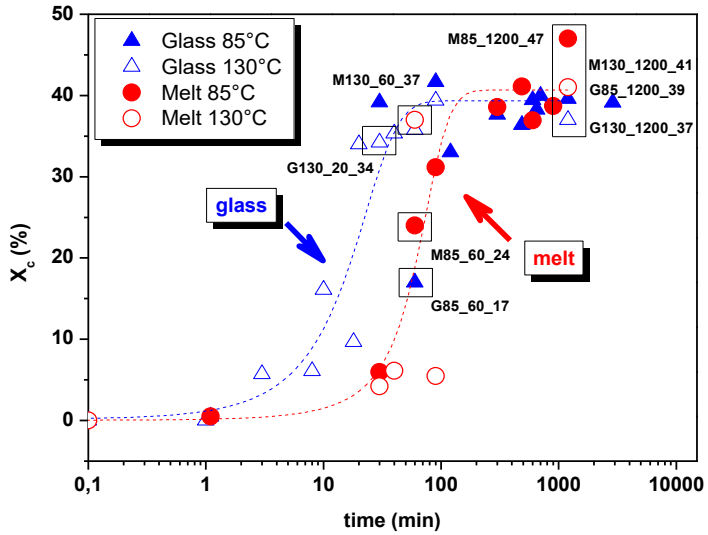

Figure 3.2. Crystallization kinetics of PLA in the oven at different temperatures upon annealing from the glassy state and from the melt.

3.4.2. Crystalline structure and space filling

Figure 3.3 shows the micrographs obtained from polarizing optical microscopy (POM). Looking at the pictures obtained at 85°C and at 130°C, one observes that the spherulites obtained from the melt were much larger than the ones obtained from the glass. Their maximum diameter was about 50 µm while the spherulites were barely observable after crystallizing from the glass. Pluta and Galeski [33] working in similar conditions reported that spherulites crystallized via cooling from the melt were larger than in those crystallized via heating from the glassy, amorphous state. They attributed this result to the formation of many pre-nuclei during the cooling of the samples to the glassy state that give rise to primary nuclei of crystallization at a higher temperature than the annealing temperature. They also observed like several authors that the sizes of the spherulites obtained by crystallization from the melt or the glass increased with the crystallization temperature [10,14,34,35]. The observation that our samples presented almost equally large spherulites when crystallized from the melt at 85 and 130 °C can be explained by assuming non-isothermal crystallization conditions. Under such conditions the radius of the spherulites changes with the temperature at which the precursor nuclei is formed [36]. The maximum nucleation rate of PLA at 120°C [37], a temperature which needs to be passed in the annealing procedure at 85 °C from the melt. The quenching following the melting of PLA in the thermal press to the annealing temperature in the oven was not

apparently fast enough to stop the nucleation and crystallization at temperatures higher than 85 °C. Androsch et al. [38,39] showed recently, using fast scanning chip calorimetry, that a cooling rate of 30 K min^{-1} is sufficient to prevent melt crystallization while a cooling rate of 500 K min^{-1} is required to inhibit the formation of nuclei in PLA containing 4% D-units. This is hardly compatible with processing of large samples, required for the present study.

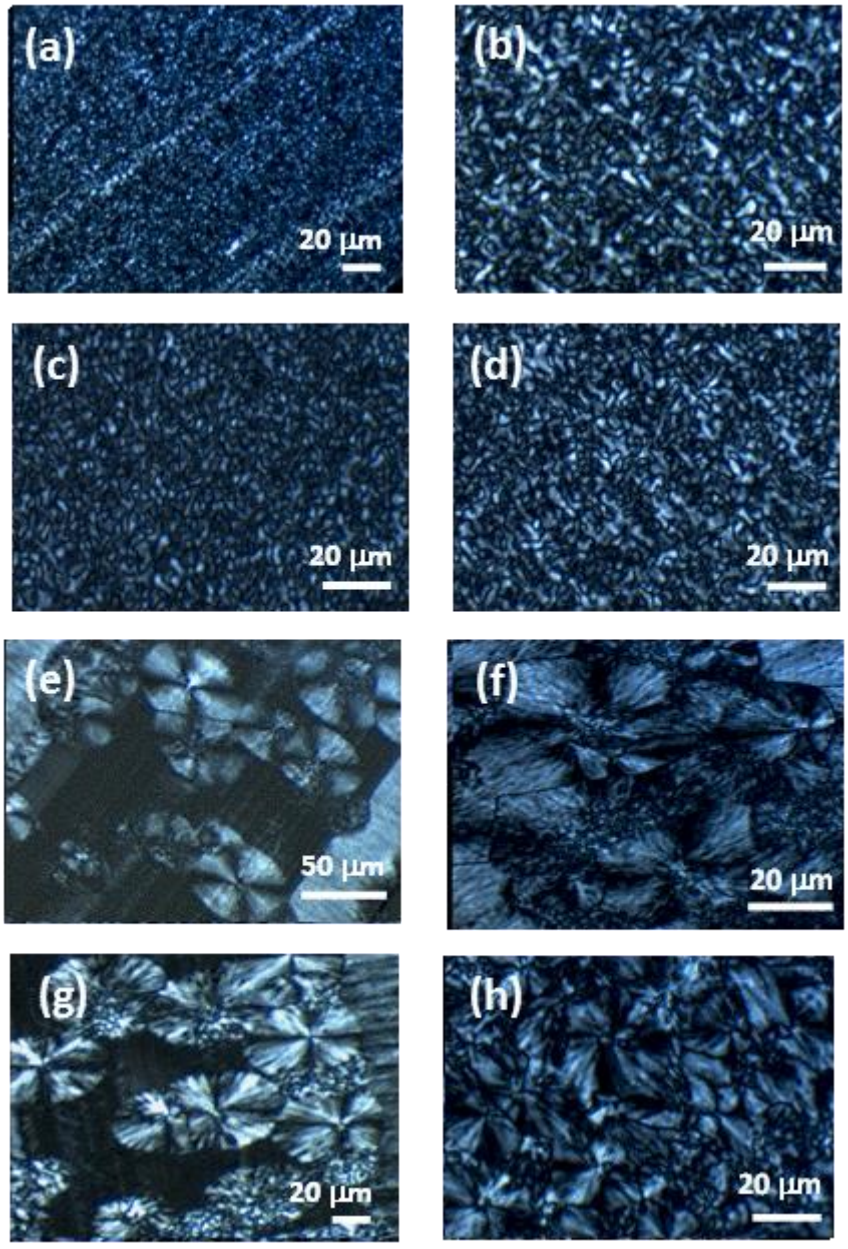

Figure 3.3. POM micrographs of PLA samples after crystallization from the glass and from the melt at two different annealing temperatures (a) G85_60_17, (b) G85_1200_39, (c) G130_20_34, (d) G130_1200_37, (e) M85_60_24, (f) M85_1200_47, (g) M130_60_37, (h) M130_1200_41.

The space-filling cannot be easily appreciated from the transmission POM pictures because of the absence of the 3D observation. The enzymatic degradation of PLA is strongly sensitive to the crystalline structure [40]. As a result one can get information about the spherulite organization by degrading the amorphous matrix outside the spherulites and trapped inside. Proteinase K works by irreversibly adsorbing on the surface of the PLA film before catalysing the hydrolysis of the ester bond. Tsuji and Miyauchi [41] studied the effect of crystallinity on the enzymatic degradation of PLLA films in the presence of proteinase K and found that the amorphous region outside of the spherulite was predominantly degraded rather than that inside. However, proteinase K can still access to the intra-spherulite amorphous phase and hydrolyse the spherulitic superstructure. It has been shown that it can even degrade a core of polylactide trapped in a crosslinked shell [42]. The SEM pictures of the sample surfaces after enzymatic degradation are shown in the *Figure 3.4*. In agreement with the POM pictures, the crystallization from the melt (*Figure 3.4*a and b) leads to the formation of bigger spherulites of about 50 μm diameter while the crystallization from the glassy state (*Figure 3.4*c and d) generates spherulites of less than 10 μm diameter. Due to this size difference the digestion of the intra-spherulite amorphous phase is only visible for samples crystallized from the melt. The degradation of the spherulites crystallized at 85°C was more pronounced (*Figure 3.4*a). Furthermore, the spherulites created by crystallization at 85°C (*Figure 3.4*a and c) looked more dispersed, separated from each other, while the spherulites crystallized at 130°C (*Figure 3.4*b and d) seemed to touch each other. This higher space-filling was particularly obvious on the picture of the G130_20_34 sample (*Figure 3.4*d). After 5 h of treatment, the enzymatic digestion penetrated barely into the sample and no single spherulites could be revealed. The high quantity of small spherulites (observed in *Figure 3.3*c) apparently hindered the access of the enzyme to the amorphous phase of the samples.

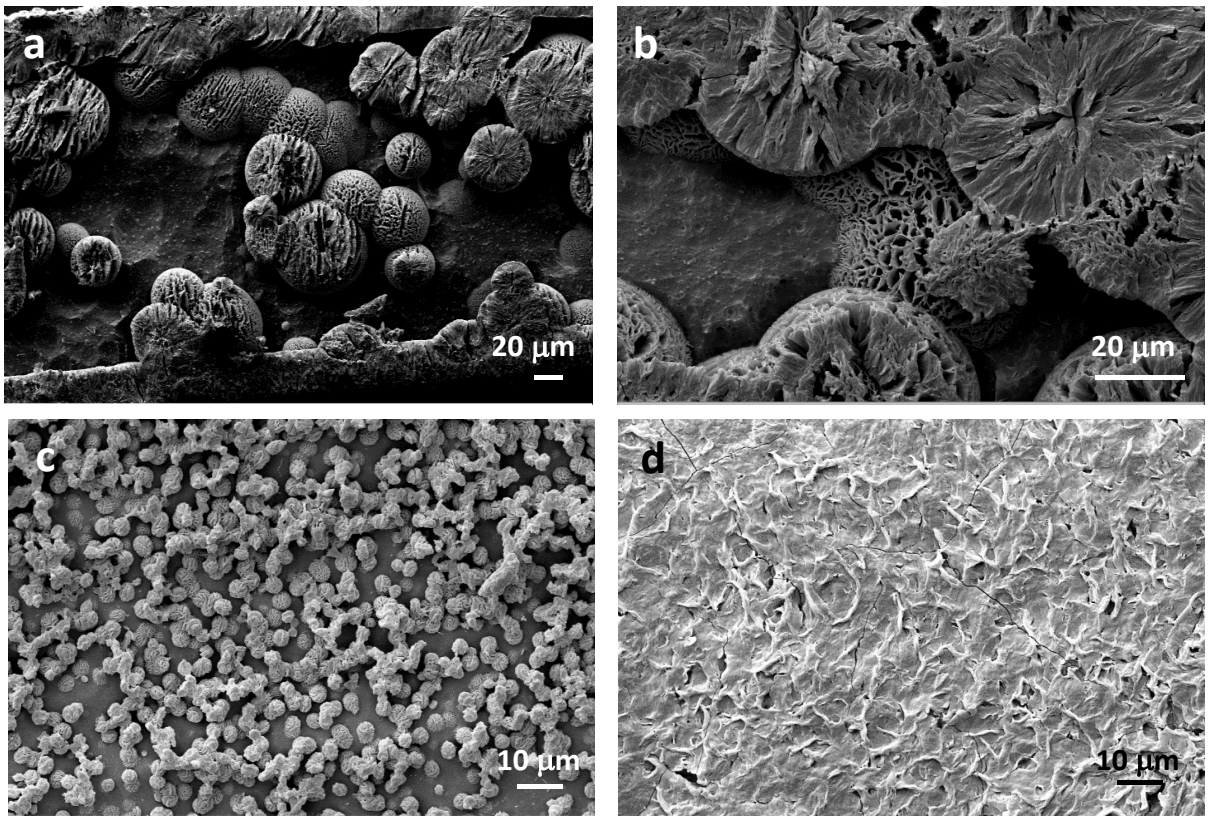

Figure 3.4. SEM pictures of PLA annealed from the glass and from the melt after 5 h enzymatic digestion (a) M85_60_24 (b) M130_60_37 (c) G85_60_17 (d) G130_20_34.

3.4.3. Crystalline morphology

The SAXS traces presented in the *Figure 3.5* show that the main diffraction peak of the samples crystallized at 130°C was located at smaller angles (smaller q) than that of the samples crystallized at 85°C. This is in coherence with existing literature [34]. The maximum of the SAXS distribution peak appears as a result of the periodicity in the arrangement of the crystalline and amorphous phases (the stacks of lamellar, amorphous regions). The samples crystallized at 130°C exhibited, as expected, a larger average long period L_z (*Table 3.1*) and a narrower distribution of the lamellae thicknesses. On the other hand, the samples crystallized at 85°C which showed a broader peak shifted towards larger angles. They present thus a more heterogeneous population of lamellar stacks, with a smaller L_z (*Table 3.1*). L_z did not depend on the crystallization pathway, *i.e*. crystallization from the glass or the melt.

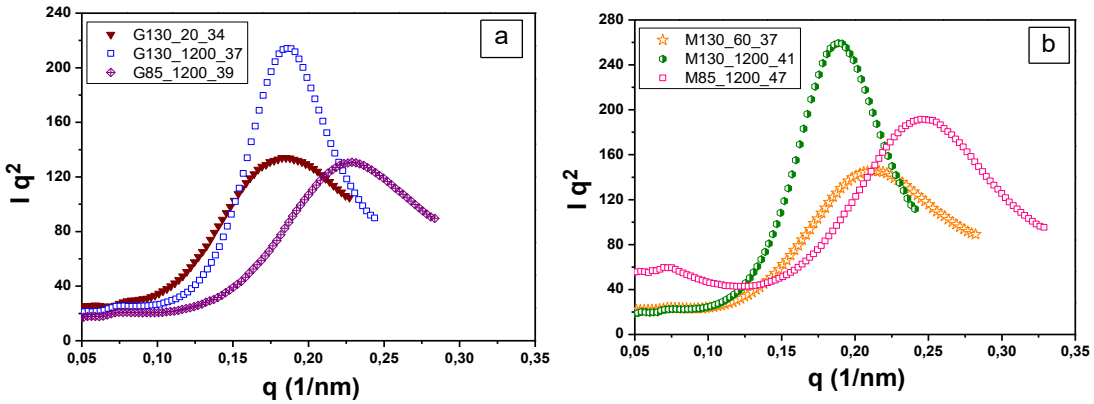

Figure 3.5. Lorentz-corrected SAXS profiles for PLA samples crystallized from the (a) glass and (b) melt at 85°C and 130°C.

The WAXS diffractograms are plotted in the *Figure 3.6*. The analysis of the reflections enables the determination of the crystalline polymorph of PLA in function of the sample preparation procedure. For easier comparison, all the diffraction were normalized using the strongest (110)/(200) reflection intensity. Di Lorenzo et al. [43] attributed the different peaks in the WAXS patterns of the α- and α'-forms of PLA. The α'-form presents small differences in the 2Θ values for the two strongest reflections, (110)/(200) and (203) planes. Based on these reflections, the d-spacings of the lattice planes can be calculated from the 2Θ positions using Bragg's law. Samples crystallized at 130°C had a smaller interplanar distance compared to samples crystallized at 85 °C (*Table 3.1*). This showed together with the results obtained from SEM and SAXS measurements that the microstructure generated at 130°C was more organized. It is worth mentioning that the WAXS spectra did not allow to discriminate the α'-and the α–polymorph as a function of the crystallization temperature. This could be the consequence of the sample annealing procedure, which involved non-isothermal nucleation.

Table 3.1. Long period and d-spacings respectively obtained from SAXS and WAXS analyses.

	L_z (nm)	d-sp. 110/200 (nm)	d-sp. 203 (nm)
G85_60_17	n.d.	0.5290	0.4637
G85_1200_39	27.5	0.5270	0.4615
G130_20_34	34	0.5255	0.4606
G130_1200_37	33.3	0.5249	0.4601
M85_60_24	n.d.	0.5274	0.4608
M85_1200_47	25.6	0.5280	0.4613
M130_60_37	29.9	0.5249	0.4615
M130_1200_41	33.3	0.5255	0.4599

n.d. non determined

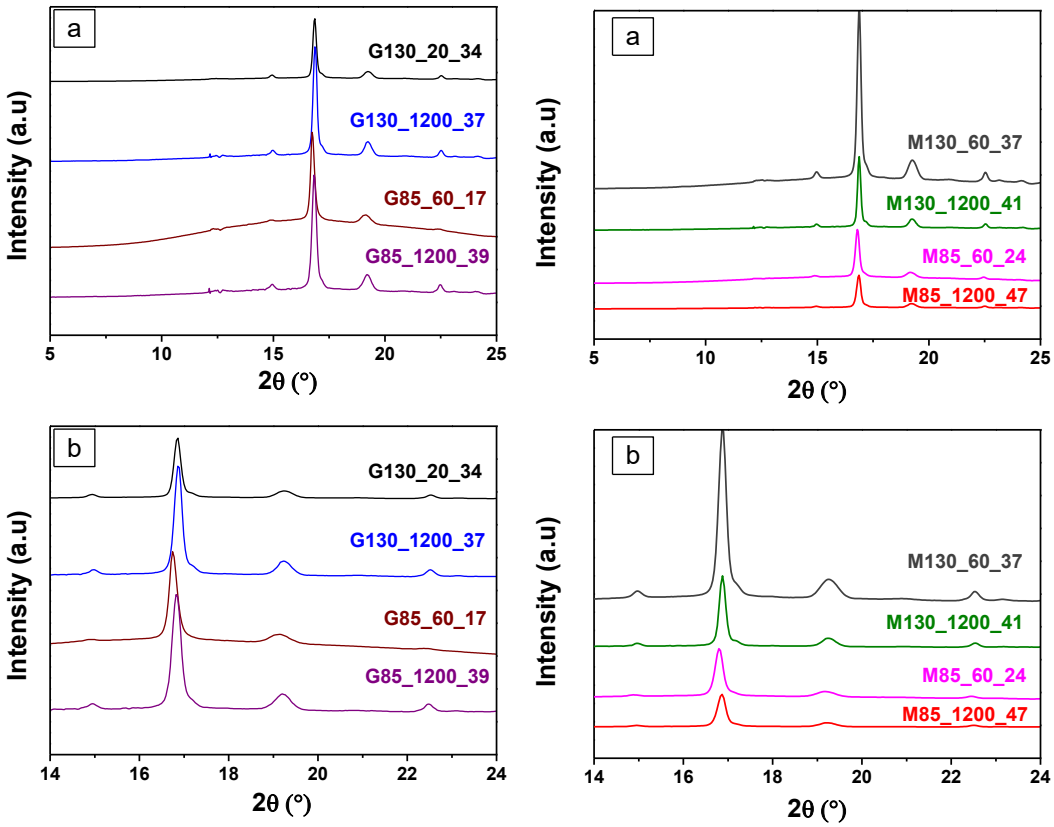

Figure 3.6. (a) WAXS patterns and (b) enlarged patterns of PLA samples crystallized from the glassy state and from the melt.

3.4.4. Structural description of the amorphous phase and its cooperativity at the glass transition

As for many semi-crystalline polymers, the classic structural representation of PLA separates the amorphous phase into a fraction relaxing at the glass transition, *i.e*., the mobile amorphous fraction (MAF), and its counterpart, the rigid amorphous fraction (RAF) which devitrifies at higher temperatures [21,43–46]. The RAF existence is due to the length of the polymer molecules that is much higher than the dimensions of the crystalline phase, leading to an incomplete decoupling between the amorphous phase and the crystals. The content of RAF in polylactide, X_{RA}, depends on the conditions of crystallization and can vary from 0% to 35% [30]. Although this approach may look simplistic since it limits the description of the amorphous phase to its structure without considering its dynamics, the studies of Guinault et al. [14], Drieskens et al. [13], and Delpouve et al. [11] proposed that an important amount of RAF is prejudicial for the barrier properties of PLA.
The content of the RAF can be calculated after

$$X_c + X_{MA} + X_{RA} = 100\% \text{ with } X_{MA} = \frac{\Delta C_p}{\Delta C_p^0} \qquad \text{Equation 3.3}$$

where X_{MA} is the content of MAF, ΔC_p is the heat capacity change measured at the glass transition and ΔC_P^0 the heat capacity change of the fully amorphous sample. The quantitative analysis of the thermal events was done thanks to MT-DSC by separating the events related to the variations of the heat capacity, which appear in the reversing heat flow, from the kinetic events, which appear in the non-reversing heat flow. An example of this protocol is given in *Figure 3.7*a. The difference between the enthalpy of cold-crystallization and the enthalpy of melting for the determination of the degree of crystallinity was double checked using, on the one hand, the average heat flow signal as usually performed in classical DSC, and, on the other hand, the reversing and the non-reversing heat flow signals from the MT-DSC. At the same time, the glass transition temperature and ΔC_p was systematically measured from the reversing heat flow (*Figure 3.7*b) with ΔC_P^0 determined to be 0.52 J (g. K)$^{-1}$. The results are presented in *Table 3.2*.

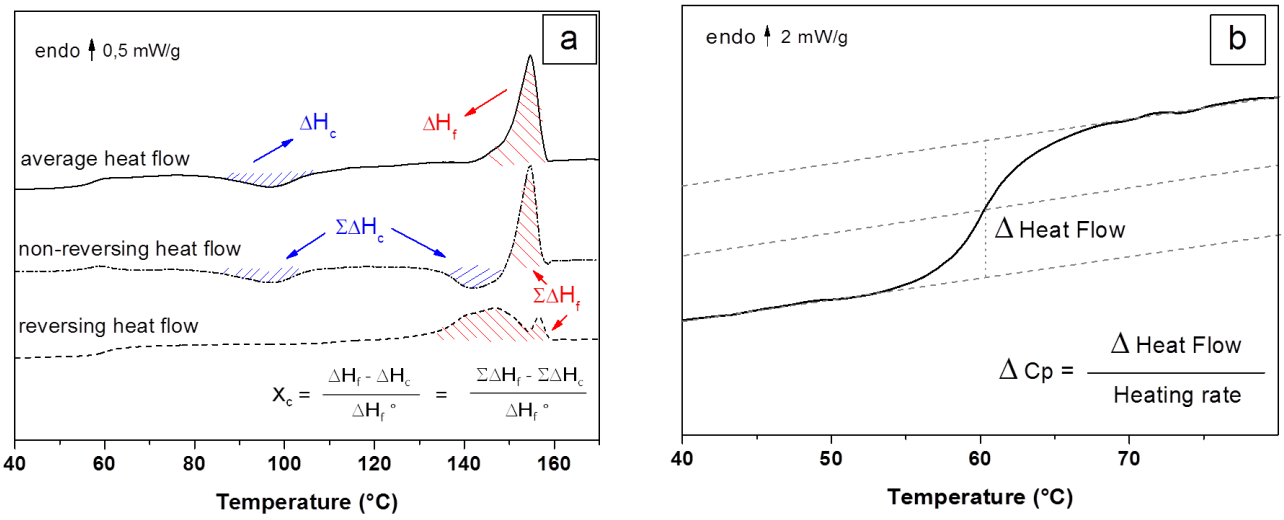

Figure 3.7. (a) Protocol for the determination of the degree of crystallinity from MT-DSC curves obtained for G85_60_17: Average heat flow (Solid line); reversing heat flow (dashed line); and non-reversing heat flow (dotted line) versus temperature; (b) reversing heat flow in the glass transition domain.

An increasing time of annealing increased the degree of crystallinity. Only two materials did not reach their maximum degree of crystallinity according to their values of enthalpy of cold-crystallization that differ from zero (*Table 3.2*). Among the others and in concordance with the *Figure 3.2*, the crystallization from the melt lead to higher ΔH_f and consequently to higher X_C after prolonging annealing although the variations are small. The quantity of measured X_{MA} at long annealing times seemed to depend on the annealing temperature. It was about 9% lower when crystallizing PLA at 85°C compared to 130 °C. One could interpret in a first time this result as evidence that the MAF underwent a stronger confinement. However, it may be hasty to do such a comparison since it would consider that the mobility landscape of the MAF was independent from the temperature of annealing. On the other hand the values of X_{RA} clearly evidenced a higher coupling between crystals and amorphous phase when crystallizing at 85°C. This means that the repartition between RAF and MAF depended on the temperature and time of annealing, even if nucleation pre-existed in the material. A high temperature of annealing allowed thus both perfecting the crystalline structure (more homogenous structure shown by XRD in *Figure 3.5* and *Figure 3.6*) and better decoupling amorphous and crystal phases.

For equivalent annealing temperatures, T_g was slightly higher, about 2°C, when crystallizing from glassy state. For an equivalent path of crystallization, T_g was higher when crystallizing at 85°C. The shift of T_g towards higher values upon crystallization is characteristic of the

constrained amorphous phase between crystalline lamellae, which relaxes only at higher temperatures [19,20]. Among crystallized samples, it has been shown that T_g also shifts to higher temperatures when the crystallization conditions did not allow a correct decoupling between the amorphous and the crystalline phase [26]. The RAF was more important when samples were crystallized at a lower temperature. This seems consistent with the results of Guinault et al. [14] who described that important formation of RAF was linked to imperfect crystallization of PLA. It is assumed that at low crystallization temperature, typically 85°C, the lack of chain mobility hinders the reorganization of polymeric segments in crystals and induces many chain segments subjected to geometrical restrictions in the amorphous phase [47]. Most interestingly, we show here that this observation could be extended to imperfect conditions of crystallization in general, including the predominance of germination over growth that lead to the formation of low-size spherulites. In particular, G85_1200_39 sample had the highest RAF degree (21%, *Table 3.2*).

Table 3.2. Thermal and structural parameters obtained from MT-DSC heat-only analyses and oxygen permeability data of PLA crystallized from the melt and from the glass at different annealing temperatures.

	T_g (°C)	ΔC_p ($Jg^{-1}K^{-1}$)	ΔH_c (Jg^{-1})	ΔH_f (Jg^{-1})	X_c (%)	X_{ma} (%)	X_{ra} (%)	$P.10^{18}$ ($m^3.m.m^{-2}.s^{-1}.Pa^{-1}$)	$D.10^{12}$ ($m^2.s^{-1}$)	$S.10^6$ ($m^3.m^{-3}.Pa^{-1}$)
Amorphous	58.0	0.52	-	-	0	-	-	2.30	1.8	1.3
G85_60_17	57.2	0.39	11	27	17	75	8	1.73	1.5	1.1
G85_1200_39	56.1	0.21	0	36	39	40	21	1.33	1.7	0.8
G130_20_34	56.1	0.31	0	32	34	60	6	0.58	0.7	0.8
G130_1200_37	53.5	0.26	0	34	37	50	13	0.93	1.2	0.8
M85_60_24	56.9	0.38	10	32	24	73	3	1.29	1.1	1.2
M85_1200_47	54.8	0.20	0	43	47	38	15	0.88	1.2	0.8
M130_60_37	56.3	0.30	0	34	37	58	5	0.87	0.9	0.9
M130_1200_41	53.2	0.24	0	38	41	46	13	0.77	1.1	0.7

n.d. non determined

To understand how the mobile amorphous phase was itself impacted by the presence of RAF, the size of cooperative rearranging region (CRR) $\xi_{T\alpha}$ was calculated. A CRR is defined as the

smallest amorphous domain where a conformational rearrangement may occur without causing rearrangements in the surrounding [48]. This approach probes the amorphous phase dynamics by providing a picture of the relaxation time at the glass transition which is directly observable through calorimetric measurements [49], and more precisely from the analysis of the in-phase component C' and the out-of-phase component C'' of the complex heat capacity measured by MT-DSC. An example of these two signals is given in *Figure 3.8*. According to this approach [50], the cooperativity volume $\xi_{T\alpha}^3$ of a CRR at the dynamic glass transition temperature T_α can be estimated from the following equation:

$$\xi_{T\alpha}^3 = \frac{\left(1/C_p\right)_{Glass\ T\alpha} - \left(1/C_p\right)_{Liquid\ T\alpha}}{\rho\left(\delta T\right)^2} k_B T_\alpha^2 \qquad \text{Equation 3.4}$$

with k_B the Boltzmann constant, δT the average temperature fluctuation related to the dynamic glass transition of a CRR which is determined from the Gaussian fit of C'' [49], ρ the density, and C_p the heat capacity at constant pressure. The values of $C_{p\ glass\ T\alpha}$ and $C_{p\ liquid\ T\alpha}$ were obtained by prolonging the glass and liquid lines to dynamic glass transition temperature after normalization to the MAF content [18]. When the crystallization is not performed to its maximum extent, the MAF splits into intra- and inter-spherulitic amorphous regions and calorimetric measurements can show two separate signatures within the glass transition temperature range [20]. To overcome the issues related to such a complex molecular mobility landscape, the investigation of the CRR size was limited to the samples having reached their maximum degree of crystallinity. The results are presented in *Table 3.3*. As expected all materials exhibited a lower CRR size compared to an amorphous sample which is 3.0 nm [30]. Investigating the semicrystalline materials, the variations of T_α followed the variations of T_g as expected. While the values of C_p were barely affected by the thermal treatments, δT was clearly higher for the samples crystallized at 85°C which resulted in a lower size of CRR [26]. This behaviour can also be seen when comparing the amount of rigid amorphous fraction and CRR. At 85°C the RAF was higher and influenced the CRR size. The impact of crystallization processes on CRR size was shown in previous articles [19,25,30,51–53] evidencing the role of the geometric confinement induced by the crystals and the incomplete decoupling between the amorphous and crystalline phases. Obviously the dynamics of the amorphous phase, including the processes of vitrification and relaxation strongly differed when varying the temperature of annealing.

Table 3.3. Amorphous phase relaxation parameters obtained from MT-DSC heat-cool analyses.

	Tα (°C)	Cp glass Tα ($Jg^{-1}K^{-1}$)	Cp liquid Tα ($Jg^{-1}K^{-1}$)	δT (°C)	CRR size (nm)
Amorphous [29]	60.5	1.46	1.97	3	3.0
G85_1200_39	54.4	1.45	1.95	4.7	2.1
G130_20_34	58.4	1.25	1.85	4	2.5
G130_1200_37	53.3	1.22	1.76	4.1	2.4
M85_1200_47	56.5	1.20	1.70	5.5	1.9
M130_60_37	57.6	1.20	1.75	3.4	2.8
M130_1200_41	52.7	1.25	1.75	3.9	2.4

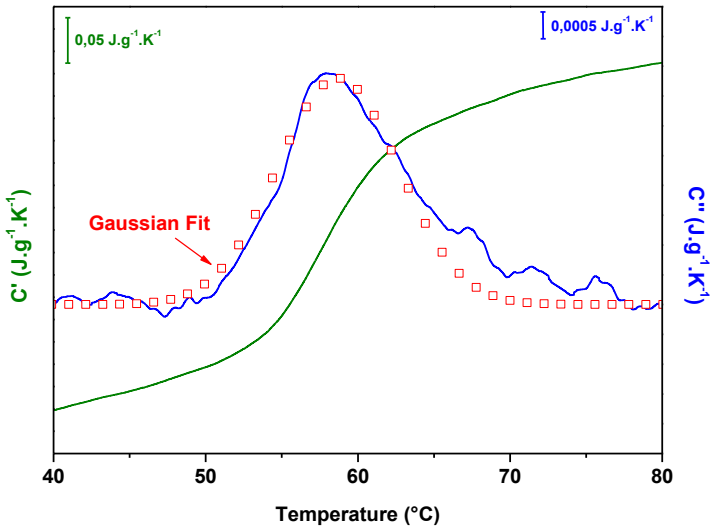

Figure 3.8. In-phase component C' (green line) and out-of-phase component C'' (blue line) from heat-cool mode in MT-DSC obtained for the G130_20_34. The red squares correspond to the adjusted Gaussian fit of C''.

3.4.5. Oxygen permeability study

The *Table 3.2* reports the oxygen permeability of the different samples. The barrier properties of PLA were globally improved after the crystallization, and this effect was higher at T_c = 130°C no matter if the crystallization was carried out from glass or from the melt. At the annealing temperature of 85°C, the crystallization from the melt lead to higher barrier properties. The

excluded volume hypothesis provides an explanation of the relationship between the crystallinity degree and barrier properties. Crystalline zones are presumed to be excluded volumes through which molecules cannot diffuse and in which they cannot sorb [4]. This is in contrast to the amorphous zones where diffusion and sorption is possible. The crystallites force a more tortuous diffusive pathway of permeants, which, macroscopically, decreases the diffusion coefficient. In addition, crystallites decrease the available volume for permeant sorption, which decreases the overall solubility coefficient of the material.

Two groups of samples could be distinguished in the oxygen permeability data presented in the *Table 3.2*: the first one was composed of samples obtained with a short crystallization time (example M85_60_24 and G85_60_17). In that case the space filling of the spherulites was not complete (see also *Figure 3.3*a, e and *Figure 3.4*a, c), which lead to a relatively low gain in the oxygen barrier properties. This gain was driven by the decrease of the diffusion coefficient due to the tortuosity effect induced by the presence of the crystallites. The impact of the crystallinity degree on the oxygen solubility coefficient was smaller than the measurement variability.

The second group was composed of samples, which were crystallized for a long time (1200 minutes, *Figure3.3*b, d, f, h), where complete space filling was reached. In that case, the quantity of RAF guided the results of permeability, while the size and structure of the crystallites had a negligible influence on the barrier properties. This can be concluded by the comparison of sample G130_1200_37 (*Figure 3.3*d) and M130_1200_41 (*Figure 3.3*h). These samples have a similar RAF content and that is why they had equal gas barrier properties, even if the spherulite sizes were very different (*Table 3.2*). The importance of the RAF for the barrier properties of semicrystalline PLA can be observed by the comparison of the samples G130_20_34 and G130_1200_37, which had almost the same crystallinity degree, similar crystalline morphology and similar relaxation dynamics in the MAF. The oxygen diffusion coefficient of G130_1200_37 was more than two times higher than that of G130_20_34 and also the RAF of G130_1200_37 was about two times higher than that of G130_20_34. The low RAF of sample G130_20_34 can be explained by the hypothesis that this sample was highly nucleated before crystallization. This caused a rapid crystallization not leaving enough time for the formation of the RAF. The sample G85_1200_39 presented the highest quantity of RAF (21 %). The oxygen diffusion coefficient of this sample was almost equal to that of amorphous PLA, and the permeability gain was uniquely obtained by the decrease of oxygen solubility in the annealed sample. These results point to the importance of the RAF for the gas barrier

properties of PLA. In that, they confirm essentially the hypothesis proposed by Guinault et al. [14] and allow ruling out other effects linked to crystalline morphology and structure.
A global summary of the impact of the sample morphology and amorphous phase dynamics is given in *Table 3.4*.

Table 3.4. Summary of morphological and structural characteristics of PLA in relation to the thermal treatment and improvement of oxygen barrier properties.

		T (crystallization) = 85 °C	**T (crystallization) = 130 °C**
Crystallization from the glass	Spherulite morphology	- Small spherulites due to preponderant nucleation	- Small spherulites due to preponderant nucleation
	Crystalline morphology	- Disordered small crystallites - More heterogeneous lamellar stacks	- Organized phase of crystallites - Less heterogeneous lamellar stacks
	Amorphous phase dynamics	- Low intermolecular interactions in the MAF (small CRR) - High coupling between amorphous and crystalline phase (high RAF content)	- Average intermolecular interactions in the MAF (intermediate CRR) - Low coupling between amorphous and crystalline phase (low RAF content)
	Gain in barrier properties	Low	**Best**
Crystallization from the melt	Spherulite morphology	- Big spherulites due to coexistence of germination and growth	- Big spherulites due to coexistence of germination and growth
	Crystalline morphology	- Disordered small crystallites - More heterogeneous lamellar stacks	- Organized phase of crystallites - Less heterogeneous lamellar stacks
	Amorphous phase dynamics	- Low intermolecular interactions in the MAF (small CRR) - Average coupling between amorphous and crystalline phase (average RAF content)	- Average intermolecular interactions in the MAF (intermediate CRR) - Average coupling between amorphous and crystalline phase (average RAF content)
	Gain in barrier properties	Average	Average

We conclude that the RAF increased locally the diffusion coefficient. It is composed of insufficiently decoupled tie molecules between the crystalline and the amorphous phase, which hinders the relaxation of the polymer chains and thereby increases the free volume at the crystallite/amorphous phase interface. This free volume is available for the accelerated diffusive transport of small molecules. The sample G130_20_34, which had the best barrier properties of the sample set, was particularly interesting because it showed a means for optimizing PLA barrier properties. In brief, PLA should be pre-nucleated and crystallized from the glass in the

aim to obtain a high crystallinity degree very quickly. The prolongation of the annealing during a long time in the aim of obtaining a higher crystallinity is yet disadvantageous, because of the mobility of macromolecular chains in the MAF (in particular at high temperatures). This mobility can be the reason for gradual conversion of MAF into RAF with time.

3.5.Conclusion

In the present work, the impact of the crystalline structure and the amorphous phase dynamics of PLA on its oxygen barrier properties were studied. We conclude that the quantity of the rigid amorphous phase is the preponderant factor governing the oxygen diffusion coefficient. The crystalline morphology and structure (in the limit of the here used methodology of thermal annealing) and the relaxation dynamics of the mobile amorphous phase have negligible impact on the diffusion coefficient and the solubility coefficient is ruled by the crystallinity degree. We propose that the insufficient decoupling between the amorphous and the crystalline phase in PLA generates supplementary free volume at the vicinity of the crystallites. This free volume can accelerate the diffusive transport of the gas molecules and cancel out the tortuosity effect induced by the presence of crystallites. From these observations the following recommendation can be formulated: In the aim of achieving optimal gas barrier properties, PLA should be pre-nucleated and crystallized at a high temperature (yielding the α-polymorph) for short time to obtain a high crystallinity degree without the formation of the rigid amorphous fraction.

Acknowledgements

The authors acknowledge the Coordenação de Aperfeiçoamento de Pessoal de Nível Superior - CAPES for the doctorate grant n° 9712-13-5 of Samira Fernandes Nassar.
The authors acknowledge furthermore the synchrotron facility SOLEIL – Beam line SWING, proposal number 20110361 for DRX measurements and Dr. Florian Meneau for his precious technical help.

3.6.References

[1] M. Schmid, K. Dallmann, E. Bugnicourt, D. Cordoni, F. Wild, A. Lazzeri, K. Noller, Properties of Whey-Protein-Coated Films and Laminates as Novel Recyclable Food Packaging Materials with Excellent Barrier Properties, Int. J. Polym. Sci. 2012 (2012) 1–7. doi:10.1155/2012/562381.

[2] R. Salazar, S. Domenek, V. Ducruet, Interactions of flavoured oil in-water emulsions with polylactide, Food Chem. 148 (2014) 138–146. doi:10.1016/j.foodchem.2013.10.018.

[3] S. Saeidlou, M.A. Huneault, H. Li, C.B. Park, Poly(lactic acid) crystallization, Prog. Polym. Sci. 37 (2012) 1657–1677. doi:10.1016/j.progpolymsci.2012.07.005.

[4] Michaels A. S.; Bixler H. J., Solubility of gases in polymers, J. Polym. Sci. L (1961) 393–412.

[5] A. Colomines, G; Domenek, S.; Ducruet, V.; Guinault, Integrated process simulation and die-design in sheet metal forming, Int. J. Mater. Form. 1 (2008) 607–610. doi:10.1007/s12289-008-0 329 0.

[6] G. Colomines, V. Ducruet, Ć. Courgneau, A. Guinault, S. Domenek, Barrier properties of poly(lactic acid) and its morphological changes induced by aroma compound sorption, Polym. Int. 59 (2010) 818–826. doi:10.1002/pi.2793.

[7] S. Sato, T. Nyuui, G. Matsuba, K. Nagai, Correlation between interlamellar amorphous structure and gas permeability in poly(lactic acid) films, J. Appl. Polym. Sci. 131 (2014) n/a–n/a. doi:10.1002/app.40626.

[8] C. Courgneau, S. Domenek, R. Lebossé, A. Guinault, L. Avérous, V. Ducruet, Effect of crystallization on barrier properties of formulated polylactide, Polym. Int. 61 (2012) 180–189. doi:10.1002/pi.3167.

[9] H. Sawada, Y. Takahashi, S. Miyata, S. Kanehashi, S. Sato, K. Nagai, Gas Transport Properties and Crystalline Structures of Poly(lactic acid) Membranes, Trans. Mater. Res. Soc. Japan. 35 (2010) 241–246. doi:10.14723/tmrsj.35.241.

[10] M. Cocca, M.L. Di Lorenzo, M. Malinconico, V. Frezza, Influence of crystal polymorphism on mechanical and barrier properties of poly(l-lactic acid), Eur. Polym. J. 47 (2011) 1073–1080. doi:10.1016/j.eurpolymj.2011.02.009.

[11] N. Delpouve, A. Saiter, E. Dargent, Water Barrier Properties in Biaxially Drawn Poly (lactic acid) Films, J. Phys. Chem. B. 116 (2012) 4615–4625. doi:10.1021/jp211670g.

[12] S. Kanehashi, A. Kusakabe, S. Sato, K. Nagai, Analysis of permeability; solubility and diffusivity of carbon dioxide; oxygen; and nitrogen in crystalline and liquid crystalline polymers, J. Memb. Sci. 365 (2010) 40–51. doi:10.1016/j.memsci.2010.08.035.

[13] M. Drieskens, R. Peeters, J. Mullens, D. Franco, P. Lemstra, D. Hristova-Bogaerds, Structure Versus Properties Relationship of Poly(lactic acid). I. Effect of Crystallinity on Barrier Properties, J. Polym. Sci. Part B Polym. Phys. 47 (2009) 2247–2258. doi:10.1002/polb.21822.

[14] A. Guinault, C. Sollogoub, V. Ducruet, S. Domenek, Impact of crystallinity of poly(lactide) on helium and oxygen barrier properties, Eur. Polym. J. 48 (2012) 779–788. doi:10.1016/j.eurpolymj.2012.01.014.

[15] K. Wasanasuk, K. Tashiro, Crystal structure and disorder in Poly(l-lactic acid) δ form (α' form) and the phase transition mechanism to the ordered α form, Polymer (Guildf). 52 (2011) 6097–6109. doi:10.1016/j.polymer.2011.10.046.

[16] K. Wasanasuk, K. Tashiro, Structural regularization in the crystallization process from the glass or melt of poly(l-lactic acid) viewed from the temperature-dependent and time-resolved measurements of FTIR and wide-angle/small-angle X-ray scatterings, Macromolecules. 44 (2011) 9650–9660. doi:10.1021/ma2017666.

[17] T. Kawai, N. Rahman, G. Matsuba, K. Nishida, T. Kanaya, M. Nakano, H. Okamoto, J. Kawada, A. Usuki, N. Honma, K. Nakajima, M. Matsuda, Crystallization and Melting Behavior of Poly (L-lactic Acid), Macromolecules. 40 (2007) 9463–9469.

[18] H. Bai, C. Huang, H. Xiu, Q. Zhang, H. Deng, K. Wang, F. Chen, Q. Fu, Significantly improving oxygen barrier properties of polylactide via constructing parallel-aligned shish-kebab-like crystals with well-interlocked boundaries, Biomacromolecules. 15 (2014) 1507–1514. doi:10.1021/bm500167u.

[19] N. Delpouve, A. Saiter, J.F. Mano, E. Dargent, Cooperative rearranging region size in semi-crystalline poly(L-lactic acid), Polymer (Guildf). 49 (2008) 3130–3135. doi:10.1016/j.polymer.2008.04.045.

[20] N. Delpouve, M. Arnoult, A. Saiter, E. Dargent, J. Saiter, Evidence of Two Mobile Amorphous Phases in Semicrystalline Polylactide Observed from Calorimetric Investigations, Polym. Eng. Sci. 54 (2014) 1144–1150. doi:10.1002/pen.23657.

[21] M. Arnoult, E. Dargent, J.F. Mano, Mobile amorphous phase fragility in semi-crystalline polymers: Comparison of PET and PLLA, Polymer (Guildf). 48 (2007) 1012–1019. doi:10.1016/j.polymer.2006.12.053.

[22] E. Zuza, J.M. Ugartemendia, A. Lopez, E. Meaurio, A. Lejardi, J.R. Sarasua, Glass transition behavior and dynamic fragility in polylactides containing mobile and rigid amorphous fractions, Polymer (Guildf). 49 (2008) 4427–4432. doi:10.1016/j.polymer.2008.08.012.

[23] B. Wunderlich, Reversible crystallization and the rigid-amorphous phase in semicrystalline macromolecules, Prog. Polym. Sci. 28 (2003) 383–450. doi:10.1016/S0079-6700(02)00085-0.

[24] J. Del Rıó, A. Etxeberria, N.L. Lopez-Rodrıuez, E. Lizundia, J.R. Sarasua, A PALS Contribution to the Supramolecular Structure of Poly(L-lactide), Macromolecules. 43 (2010) 4698–4707. doi:10.1021/ma902247y.

[25] N. Delpouve, L. Delbreilh, G. Stoclet, A. Saiter, E. Dargent, Structural dependence of the molecular mobility in the amorphous fractions of polylactide, Macromolecules. 47 (2014) 5186–5197. doi:10.1021/ma500839p.

[26] A. Saiter, N. Delpouve, E. Dargent, W. Oberhauser, L. Conzatti, F. Cicogna, E. Passaglia, Probing the chain segment mobility at the interface of semi-crystalline polylactide/clay nanocomposites, Eur. Polym. J. 78 (2016) 274–289. doi:10.1016/j.eurpolymj.2016.03.040.

[27] J.M. Hutchinson, Studying the glass transition by DSC and TMDSC, J. Therm. Anal. Calorim. 72 (2003) 619–629. doi:10.1023/A:1024542103314.

[28] B.E.W. Fischer, H.J. Sterzel, G. Wegner, Investigation of the structure of solution grown crystals of lactide copolymers by means of chemical reactions by means of chemical reactions, Kolloid-Z. U. Z. Polym. 251 (1973) 980–990.

[29] M.C. Righetti, M. Gazzano, M.L. Di Lorenzo, R. Androsch, Enthalpy of melting of α′- and α-crystals of poly(L-lactic acid), Eur. Polym. J. 70 (2015) 215–220. doi:10.1016/j.eurpolymj.2015.07.024.

[30] N. Delpouve, a. Saiter, E. Dargent, Cooperativity length evolution during crystallization of poly(lactic acid), Eur. Polym. J. 47 (2011) 2414–2423. doi:10.1016/j.eurpolymj.2011.09.027.

[31] T. Funaki, A; Kondo, K; Kanai, Analysis of Contributing Factors to Production of Highly Transparent Isotactic Polypropylene Extrusion Sheets. Part 2, Polym. Eng. Sci. 51 (2011) 1068–1077.

[32] T. Funaki, A; Kanai, T; Saito, Y; Yamada, Analysis of Contributing Factors to Production of Highly Transparent Isotactic Polypropylene Extrusion Sheets. Part I, Polym. Eng. Sci. 50 (2010) 2356–2365.

[33] M. Pluta, A. Galeski, Crystalline and supermolecular structure of polylactide in relation to the crystallization method, J. Appl. Polym. Sci. 86 (2002) 1386–1395. doi:10.1002/app.11280.

[34] P. Pan, B. Zhu, W. Kai, T. Dong, Y. Inoue, Effect of crystallization temperature on crystal modifications and crystallization kinetics of poly(L-lactide), J. Appl. Polym. Sci. 107 (2008) 54–62. doi:10.1002/app.27102.

[35] M. Yasuniwa, S. Tsubakihara, K. Iura, Y. Ono, Y. Dan, K. Takahashi, Crystallization behavior of poly(l-lactic acid), Polymer (Guildf). 47 (2006) 7554–7563. doi:10.1016/j.polymer.2006.08.054.

[36] X.J. Li, G.J. Zhong, Z.M. Li, Non-isothermal crystallization of poly(L-lactide) (PLLA) under quiescent and steady shear conditions, Chinese J. Polym. Sci. 28 (2010) 357–366. doi:10.1007/s10118-010-9015-z.

[37] M.L. Di Lorenzo, Determination of spherulite growth rates of poly(l-lactic acid) using combined isothermal and non-isothermal procedures, Polymer (Guildf). 42 (2001) 9441–9446. doi:http://dx.doi.org/10.1016/S0032-3861(01)00499-2.

[38] R. Androsch, M.L. Di Lorenzo, C. Schick, Crystal nucleation in random l/d-lactide copolymers, Eur. Polym. J. 75 (2016) 474–485. doi:10.1016/j.eurpolymj.2016.01.020.

[39] R. Androsch, H.M.N. Iqbal, C. Schick, Non-isothermal crystal nucleation of poly (l-lactic acid), Polymer (Guildf). 81 (2015) 151–158. doi:10.1016/j.polymer.2015.11.006.

[40] R.T. MacDonald, R.A. Gross, S.P. McCarthy, Enzymatic degradability of poly(lactide): Effects of chain stereochemistry and material crystallinity, Macromolecules. 29 (1996) 7356–7361. doi:10.1021/ma960513j.

[41] H. Tsuji, S. Miyauchi, Enzymatic hydrolysis of free and restricted amorphous regions in poly(L-lactide) films with different crystallinities and a fixed crystalline thickness, Polymer (Guildf). 42 (2001) 4463–4467. doi:10.1016/S0032-3861(00)00792-8.

[42] S. Samarajeewa, R. Shrestha, Y. Li, K.L. Wooley, Degradability of poly(lactic acid)-containing nanoparticles: Enzymatic access through a cross-linked shell barrier, J. Am. Chem. Soc. 134 (2012) 1235–1242. doi:10.1021/ja2095602.

[43] M.L. Di Lorenzo, M. Cocca, M. Malinconico, Crystal polymorphism of poly(l-lactic acid) and its influence on thermal properties, Thermochim. Acta. 522 (2011) 110–117. doi:10.1016/j.tca.2010.12.027.

[44] S. Iannace, L. Nicolais, Isothermal Crystallization and Chain Mobility of Poly (L - lactide), J. Appl. Polym. Sci. (1997) 911–919.

[45] M. Pyda, R.C. Bopp, B. Wunderlich, Heat capacity of poly(lactic acid), J. Chem. Thermodyn. 36 (2004) 731–742. doi:10.1016/j.jct.2004.05.003.

[46] M. Kanchanasopa, J. Runt, Broadband Dielectric Investigation of Amorphous and Semicrystalline l-Lactide/ meso-Lactide Copolymers, Macromolecules. 37 (2004) 863–871. doi:10.1021/ma035597s.

[47] M.C. Righetti, E. Tombari, Crystalline, mobile amorphous and rigid amorphous fractions in poly(L-lactic acid) by TMDSC, Thermochim. Acta. 522 (2011) 118–127. doi:10.1016/j.tca.2010.12.024.

[48] G. Adam, J.H. Gibbs, On the Temperature Dependence of Cooperative Relaxation Properties in Glass-Forming Liquids, J. Chem. Phys. 43 (1965) 139–146. doi:10.1063/1.1696442.

[49] E. Hempel, G. Hempel, a. Hensel, C. Schick, E. Donth, Characteristic Length of Dynamic Glass Transition near T g for a Wide Assortment of Glass-Forming Substances, J. Phys. Chem. B. 104 (2000) 2460–2466. doi:10.1021/jp991153f.

[50] E. Donth, The size of cooperatively rearranging regions at the glass transition, J. Non. Cryst. Solids. 53 (1982) 325–330. doi:10.1016/0022-3093(82)90089-8.

[51] A. Saiter, N. Delpouve, E. Dargent, J.M. Saiter, Cooperative rearranging region size determination by temperature modulated DSC in semi-crystalline poly(l-lactide acid), Eur. Polym. J. 43 (2007) 4675–4682. doi:10.1016/j.eurpolymj.2007.07.039.

[52] C. Lixon, N. Delpouve, a. Saiter, E. Dargent, Y. Grohens, Evidence of Cooperative Rearranging Region size anisotropy for drawn PET, Eur. Polym. J. 44 (2008) 3377–3384. doi:10.1016/j.eurpolymj.2008.08.001.

[53] N. Delpouve, C. Lixon, a. Saiter, E. Dargent, J. Grenet, Amorphous phase dynamics at the glass transition in drawn semi-crystalline polyester : DDDMA and TMDSC comparative studies, J. Therm. Anal. Calorim. 97 (2009) 541–546. doi:10.1007/s10973-008-9670-2.

Chapter 4 - Structural and dynamic heterogeneity in the amorphous phase of PLLA confined at the nanoscale by co-extrusion process

Les films polystyrène/poly (acide L-lactique) (PS/PLLA) ont été obtenus par le procédé de co-extrusion multi-nanocouches. Le PLLA a été confiné par le PS jusqu'à une épaisseur limite de 20 nm pour maintenir une bonne homogénéité et continuité des couches. Classiquement, l'isolement du PLLA amorphe induit un changement dans la mobilité moléculaire qui se manifeste par une baisse de la taille de la Région de Réorganisation Coopérative (CRR) lors de la transition vitreuse. Le recuit du PLLA sous confinement révèle que la cinétique de cristallisation est ralentie et que la géométrie de croissance cristalline est réduite à deux dimensions dans les couches confinées. Dans les systèmes avec des couches nanométriques, nous observons un découplage parfait entre les phases amorphes et cristallines, montré par l'absence de fraction rigide amorphe (RAF) lors de la cristallisation. En conséquence, l'hétérogénéité dynamique à la transition vitreuse reste étonnamment inchangée par la procédure de recuit. D'autre part, dans les polymères moins confinés où le niveau de couplage entre la phase amorphe et cristalline est élevé, la température de transition vitreuse augmente de manière significative tandis que la taille de la CCR diminue. On déduit que la dynamique de transition vitreuse dans les polymères semi-cristallins est fortement liée au paysage de la mobilité à l'interface avec des cristaux.

4. Structural and dynamic heterogeneity in the amorphous phase of PLLA confined at the nanoscale by co-extrusion process

Samira Fernandes Nassar[a], Sandra Domenek[a], Alain Guinault[b], Gregory Stoclet[d], Nicolas Delpouve[c], Cyrille Sollogoub[b*]

[a]UMR Ingénierie Procédés Aliments, AgroParisTech, INRA, Université Paris-Saclay, 1 avenue des Olympiades, F-91300 Massy, France

[b]PIMM, ENSAM - CNRS - CNAM, 151, Boulevard de l'Hôpital, F-75013 Paris, France

[c]Normandie Univ, UNIROUEN Normandie, INSA Rouen, CNRS, Groupe de Physique des Matériaux, 76000 Rouen, France

[d]UMR CNRS 8207, Unité Matériaux et Transformations, Université Lille1 Sciences et Technologies, Bâtiment C6, Université de Lille Nord de France, 59655 Villeneuve d'Ascq, France

Corresponding author: Cyrille Sollogoub, PIMM, Arts et Métiers ParisTech/CNRS/CNAM, 151 Bd de l'Hôpital, F-75013 Paris Cedex, France

Email: cyrille.sollogoub@cnam.fr

4.1. Abstract

Multi nanolayered Polystyrene/Poly(L-lactic acid) (PS/PLLA) films were obtained by layer multiplication coextrusion process. PLLA was confined by PS until a limit thickness of 20 nm to maintain good layer homogeneity and continuity. Classically the confinement of the amorphous PLLA induces a change in the molecular mobility which manifests by a drop of the Cooperative Rearranging Region (CRR) size at the glass transition. A subsequent annealing reveals that the crystallization kinetic is slowed down and that the crystalline growth geometry is reduced to two-dimensions in the confined layers. In the resulting nano-layered systems we observe a perfect decoupling between both amorphous and crystalline phases as no Rigid Amorphous Fraction (RAF) is generated during crystallization. As a consequence the dynamic heterogeneity at the glass transition remains surprisingly unaffected by the annealing procedure. On the other hand in bulk polymers where the level of coupling between amorphous and crystals is high, the glass transition temperature increases significantly whereas the CCR size falls. It is deduced that the glass transition dynamics in semi-crystalline polymers are strongly related to the mobility landscape at the interface with crystals.

Key words: PLLA, poly(lactic acid), confinement, RAF, rigid amorphous fraction, CRR

4.2.Introduction

Confining a polymer to a scale comparable to its different characteristic lengths (gyration radius or dimensions of the crystalline structure for example) leads to strong deviations of the structural and dynamical properties from the bulk. Since the pioneering work of Jackson and McKenna [1] on T_g deflection of organic liquids in nanopores, many studies [2–4] have discussed the effect of geometrical confinement on the molecular mobility and the glass transition temperature deviations of amorphous polymers. Similarly, crystallization under confinement has been shown to generate new mechanisms other than those usually observed in bulk crystallization, possibly leading to a great variety of crystalline morphologies, exhibiting unique preferential orientations [5–8]. In the aim of searching for finite size effects, a variety of experimental systems and geometries has been proposed to confine both amorphous and semi-crystalline polymers: droplet dispersions [9], thin films [10–12] or nano-layers [5,13], polymers infiltrated in inorganic nanotemplates (nanocylinders, nanolayers, nanospheres and nanopores) [14,15], self-assembled block copolymers [16–18]. Confinement can also be present, probably in a less regular and controllable way, in systems like polymer blends [19,20], nanocomposites [21,22] and semi-crystalline polymers [23–25].

In semi-crystalline polymers, amorphous phase appears to be constrained in the intra-spherulitic zone by the crystalline lamellae. This constraint is the consequence of both a geometrical confinement and a covalent coupling between the lamellae and the non-crystalline regions through tie molecules. The effect of this constraint on the molecular dynamics of the amorphous phase has been studied for several semi-crystalline polymers: polyethylene terephtalate (PET) [26,27], isotactic polypropylene (iPP) [28,29], polyamide 6 (PA6) [30], polyhydroxybutyrate (PHB) [31], polylactic acid PLA [32,33]. In many cases, a broadening of the glass transition temperature as well as a T_g shift to higher temperatures have been evidenced, reflecting a loss of mobility of the amorphous chain segments in the vicinity of the crystalline structure. When the coupling between the lamellae and the non-crystalline regions is strong enough, a separate nanophase can be produced at the interface between the two phases. A three phase model is therefore necessary to fully describe the semi-crystalline structure, in which the amorphous phase is split into two differently mobile fractions: the rigid amorphous fraction (RAF) as opposed to the mobile amorphous fraction (MAF) [34–36]. While the latter relaxes at the glass transition, the former devitrifies at higher temperatures than T_g. The exact temperature at which the RAF vitrifies and devitrifies has been extensively studied and seems to highly depend on

the type of polymer investigated [34]. Moreover, the presence of RAF, having its own specific properties, not only modifies the mobility of the amorphous phase but may impact also the macroscopic properties, especially mechanical [37,38] and gas barrier properties [39,40]. Therefore, this RAF must be taken into account and thoroughly characterized in order to propose a complete understanding of the structure – property relationships in semi-crystalline polymers. It seems besides of prime importance to identify the parameters responsible for the RAF formation, in order to be able to tailor the RAF and thus to optimize the macroscopic properties.

Poly Lactic acid (PLA), a biobased and biodegradable semi crystalline polymer, is a promising candidate to replace petroleum-based polymers [41,42], due to its several advantages like processability, satisfying stiffness, and high transparence. Due to its slow crystallization rate and its various polymorphic forms [43], it is possible to create many samples with various crystallinity degrees and morphologies, which makes PLA interesting candidate to better understand the coupling between the amorphous phase and the crystal development. Depending on the crystallization conditions, the RAF content created in PLLA varies from 10% to 30% [44–52], and deteriorates the gas barrier properties of PLA [50,51,53], due to the fact that the RAF is a dedensified phase [47]. Cocca et al. [54] suggested that the presence of RAF can also influence the mechanical behavior of PLLA.

The RAF formation in PLA has been clearly correlated with the crystal growth [50,52,55]: at low crystallization temperature, the RAF develops in parallel with the crystals, whereas for higher crystallization temperatures, the RAF appears at long crystallization time in correspondence with the secondary crystallization, occurring after spherulite impingement, highlighting the link between RAF formation and the chain mobility in the amorphous phase. Different theoretical approaches and experimental techniques (thermal analysis, dielectric relaxation spectroscopy, and dynamic mechanical analysis) have been used to investigate the effect of the geometrical confinement induced by the spherulitic structures on the dynamics of amorphous phase in semi-crystalline PLA. While Mijovic et al. [56] haven't observed any change in the glass transition dynamics upon crystallization, some other authors [46,57] have evidenced a clear confinement effect appearing during primary crystallization, inducing RAF formation, T_g elevation and increased dynamic fragility around T_g. For example, Delpouve et al.[58], using the concept of Cooperative Rearranging Regions (CRR), originally introduced by Adam and Gibbs [59], and following Donth's approach [60], have evidenced [48,58,61] a

confining effect due to the crystallization and leading to a drastic reduction in the characteristic length of this CRR.

Common techniques have been used to study PLA behavior in confined nanometer space, using block copolymers [62,63] or thin films [64,65]. Nevertheless, all these studies were focused only on the impact of confinement on the crystallization of PLA. In the present work, PLA is confined using the original nanolayer coextrusion process, a relevant tool to investigate the effect of confinement on crystallization [5,66,67] or macromolecular dynamics [68–70]. The study of amorphous and crystallized PLA nanolayered films should shed additional light above the macromolecular mobility in the amorphous phase and the coupling between the amorphous and crystalline phases in PLA.

4.3.Experimental

4.3.1. Process and crystallization parameters

Polylactide (PLLA) pellets were purchased from Corbion Purac (PLA REVODE 190). The content of L-lactide was higher than 99%. Polystyrene (PS) pellets were obtained from Total Petrochemicals (PS 1340).

A layer multiplication coextrusion process was used to fabricate multilayered films of 3, 512 and 2049 alternating layers of PLLA and PS. The process is presented in the *Figure 4.1*. It consists in two single screw extruders of 20 mm with gear pumps, a three-layer feed block (A-B-A), a series of layer-multiplying elements, a flat die and chill rolls. The PLLA was extruded to form the external layers of the films and PS the central layer. The composition of the PS/PLLA films is 75/25 (m/m). The initial three-layer polymer flow enters a mixing section, followed by a sequence of layer-multiplying elements. The melt was initially cut in half vertically, and then both flows were superposed, compressed and stretched to its original width, hence doubling the number of layers with each layer-multiplying element. A series of n elements leads thus to $2^{n+1}+1$ alternating layers. The extrusion conditions are given in Supplementary Information (SI 1).

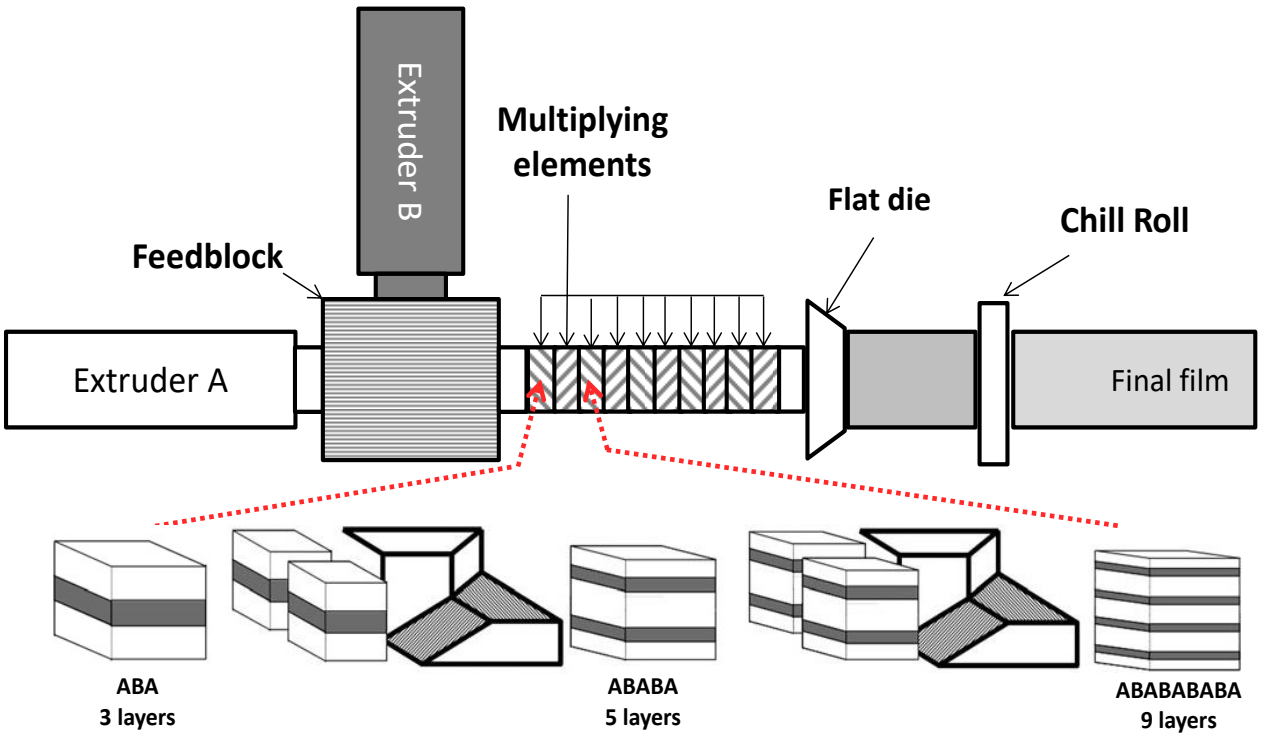

Figure 4.1. Principle of the multilayer coextrusion process

Our objective was to obtain films with individual PLLA layer thicknesses of 30000, 300, and 20 nm. This individual thickness was dependent on the final thickness of the film and the number of multiplying elements. The conditions of process and the films characteristics are given in *Table 4.1*. After extrusion the multilayered PLLA/PS films were isothermally recrystallized. For the annealing treatment, the films were sandwiched between two sheets of Teflon and two stainless steel plates, then thermocompressed for 180 minutes using a heat press (Darragon, France), at 85°C, i.e., a temperature situated between the glass transition temperature of PLLA and PS, and a pressure set to 5 x 10^6 Pa. The annealing temperature for crystallization was chosen in relation with the glass transition temperature of the two coextruded polymers. In order to preserve the layer integrity of the confining polymer, and therefore to maintain the geometrical confinement, the annealing temperature has to be below the glass transition temperature of the confining polymer ($T_{g\ PS}$ = 100°C). The crystallization temperature must besides be higher than $T_{g\ PLLA}$, located around 60°C.

Table 4.1. PS/PLLA multilayered films technical characteristics and process conditions.

Number of multiplying elements	Number of layers	Draw ratio	Film total thickness (μm)	PLLA nominal thickness (nm)
0	3	2	120	30000
8	512	2	300	300
10	2049	6	80	20

4.3.2. Characterization

Melt rheology. The melt viscosity of PLLA and PS was measured using an Anton Paar MCR 502 rheometer in an oscillatory mode between 0.01 and 100 rad/s. The deformation was previously determined by performing preliminary deformation sweeps, and was set to 1% for both polymers. The shear viscosity as a function of shear rate can be deduced from these measurements using the Cox-Merz rule.

Atomic force microscopy (AFM). AFM was used to characterize the layered morphology of the coextruded films. AFM images were obtained in tapping mode using a multimode microscope controlled by a Veeco Nanoscope V controller. The tips (silicon, spring constant 40 N/m, oscillation frequency ca. 300 kHz) had a radius of curvature less than 10 nm. Specimens were taken from the center of the extruded films and were cut from the cross section with an ultramicrotome 2088 Ultrotome V (LKB) equipped with a diamond knife at a cutting speed of 1 mm/s. 15 images were recorded at full resolution (4096 × 4096 pixels), with a scan rate of 0.9 Hz, throughout the thickness of the film. Following the analysis developed by Bironeau et al [71], the analysis of these 15 images containing each around 20 layers is representative of the whole sample with an uncertainty of 10%.

Wide Angle X-Ray Scattering (WAXS). WAXS analyses were carried out using a PANanalytical sealed tube operating at 40 kV and 20 mA. The Cu Kα radiation (λ = 1.54 Å) was selected with a nickel filter. The WAXS patterns were recorded on a 2-D CCD camera (Photonic Science). Analyzes of the kinetics of isothermal crystallization were made using the same X-ray generator and heating in situ the sample in a hot plate.

Modulated Temperature Differential Scanning Calorimetry (MT-DSC). The MT-DSC analysis was performed on a Thermal Analysis® Instrument DSC Q100. Nitrogen was used as purge gas (50 mL/min). The samples weights were about 5-10 mg, encapsulated in Tzero hermetic aluminum pans. Calibration in temperature and enthalpy was carried out using an indium standard. The specific heat capacity of each sample was measured using sapphire as a reference. The glass transition region of PLLA was analyzed using a heat-cool temperature modulation (oscillation amplitude of 3 K, oscillation period of 120 s, and heating rate of 1 K min^{-1}). The crystallization and melting of PLLA was analyzed using a heat-only temperature modulation (oscillation amplitude of 0.32 K, oscillation period of 60 s, and heating rate of 2 K min^{-1}). By MT-DSC, in addition of the modulated heat flow, the apparent specific complex heat capacity C* is obtained from the complete deconvolution procedure proposed by Reading and co-authors [72]. Its in-phase component versus temperature C' appears as a step, when its out-of-phase component C'' draws a peak in the glass transition region.

4.4. Results and discussion

4.4.1. Optimization of the layer multiplying co-extrusion process

The uniformity and continuity of the layers depend strongly on the viscosity ratio ρ between two polymers, defined as follows:

$$\rho = \frac{\eta_{confined}}{\eta_{confining}} \qquad \text{Equation 4.1}$$

Where $\eta_{confined}$ and $\eta_{confining}$ are respectively the viscosity of the confined polymer (in our case PLA) and confining polymer (PS). A poor viscosity ratio can result in phenomena of encapsulation of the polymer of high viscosity by the polymer of lower viscosity [13].
Figure 4.2 plots the viscosity of PLLA and PS (*Figure 4.2*a) and the viscosity ratio (*Figure 4.2*b) as a function of the shear rate. In the shear rate range of coextrusion process, typically between 1 and 50 s^{-1}, the viscosity ratio is close to 1, which ensures homogeneity of the stratified flow.

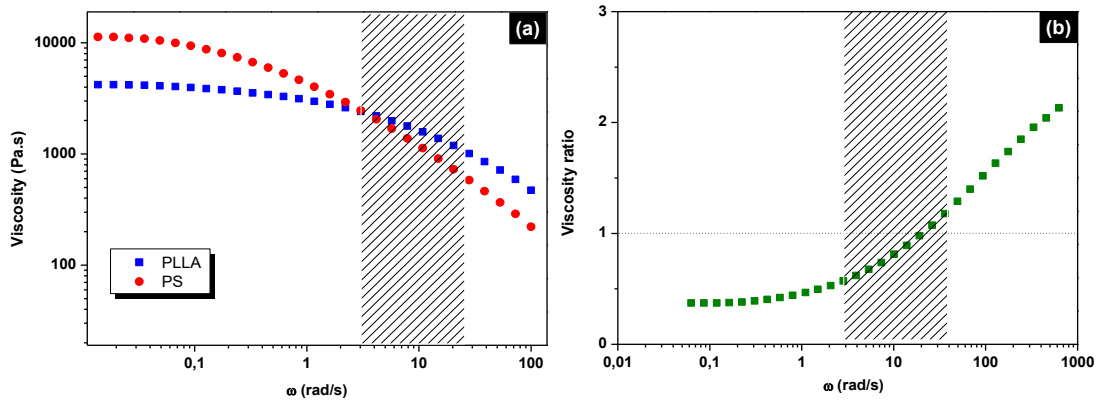

Figure 4.2. (a) Viscosity curves of PLLA and PS (b) Viscosity ratio for PS/PLLA. The hatched zone corresponds to the shear rates found in the co-extrusion process, considering the law of Cox-Merz.

This homogeneity is confirmed by the images obtained with AFM. *Figure 4.*3 exhibits the AFM phase images obtained on as-extruded and annealed films. A reasonable contrast between the two components (PS appears bright and PLLA dark) enables to reveal the layered structure and to perform image analysis in order to measure a thickness distribution of the layers.

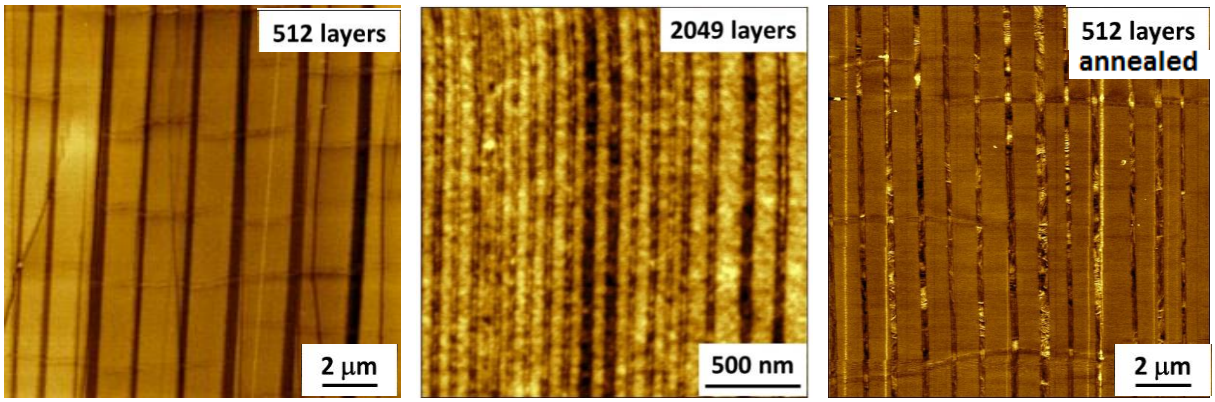

Figure 4.3. Tapping mode AFM phase images of nanolayered amorphous PS/PLLA containing different number of layers as indicated.

The AFM images show continuous and relatively uniform layers of PS and PLLA. The average layer thicknesses of PLLA is 220 ± 50 nm for the films containing 512 layers and 20 ± 5 nm for the films with 2049 layers, which is in reasonable agreement with the expected nominal thickness given in *Table 4.2*. The observed distributions of thickness of PLLA layers for each

sample (8 multiplying elements) and (10 multiplying elements) are shown in *Figure 4.4*a and 4.4b, respectively. As represented in red lines, normal distribution curves have been fitted to the experimental data. Experimental data and fit are in good agreement. After crystallization, it can be observed that the layer continuity is maintained (*Figure 4.3*).

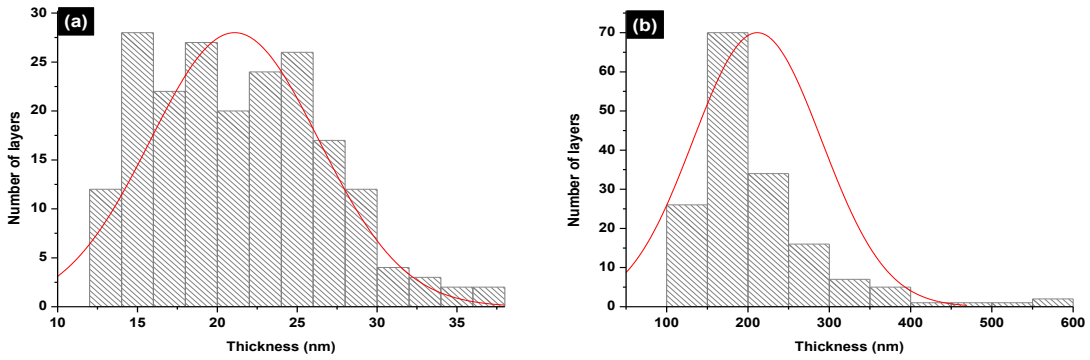

Figure 4.4. Distribution of PLLA layer thickness for 10 (a) and 8 (b) multiplying elements. The red lines represent the normal distribution curves.

4.4.2. Crystallization of PLLA under confinement

*Figure 4.5*a shows the WAXS patterns obtained on as extruded PS/PLLA films. Only the amorphous halo of PLLA and PS was visible, indicating that PLLA was amorphous at the end of extrusion. This was expected because it is known that PLA has a slow crystallization kinetic [73,74] although the stereoregularity of the polymer chain decreases this time, which is around 11 min for PLLA at 85 °C [73]. *Figure 4.5*b shows the WAXS diffractograms of annealed PLLA after 3 h at 85 °C. The strong reflections of PLLA attributed to the 200/110 and 203 planes can be observed for all samples.[75,76] The present crystallization temperature would theoretically favor the α'-polymorph of PLLA [49,51]. However the minor reflections characteristic of the α'-polymorph were not observed. As a consequence, those investigations do not allow describing the crystalline polymorph.

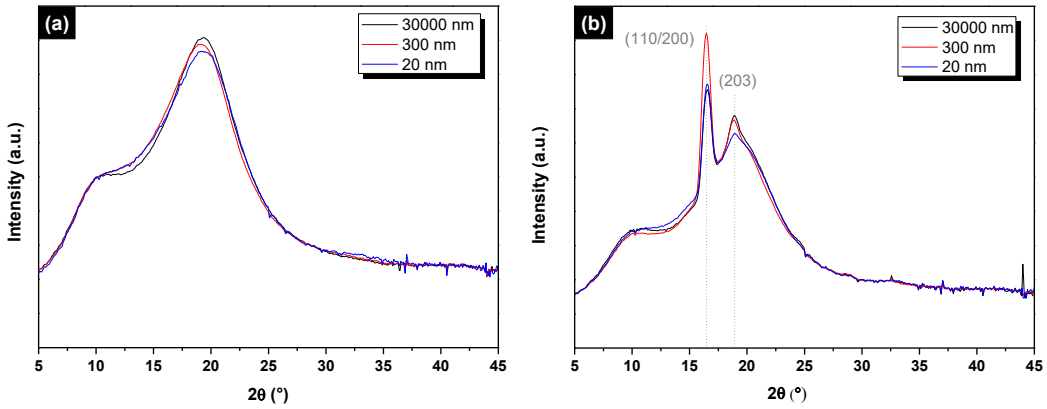

Figure 4.5. WAXS intensity profiles of PS/PLLA films (a) before annealing (b) after annealing at 85°C during 180 minutes.

In the aim to study the impact of the confinement on the crystallization kinetics of PLLA, the relative crystallinity of PLLA was recorded by WAXS during isothermal annealing at 85 °C for different layer thicknesses. The results are shown in the *Figure 4.6*. While the crystallization kinetic of the three-layer extruded films (30000 nm) superimposes with the pure PLLA film one, the overall crystallization rate is delayed as the layer thickness decreases. which has been already observed on multilayer coextruded PEO and PET by Baer et al.[77][78].

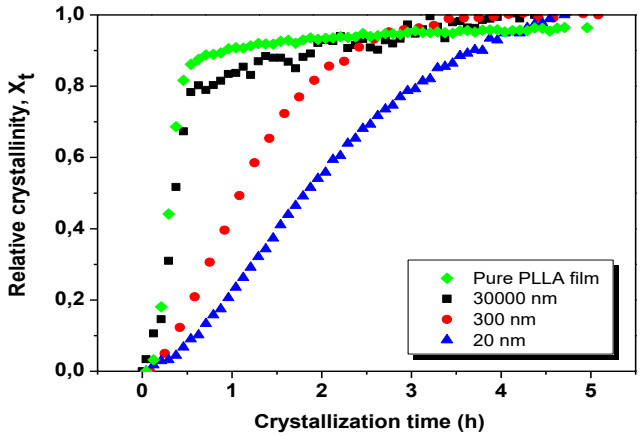

Figure 4.6. Relative crystallinity of PLLA (X_t) versus crystallization time for isothermal crystallization at 85 °C

Isothermal crystallization behavior of PLLA has been analyzed from Avrami equation.

$$\alpha(t) = 1 - \exp(-K \cdot t^n) \qquad \text{Equation 4.2}$$

Where $\alpha(t)$ is the relative crystallinity fraction at time t, K is the crystallization rate constant and n is the Avrami exponent depending on the nucleation (homogeneous or heterogeneous) and the growth geometry (sphere, disc, etc.) [79]. *Equation 4.2* can be transformed into the following form:

$$\ln(-\ln(1-\alpha(t))) = n\ln(t) + \ln K \qquad \text{Equation 4.3}$$

The kinetic parameters n and K can therefore be obtained by plotting $\ln(-\ln(1-\alpha(t)))$ as a function of ln(t). In literature, the curvature in the Avrami plots (non-linear behavior) is attributed to the secondary crystallization [80]. The Avrami model in *Figure 4.7*a for 20 and 300 nm samples fits well with experiments, which corresponds to linear curves for the double logarithm of the relative crystallinity in *Figure 4.7*b. For 20 nm and 300 nm, n=1.7 and 1.6 respectively (*Table 4.2*), which corresponds, according to the Avrami theory [79], to a two dimensional crystallization growth with an instantaneous nucleation. For 30000 nm sample, it appears that the Avrami model fits well for relative crystallinity below 0.8 with an Avrami exponent n=3.3 which is associated to a three dimensional crystallization growth with an instantaneous nucleation. However, a non-linear behavior can be observed, suggesting a secondary crystallization in 30000 nm sample (*Figure 4.7*). The crystallization rate (K) and crystallization half-time ($t_{1/2}$) are shown in *Table 4.2*. We observed a decrease in K when PLLA thickness decreases, which is consistent with the increase in $t_{1/2}$. To summarize, in the confined layer the crystalline growth is restricted to two dimensions and occurs slower.

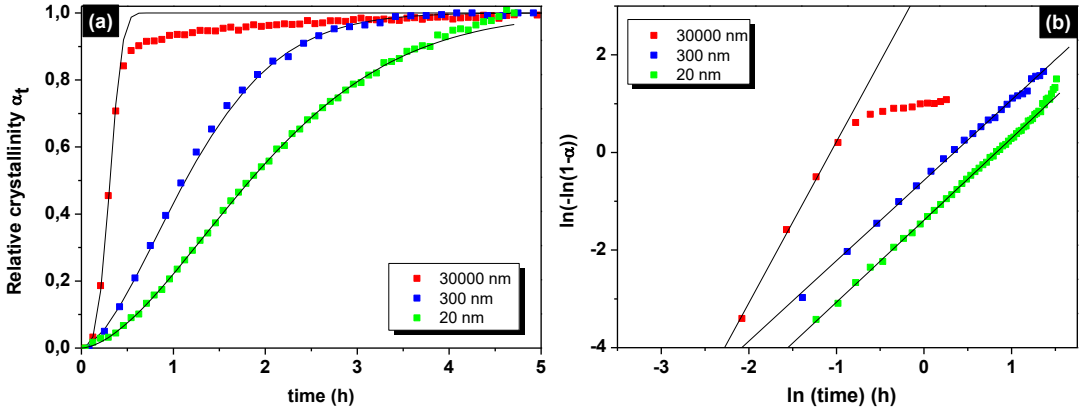

Figure 4.7. (a) Relative crystallization and Avrami model versus time for 30000 nm, 300 nm and 20 nm isothermal crystallization at 85°C. (b) Double logarithm versus ln(time) and the Avrami model (black lines) for annealed samples (30000 nm, 300 nm and 20 nm) at 85°C.

As previously mentioned PLLA is described by a three-phase model and the quantification of each fraction is possible from calorimetric analysis. The degree of crystallinity (X_c) of the PLA samples was calculated from

$$X_c = \frac{\Delta H_f - \Delta H_{cc}}{\Delta H_f^0} \qquad \text{Equation 4.4}$$

Where ΔH_f is the enthalpy of fusion or melting after subtraction of the small exothermal event at the beginning of the melting peak, ΔH_{cc} is the enthalpy of the cold crystallization (both ΔH_f and ΔH_{cc} are normalized to PLLA content), and $\Delta H_f°$ is the enthalpy of the melting of the perfect crystal of infinite size, i.e. the totally crystalline polymer (93.1 J/g) [81]. The use of MT-DSC is specifically required in the present study as the glass transition of PS falls in the same temperature domain than the cold crystallization of PLLA. An example of the analysis procedure is given in supplementary material (SI 2). The difference between the enthalpy of cold-crystallization and the enthalpy of melting for the determination of the degree of crystallinity has been double checked using the average heat flow signal on the one hand as usually performed from classical DSC, and both the reversing and the non-reversing heat flow signals from MT-DSC on the other hand. At low crystallization temperature (i.e. crystallization temperatures near the glass transition), polymer chains have low mobility, which hampers the

organization of the polymeric segments in ordered crystal structures and causes coupling of the crystalline and amorphous phase by tie chains. The coupling can be observed by the existence of the RAF, which does not devitrify at the polymer glass transition and develops at the early stages of crystallization. Many studies observed the presence of rigid amorphous phase (RAF) in polylactide when it is isothermally crystallized at 85°C [46,48,50,51,55]. The content of the RAF X_{RA} can be calculated from

$$X_c + X_{MA} + X_{RA} = 100\% \text{ with } X_{MA} = \frac{\Delta C_p}{\Delta C_p^0} \qquad \text{Equation 4.5}$$

Where X_{MA} is the content of MAF, ΔCp is the heat capacity change measured at the glass transition and ΔCp^0 the heat capacity change of the fully amorphous sample. ΔCp^0 was recorded and used in comparison with the bulk to check the absence of crystallites in the PLLA films after the fabrication. The numerical results are presented in *Table 4.2*. The crystallinity degree of PLLA after annealing increased with the decrease of the layer thickness. The underlying physics are not yet established and different types of behaviour were already observed. Mackey et al.[82] showed a slight decrease in crystallinity for confined polyvinylidene fluoride (PVDF), while Wang et al.[66] did not observe any difference in crystallinity for confined poly(ethylene oxide) (PEO). Our result is comparable to the one of Boufarguine et al.[67] for the couple PLA/PHBV, who showed an increased crystallinity degree for PHBV when confined in thin layers, possibly attributed to the strong molecular orientation induced by the polymer flow in multiplying elements [67]. On the other hand the RAF of PLLA decreases from about 40 to 10% as the layer thickness decreases (from 30000 to 300 nm) and it disappeared when PLLA was confined in layers of 20 nm thicknesses although its degree of crystallinity is the highest. This means that the decoupling between both crystalline and amorphous phases is more successful when reducing the size of the layer. Several hypotheses can be suggested to explain this result. It might be associated to a pure geometric constraint effect. It has been proposed that the domain of molecular segments involved in the coupling should reach a critical length to produce an intermediate phase [39]. In a layer space of 20 nm the amorphous phase is strongly confined by the few crystalline lamellae allowed to form and its size is dramatically reduced. This effect is even more pronounced due to the increase of the crystallinity degree with the number of layers. One may also relate this result to the change in the crystalline growth from a three dimensional to a two dimensional order as deduced from the Avrami equation.

Nevertheless the Avrami exponents are the same for both 300 and 20 nm PLLA layer while the RAF content decreases with the thickness. Finally the development of RAF may be impacted by the crystallization kinetic. As shown in *Figure 4.6*, for three hours annealing and depending on the layer nominal thickness, the maximum crystallinity degree has been reached hours ago (30000 nm), minutes ago (300 nm), or roughly reached (20 nm). In a previous work we reported that prolonging the annealing time favours the gradual conversion of MAF into RAF with time [50]. One can consider that the shift in the crystallization kinetic to longer durations offers the opportunity to manage the time of crystallization in order to suppress the occurrence of the Rigid Amorphous Fraction. Whatever the predominant cause for the critical difference in coupling between confined and non confined samples, the impact of the multilayer coextrusion process is obvious in the same annealing conditions. This observation is not limited to the crystalline phase development, but it also concerns the structural heterogeneity in the amorphous phase.

Table 4.2. Structural and thermal parameters of PLLA confined at different thickness obtained from in-situ WAXS and MT-DSC heat-only analyses.

PLLA nominal thickness	$t_{1/2}$ (h)	n	K (h^{-n})	ΔC_p^0 ($Jg^{-1}K^{-1}$)	ΔC_p ($Jg^{-1}K^{-1}$)	X_c (%)	X_{MA} (%)	X_{RA} (%)
30000 nm	0.31	3.3	33.52	0.48	0.16	28	33	39
300 nm	1.13	1.6	0.57	0.44	0.24	36	55	9
20 nm	1.84	1.7	0.25	0.44	0.25	44	56	0

Annealing conditions: 85 °C during 3h
$t_{1/2}$ the crystallization half-time
n the Avrami exponent
K the crystallization rate constant
ΔC_p^0 the heat capacity step of PLLA with a nil crystallinity degree
ΔC_p the heat capacity step of annealed PLLA
X_c the crystallinity degree
X_{MA} the content of the mobile amorphous phase fraction (MAF)
X_{RA} the content of the rigid amorphous phase fraction (RAF)

4.4.3. Dynamic heterogeneity of confined PLLA

The mobility landscape of the amorphous phase can be pictured by the size of the cooperative rearranging regions (CRR), which can be calculated directly from MT-DSC measurements using Donth's approach.[60,83] An example of how to retrieve the required physical quantities is shown in Supplementary Information (SI 3). The cooperativity volume $\xi_{T\alpha}{}^3$ of a CRR at the dynamic glass transition temperature T_α can be estimated from the equation below:

$$\xi_{T\alpha}^{3} = \frac{\left(1/C_p\right)_{Glass\ T\alpha} - \left(1/C_p\right)_{Liquid\ T\alpha}}{\rho(\delta T)^2} k_B T_\alpha^2 \qquad \text{Equation 4.6}$$

Where k_B is the Boltzmann constant, δT the average temperature fluctuation related to the dynamic glass transition of a CRR determined from the Gaussian fit of C'' [83], ρ the density equal to 1.25 g cm^{-3} for the amorphous phase of PLLA, and C_p the heat capacity at constant pressure. The values of $C_{p\ glass\ T\alpha}$ and $C_{p\ liquid\ T\alpha}$ are obtained from the C' signal by prolonging the glass and liquid lines to dynamic glass transition temperature after normalization to the quantity relaxing at the glass transition.

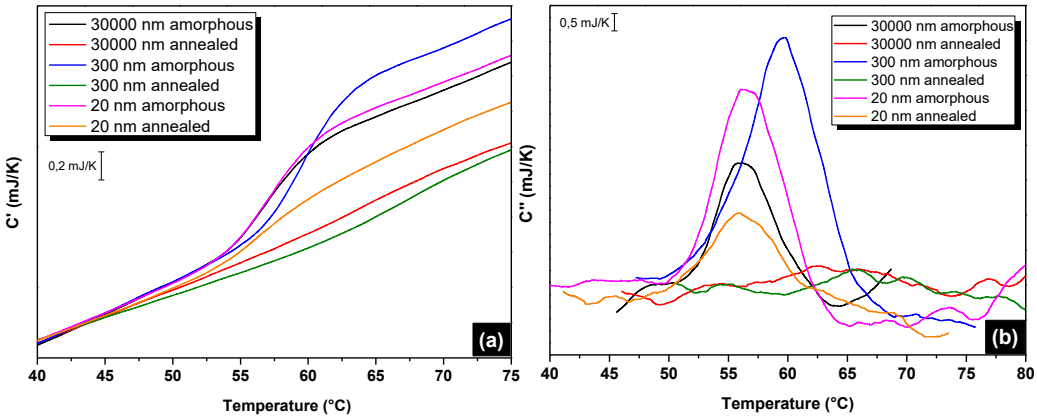

Figure 4.8. Temperature dependence of (a) real part (C') (b) imaginary part (C'') of complex heat capacity (C*) for different multilayered PS/PLLA film when PLLA is amorphous and crystallized.

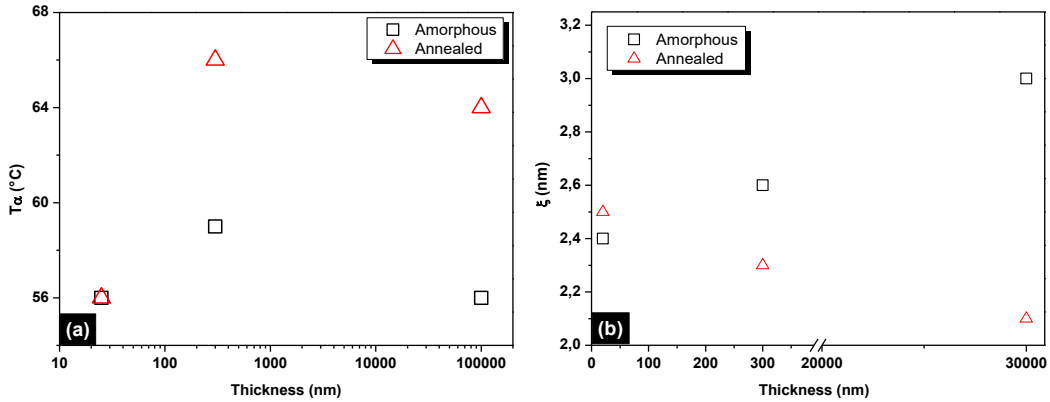

Figure 4.9. (a) Variation of dynamic glass transition temperature (Ta) for amorphous and crystallized PLLA (b) Cooperativity length of amorphous and crystallized PLLA; as a function of layers thickness

The real part and imaginary part of the complex heat capacity during the glass transition of PLLA are presented in *Figure 4.8*. The curves are presented before any normalization; however the C' curves have been shifted for the consistency of Cp_{glass} with the computed values linked to the vibrational molecular motions as recommended by Pyda et al. [84]. For all samples the increase of the crystallinity degree (X_c) of PLLA induced by the annealing causes the decrease of the amplitude of the heat capacity change because less amorphous phase is available for relaxation (*Figure 4.8*a). For the thicker layers (30000 and 300 nm) one can observe the classic effect of crystallization on the amorphous phase relaxation. The dynamic glass transition T_α is shifted of about 7°C to higher temperatures (*Figure 4.8*b) due to the constraints generated by the crystalline environment. This effect is largely described in bulk materials, because the amorphous phase requires more thermal energy for relaxation in presence of crystallites [71]. Zuza et al. among others reported an increase of T_g associated with the concomitant presence of crystals and RAF [46]. Moreover the glass transition domain significantly broadens meaning that δT increases. Therefore the peak of C" of annealed PLLA in the thicker layers almost disappeared due to its lower intensity and important enlargement. For a nominal thickness of 20 nm the C'' peak is perfectly discernible. Moreover neither the shift of T_α nor the increase of δT is observed. This reveals a different impact of crystallization on the relaxation dynamics for the most confined sample. As previously mentioned, the two multilayer coextruded annealed materials mostly differ structurally by their crystalline phase and RAF content. In the 20 nm nominal thickness PLLA the decoupling between the amorphous and crystalline phase is the

most successful leading to both the highest crystallinity degree and the absence of RAF. Saiter et al. reported that the glass transition temperature of polylactide is barely impacted by crystallization when the annealing conditions favor the decoupling [85]. This is apparent in *Figure 4.9*a presenting the values of T_α for both amorphous and crystallized samples. The highest shift of T_α after annealing that is equal to 8 °C, is observed for the material exhibiting the lowest X_c but the highest X_{RA}. Besides there is no evidence of a relation between T_α and the relaxing layer thickness even in the amorphous state. As shown in *Figure 4.9*b the cooperativity length in amorphous PLLA decreases with the PLLA nominal layer thickness. For the amorphous phase, the effect of confinement on the CRR size is in agreement with other studies on amorphous polymers, where the cooperativity at T_g decreases in confined systems ((Tran et al. [86] for poly(methyl methacrylate), Arabeche et al.[68] for poly(methyl methacrylate) and polycarbonate, Tomczak et al. [87] for PS). This cooperativity decrease should normally result in a T_g depression, which is not exactly observed in our case. The more complex T_g variation may reveal antagonist mechanisms involved in the relaxation such as confinement, tortuosity, coupling, and interface interactions (PS/PLLA). Since the dimension of the MAF decreases during the crystallization, it is expected that the cooperativity length will follow the same tendency as reported by several authors for bulk PLA [46,50,58]. However by decreasing the PLLA layer thickness the drop of the cooperativity length caused by the annealing tends to minimize. For the most confined material one can even observe that the cooperativity length remains unchanged after the crystallization. Esposito et al. [88] have shown that the width of the glass transition in semi-crystalline materials is strongly related to the level of coupling between both amorphous and crystalline phases. If the level of coupling is high the structural constraints generated by the crystalline phase progressively transfer in the non-crystalline part of the material. This leads to a gradient of mobility in the amorphous phase that translates in a broad distribution of relaxation temperatures during a MT-DSC analysis and therefore to significantly reduced CRR sizes. The progressive disappearance of the RAF with the reduction of the PLLA nominal thickness is consistent with the progressive invariance of the CRR size in comparison to an amorphous sample. A schematic representation of the respective influence of confinement and coupling on the dynamic heterogeneity is proposed in *Figure 4.10*. For the amorphous materials the reduction of the CRR size with the PLLA layer thickness is mostly guided by geometric restrictions imposed by the neighboring layers of PS. Because the volume allowed for relaxation is decreasing, this fall of cooperativity can be considered as a pure confinement effect. The additional constraint brought by the crystal growth

differs from a pure confinement effect because the macromolecule is both part of the confining and the confined part. In such a landscape the role of the RAF is underlined since the volume of the MAF involved in the relaxation is dependent on its decoupling from the crystal.

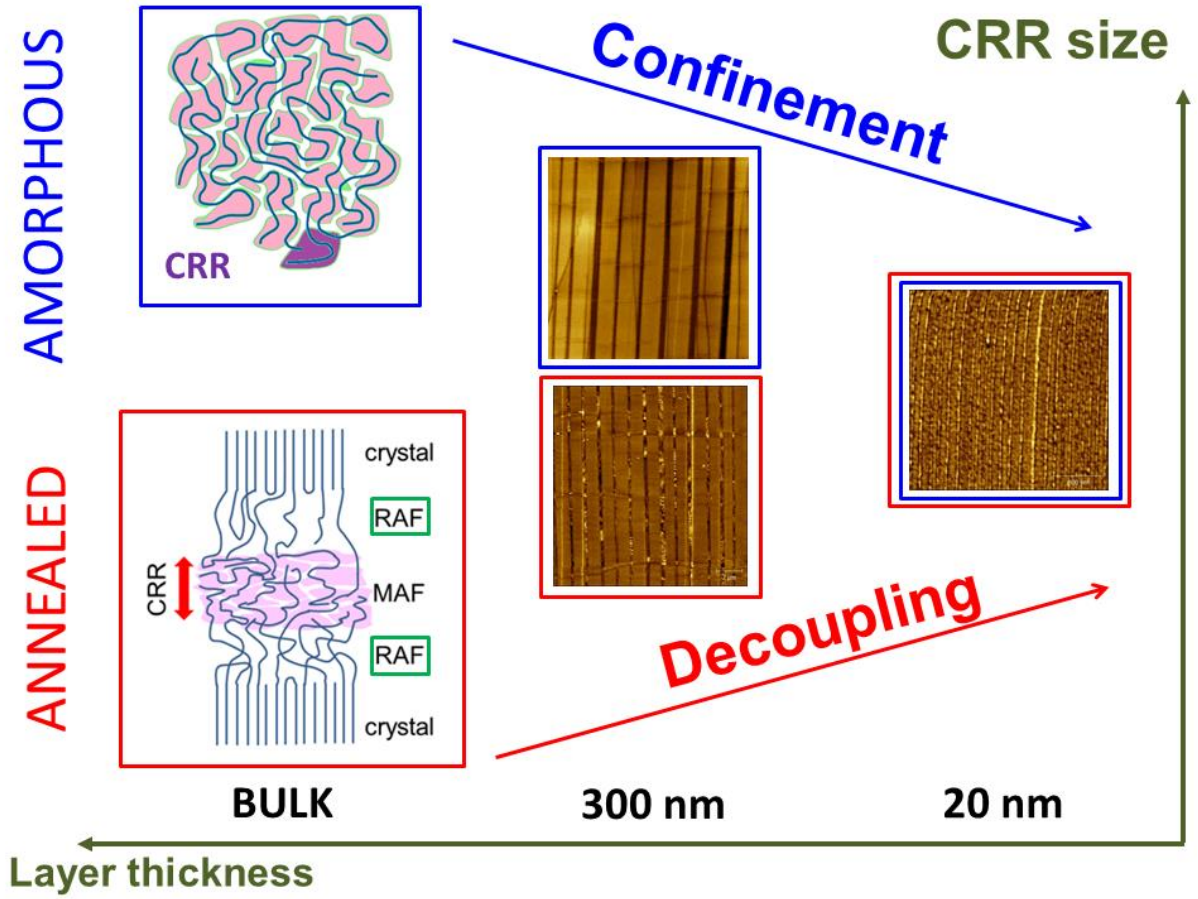

Figure 4.10. Role of confinement and coupling on the variations of cooperativity in multilayer coextruded samples

4.5. Conclusion

In a nanoscale confined area created from multilayer coextrusion process, the crystallization of PLLA is modified in terms of kinetic and dimensional growth. By multiplying the number of alternating layers of PS and PLLA, the crystallization conditions can be sufficiently disturbed to also impact the level of coupling between both amorphous and crystals. The coupling has a major role in the glass transition dynamics of semi-crystalline polymers as it brings an additional mobility constraint to the system which results in an increase of the dynamic

heterogeneity. Thus the broadening of the glass transition during crystallization is the caused by both geometric restrictions and interfacial interactions.

4.6. References

[1] C.L. Jackson, G.B. McKenna, The glass transition of organic liquids confined to small pores, J. Non. Cryst. Solids. 131-133 (1991) 221–224. doi:10.1016/0022-3093(91)90305-P.

[2] M. Alcoutlabi, G.B. McKenna, Effects of confinement on material behaviour at the nanometre size scale, J. Physics-Condensed Matter. 17 (2005) 461–524. doi:10.1088/0953-8984/17/15/R01.

[3] J.A. Forrest, K. Dalnoki-Veress, The glass transition in thin polymer films, Adv. Colloid Interface Sci. 94 (2001) 167–196. doi:10.1016/S0001-8686(01)00060-4.

[4] F. Kremer, M. Tress, E.U. Mapesa, Glassy dynamics and glass transition in nanometric layers and films: A silver lining on the horizon, J. Non. Cryst. Solids. 407 (2015) 277–283. doi:10.1016/j.jnoncrysol.2014.08.016.

[5] J.M. Carr, D.S. Langhe, M.T. Ponting, A. Hiltner, E. Baer, Confined crystallization in polymer nanolayered films: A review, J. Mater. Res. 27 (2012) 1326–1350. doi:10.1557/jmr.2012.17.

[6] Y.X. Liu, E.Q. Chen, Polymer crystallization of ultrathin films on solid substrates, Coord. Chem. Rev. 254 (2010) 1011–1037. doi:10.1016/j.ccr.2010.02.017.

[7] R.M. Michell, A.J. Müller, Confined crystallization of polymeric materials, Prog. Polym. Sci. 54-55 (2016) 183–213. doi:10.1016/j.progpolymsci.2015.10.007.

[8] R.E. Prud'homme, Crystallization and morphology of ultrathin films of homopolymers and polymer blends, Prog. Polym. Sci. 54-55 (2015) 214–231. doi:10.1016/j.progpolymsci.2015.11.001.

[9] M. V. Massa, K. Dalnoki-Veress, Homogeneous crystallization of poly(ethylene oxide) confined to droplets: The dependence of the crystal nucleation rate on length scale and temperature, Phys. Rev. Lett. 92 (2004) 255509–1. doi:10.1103/PhysRevLett.92.255509.

[10] C.W. Frank, V. Rao, M.M. Despotopoulou, R.F.W. Pease, W.D. Hinsberg, R.D. Miller, J.F. Rabolt, Structure in Thin and Ultrathin Spin-Cast Polymer Films, Science (80-.). 273 (1996) 912–915. doi:10.1126/science.273.5277.912.

[11] J.L. Keddie, R. a L. Jones, R. a Cory, Size-Dependent Depression of the Glass Transition Temperature in Polymer Films, Epl. 27 (1994) 59–64. doi:10.1209/0295-5075/27/1/011.

[12] J.A. Forrest, J.R. Dutcher, Interface and chain confinement effects on the glass transition temperature of thin polymer film, Phys. Rev. E. 56 (1997) 5705–5716.

[13] M. Ponting, A. Hiltner, E. Baer, Polymer nanostructures by forced assembly: Process, structure, and properties, Macromol. Symp. 294 (2010) 19–32. doi:10.1002/masy.201050803.

[14] C.L. Jackson, G.B. McKenna, Vitrification and Crystallization of Organic Liquids Confined to Nanoscale Pores, Chem. Mater. 8 (1996) 2128–2137. doi:10.1021/cm9601188.

[15] R.M. Michell, I. Blaszczyk-Lezak, C. Mijangos, A.J. Müller, Confined crystallization of polymers within anodic aluminum oxide templates, J. Polym. Sci. Part B Polym. Phys. 52 (2014) 1179–1194. doi:10.1002/polb.23553.

[16] B.Y. Wang, S. Krause, Properties of Dimethylsiloxane Microphases in Phase-Separated Dimethylsiloxane Block Copolymers, Macromolecules. 20 (1987) 2201–2208. doi:10.1021/ma00175a026.

[17] I.W. Hamley, Crystallization in Block Copolymers .pdf, Adv. Polym. Sci. 148 (1999) 113–137. doi:10.1007/3-540-48836-7_2.

[18] A.J. Müller, V. Balsamo, M.L. Arnal, Crystallization Copolymers in Diblock and Triblock, (2004) 1–62.

[19] G. Zhong, R. Su, L. Zhang, K. Wang, Z. Li, H. Fong, L. Zhu, Evolution of nanodroplets and fractionated crystallization in thermally annealed electrospun blend fibers of poly(vinylidene fluoride) and polysulfone, Polym. (United Kingdom). 53 (2012) 4472–4480. doi:10.1016/j.polymer.2012.08.014.

[20] T. Wang, H. Li, F. Wang, S. Yan, J.M. Schultz, Confined growth of poly(butylene succinate) in its miscible blends with poly(vinylidene fluoride): Morphology and growth kinetics, J. Phys. Chem. B. 115 (2011) 7814–7822. doi:10.1021/jp203680e.

[21] Z. Wang, X. Fan, K. Wang, H. Deng, F. Chen, Q. Fu, B. Na, Ordered long-helical conformation of isotactic polypropylene obtained in constrained environment of nanoclay, Polym. Adv. Technol. 22 (2011) 1375–1380. doi:10.1002/pat.1827.

[22] H.D. Huang, J.Z. Xu, Y. Fan, L. Xu, Z.M. Li, Poly(l-lactic acid) crystallization in a confined space containing graphene oxide nanosheets, J. Phys. Chem. B. 117 (2013) 10641–10651. doi:10.1021/jp4055796.

[23] C. Schick, E. Donth, Characteristic length of glass transition: experimental evidence Characteristic Length of G lass Transition : Experimenta I Evidence, Phys. Scr. 43 (1991) 423–429. http://iopscience.iop.org/1402-4896/43/4/010.

[24] S. Aharoni, Increased glass transition temperature in motionally constrained semicrystalline polymers, Polym. Adv. Technol. 9 (1998) 169–201. doi:papers://590F92D9-0B76-4B88-8729-9AF064BE5AC8/Paper/p5653.

[25] J. Dobbertin, A. Hensei, C. Schick, Dielectric Spectroscopy and Calorimetry in the Glass Transition Region of Semi- Crystalline Poly (Ethylene Terephthalate), J. Therm. Anal. Calorim. 47 (1996) 1027–1040. doi:10.1007/BF01979446.

[26] B.W. J. Menczel, Heat capacity hysteresis of semicrystalline macromolecular glasses, J. Polym. Sci. Polym. Lett. Ed. 19 (1981) 261–264. doi:10.1002/pol.1981.130190506.

[27] R. Androsch, B. Wunderlich, The link between rigid amorphous fraction and crystal perfection in cold-crystallized poly(ethylene terephthalate), Polymer (Guildf). 46 (2005) 12556–12566. doi:10.1016/j.polymer.2005.10.099.

[28] Q. Zia, D. Mileva, R. Androsch, Rigid amorphous fraction in isotactic polypropylene, Macromolecules. 41 (2008) 8095–8102. doi:10.1021/ma801455m.

[29] C. Hedesiu, D.E. Demco, R. Kleppinger, G. Vanden Poel, W. Gijsbers, B. Blümich, K. Remerie, V.M. Litvinov, Effect of temperature and annealing on the phase composition, molecular mobility, and the thickness of domains in isotactic polypropylene studied by proton solid-state NMR, SAXS, and DSC, Macromolecules. 40 (2007) 3977–3989. doi:10.1021/ma070014q.

[30] H. Chen, P. Cebe, Investigation of the rigid amorphous fraction in nylon-6, 89 (2007) 417–425.

[31] C. Schick, A. Wurm, A. Mohamed, Dynamics of reversible melting revealed from frequency dependent heat capacity, Thermochim. Acta. 392-393 (2002) 303–313. doi:10.1016/S0040-6031(02)00116-8.

[32] Y. Wang, J.L. Gómez Ribelles, M. Salmerón Sánchez, J.F. Mano, Morphological Contributions to Glass Transition in Poly (L -lactic acid), Macromolecules. 38 (2005) 4712–4718. doi:10.1021/ma047934i.

[33] Y. Wang, S.S. Funari, J.F. Mano, Influence of semicrystalline morphology on the glass transition of poly(L-lactic acid), Macromol. Chem. Phys. 207 (2006) 1262–1271. doi:10.1002/macp.200600114.

[34] B. Wunderlich, Reversible crystallization and the rigid amorphous phase in semicrystalline macromolecules, Prog. Polym. Sci. 28 (2003) 408–409.

[35] C. Schick, A. Wurm, A. Mohammed, Formation and disappearance of the rigid amorphous fraction in semicrystalline polymers revealed from frequency dependent heat capacity, Thermochim. Acta. 396 (2003) 119–132. doi:10.1016/S0040-6031(02)00526-9.

[36] H. Suzuki, J. Grebowicz, B. Wunderlich, Transition of Poly(oxymethy1ene), (1984) 1984–1986.

[37] I. Kolesov, R. Androsch, The rigid amorphous fraction of cold-crystallized polyamide 6, Polym. (United Kingdom). 53 (2012) 4770–4777. doi:10.1016/j.polymer.2012.08.017.

[38] R. Rastogi, W.P. Vellinga, S. Rastogi, C. Schick, H.E.H. Meijer, The three-phase structure and mechanical properties of poly(ethylene terephthalate), J. Polym. Sci. Part B Polym. Phys. 42 (2004) 2092–2106. doi:10.1002/polb.20096.

[39] J. Lin, S. Shenogin, S. Nazarenko, Oxygen solubility and specific volume of rigid amorphous fraction in semicrystalline poly(ethylene terephthalate), Polymer (Guildf). 43 (2002) 4733–4743. doi:10.1016/S0032-3861(02)00278-1.

[40] Y.S. Hu, R.Y.F. Liu, L.Q. Zhang, M. Rogunova, D. a. Schiraldi, S. Nazarenko, a. Hiltner, E. Baer, Oxygen transport and free volume in cold-crystallized and melt-crystallized poly(ethylene naphthalate), Macromolecules. 35 (2002) 7326–7337. doi:10.1021/ma0205156.

[41] R. Auras, B. Harte, S. Selke, An overview of polylactides as packaging materials, Macromol. Biosci. 4 (2004) 835–864. doi:10.1002/mabi.200400043.

[42] I. Armentano, N. Bitinis, E. Fortunati, S. Mattioli, N. Rescignano, R. Verdejo, M. a. Lopez-Manchado, J.M. Kenny, Multifunctional nanostructured PLA materials for packaging and tissue engineering, Prog. Polym. Sci. 38 (2013) 1720–1747. doi:10.1016/j.progpolymsci.2013.05.010.

[43] P. Pan, Y. Inoue, Polymorphism and isomorphism in biodegradable polyesters, Prog. Polym. Sci. 34 (2009) 605–640. doi:10.1016/j.progpolymsci.2009.01.003.

[44] M. Kanchanasopa, J. Runt, Broadband Dielectric Investigation of Amorphous and Semicrystalline l-Lactide/ meso-Lactide Copolymers, Macromolecules. 37 (2004) 863–871. doi:10.1021/ma035597s.

[45] M. Arnoult, E. Dargent, J.F. Mano, Mobile amorphous phase fragility in semi-crystalline polymers: Comparison of PET and PLLA, Polymer (Guildf). 48 (2007) 1012–1019. doi:10.1016/j.polymer.2006.12.053.

[46] E. Zuza, J.M. Ugartemendia, A. Lopez, E. Meaurio, A. Lejardi, J.R. Sarasua, Glass transition behavior and dynamic fragility in polylactides containing mobile and rigid amorphous fractions, Polymer (Guildf). 49 (2008) 4427–4432. doi:10.1016/j.polymer.2008.08.012.

[47] J. Del Rıó, A. Etxeberria, N.L. Lopez-Rodrıuez, E. Lizundia, J.R. Sarasua, A PALS Contribution to the Supramolecular Structure of Poly(L-lactide), Macromolecules. 43 (2010) 4698–4707. doi:10.1021/ma902247y.

[48] N. Delpouve, a. Saiter, E. Dargent, Cooperativity length evolution during crystallization of poly(lactic acid), Eur. Polym. J. 47 (2011) 2414–2423. doi:10.1016/j.eurpolymj.2011.09.027.

[49] M.L. Di Lorenzo, M. Cocca, M. Malinconico, Crystal polymorphism of poly(l-lactic acid) and its influence on thermal properties, Thermochim. Acta. 522 (2011) 110–117. doi:10.1016/j.tca.2010.12.027.

[50] S. Fernandes Nassar, A. Guinault, N. Delpouve, V. Ducruet, C. Sollogoub, S. Domenek, Multi-scale analysis of the impact of polylactide morphology on gas barrier properties, 108 (2017) 163–172. doi:10.1016/j.polymer.2016.11.047.

[51] A. Guinault, C. Sollogoub, V. Ducruet, S. Domenek, Impact of crystallinity of poly(lactide) on helium and oxygen barrier properties, Eur. Polym. J. 48 (2012) 779–788. doi:10.1016/j.eurpolymj.2012.01.014.

[52] M.C. Righetti, D. Prevosto, E. Tombari, Time and Temperature Evolution of the Rigid Amorphous Fraction and Differently Constrained Amorphous Fractions in PLLA, Macromol. Chem. Phys. (2016) 1–14. doi:10.1002/macp.201600210.

[53] M. Drieskens, R. Peeters, J. Mullens, D. Franco, P. Lemstra, D. Hristova-Bogaerds, Structure Versus Properties Relationship of Poly(lactic acid). I. Effect of Crystallinity on Barrier Properties, J. Polym. Sci. Part B Polym. Phys. 47 (2009) 2247–2258. doi:10.1002/polb.21822.

[54] M. Cocca, M.L. Di Lorenzo, M. Malinconico, V. Frezza, Influence of crystal polymorphism on mechanical and barrier properties of poly(l-lactic acid), Eur. Polym. J. 47 (2011) 1073–1080. doi:10.1016/j.eurpolymj.2011.02.009.

[55] M.C. Righetti, E. Tombari, Crystalline, mobile amorphous and rigid amorphous fractions in poly(L-lactic acid) by TMDSC, Thermochim. Acta. 522 (2011) 118–127. doi:10.1016/j.tca.2010.12.024.

[56] J. Mijovic, M. Sun, Y. Han, Normal and segmental mode dynamics of end-functionalized poly(propylene oxide) by dielectric relaxation spectroscopy and dynamic mechanical spectroscopy, Macromolecules. 35 (2002) 6417–6425. doi:10.1021/ma020293b.

[57] A.R. Bras, T. Viciosa, Y. Wang, M. Dionisio, J.F. Mano, Crystallization of Poly (L - lactic acid) Probed with Dielectric Relaxation Spectroscopy, Macromolecules. 39 (2006) 6513–6520.

[58] N. Delpouve, A. Saiter, J.F. Mano, E. Dargent, Cooperative rearranging region size in semi-crystalline poly(L-lactic acid), Polymer (Guildf). 49 (2008) 3130–3135. doi:10.1016/j.polymer.2008.04.045.

[59] G. Adam, J.H. Gibbs, On the Temperature Dependence of Cooperative Relaxation Properties in Glass-Forming Liquids, J. Chem. Phys. 43 (1965) 139–146. doi:10.1063/1.1696442.

[60] E. Donth, The size of cooperatively rearranging regions at the glass transition, J. Non. Cryst. Solids. 53 (1982) 325–330. doi:10.1016/0022-3093(82)90089-8.

[61] A. Saiter, N. Delpouve, E. Dargent, J.M. Saiter, Cooperative rearranging region size determination by temperature modulated DSC in semi-crystalline poly(l-lactide acid), Eur. Polym. J. 43 (2007) 4675–4682. doi:10.1016/j.eurpolymj.2007.07.039.

[62] R.-M. Ho, F.-H. Lin, C.-C. Tsai, C.-C. Lin, B.-T. Ko, B.S. Hsiao, I. Sics, Crystallization-Induced Undulated Morphology in Polystyrene-b-Poly(L-lactide) Block Copolymer, Macromolecules. 37 (2004) 5985–5994. doi:10.1021/ma0492869.

[63] R.V. Castillo, A.J. Müller, M. Lin, H. Chen, U. Jeng, M. a Hillmyer, Confined Crystallization and Morphology of Melt Segregated PLLA- b -PE and PLDA- b -PE Diblock Copolymers, Macromolecules. 41 (2008) 6154–6164. doi:10.1021/ma800859y.

[64] D. Maillard, R.E. Prud'homme, Crystallization of ultrathin films of polylactides: From chain chirality to lamella curvature and twisting, Macromolecules. 41 (2008) 1705–1712. doi:10.1021/ma071306u.

[65] D.E. Martinez-Tong, B. Vanroy, M. Wu, A. Nogales, S. Napolitano, Crystallization of Poly (L- lactide) Confined in Ultrathin Films : Competition between Finite Size Effects and Irreversible Chain Adsorption, 47 (2014) 2354–2360.

[66] H. Wang, J.K. Keum, A. Hiltner, E. Baer, Confined crystallization of peo in nanolayered films impacting structure and oxygen permeability, Macromolecules. 42 (2009) 7055–7066. doi:10.1021/ma901379f.

[67] M. Boufarguine, A. Guinault, G. Miquelard-Garnier, C. Sollogoub, PLA/PHBV films with improved mechanical and gas barrier properties, Macromol. Mater. Eng. 298 (2013) 1065–1073. doi:10.1002/mame.201200285.

[68] K. Arabeche, L. Delbreilh, R. Adhikari, G.H. Michler, A. Hiltner, E. Baer, J.M. Saiter, Study of the cooperativity at the glass transition temperature in PC/PMMA multilayered films: Influence of thickness reduction from macro- to nanoscale, Polymer (Guildf). 53 (2012) 1355–1361. doi:10.1016/j.polymer.2012.01.045.

[69] K. Arabeche, L. Delbreilh, J.-M. Saiter, G.H. Michler, R. Adhikari, E. Baer, Fragility and molecular mobility in micro- and nano-layered PC/PMMA films, Polymer (Guildf). 55 (2014) 1546–1551. doi:10.1016/j.polymer.2014.02.006.

[70] R. Casalini, L. Zhu, E. Baer, C.M. Roland, Segmental dynamics and the correlation length in nanoconfined PMMA, Polym. (United Kingdom). 88 (2016) 133–136. doi:10.1016/j.polymer.2016.02.030.

[71] A. Bironeau, J. Dirrenberger, C. Sollogoub, G. Miquelard-Garnier, S. Roland, Evaluation of morphologically representative sample sizes for nanolayered polymer blends, J. Microsc. 00 (2016) 1–11. doi:10.1111/jmi.12415.

[72] A.A. Lacey, D.M. Price, M. Reading, Theory and Practice of Modulated Temperature Differential Scanning Calorimetry, Springer. (2006) 1–82. doi:10.1007/1-4020-3750-3_1.

[73] S. Saeidlou, M.A. Huneault, H. Li, C.B. Park, Poly(lactic acid) crystallization, Prog. Polym. Sci. 37 (2012) 1657–1677. doi:10.1016/j.progpolymsci.2012.07.005.

[74] C. Courgneau, S. Domenek, R. Lebossé, A. Guinault, L. Avérous, V. Ducruet, Effect of crystallization on barrier properties of formulated polylactide, Polym. Int. 61 (2012) 180–189. doi:10.1002/pi.3167.

[75] J. Zhang, K. Tashiro, H. Tsuji, A.J. Domb, Disorder-to-order phase transition and multiple melting behavior of poly(L-lactide) investigated by simultaneous measurements of WAXD and DSC, Macromolecules. 41 (2008) 1352–1357. doi:10.1021/ma0706071.

[76] G. Stoclet, R. Séguéla, J.M. Lefebvre, S. Li, M. Vert, Thermal and strain-induced chain ordering in lactic acid stereocopolymers: Influence of the composition in stereomers, Macromolecules. 44 (2011) 4961–4969. doi:10.1021/ma200469t.

[77] H. Wang, J.K. Keum, A. Hiltner, E. Baer, Crystallization kinetics of poly(ethylene oxide) in confined nanolayers, Macromolecules. 43 (2010) 3359–3364. doi:10.1021/ma902780p.

[78] A. Flores, F. Ania, C. Arribas, A. Ochoa, S. Scholtyssek, F.J. Baltá-Calleja, E. Baer, Confined crystallization of nanolayered poly(ethylene terephthalate) using X-ray diffraction methods, Polym. (United Kingdom). 53 (2012) 3986–3993. doi:10.1016/j.polymer.2012.06.047.

[79] Melvin Avrami, M. Avrami, Kinetics of phase change. I general theory, J. Chem. Phys. 7 (1939) 1103–1112. doi:10.1063/1.1750380.

[80] Y. Liu, L. Wang, Y. He, Z. Fan, S. Li, Non-isothermal crystallization kinetics of poly(L-lactide), Polym. Int. 59 (2010) 1616–1621. doi:10.1002/pi.2894.

[81] B.E.W. Fischer, H.J. Sterzel, G. Wegner, Investigation of the structure of solution grown crystals of lactide copolymers by means of chemical reactions by means of chemical reactions, Kolloid-Z. U. Z. Polym. 251 (1973) 980–990.

[82] M. MacKey, L. Flandin, A. Hiltner, E. Baer, Confined crystallization of PVDF and a PVDF-TFE copolymer in nanolayered films, J. Polym. Sci. Part B Polym. Phys. 49 (2011) 1750–1761. doi:10.1002/polb.22375.

[83] E. Hempel, G. Hempel, a. Hensel, C. Schick, E. Donth, Characteristic Length of Dynamic Glass Transition near T g for a Wide Assortment of Glass-Forming Substances, J. Phys. Chem. B. 104 (2000) 2460–2466. doi:10.1021/jp991153f.

[84] M. Pyda, R.C. Bopp, B. Wunderlich, Heat capacity of poly(lactic acid), J. Chem. Thermodyn. 36 (2004) 731–742. doi:10.1016/j.jct.2004.05.003.

[85] A. Saiter, N. Delpouve, E. Dargent, W. Oberhauser, L. Conzatti, F. Cicogna, E. Passaglia, Probing the chain segment mobility at the interface of semi-crystalline polylactide/clay nanocomposites, Eur. Polym. J. 78 (2016) 274–289. doi:10.1016/j.eurpolymj.2016.03.040.

[86] T.A. Tran, S. Saïd, Y. Grohens, Nanoscale characteristic length at the glass transition in confined syndiotactic poly(methyl methacrylate), Macromolecules. 38 (2005) 3867–3871. doi:10.1021/ma0487296.

[87] N. Tomczak, R. a L. Vallée, E.M.H.P. Van Dijk, L. Kuipers, N.F. Van Hulst, G.J. Vancso, Segment Dynamics in Thin Polystyrene Films Probed by Single-Molecule Optics, J. Am. Chem. Soc. 126 (2004) 4748–4749. doi:10.1021/ja039249h.

[88] A. Esposito, N. Delpouve, V. Causin, A. Dhotel, L. Delbreilh, E. Dargent, From a Three-Phase Model to a Continuous Description of Molecular Mobility in Semicrystalline Poly(hydroxybutyrate- *co* -hydroxyvalerate), Macromolecules. (2016) acs.macromol.6b00384. doi:10.1021/acs.macromol.6b00384.

Structural and dynamic heterogeneity in the amorphous phase of PLLA confined at the nanoscale by coextrusion process

Samira Fernandes Nassar[a], Sandra Domenek[a], Alain Guinault[b], Gregory Stoclet[d], Nicolas Delpouve[c], Cyrille Sollogoub[b*]

4.7. Supplementary information

SI 1. The extrusion conditions to fabricate PLLA/PS films.

PLLA extruder (°C)	190/200/200/200
PS extruder (°C)	200/200/200/210
Pump + Feed bloc (°C)	200
Layers multipliers blocks (°C)	200
Flat die (°C)	200
Material temperature (°C)	200
PLLA screw speed (rpm)	22
PS screw speed (rpm)	57
PLLA throughput (g/h)	600
PS throughput (g/h)	1800

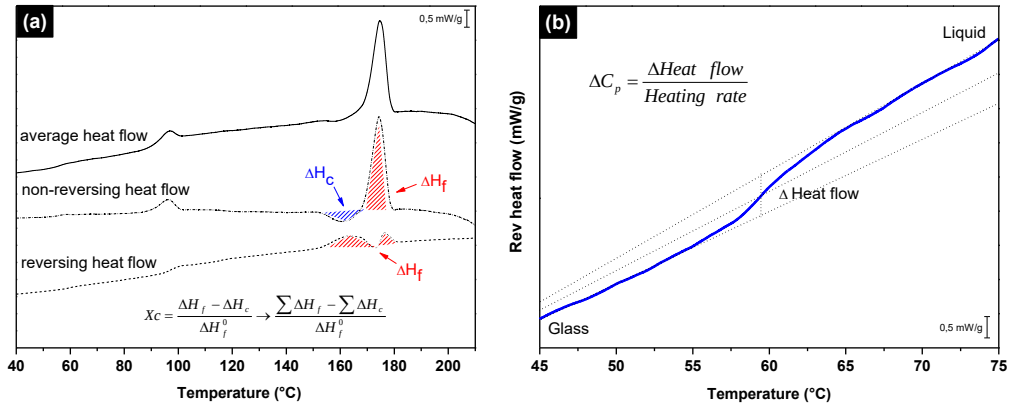

SI 2. (a) Protocol for the determination of the degree of crystallinity from MT-DSC curves obtained for the 20 nm annealed sample; Average heat flow (Solid line); reversing heat flow (dashed line); and non-reversing heat flow (dotted line) versus temperature (b) Reversing heat flow in the glass transition domain for the 20 nm annealed sample.

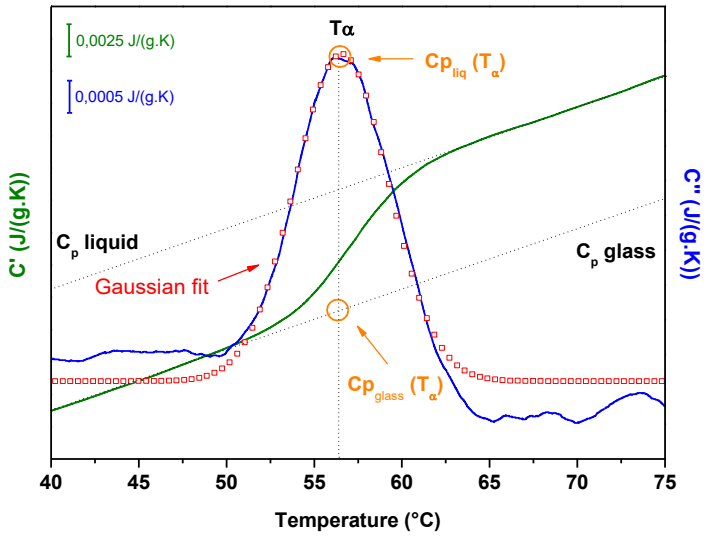

SI 3. Example of C' (T) and C'' (T) of confined amorphous PLLA at 20 nm of thickness obtained by TMDSC on PS/PLLA sample (2049 layers)

Chapter 5 – The impact of nanoconfinement on PLLA crystallization and gas barrier properties

Le procédé multicouches a été utilisé pour confiner le PLLA par deux polymères amorphes (PS et PC) qui ont une affinité chimique différente avec le PLLA. Ce procède a permis d'obtenir le PLLA confiné dans des couches d'épaisseur 20 nm chaque. Le PLLA est à l'état amorphe dans les films extrudés mais avec un recuit thermique des taux de cristallinité très élevées ont été obtenus. Nous avons observé des lamelles très orientées dans les films cristallisés multi-nanocouches, avec différentes orientations de cristaux en fonction du polymère confineur. Pour le couple PLLA / PS, des lamelles dans deux directions ont été obtenues (parallèles et perpendiculaire aux couches), et pour PLLA / PC, seules des lamelles dans le plan, c'est-à-dire parallèles aux couches, ont été obtenues. Les résultats de PLLA / PC recuits à 85 ° C suggèrent la présence possible d'une interphase, ce qui peut expliquer une perméabilité plus élevée par rapport aux échantillons amorphes. Dans le cas de PLLA / PC recuit à 120 ° C et PLLA / PS recuit à 85 ° C, comme nous l'avons montré au chapitre 3, les propriétés barrière aux gaz étaient régies par la fraction amorphe rigide (RAF).

5. The impact of nanoconfinement on PLLA crystallization and gas barrier properties

Samira Fernandes Nassar[a], Alain Guinault[b], Gregory Stoclet[d], Nicolas Delpouve[c], Cyrille Sollogoub[b], Sandra Domenek[a *]

[a]UMR Ingénierie Procédés Aliments, AgroParisTech, INRA, Université Paris-Saclay, 1 avenue des Olympiades, F-91300 Massy, France

[b]PIMM, ENSAM - CNRS - CNAM, 151 Boulevard de l'Hôpital, F-75013 Paris Cedex, France

[c]AMME-LECAP EA 4528 International Lab., Normandie Univ, UNIROUEN, LECAP, F-76000 Rouen, France

[d]UMR CNRS 8207, Unité Matériaux et Transformations, Université Lille1 Sciences et Technologies, Bâtiment C6, Université de Lille Nord de France, 59655 Villeneuve d'Ascq, France

Corresponding author: Sandra Domenek, UMR Ingénierie Procédés Aliments, AgroParisTech, INRA, Université Paris-Saclay, 1 avenue des Olympiades, F-91300 Massy, France

Email: sandra.domenek@agroparistech.fr

5.1.Abstract

The multi-nanolayered process was used to confine PLLA by two amorphous polymers (PS and PC) which have different chemical affinity with PLLA. This process allowed to obtain PLLA confined in 20 nm each individual thickness. PLLA was amorphous in extrude films however, applying thermal annealing, high degrees of crystallinity were achieved. We observed highly oriented lamellas in crystallized multi-nanolayered films, with different crystals orientations depending of confiner polymer. For PLLA/PS couple, mixed lamellas was obtained (in-plane and on-edge), and for PLLA/PC, only in-plane lamellas was obtained. The results of PLLA/PC annealed at 85°C suggest the possible presence of an interphase, which can explain the higher permeability compared to amorphous samples. In the case of PLLA/PC annealed at 120°C and PLLA/PS annealed at 85°C, as we showed in chapter 3, gas barrier properties was governed by the rigid amorphous fraction (RAF).

Key words: PLLA, confinement, interphase, RAF, permeability

5.2.Introduction

Polylactide is produced for numerous applications for example packaging material or in the biomedical sector [1]. However, compared to other high performance polymers, its barrier properties hinder its large-scale commercial application. A huge effort has been focused on this polymer for optimizing its barrier properties and improvements were often achieved by optimizing crystallization [2,3], by drawing [4], and by compounding or blending with less permeable fillers/polymers with high aspect ratio [5,6]. Still, the decrease in barrier properties is rather limited and generally, other properties (like optical clarity, degradability, mechanical toughness) are affected or sacrificed. Alternative strategies must therefore be explored.

Substantial gas barrier improvements have been recently measured on multilayered films obtained with layer-multiplying coextrusion, especially when decreasing the individual layer thicknesses below the diameter of spherulites [7–12]. It is well known that in semi-crystalline polymers, crystallization can be profoundly affected by nanoscale confinement [13]: spherulite growth is greatly hampered and specific lamellar crystal orientations are created. In particular, it was observed that coextruding PEO, PCL or PP between hard confining layers led to unique single crystalline lamellae, oriented parallel to the layers (in-plane) [8,9,12,14,15]. Since the impermeable lamellas with large aspect ratios were oriented perpendicularly to the permeant flux, multiple orders of magnitude reduction in gas permeability was achieved compared to the bulk.

Nevertheless, the control of crystal orientation is crucial for barrier enhancement and more understanding of the parameters governing it is still needed [16]. The difficulty lies in the fact that it is not a simple task to split the substrate effect from the size effect, as well as the kinetics effect from the nucleation effect. The layer multiplying co-extrusion appeared as a relevant tool allowing to provide insight into the effect of confinement on the crystallization behavior of polymers [13,14]. Thermal annealing after extrusion to (re-)crystallize the confined polymer was used to better control the orientation habit. In addition to space confinement (i.e. layer thickness), other parameters were found to impact the lamellar crystal orientation, like chemical interaction between confining and confined polymers or the annealing conditions [13]. With the decrease of the layer thickness, a transition from on-edge lamellas (i.e. polymeric chains parallel to the polymer layer) to in-plane lamellas (i.e. polymeric chains perpendicular to the polymer layer) was observed. A similar transition was found when the (re-)crystallization temperature was increased, both on substrate supported thin films [17,18] and nanolayered films

[13]. This transition in orientation was attributed to a transition from heterogeneous nucleation to surface nucleation, deactivated at high temperatures [19], suggesting that the lamellar orientation is mainly nucleation controlled.

The substrate effect is still poorly understood. Enhancing polymer-substrate interaction may impose the polymer chains to lie down, favoring on-edge lamellar orientation. Still, some experimental results on substrate supported thin films contradict this scenario [17]. The substrate effect on the confined crystallization of PCL in coextruded nanolayered films was investigated [13] and it was shown that increased interaction tended to retard the formation of in-plane crystalline lamellae. As an attempt to understand the substrate effect, Ma et al. [20,21] performed dynamic Monte Carlo simulations considering two kinds of interactions with the substrate: sticky walls (related to the case of strong adhesion between polymer and wall) and slippery walls (neutral repulsion between polymer and wall). On-edge lamellas were dominant at the whole range of crystallization temperature and film thickness for slippery walls, while for sticky walls, in-plane lamellas tended to be dominant

There are some studies carried out with spin-coated ultra-thin PLA films on the influence of annealing temperature on lamellar crystal formation in PLLA. Wu et al. [22] showed that on-edge lamellar crystals of PLLA thin films are mainly formed by cold crystallization at low temperatures, whereas the in-plane crystals occur when the crystallization temperature approaches 100°C. However, in another study, Maillard and Prud'homme [23] showed that thin PLLA crystallized at 125°C and 160°C had on-edge lamellae. The conflicting literature results inform that the main factors influencing the orientation of PLA lamella in thin films are still unknown. Furthermore, no study of the PLA crystallization in coextruded nanolayered films has been carried out today.

In the present work, we investigate the impact PLLA confinement between slippery or stick walls by polystyrene (PS) or polycarbonate (PC) on its crystallization behavior and its macromolecular mobility. PS and PLLA are immiscible [24–26] and the different surface tensions [27] of both polymers let us anticipate low compatibility, leading rather to slippery interfaces. On the contrary PC and PLA have a greater compatibility. Imre et al. [28] showed that up to approximately 5 wt% of PC, the Tg o PLLA increased due to the small admixture. The wall of the confiner polymer PC should as a consequence be more sticky for PLLA compared to PS walls. We study furthermore the impact of the microstructural changes of confined PLA on the macroscopic gas barrier properties in the aim to deduce engineering rules for increasing the performance of the multilayer materials.

5.3.Materials and methods

5.3.1. Materials and processing

Two couples of polymers was used in this study: polylactide (PLLA) - polystyrene (PS) (PLLA/PS) and polylactide (PLLA) - polycarbonate (PC) (PLLA/PC). All the information related to the polymer PS and the couple PLLA/PS (processing and characterization) are described in Chapter 4. PLLA pellets were purchased from Corbion Purac (PLA REVODE 190). The content of L-lactide was higher than 99%. Polycarbonate (PC) pellets were obtained from Gazechim (PC121R). A multilayer coextrusion process was used to fabricate multilayered films composed of 512 and 2049 alternating layers of PLLA and PC. The composition of the PC/PLLA films is 75/25 (m/m). The process is described in Chapter 4. In brief, the extrusion conditions are presented in *Table 5.1*.

Table 5.1. The extrusion conditions to fabricate PLLA/PC films.

PLLA extruder (°C)	230/220/210/210
PC extruder (°C)	280/260/260/260
Pump + Feed bloc (°C)	240
Layers multipliers blocks (°C)	240
Flat die (°C)	220
Material temperature (°C)	210
PLLA screw speed (rpm)	15
PS screw speed (rpm)	34
PLLA throughput (g/h)	600
PC throughput (g/h)	1800

Our objective was to obtain films with individual PLLA layer thickness of 300 nm and 20 nm. For that the final thickness of the film is defined by the chill-roll speed and the number of multiplying elements. The *Table 5.2* presents different conditions to obtain these films.

Table 5.2. PC/PLLA multilayered films used to study the effect of PLLA layer thickness on the confinement effect.

Number of multiplying elements	Number of layers	Draw ratio	Film total thickness (μm)	PLLA nominal thickness (nm)
8	512	2	300	300
10	2049	6	80	20

The annealing procedure of PLLA/PS films was already described in chapter 4. The same method was used for PLLA/PC films after cutting the edges of the samples to avoid edge effects. The extruded PLLA/PC films were hot-pressed at 85°C or 120°C for 180 minutes at a pressure of 5 x 10^6 Pa using a heating press (Darragon, France).

5.3.2. Methods

Melt rheology, Atomic force microscopy (AFM) and Differential Scanning Calorimetry (DSC) methods was described in Chapter 4.

Wide Angle X-Ray Scattering (WAXS). WAXS analyses were carried out using the synchrotron radiation on the BM02 beamline at European Synchrotron Radiation Facility (Grenoble, France). Experiments were carried out using an energy of λ=0,995058 Å. The WAXS patterns were recorded on a 2-D CCD camera from Princeton Instruments. The intensity profiles were obtained by 360° azimuthal integration of the 2D patterns using the fit2D software.

Analyzes of the kinetics of isothermal crystallization were made using X-ray diffraction. The samples were crystallized in a heating plate in situ in an X-ray diffraction machine (PANanalytical). The parameters were: beam at 40 kV and 20 mA, the CuKa radiation (λ = 1.54Å) was chosen with a nickel filter. The WAXS diffractrograms were recorded by a CDD camera (Photonic Science) in 2-D.

The equation and methodology used to determine Avrami parameters are described in Chapter 4.

Dynamic Mechanical Thermal Analysis (DMTA). DMTA was carried out on small film samples (10.25 mm length, 5.00 mm width, and a thickness between 0.08 and 0.12 mm) using a Triton Tritec apparatus, working in dynamic tensile mode. The frequency was set at 1Hz and the dynamic displacement at 10 microns. The samples were heated from 25 to 200°C at a heating rate of 2°C.min^{-1}.

Helium permeability. The helium permeability was measured at room temperature and 0% RH, by a specific lab-made analyser, based on the ISO 15105-2:2003 method. The helium permeability was determined from the transmission rate by taking into account the thickness of the films.

Oxygen permeability. The oxygen permeability was measured with a Systech analyser 8001 at 23°C and 0% RH. Oxygen permeability is calculated from the measured oxygen transmission rate (OTR) by multiplying it by the sample thickness (measured with a micrometer on 9 points). For assessing reproducibility of permeability measurements were carried out on at least two different samples obtained by the same protocol.
The permeability of PLLA is calculated using the equation below, derived from the series model for multi-layered assemblies. In this equation, 75% by weight of PS or PC and 25% by weight of PLLA are considered.

$$\frac{1}{P_{film}} = \frac{0{,}25}{\rho_{PLLA} \cdot P_{PLLA}} + \frac{0{,}75}{\rho_{confining} \cdot P_{confining}} \qquad \text{Equation 5.1}$$

Where PLLA density (ρ_{PLLA}) is 1,25 g/cm^3, PS density (ρ_{PS}) is 1,05 g/cm^3 and PC density (ρ_{PC}) is 1,2 g/cm^3.

5.4.Results and discussion

5.4.1. Optimization of the layer multiplying co-extrusion process

As for PLLA/PS, the uniformity and continuity of the layers are mainly dependent on the viscosity ratio between the coextruded polymers. The viscosity ratio is defined as:

$$\rho = \frac{\eta_{confined}}{\eta_{confining}}$$ Equation 5.2

where $\eta_{confined}$ and $\eta_{confining}$ are respectively the viscosity of the confined polymer (in our case PLLA) and confining polymer (PC).

Figure *5.1* shows the viscosity of PLLA and PC and viscosity ratio as a function of the shear rate. In the shear rate range of co-extrusion process, typically between 1 and 50 s^{-1}, the viscosity ratio should be close to 1, which ensures homogeneity of the stratified flow. In the case of PLLA/PC, the PC grade chosen for this study is very fluid, but not enough to achieve a viscosity ratio close to 1.

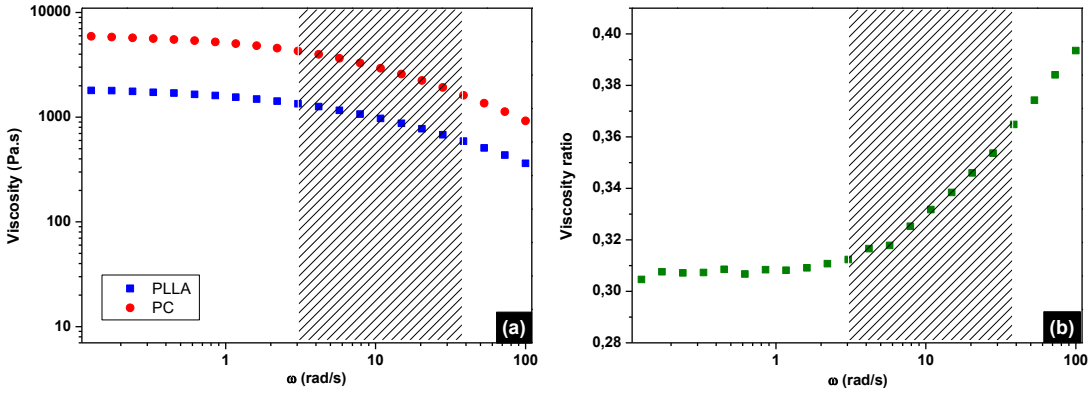

Figure 5.1. a) Viscosity curves of PLLA and PC (b) Viscosity ratio for PLLA/PC. The hatched zone corresponds to the shear rates found in the co-extrusion process, considering the law of Cox Merz

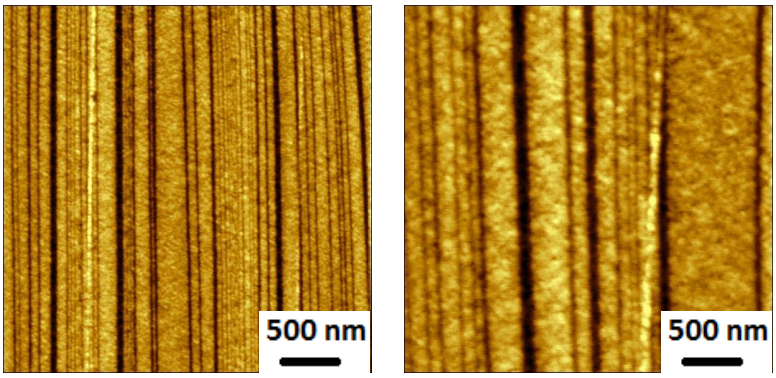

Figure 5.2. Tapping mode AFM phase image of nanolayered PLLA/PC containing 2049 layers.

Figure 5.2 shows AFM images for PLLA/PC, where PC appears bright while PLLA appears dark. The observed layers are continuous but thickness heterogeneities are also observed, probably due to viscosity ratio far from 1. However, the sample preparation as well as the acquisition of images with AFM were extremely delicate and few images were obtained, which prevented from a complete statistical analysis of the sample. Based on a sampling composed of several tens of layers, the measured mean thickness was in a reasonable agreement with the nominal thickness.

5.4.2. Crystallization kinetics and crystalline lamellae orientation of confined PLLA layers

The annealing temperatures of the couple PLLA/PC were chosen below the glass transition temperature of the confining polymer (140°C) to preserve the continuity of the layers and to ensure a hard confinement imposed by hard glassy PC. PLLA was crystallized at 85 °C to yield the α'-polymorph and at 120 °C to obtain the α-polymorph. The glass transition temperature of PS is 100 °C. In this case, the crystallization of PLLA was carried out uniquely at 85 °C.
The crystallization kinetics of PLLA confined by PS were shown in Chapter 4. The impact of the confinement of PLLA by PC to 20 nm thick layers on the crystallization kinetics of PLLA was measured with the help of in-situ WAXS analysis. The results are shown in *Figure 5.3*. As already discussed in Chapter 4 for PS/PLLA films, the PLLA crystallization rate at 85°C was retarded when PLLA was confined. The same result was observed for other confined polymers (PEO, PCL, PP) [9,29,30]. However, the overall crystallization rate for confined PLLA annealed at 120°C had the same kinetics as bulk PLLA. The kinetic parameters were modeled

with the help of the Avrami theory. The Avrami exponent and the crystallization rate constant were retrieved from the slope and intercept of the linearized crystallization kinetics shown in *Figure 5.4*. For bulk PLLA annealed at 85°C and the confined film annealed at 120°C, non-linear behavior was observed in the double-logarithmic curve, which suggested the existence of a secondary crystallization [31,32]. The apparition of the secondary crystallization in annealed sample at 120°C is consistent with the literature because in high-annealed temperature (closer to fusion temperature), macromolecules are more mobile allowing easier its generation [33,32]. The Avrami model of 20 nm annealed at 85°C fitted well and its curve was linear for the double logarithm of the relative crystallinity without secondary crystallization. The Avrami exponent was n=1,8 (*Table 5.3*), which approximately corresponded to a two dimensional crystallization growth with an instantaneous nucleation. The half-time of crystallization ($t_{1/2}$) is related to the n and K parameters and was defined as the time at which the extent of relative crystallization reached a value of 50%. Similarly to the results obtained for PLLA confined by PS, half-time crystallization for PLLA confined by PC increased compared to bulk PLLA at 85°C. K was strongly dependent on the annealing temperature and increased at 120°C, which was expected from the known behavior of PLLA crystallization in bulk.

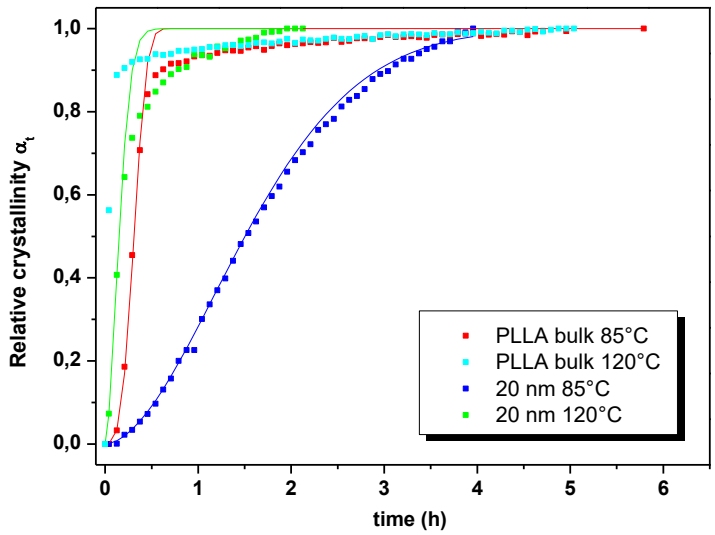

Figure 5.3. Relative crystallinity and Avrami model (continuous lines) versus crystallization time for isothermal crystallization for bulk PLLA and 20 nm samples at 85°C and 120°C.

Table 5.3. Parameters of isothermal crystallization with Avrami model

	$t_{1/2}$ (h)	n	K (h^{-n})
PLLA bulk 85°C	0,31	3,3	33,52
20 nm 85°C	1,54	1,8	0,32
20 nm 120°C	0,15	1,6	20,20

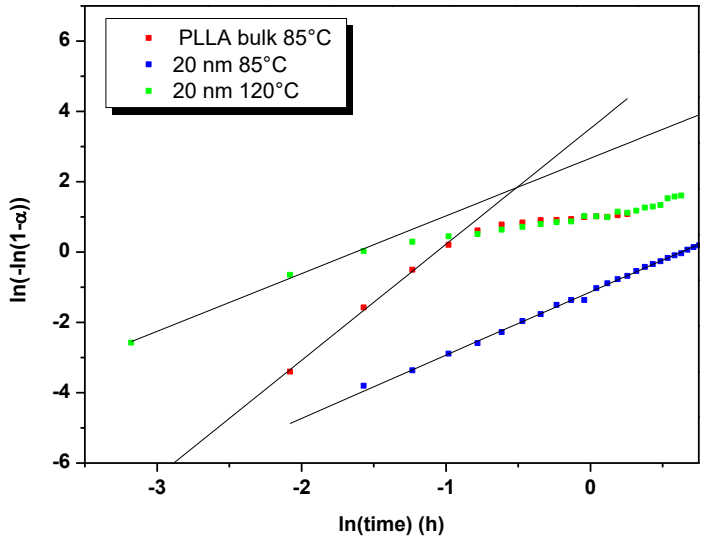

Figure 5.4. Double logarithm versus ln(time) and the Avrami model (black lines) for PLLA annealed at 85°C, 20 nm annealed at 85°C and 120°C.

The orientation of crystalline lamellae and the crystalline polymorph of extruded and annealed PLLA/PS and PLLA/PC multilayer films were analyzed by WAXS. The WAXS patterns of PLLA/PS films are shown in *Figure 5.5*. In all samples after extrusion, no arc reflections of crystalline structures were observed (*Figure 5.5*a-c). In the corresponding normalized WAXS intensity (*Figure 5.7*a), there is no pic characteristic of crystallized PLLA, indicating that the as-extruded films were amorphous. WAXS patterns of 30 μm and 300 nm PLLA/PS films after annealing at 85°C exhibited isotropic reflection rings from (110)/(200) plane of PLLA. In the case of PLLA/PS 20 nm, crystallization at 85°C resulted in crystallization forming lamellae apparently oriented in both directions, on-edge and in-plane. The presence of on-edge lamellae was confirmed by meridional reflections for (110)/(200) crystal plane while in-plane crystals led to the formation of equatorial arcs for the same crystal plane. The formation of mixed

lamellas was also observed on polypropylene confined by PC [15] or PCL confined by PS/PP [11].

The WAXS patterns of PLLA/PC films are shown in *Figure 5.6*. In both samples of PLLA/PC 20 nm annealed at 85°C and 120°C, there were equatorial reflections for (110)/(200) crystal plane indicating the presence of in-plane lamellas. Another evidence for in-plane lamellae in PLLA/PC samples was the reflections at about 30° for (203) crystal plan. For this crystal plan with in-plane lamellae, and since PLLA has a orthorhombic form [34,35] with parameters a=1.06 nm, b=0.610 nm and c=2.88 nm [36], the beam hits lamellae at 60°, reflecting an arc at about 30°.

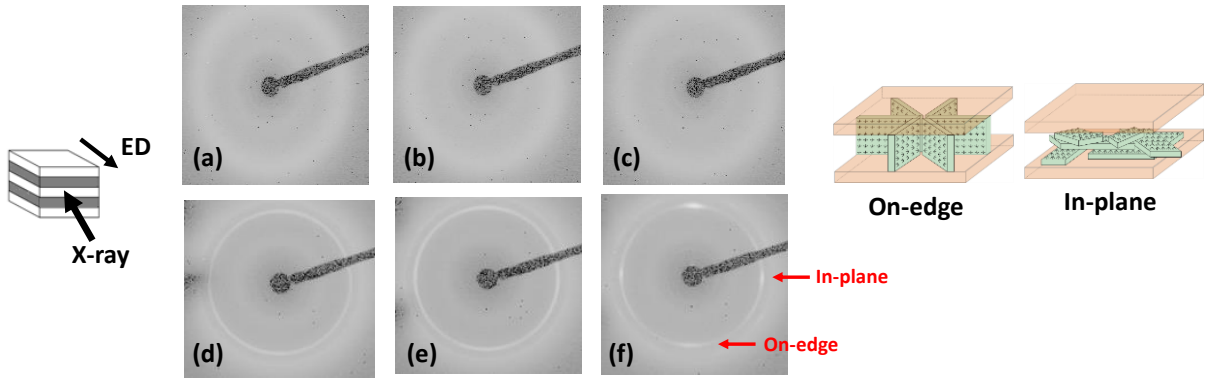

Figure 5.5. WAXS pattern obtained in extrusion direction (ED) for PS/PLLA (a) 30 μm, (b) 300 nm and (c) 20 nm after extrusion and (d) 30 μm, (e) 300 nm and (f) 20 nm after annealing at 85°C during 180 min

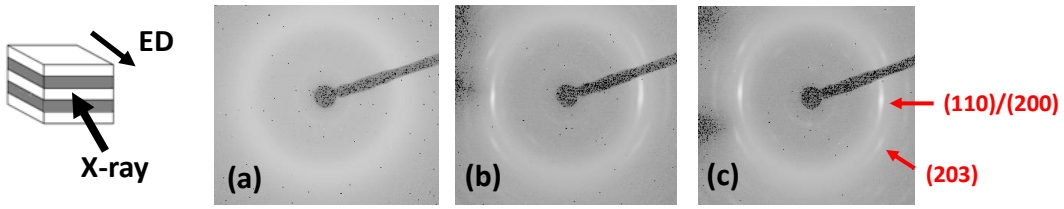

Figure 5.6. WAXS pattern obtained in extrusion direction (ED) for PC/PLLA samples (a) 20 nm after extrusion, (b) 20 nm after annealing at 85°C during 180 min and (c) 20 nm after annealing at 120°C during 180 min.

*Figure 5.7*b shows the WAXS intensity profile of amorphous PLLA/PC and annealed at 85°C and 120°C during 180 minutes. The strong reflections of PLLA attributed to the 200/110 and 203 planes could be observed for both annealed samples [37–40]. It is well known that ta

crystallization temperature at 85°C favors the α'-polymorph of PLLA and 120°C favors the α–form of PLLA [2,41,42] . These crystalline forms can be differentiated in the WAXS patterns with small differences in 2θ values for the two strongest reflections, assigned to the (110)/(200) and (203) planes[41]. In both planes, it is possible to see a gap between the peaks, with the peak of annealed PLLA at 85°C shifted towards lower angles, characteristic of the α' form. As we described in Chapter 4, in all PLLA/PS annealed samples (*Figure 5.7*a), the strong reflections of PLLA attributed to the (200)/(110) and (203) planes could be observed. However, due to small amount of PLLA in the multilayer samples the minor reflections characteristics of α'-form (PLLA annealed at 85°C) were not observed and the crystalline polymorph could not be described.

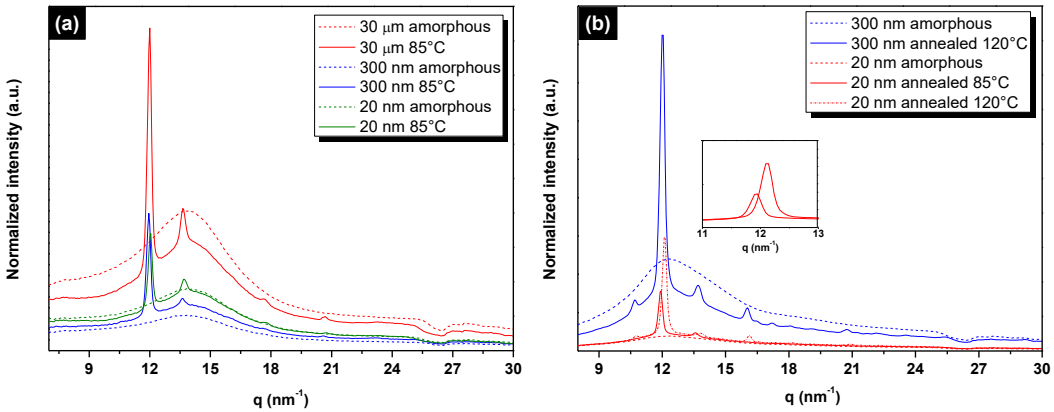

Figure 5.7. Normalized WAXS intensity profile of (a) PLLA/PS 30 μm amorphous and annealed 85°C, 300 nm amorphous and annealed 85°C and 20 nm amorphous and annealed 85°C (b) PLLA/PC 20 nm amorphous, annealed 85°C and 120°C with enlarged pattern of (110)/(200) plan.

5.4.3. Impact of the layer multiplying co-extrusion on the confining polymer PC

PLLA and PC have a certain degree of compatibility [28] and a shift in Tg of PLLA and PC can be observed in polymer blends [6,43], which should have as an effect that PLLA layers will be confined between sticky PC walls. Therefore, we analyzed the glass transition of both polymers, PLLA and PC, in the multilayered films. *Figure 5.8* shows the heat flow in the range of the glass transition of PC and *Table 5.4* gives the corresponding numerical data. The glass transition of PC layers was clearly affected by the layer-multiplying co-extrusion process. The

dynamic heterogeneity increased, which can be observed by the change on the shape and enlargement of the glass transition curve in PLLA/PC films in comparison to the PC bulk sample (*Figure 5.8*). The Tg of the PLLA/PC films with 20 nm PLLA layer thickness, which had therefore the largest interface shifted to lower values. Furthermore, the heat capacity step of the sample containing 20 nm PLLA layers and annealed 300 nm PLLA layers at 85 °C, was clearly smaller than that of the PC bulk. We suggest that an interphase of PLLA and PC might have formed. This interphase could represent a quantitatively non-negligible amount in the 20 nm PLLA samples. The recovered quantity of PC in the multilayer samples was recalculated from the heat capacity step and it is printed in Table *5.4*. Remembering that the amount of PC in the films is 75%, one observes that in the case of those two samples, not all PC can be found. However, experimental uncertainty of these data was high, because the end of the PC glass transition became superposed with the melting/recrystallization transition of the α'-polymorph of PLLA.

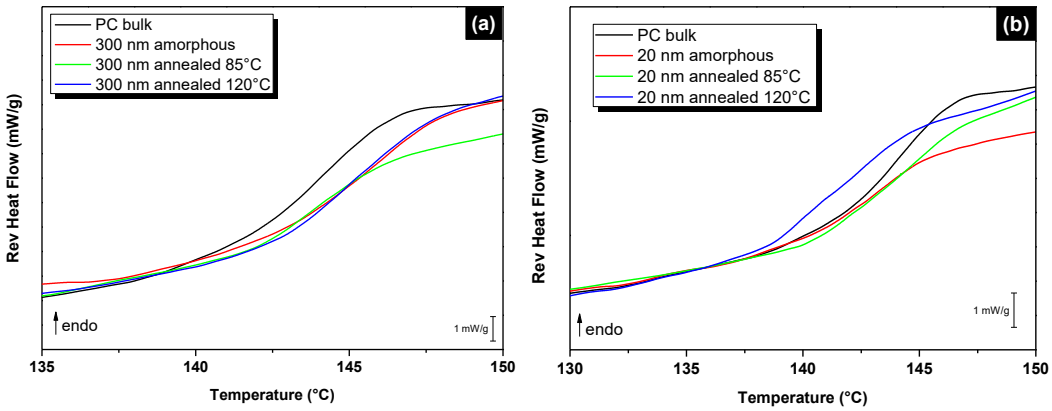

Figure 5.8. Glass transition (Tg) of (a) PC bulk and PC in 300 nm, (b) PC bulk and PC in 20 nm multi-nanolayers films.

Table 5.4. Glass transition temperature (Tg) heat capacity (ΔCp) of PC in PLLA/PC multi-nanolayers films.

	Tg (°C)	ΔCp ($J.g^{-1}.K^{-1}$)	% of PC in PLLA/PC films
PC bulk	143,5 ± 0,1	0,24 ± 0,01	100
300 nm amorphous	144,3 ± 0,3	0,19 ± 0,03	78 ± 10
20 nm amorphous	142,0 ± 0,2	0,14 ± 0,02	60 ± 10
300 nm annealed 85°C	143,6 ± 0,4	0,13 ± 0,03	52 ± 10
300 nm annealed 120°C	144,9 ± 0,9	0,17 ± 0,03	73 ± 10
20 nm annealed 85°C	142,8 ± 0,2	0,17 ± 0,02	70 ± 10
20 nm annealed 120°C	140,6 ± 0,3	0,17 ± 0,02	72 ± 10

In the aim of better separating the phenomena of PC glass transition and PLLA crystallization and melting, DMA measurements were carried out. *Figure 5.9* shows tan δ curves of PC and PLLA bulk, and amorphous and annealed multi-nanolayered films. It is possible to observe that the tan δ peak of PC shifted to lower temperatures for more confined PLLA layers. This shift confirmed DSC data, which fortified the hypothesis of the occurrence of a PLLA/PC interphase. In literature, the appearance of an interphase between PC and PLLA in polymer blends was described and attributed to a transesterification reaction [44,45]. Liu et al.[46] studied the transesterification mechanism between PLA and PC under flow field by adding catalyst to the PLA/PC blend. They found that transesterification reaction between PLA and PC could occur even without catalyst.

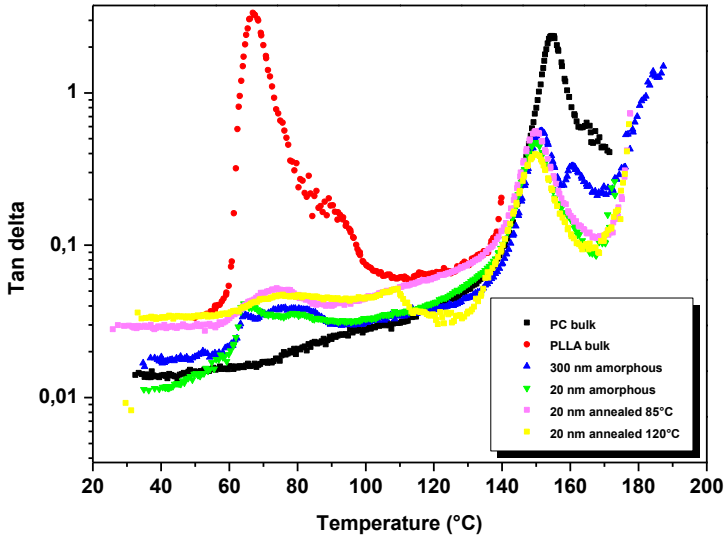

Figure 5.9. DMTA of PC and PLLA bulk and amorphous and annealed (85°C and 120°C) PLLA/PC at 300 nm and 20 nm.

5.4.4. Maximum crystallinity degree and amorphous phase dynamics and of confined PLLA

In the aim to quantify the crystallinity degree of the annealed PLLA in PLLA/PC films, a TM-DSC study was carried out. The glass transition of PC falls in the same temperature domain as the end of cold crystallization and the start of PLLA melting, as shown in the example of 20 nm amorphous PLLA films given in *Figure 5.10*. The superposition of both phenomena makes it difficult to quantify precisely the cold crystallization enthalpy of PLLA. Therefore, we

neglected a possible contribution of the enthalpic relaxation of PC in the non-reversing heat flow signal and quantified the PLLA crystallinity degree as shown in *Figure 5.10*. The amount of crystallinity is given in the Table *5.5*.

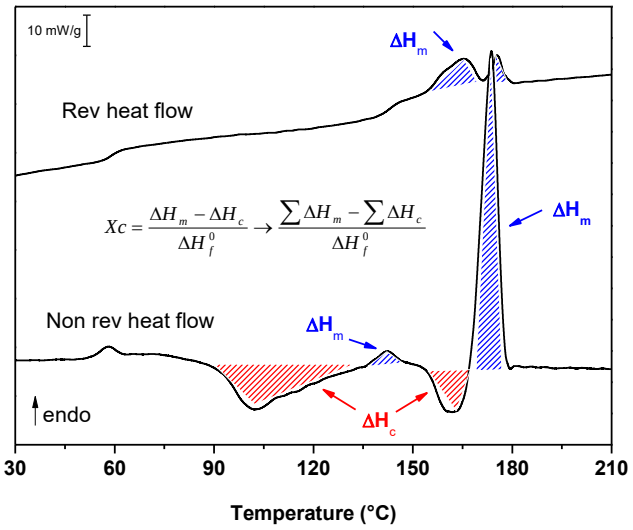

Figure 5.10. Reversing heat flow and Non reversing heat flow of amorphous PC/PLLA (layer thickness 20 nm).

Table 5.5. Glass transition temperature (Tg), Heat capacity (ΔCp), normalized heat capacity to amount of PLLA in multi-nanolayered films($\Delta Cp_{25\%PLLA}$), enthalpy of crystallization (ΔHc) and crystallinity degree normalized to amount of PLLA in multi-nanolayered films ($Xc_{25\%PLLA}$) of PLLA in PLLA/PC multi-nanolayered films.

	Tg (°C)	ΔCp ($J.g^{-1}.K^{-1}$)	$\Delta Cp_{25\%PLLA}$ ($J.g^{-1}.K^{-1}$)	ΔHc (J/g)	$Xc_{25\%PLLA}$
PLLA bulk amorphous	58 ± 0,1	0,44		-	-
300 nm amorphous	59,3 ± 0,2	0,1 ± 0,03	0,4 ± 0,1	3,5 ± 2	15 ± 8
20 nm amorphous	58,3 ± 0,1	0,1 ± 0,02	0,4 ± 0,1	6,2 ± 2	26,7 ± 8
300 nm annealed 85°C	67,5 ± 0,3	0,06 ± 0,01	0,24 ± 0,1	8,9 ± 2	38,6 ± 8
300 nm annealed 120°C	69,7 ± 0,7	0,05 ± 0,01	0,20 ± 0,1	11,4 ± 2	49,0 ± 8
20 nm annealed 85°C	62,1 ± 0,5	0,06 ± 0,01	0,24 ± 0,1	10,9 ± 2	46,8 ± 8
20 nm annealed 120°C	67,0 ± 0,2	0,07 ± 0,01	0,28 ± 0,1	14,5 ± 2	62,5 ± 8

Figure *5.11* shows a zoom on the PLLA glass transition in an In-phase Cp signal for both 20 nm couple (PLLA/PS and PLLA/PC) amorphous and annealed at 85°C. The correspondent values of Tg is given in Table *5.5*. One observes that, in PLLA/PC the Tg of crystallized

samples shifts higher than amorphous samples. This behavior was not expected because, according to Chapter 4, it should not shift when PLLA is confined. We can consider, for PLLA/PC, an effect like confinement in spherulites. However, Tg of amorphous samples doesn't shift compared to bulk PLLA, thus it has no interphase effect. Another observation is the high crystallinity in 20 nm samples annealed at 120°C. This result suggests that, crystallization at 120°C under confinement is effective even if there is a high uncertainty in this result as we explained in the determination part of crystallinity degree.

Heat capacity of PLLA in annealed samples is very high compared usual crystallized PLLA[47], suggesting the presence of an interphase. In samples annealed at 120°C, the width of Tg and the high amount of crystallinity suggests a rather heterogeneous sample. The great heterogeneity of the samples reflects in the PLLA heat capacity height, which is very small, not allowing its measurement (*Figure 5.12*). Contrary to PLLA/PS, which mobile amorphous phase and rigid amorphous phase was calculated, in PLLA/PC due to the fact that heat capacity cannot be well determined, the three phases in PLLA was not calculated. Another important point is linked with the interphase mentioned earlier, the existence of which might affect the values of heat capacity in PLLA as we showed for PC in Table *5.4*.

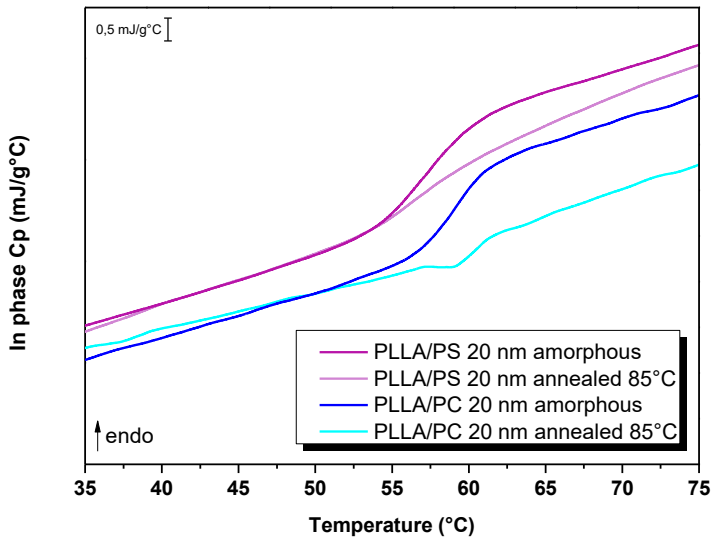

Figure 5.11. In phase Cp of PLLA/PC and PLLA/PS 20 nm amorphous and annealed at 85°C during 180 minutes.

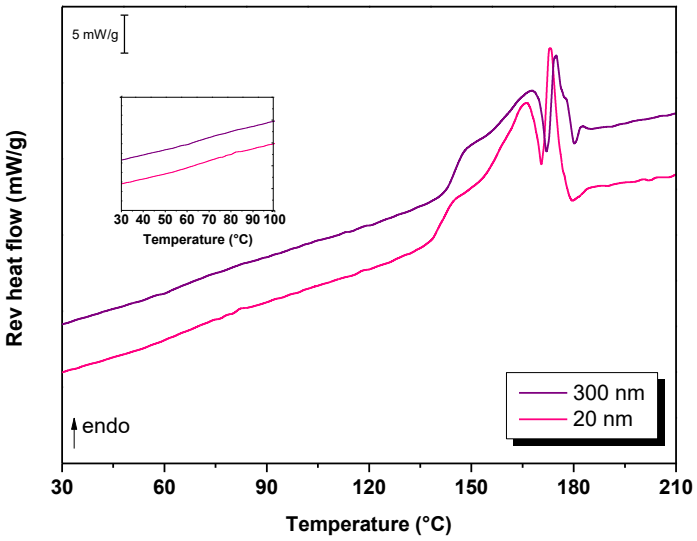

Figure 5.12. Reversing heat flow of PLLA/PC 300 nm and 20 nm annealed at 120°C during 180 minutes.

5.4.5. Impact of PLLA microstructure on helium and oxygen permeability

Table 5.*6* and Table 5.*7* report the oxygen and helium permeability of PLLA/PS and PLLA/PC films. We shall discuss first the impact on the oxygen permeability. In PLLA/PS films, the barrier properties of films were improved after annealing, and this effect is greater on the sample which confined PLLA (20 nm) (*Table 5.6*). In Chapter 4 we showed that this sample does not contain any RAF, which is a phase that does not allow to decouple crystalline and amorphous phases, hindering the relaxation of the polymers chains and thereby accelerating the transport of small molecules (Chapter 3) [3]. We have shown in chapter 3 that the presence of the RAF is the factor determining the gas barrier properties of annealed PLLA. The absence of RAF explains thus the improvement in oxygen permeability of annealed PLLA confined by PS. One should note however, that the final oxygen barrier properties of the confined and annealed PLLA at 85 °C were not better than the properties which were obtained by bulk crystallization of PLLA at 120 °C in absence of RAF and that they were near to amorphous PLLA. The confining of PLLA in the 20 nm film thickness and the mixed orientation of the crystalline lamellae (partly on-edge and partly in-plane), did therefore not allow to increase the tortuosity of permeant pathway beyond the effects of spherulites in the bulk.

PLLA/PC had a different behavior than PLLA/PS. We have two groups with different behaviors. The first group is composed of samples annealed at 85°C. In that case, independently of the thickness of the PLLA layer, the oxygen permeability largely increased compared to amorphous samples. We suggest that this could be caused by two cumulative effects. The PLLA/PC interphase would much likely have higher oxygen permeability than the PLLA bulk. If present in sufficient in non-negligible amount, it would increase the permeability of the films. The 20 nm amorphous sample had smaller permeability than the 300 nm amorphous PLLA sample, most likely caused by its bigger crystallinity degree (*Table 5.5*). Furthermore, the presence of the interphase could hinder the decoupling of amorphous and crystalline phases, because of the existence of supplementary tie molecules between interphase and crystallites. The large dynamic heterogeneity of the PLLA/PC samples annealed at 85 °C would point in this direction. The result would also be a permeability increase. The second group is composed of samples annealed at 120°C, which have the same properties as the 85°C PS/PLLA films. At 120°C, there is a low coupling between amorphous and crystalline phase [3]. Even with the presence of interphases, the coupling between amorphous and crystalline phases plays the most important role in permeability (*Table 5.7*). The in-plane morphology of the crystalline lamellae did not allow to increase the tortuosity of the permeant pathway. Our hypothesis is that the crystallites might be not overlapping, but separated from each other by large spaces of amorphous phase, which represents roughly 50-60% of the PLLA mass. In that case, permeants diffuse almost unhindered through the amorphous zones, which explains that the properties are near to the value of amorphous PLLA.

Considering the helium permeability, we must first notice that the measurements obtained with PLLA/PS exhibited a significant scatter, making interpretation difficult. Nevertheless this scatter was much less important for PLLA/PC films and tendencies could be discussed. An interesting point is related with the fact that PC and PLLA have the same helium permeability, which means that the presence of an interphase would not perturb the helium permeability values as it was the case for oxygen. We can assume that this probe may therefore decouple the interphase effect from the geometrical confinement. Even for amorphous PLLA, a factor around 2 was obtained when reducing the layer thickness. Crystallization at 85°C did not lead to barrier properties improvement, due to the presence of RAF as previously shown in chapter 3. Annealing at 120°C hindered the formation of RAF, leading to another factor 2 improvement on helium permeability. The best helium barrier properties was thus obtained for the confined PLLA crystallized at 120°C.

Table 5.6. Oxygen and helium permeability of PLLA in PLLA/PS films.

	Oxygen permeability (10^{18}.m^3.m.m^{-2}.s^{-1}.Pa^{-1})	Helium permeability (m^3.m/m^2.s.Pa)
PLLA bulk amorphous	1,8 ± 0,5	84 ± 4
PLLA bulk annealed 85°C/180 min	2,2 ± 0,3	85 ± 11
PS bulk	13,2 ± 0,2	198 ± 5
30 µm amorphous	2,0 ± 0,2	55 ± 10
30 µm annealed 85°C/180 min	1,1 ± 0,1	50 ± 9
300 nm amorphous	2,0 ± 0,1	31 ± 15
300 nm annealed 85°C/180 min	1,1 ± 0,1	63 ± 25
20 nm amorphous	1,9 ± 0,1	68 ± 6
20 nm annealed 85°C/180 min	0,3 ± 0,1	32 ± 10

Table 5.7. Oxygen and helium permeability of PLLA in PLLA/PC films.

	Oxygen permeability (10^{18}.m^3.m.m^{-2}.s^{-1}.Pa^{-1})	Helium permeability (m^3.m/m^2.s.Pa)
PLLA bulk amorphous	1,8 ± 0,5	84 ± 4
PLLA bulk annealed 85°C/180 min	2,2 ± 0,3	85 ± 11
PLLA bulk annealed 120°C/180 min	0,4 ± 0,01	53 ± 3
PC bulk	10,1 ± 0,1	90 ± 8
300 nm amorphous	1,9 ± 0,07	49 ± 1
300 nm annealed 85°C/180 min	3,0 ± 0,5	52 ± 3
300 nm annealed 120°C/180 min	0,3 ± 0,01	27 ± 4
20 nm amorphous	1,1 ± 0,03	46 ± 5
20 nm annealed 85°C/180 min	2,2 ± 0,2	54 ± 1
20 nm annealed 120°C/180 min	0,3 ± 0,03	26 ± 2

5.5.Conclusion

The innovative layer multiplying coextrusion process allowed the fabrication of multilayered films composed of alternating layers of PLLA and an amorphous polymer (PS or PC). Continuous layers with individual thicknesses of PLLA down to 30 nanometers were obtained. The study of those films extended our insights into PLLA crystallization under confinement. In particular, by choosing two amorphous polymers (PS and PC) having different chemical affinity with PLLA, the role of the confining polymer was investigated.

While in the as-extruded films PLLA was amorphous, high degrees of crystallinity were achieved by cold-crystallizing PLLA after extrusion. For that, thermal annealing was applied to the nanolayered films at temperatures below the glass transition of the confining amorphous polymer: 85°C for PS/PLLA films, 85°C and 120°C for PC/PLLA films. Highly orientated lamellas were obtained in the crystallized nanolayered films: in-plane lamellas for PC/PLLA (at both temperatures) and mixed lamellas for PS/PLLA, suggesting that a higher interaction between the two polymers favors the formation of in-plane lamellas.

A complete quantitative study of the amorphous and crystalline phases in PC/PLLA films was hindered by the possible presence of an interphase between PLLA and PC layers. Still, it was pointed out that, like in bulk semi-crystalline PLLA, the gas permeability of nanolayered crystallized PLLA was mainly governed by the amorphous phase rather than by the orientation of the lamellas. The best gas barrier properties were thus achieved with the samples presenting the lowest amount of RAF.

5.6.References

[1] R. Auras, B. Harte, S. Selke, An overview of polylactides as packaging materials, Macromol. Biosci. 4 (2004) 835–864. doi:10.1002/mabi.200400043.

[2] A. Guinault, C. Sollogoub, V. Ducruet, S. Domenek, Impact of crystallinity of poly(lactide) on helium and oxygen barrier properties, Eur. Polym. J. 48 (2012) 779–788. doi:10.1016/j.eurpolymj.2012.01.014.

[3] S. Fernandes Nassar, A. Guinault, N. Delpouve, V. Ducruet, C. Sollogoub, S. Domenek, Multi-scale analysis of the impact of polylactide morphology on gas barrier properties, 108 (2017) 163–172. doi:10.1016/j.polymer.2016.11.047.

[4] N. Delpouve, A. Saiter, E. Dargent, Water Barrier Properties in Biaxially Drawn Poly (lactic acid) Films, J. Phys. Chem. B. 116 (2012) 4615–4625. doi:10.1021/jp211670g.

[5] E. Picard, E. Espuche, R. Fulchiron, Effect of an organo-modified montmorillonite on PLA crystallization and gas barrier properties, Appl. Clay Sci. 53 (2011) 58–65. doi:10.1016/j.clay.2011.04.023.

[6] M. Boufarguine, A. Guinault, G. Miquelard-Garnier, C. Sollogoub, PLA/PHBV films with improved mechanical and gas barrier properties, Macromol. Mater. Eng. 298 (2013) 1065–1073. doi:10.1002/mame.201200285.

[7] G. Zhang, P.C. Lee, S. Jenkins, J. Dooley, E. Baer, The effect of confined crystallization on high-density poly(ethylene) lamellar morphology, Polym. (United Kingdom). 55 (2014) 663–672. doi:10.1016/j.polymer.2013.12.027.

[8] H. Wang, J.K. Keum, A. Hiltner, E. Baer, B. Freeman, A. Rozanski, A. Galeski, Confined crystallization of polyethylene oxide in nanolayer assemblies., Science. 323 (2009) 757–760. doi:10.1126/science.1164601.

[9] H. Wang, J.K. Keum, A. Hiltner, E. Baer, Confined crystallization of peo in nanolayered films impacting structure and oxygen permeability, Macromolecules. 42 (2009) 7055–7066. doi:10.1021/ma901379f.

[10] M. MacKey, L. Flandin, A. Hiltner, E. Baer, Confined crystallization of PVDF and a PVDF-TFE copolymer in nanolayered films, J. Polym. Sci. Part B Polym. Phys. 49 (2011) 1750–1761. doi:10.1002/polb.22375.

[11] Y. Lin, A. Hiltner, E. Baer, Nanolayer enhancement of biaxially oriented polypropylene film for increased gas barrier, Polymer (Guildf). 51 (2010) 5807–5814. doi:10.1016/j.polymer.2010.09.070.

[12] G. Zhang, E. Baer, A. Hiltner, Gas permeability of poly(4-methylpentene-1) in a confined nanolayered film system, Polym. (United Kingdom). 54 (2013) 4298–4308. doi:10.1016/j.polymer.2013.05.074.

[13] J.M. Carr, D.S. Langhe, M.T. Ponting, A. Hiltner, E. Baer, Confined crystallization in polymer nanolayered films: A review, J. Mater. Res. 27 (2012) 1326–1350. doi:10.1557/jmr.2012.17.

[14] M. Ponting, Y. Lin, J.K. Keum, A. Hiltner, E. Baer, Effect of substrate on the isothermal crystallization kinetics of confined poly(ε-caprolactone) nanolayers, Macromolecules. 43 (2010) 8619–8627. doi:10.1021/ma101625h.

[15] D.S. Langhe, A. Hiltner, E. Baer, Melt crystallization of syndiotactic polypropylene in nanolayer confinement impacting structure, Polymer (Guildf). 52 (2011) 5879–5889. doi:10.1016/j.polymer.2011.10.018.

[16] Y. Wang, C.M. Chan, K.M. Ng, N. Li, What controls the lamellar orientation at the surface of polymer films during crystallization?, Macromolecules. 41 (2008) 2548–2553. doi:10.1021/ma7021309.

[17] Y.X. Liu, E.Q. Chen, Polymer crystallization of ultrathin films on solid substrates, Coord. Chem. Rev. 254 (2010) 1011–1037. doi:10.1016/j.ccr.2010.02.017.

[18] R.E. Prud'homme, Crystallization and morphology of ultrathin films of homopolymers and polymer blends, Prog. Polym. Sci. 54-55 (2015) 214–231. doi:10.1016/j.progpolymsci.2015.11.001.

[19] H. Wang, J.K. Keum, A. Hiltner, E. Baer, Impact of nanoscale confinement on crystal orientation of poly(ethylene oxide), Macromol. Rapid Commun. 31 (2010) 356–361. doi:10.1002/marc.200900653.

[20] Y. Ma, G. Reiter, W. Hu, Lamellar Crystal Orientations Biased by Crystallization Kinetics in Polymer Thin Films Lamellar Crystal Orientations Biased by Crystallization Kinetics in Polymer Thin Films, Society. (2006) 5159–5164. doi:10.1021/ma060798s.

[21] Y. Ma, W. Hu, J. Hobbs, G. Reiter, Understanding crystal orientation in quasi-one-dimensional polymer systems, Soft Matter. 4 (2008) 540. doi:10.1039/b715065b.

[22] N. Wu, M. Ding, C. Li, Y. Yuan, J. Zhang, Lamellar orientation and crystallization dynamics of poly (L-lactic acid) thin films investigated by in-situ reflection absorption infrared spectroscopy, J. Phys. Chem. B. 115 (2011) 11548–11553. doi:10.1021/jp203110u.

[23] D. Maillard, R.E. Prud'homme, Crystallization of ultrathin films of polylactides: From chain chirality to lamella curvature and twisting, Macromolecules. 41 (2008) 1705–1712. doi:10.1021/ma071306u.

[24] A. Mohamed, S.H. Gordon, G. Biresaw, Poly(lactic acid)/Polystyrene Bioblends Characterized by Thermogravimetric Analysis, Differential Scanning Calorimetry, and Photoacoustic Infrared Spectroscopy, J. Appl. Polym. Sci. 106 (2007) 1689–1696. doi:10.1002/app.

[25] B.O. Leung, A.P. Hitchcock, J.L. Brash, A. Scholl, A. Doran, Phase Segregation in Polystyrene - Polylactide Blends, Macromolecules. 42 (2009) 1679–1684. doi:10.1021/ma802176b.

[26] P. Sarazin, B.D. Favis, Morphology control in co-continuous poly(L-lactide)/polystyrene blends: A route towards highly structured and interconnected porosity in poly(L-lactide) materials, Biomacromolecules. 4 (2003) 1669–1679. doi:10.1021/bm030034+.

[27] G. Biresaw, C.J. Carriere, Interfacial tension of poly(lactic acid)/polystyrene blends, J. Polym. Sci. Part B Polym. Phys. 40 (2002) 2248–2258. doi:10.1002/polb.10290.

[28] B. Imre, K. Renner, B. Pukánszky, Interactions, structure and properties in poly (lactic acid)/thermoplastic polymer blends, Express Polym. Lett. 8 (2014) 2–14. doi:10.3144/expresspolymlett.2014.

[29] H. Wang, J.K. Keum, A. Hiltner, E. Baer, Crystallization kinetics of poly(ethylene oxide) in confined nanolayers, Macromolecules. 43 (2010) 3359–3364. doi:10.1021/ma902780p.

[30] A. Flores, F. Ania, C. Arribas, A. Ochoa, S. Scholtyssek, F.J. Baltá-Calleja, E. Baer, Confined crystallization of nanolayered poly(ethylene terephthalate) using X-ray diffraction methods, Polym. (United Kingdom). 53 (2012) 3986–3993. doi:10.1016/j.polymer.2012.06.047.

[31] S. Iannace, L. Nicolais, Isothermal Crystallization and Chain Mobility of Poly (L - lactide), J. Appl. Polym. Sci. (1997) 911–919.

[32] S.H. Park, S.G. Lee, S.H. Kim, Isothermal crystallization behavior and mechanical properties of polylactide/carbon nanotube nanocomposites, Compos. Part A Appl. Sci. Manuf. 46 (2013) 11–18. doi:10.1016/j.compositesa.2012.10.011.

[33] M. Dasriaux, S. Castagnet, L. Thilly, L. Chocinski-Arnault, S. a E. Boyer, Evolution of the amorphous fraction of PEEK during annealing at atmospheric and high pressure

above the glass transition temperature, J. Appl. Polym. Sci. 130 (2013) 1148–1157. doi:10.1002/app.39297.

[34] M. Yasuniwa, S. Tsubakihara, K. Iura, Y. Ono, Y. Dan, K. Takahashi, Crystallization behavior of poly(l-lactic acid), Polymer (Guildf). 47 (2006) 7554–7563. doi:10.1016/j.polymer.2006.08.054.

[35] G. Stoclet, R. Seguela, C. Vanmansart, C. Rochas, J.M. Lefebvre, WAXS study of the structural reorganization of semi-crystalline polylactide under tensile drawing, Polymer (Guildf). 53 (2012) 519–528. doi:10.1016/j.polymer.2011.11.063.

[36] L. Cartier, T. Okihara, Y. Ikada, H. Tsuji, J. Puiggali, B. Lotz, Epitaxial crystallization and crystalline polymorphism of polylactides, Polymer (Guildf). 41 (2000) 8909–8919. doi:10.1016/0032-3861(94)90933-4.

[37] J. Zhang, K. Tashiro, H. Tsuji, A.J. Domb, Investigation of Phase Transitional Behavior of Poly (l-lactide)/ Poly (d- lactide) Blend Used to Prepare the Highly-Oriented Stereocomplex Investigation of Phase Transitional Behavior of Poly (L -lactide)/ Poly (D -lactide) Blend Used to Prepare, Macromolecules. (2007) 1049–1054. doi:10.1021/ma061693s.

[38] G. Stoclet, R. Séguéla, J.M. Lefebvre, S. Li, M. Vert, Thermal and strain-induced chain ordering in lactic acid stereocopolymers: Influence of the composition in stereomers, Macromolecules. 44 (2011) 4961–4969. doi:10.1021/ma200469t.

[39] R.V. Castillo, A.J. Müller, M. Lin, H. Chen, U. Jeng, M. a Hillmyer, Confined Crystallization and Morphology of Melt Segregated PLLA- b -PE and PLDA- b -PE Diblock Copolymers, Macromolecules. 41 (2008) 6154–6164. doi:10.1021/ma800859y.

[40] Y. Wang, S.S. Funari, J.F. Mano, Influence of semicrystalline morphology on the glass transition of poly(L-lactic acid), Macromol. Chem. Phys. 207 (2006) 1262–1271. doi:10.1002/macp.200600114.

[41] J. Zhang, K. Tashiro, H. Tsuji, A.J. Domb, Disorder-to-order phase transition and multiple melting behavior of poly(L-lactide) investigated by simultaneous measurements of WAXD and DSC, Macromolecules. 41 (2008) 1352–1357. doi:10.1021/ma0706071.

[42] M.L. Di Lorenzo, M. Cocca, M. Malinconico, Crystal polymorphism of poly(l-lactic acid) and its influence on thermal properties, Thermochim. Acta. 522 (2011) 110–117. doi:10.1016/j.tca.2010.12.027.

[43] H. Chen, M. Pyda, P. Cebe, Non-isothermal crystallization of PET/PLA blends, Thermochim. Acta. 492 (2009) 61–66. doi:10.1016/j.tca.2009.04.023.

[44] D. Bao, X. Liao, G. He, E. Huang, Q. Yang, G. Li, Effects of enhanced compatibility by transesterification on the cell morphology of poly(lactic acid)/ polycarbonate blends using supercritical carbon dioxide, J. Cell. Plast. 51 (2015) 349–372. doi:10.1177/0021955X14537661.

[45] Y. Chen, Y. Peng, W.Y. Liu, G.S. Zeng, J.H. Yang, X.H. Yan, The Effect of Various Catalyzers on Transesterification in Reactive Blending PC/PLA Blends, Adv. Mater. Res. 741 (2013) 24–27. doi:10.4028/www.scientific.net/AMR.741.24.

[46] C. Liu, S. Lin, C. Zhou, W. Yu, Influence of catalyst on transesterification between poly(lactic acid) and polycarbonate under flow field, Polym. (United Kingdom). 54 (2013) 310–319. doi:10.1016/j.polymer.2012.11.047.

[47] M.C. Righetti, D. Prevosto, E. Tombari, Time and Temperature Evolution of the Rigid Amorphous Fraction and Differently Constrained Amorphous Fractions in PLLA, Macromol. Chem. Phys. (2016) 1–14. doi:10.1002/macp.201600210.

Chapter 6 - Physical aging in PLLA confined at the nanoscale by multilayer coextrusion

6. Physical aging in PLLA confined at the nanoscale by multilayer coextrusion

Xavier Monnier[c], Samira Fernandes Nassar[a], Sandra Domenek[a], Alain Guinault[b], Cyrille Sollogoub[b], Eric Dargent[c], Nicolas Delpouve[c]

[a]UMR Ingénierie Procédés Aliments, AgroParisTech, INRA, Université Paris-Saclay, 1 avenue des Olympiades, F-91300 Massy, France

[b]PIMM, Arts et Métiers ParisTech/CNRS/CNAM, 151 Bd de l'Hôpital, F-75013 Paris Cedex, France

[c]Normandie Univ, UNIROUEN Normandie, INSA Rouen, CNRS, Groupe de Physique des Matériaux, 76000 Rouen, France

Corresponding author: Nicolas Delpouve,
Normandie Univ, UNIROUEN Normandie, INSA Rouen, CNRS, Groupe de Physique des Matériaux, 76000 Rouen, France

Email: nicolas.delpouve1@univ-rouen.fr

This chapter results from a current joint collaboration with Xavier Monnier.
"Etude de la mobilité moléculaire dans des systèmes polymères complexes, anisotropes, et confinés".

6.1.Introduction

Physical aging is a ubiquitous phenomenon in glassy materials and originates from the fact that they are out-of-equilibrium, it is associated with molecular rearrangements at low temperatures ($T < T_g$). The aging effects can be erased by heating the material above its glass transition temperature (T_g) during a time, which allows the material achieve an equilibrium state [1]. Because many properties change when material undergoes physical aging, as increase of brittleness [2], decrease of gas permeability [3], etc., the understanding of this phenomenon is essential for the practical use of polymers. There are a lot of methods that have been used to study physical aging, including differential scanning calorimetry (DSC) [4–6], gas permeability measurement [3,7,8], dielectric spectroscopy [9–11], positron annihilation spectroscopy (PALS) [12], etc.

In DSC, physical aging is characterized by enthalpy recovery, which appears as the development of an endothermic peak after the heat capacity step of the glass transition. This peak systematically shifts to higher temperatures and its intensity increases in magnitude with increasing aging time.

Today, the recent development of Flash DSC has received much interest regarding physical aging [6,13,14]. Such technique allows to heat up and cool down polymers as fast as thousand Kelvin per second. Therefore, the sample masses are drastically reduced from few mg by standard DSC to tens ng by Flash DSC, in order to reduce thermal lag (i.e., temperature gradients occurring in sample and instrument during the measurement). With this technique, thermodynamic equilibrium can be reached much faster than standard DSC [15].

Physical aging in bulk polymer systems has been studied for many years using these techniques and others, but recently literature has focused on aging in confined polymers.

Most of the studies of physical aging using DSC have often observed accelerated aging in confinement [9,16,17] though some studies have observed decreases in the aging with confinement [18,19]. These opposite results and interpretations largely open the debate about the possible existence of antagonist causes driving the structural relaxation in confined landscapes.

Boucher et al. found that PS films with thickness in the range of hundreds of nanometers demonstrated accelerated aging [20] as well as Cangialosi et al. [21] observed accelerated aging in PMMA-silica and PS-silica nanocomposites.

An opposite behavior was seen by Langhe et al [18]. They studied physical aging of PS layers in multilayers films of PS and polycarbonate (PC) using DSC. The PS/PC films had PS layers thickness ranging from 50 to 500 nm. The T_g of the PS was independent of layers thickness and the same as bulk PS, however a reducing in the aging rate was observed when PS layer thickness decreased from 500 to 50 nm. They found a fraction of interphase material between PC and PS, containing both PS and PC, which increases as layer thickness decreases, and it was inversely correlated with aging rate. The increased T_g of the interphase material was hypothesized to lead to longer relaxation times, thus reducing the aging rate.
In this work, we studied the impact of confinement on physical aging of PLLA confined by PS in multi-nanolayers films using Flash DSC.

6.2.Materials and methods

The materials used are multi-nanolayers films PLLA/PS. Polymers and methods used in this process are described in Chapter 4 The annealing procedures, the phase content of semi-crystalline materials as well as the glass transition dynamics are also given in Chapter 4.

6.2.1. Characterization of physical aging

The experiments were carried out using a Flash DSC (Mettler-Toledo). The sample mass, typically, was of the order of magnitude of 50 ng which was roughly estimated by comparison of the value of the heat capacity step ΔCp from the one obtained through Flash DSC at 1000 $K.s^{-1}$ and the one obtained through MT-DSC at 1 $K.min^{-1}$ equal to 0,48 $J.g^{-1}.K^{-1}$ for 30 μm sample and 0,44 $J.g^{-1}.K^{-1}$ for 300 nm and 20 nm sample. Multi-nanolayers films were cut with the help of a microtome to obtain in a first preparation step thin sections, which then were reduced with the help of a scalpel.
Samples were placed on the MultiSTAR UFS1 MEMS sensors as shown in Figure *6.1*. The area to place the samples is 180 x 180 μm. An Intracooler Huber TC100 was used to cool down samples up to 178 K and operate at high cooling speeds. The thermal contact between the sample and the sensor was improved using a thin layer of silicone oil. The purge gas used was nitrogen to prevent water condensation. A flow of 20 mL min^{-1} was chosen to optimize machine performance. The temperature profile used for physical aging is shown in Figure *6.2*. The used heating rate was 1000 K s-1.

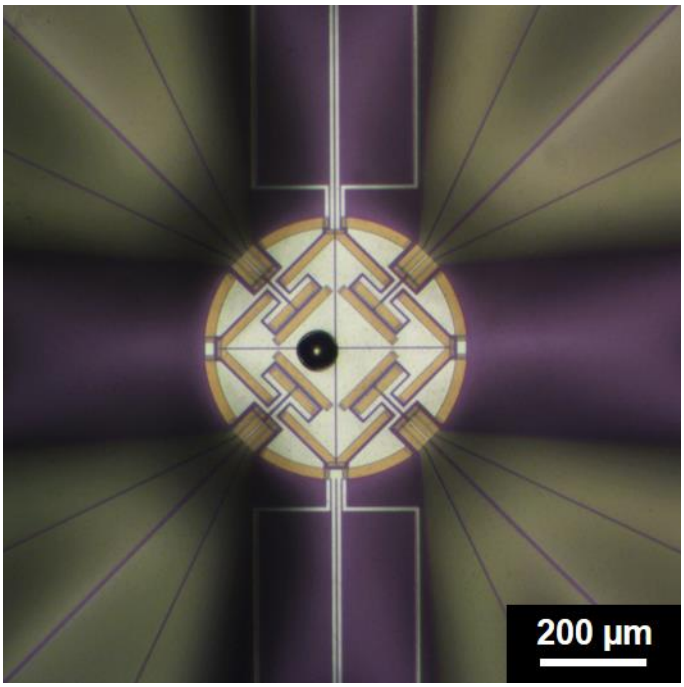

Figure 6.1. Picture of the 30000 nm PLLA nominal thickness amorphous sample.

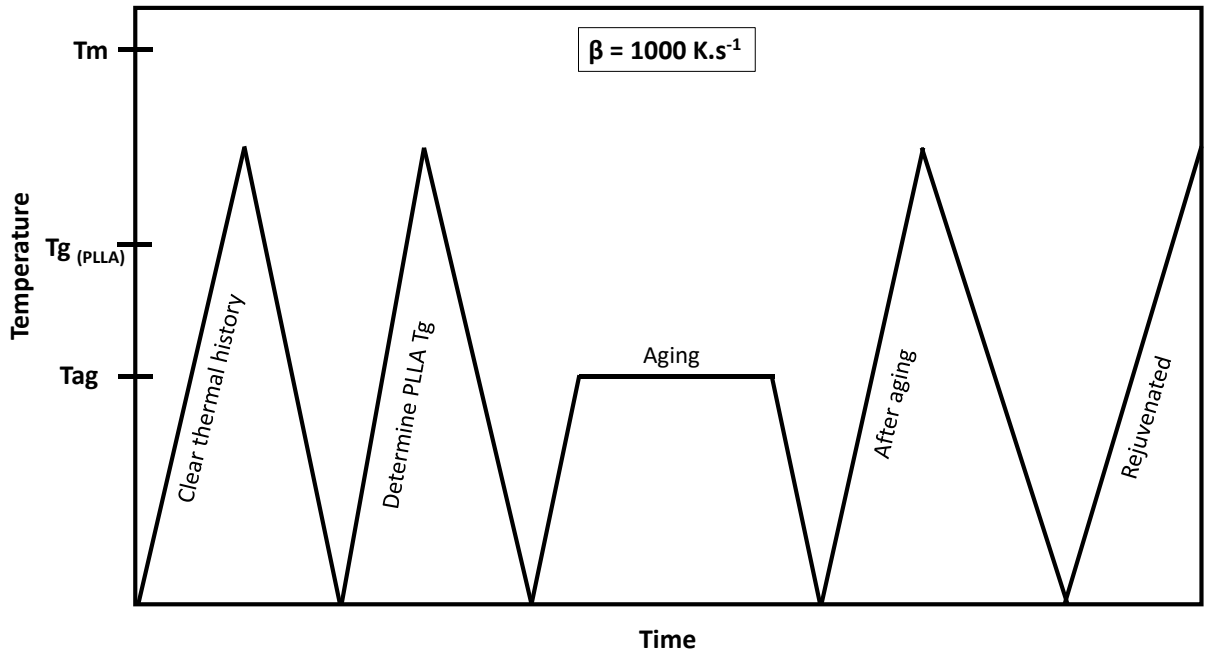

Figure 6.2. Temperature profile for the PLLA physical aging study in Flash DSC.

The aging temperature was estimated to be 18°C below the glass transition temperature determined during the cooling step in Flash DSC. Such a determination required the successive corrections of the static thermal lag (Figure *6.3*) and the dynamic thermal lag (Figure *6.4*). The

static thermal lag is related to the thickness of the sample. The dynamic thermal lag is related to the intrinsic nature of both the technique and the material themselves. As shown in Figure *6.5*, the fictive temperature is not dependent on the cooling rate for this range of cooling rates in PLLA whereas it is highly dependent on the heating rate. After correction one can find an identical fictive temperature from both heating and cooling measurements. The fictive temperature shows dependency from the cooling rate when reaching lower values as the ones usually applied in conventional DSC. Therefore the reference glass transition in this study is the invariant fictive temperature measured upon cooling. The aging time (tag) range was chosen from 0,001 to 100 min to cover the whole relaxation kinetic. This calibration procedure has been validated for bulk PLLA. More details about the procedure can be found in reference [15].

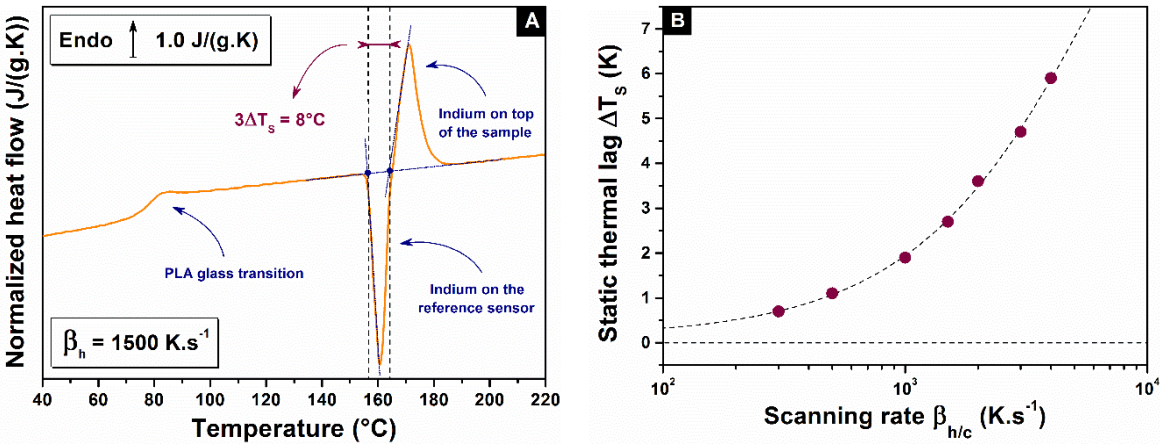

Figure 6.3. Manifestation (A) and dependence (B) of the static thermal lag with the heating/cooling rate for bulk PLLA.

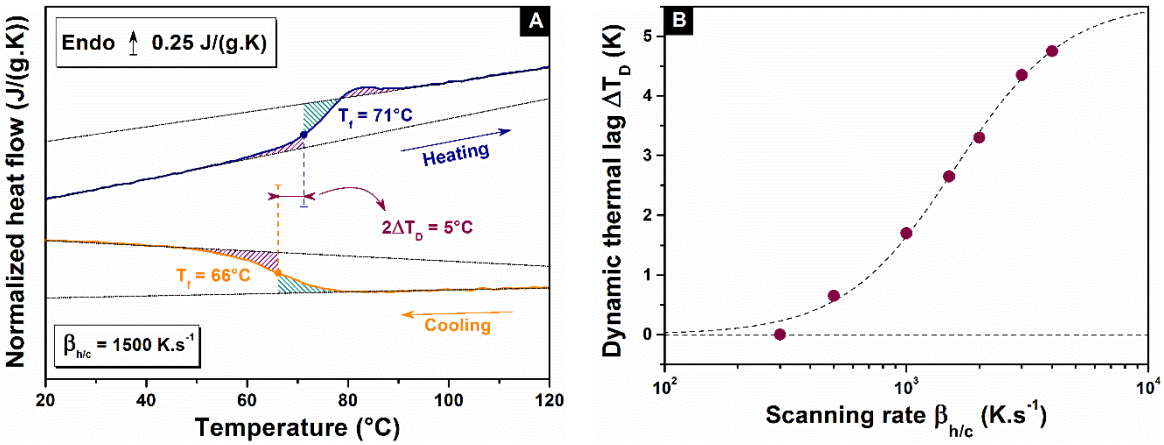

Figure 6.4. Manifestation (A) and dependence (B) of the dynamic thermal lag with the heating/cooling rate for bulk PLLA.

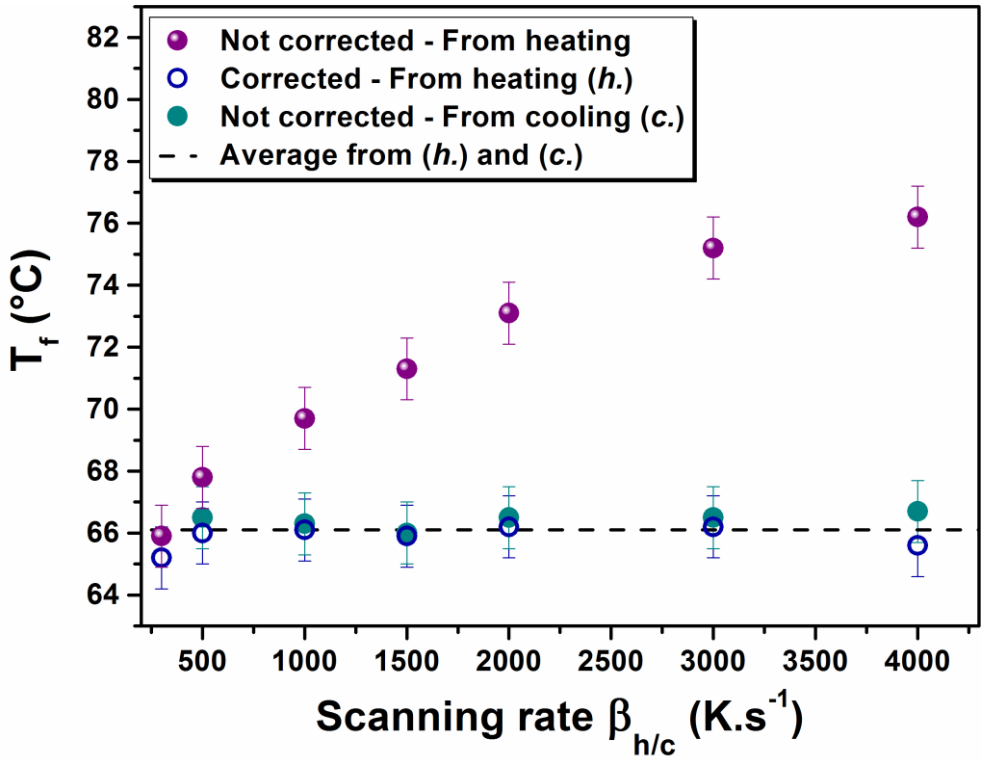

Figure 6.5. Dependence of the fictive temperature with heating and cooling rates before and after correction of the dynamic thermal lag for bulk PLLA.

6.3.Results and discussion

Questioning the aptitude of the Flash DSC to correctly picture the relaxation behavior of samples exhibiting drastically different layer dimension is relevant, expecially for high nominal

thickness. Figure *6.6* shows the heat flow curve of PS/PLLA with 30 μm PLLA thickness. The recorded heat flow was normalized as a function of sample mass. The heating scan was made from 0 to 230°C, erasing all thermal history of PLLA. All the impact and constraints that PLLA has suffered from the process, including stretching and confinement, was erased because the scan was performed above PLLA melting temperature. One observe that the amount of sample used for the Flash DSC analysis is sufficient to give a representative response of the whole film since the progressive increase of the enthalpy of recovery during aging of PLLA and PS appears explicitly. The phenomenon is obviously amplified for PLLA as the temperature of aging is closer to its glass transition temperature. Monnier et al. [15] already showed that a few ng of PLA analyzed by Flash DSC are totally representative of the bulk sample analyzed by standard DSC. Contrary to standard or TM DSC experiments for which the sensitivity/resolution compromise needed to measure the heat flow drastically limits the range for the sample mass and the scanning rate [22], in Flash DSC smother heat flow signals are observed when the scanning rate increases [15].

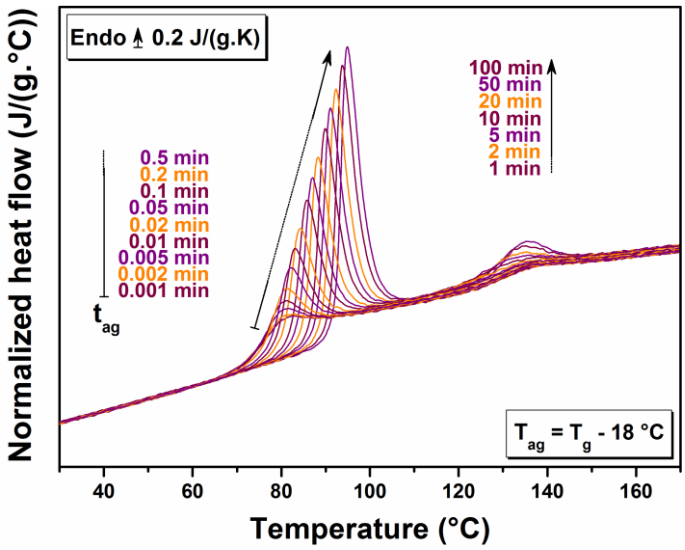

Figure 6.6. Normalized heat flow of 30000 nm PLLA nominal thickness amorphous multilayer film.

Figure *6.7*, Figure *6.8* and Figure *6.9* show the normalized heat flow curves of PS/PLLA films with 30 μm, 300 nm and 20 nm PLLA layer thickness respectively. To keep the layer integrity, the successive scans were stopped before reaching the glass transition temperature of polystyrene. In all samples, amorphous and annealed, endothermic relaxation peaks increase

and shift towards high temperatures when the aging times increase, as classically observed for glass formers including PLLA [23,24].

As shown in Figure *6.7*a the amplitude of the enthalpy recovery is significantly lower for the 30 µm PLLA/PS multilayer film (in comparison with Figure *6.6*) when the layer integrity is kept. One can also observe that the signature of the physical aging is by far broader. This evidences an effect related to the multilayer coextrusion process that disappears when destroying the layers. The comparison of the aging of 30 µm amorphous sample with those of 300 nm and 20 nm amorphous (Figure *6.7*a, Figure *6.8*a, Figure *6.9*a), at any aging time, puts in evidence that, the endothermic peak measured in the nano-layers samples appears as less pronounced and broader than that of micrometer layers. This is a typical behavior for confined materials [20] which is related to the influence of the sample dimension in the physical aging as a higher relative mass of the sample relaxes while cooling down the system from the liquid state to the aging temperature. In annealed samples, the same behavior is observed and it is possible to record the crystallization effect on the recovery enthalpy peak, which is even less pronounced in the presence of crystals because of the reducing of the amorphous phase content (Figure *6.7*b, Figure *6.8*b, Figure *6.9*b).

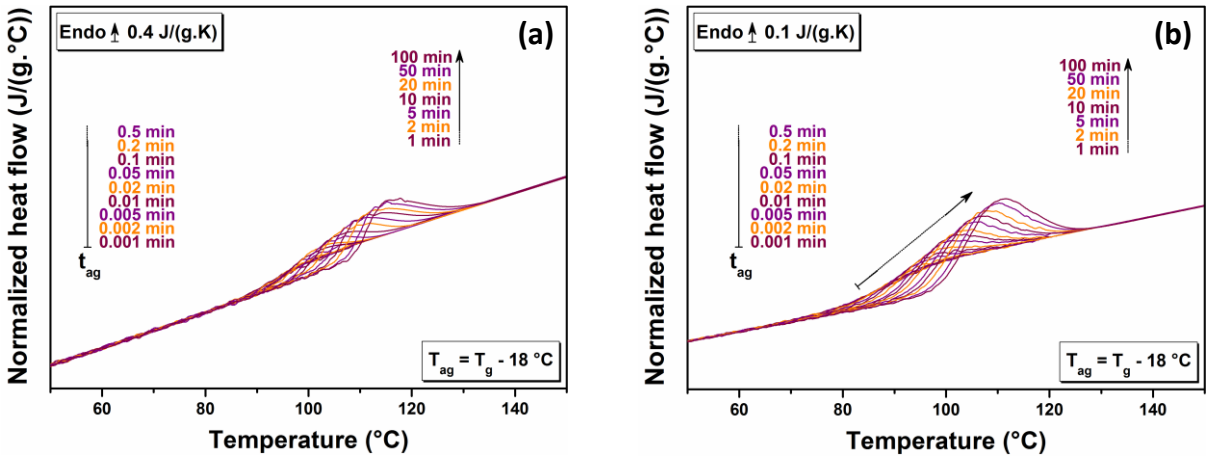

Figure 6.7. Normalized heat flow of 30 µm PLLA/PS multilayer aged when (a) PLLA is amorphous and (b) annealed.

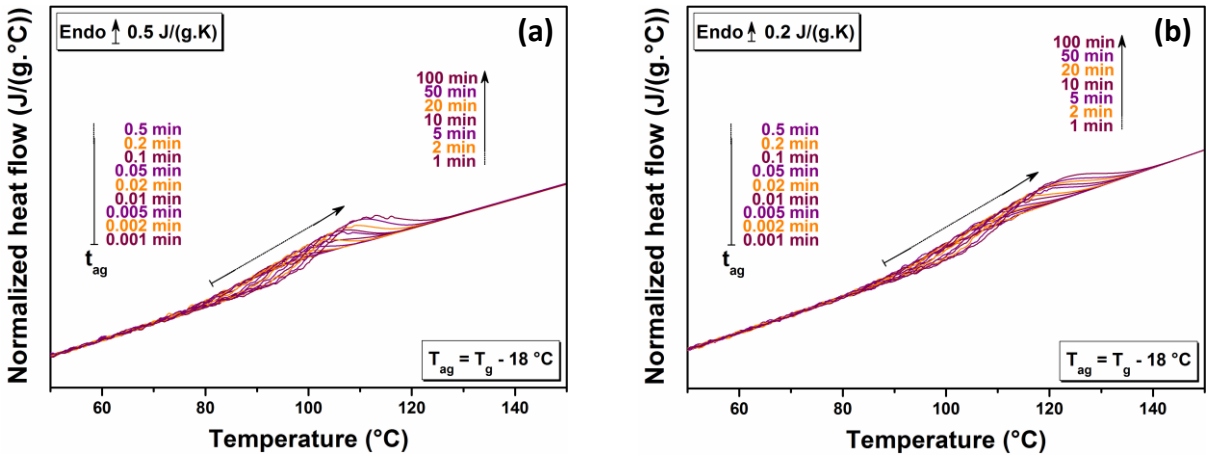

Figure 6.8. Normalized heat flow of 300 nm PLLA/PS multilayer aged when (a) PLLA is amorphous and (b) annealed.

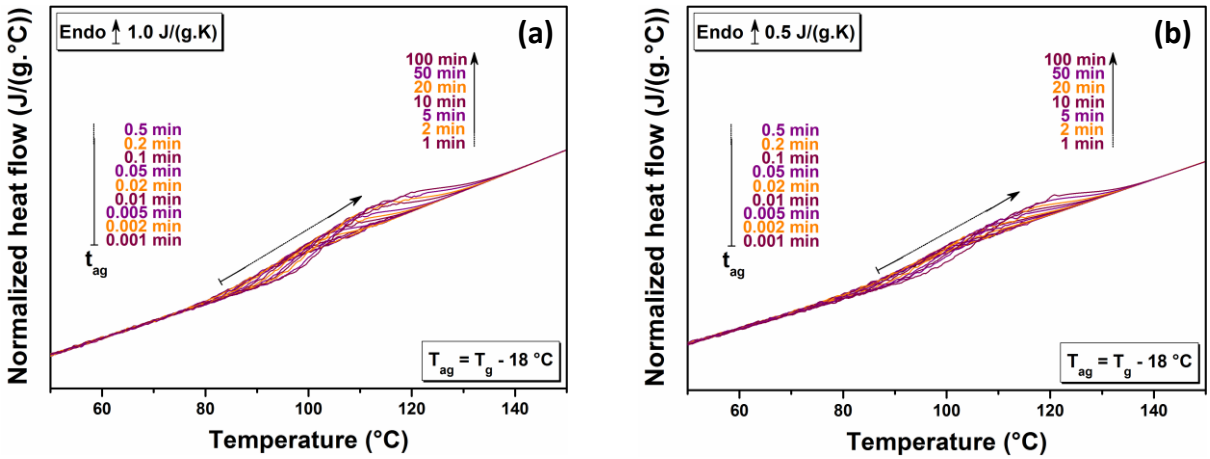

Figure 6.9. Normalized heat flow of 20 nm PLLA/PS multilayer aged when (a) PLLA is amorphous and (b) annealed

Figure *6.10* shows the shift of recovery enthalpy peak as a function of aging time for all samples. We can observe that process impacts the shift of recovery enthalpy since, in 30 μm sample which scanning rate was above PLLA melting temperature, the shift was much lighter than samples which process effects were kept. More significantly, we observe a greater shift when the thickness of PLLA layers decreases. This result might be the signature of a strong heterogeneity in the structural relaxation landscape related to non-isothermal physical aging [20].

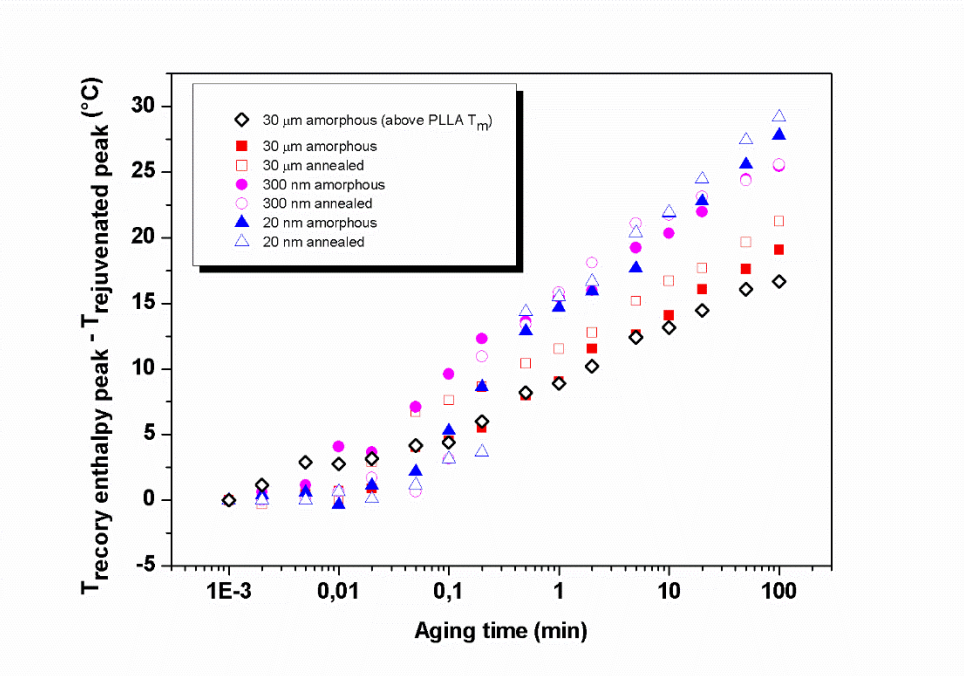

Figure 6.10. Difference between the temperatures of recovery enthalpy peak and the temperature of rejuvenated peak as a function of aging times for all samples.

In Figure *6.11*, the time dependence of the difference between the total enthalpy loss (ΔH_∞) and the enthalpy recovery (ΔH_t) is shown for all samples. ΔH_∞ is thanks to Flash DSC determinable from empirical way, confirming an acceptable description by the following equation:

$$\Delta H_\infty = \Delta C_p \cdot (T_g - T_{ag}) \qquad \text{Equation 6.1}$$

Where ΔCp is the heat capacity, T_g is the glass transition temperature determined at the cooling at 1000 $K.s^{-1}$ in Flash DSC and T_{ag} is the aging temperature. Because the content of relaxing amorphous phase varies from a sample to another, the values of enthalpy of recovery are normalized to X_{MAF} to allow comparing the structural relaxation kinetics. As can be observed in Figure *6.11*, samples annealed at 85°C (full symbols) exhibit the same trends as amorphous samples (empty symbols). This reveals a minor role of the chain constraints induced by thermal crystallization including the coupling effect.

On the other hand the physical aging kinetics slows down because of the process. We cannot attribute this tendency to pure geometric restrictions as the volume of the amorphous phase also

reduced during crystallization without any perceptible effect on the relaxation kinetic. Some studies mentioned that, physical aging in confined systems can be dramatically impacted by surface effects, which is responsible for mobility changes at the interface [10,25,26]. They invoke that the acceleration of physical aging in confined systems can be explained by a mechanism based on diffusion of free volume which is accelerated in the presence of surfaces [11]. Recent studies propose a relation between the physical aging and the inherent stress of the macromolecular system. Pye et al. showed from ellipsometry study [27] that the physical aging rate of polystyrene is independent of film thickness between 220 and 1800 nm when the applied stress is the same. Ghazaryan et al. [28] report that both uniaxial and biaxial plastic deformation in excess of 150% plastic strain, decelerates and possibly prohibits the physical ageing process. This idea of an inherent mechanical stress could explain why the impact of the process on the relaxation dynamics differs so strong from the pure thermal crystallization. Delpouve et al. [29] have already reported that the dependence of the relaxation times with temperature is identical between an amorphous PLA its analogous after crystallization at 80°C while significant changes were observed after drawing in the same temperature domain. Interestingly the most confined sample exhibits the same relaxation kinetic than a bulk PLLA. In regard to the previous assumption this would mean that there is a threshold for which the inherent stress disappears. At the last stages of confinement, the macromolecule is insulated. It seems that this environment favors the annihilation of the constraints. The system can thus be seen as the ideal amorphous state of the glass former.

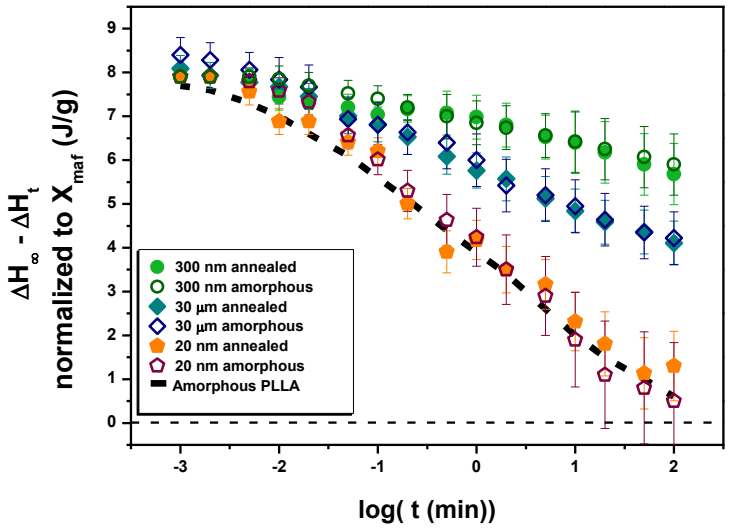

Figure 6.11. Time evolution of the difference between the total enthalpy loss ΔH∞ and the enthalpy recovery ΔHt for the 300 nm, 30 mm and 20 nm PLLA/PS multilayer aged when PLLA is amorphous (empty symbols) and annealed (full symbols). Enthalpy recovery are normalized to the mobile amorphous fraction X_{MAF}.

6.4.Conclusion

The use of Flash DSC allows obtaining information about the structural relaxation kinetic in an enhanced scale. We show here that the multilayer coextrusion process is able to slow down the physical aging on a level largely higher than thermal crystallization. This observation is however limited to a given range of thickness. For the most reduced layer scales the kinetic of the structural relaxation is the same than those of pure amorphous bulk PLLA. These results are consistent with the previous investigations about the glass transition and the dynamic heterogeneity which suggests a total disassociation or decoupling of the PLLA macromolecule to its neighboring when confined to a very limited volume.

6.5.References

[1] D. Cangialosi, V.M. Boucher, A. Alegria, J. Colmenero, A. Alegría, Physical aging in polymers and polymer nanocomposites: recent results and open questions, Soft Matter. 9 (2013) 8619. doi:10.1039/c3sm51077h.

[2] Y. Huang, D.R. Paul, Physical aging of thin glassy polymer films monitored by gas permeability, Macromolecules. 39 (2006) 1554–1559. doi:10.1016/j.polymer.2004.10.019.

[3] B.W. Rowe, B.D. Freeman, D.R. Paul, Physical aging of ultrathin glassy polymer films tracked by gas permeability, Polymer (Guildf). 50 (2009) 5565–5575. doi:10.1016/j.polymer.2009.09.037.

[4] V.M. Boucher, D. Cangialosi, A. Alegría, J. Colmenero, Enthalpy recovery of PMMA/silica nanocomposites, Macromolecules. 43 (2010) 7594–7603. doi:10.1021/ma101217y.

[5] V.M. Boucher, D. Cangialosi, A. Alegría, J. Colmenero, Enthalpy recovery of glassy polymers: Dramatic deviations from the extrapolated liquidlike behavior, Macromolecules. 44 (2011) 8333–8342. doi:10.1021/ma2018233.

[6] E. Lopez, S.L. Simon, Signatures of Structural Recovery in Polystyrene by Nanocalorimetry, Macromolecules. 49 (2016) 2365–2374. doi:10.1021/acs.macromol.5b02112.

[7] Y. Huang, D.R. Paul, Physical aging of thin glassy polymer films monitored by gas permeability, Polymer (Guildf). 45 (2004) 8377–8393. doi:10.1016/j.polymer.2004.10.019.

[8] T.M. Murphy, D.S. Langhe, M. Ponting, E. Baer, B.D. Freeman, D.R. Paul, Physical aging of layered glassy polymer films via gas permeability tracking, Polymer (Guildf). 52 (2011) 6117–6125. doi:10.1016/j.polymer.2011.10.061.

[9] V.M. Boucher, D. Cangialosi, A. Alegría, J. Colmenero, I. Pastoriza-Santos, L.M. Liz-Marzan, Physical aging of polystyrene/gold nanocomposites and its relation to the calorimetric Tg depression, Soft Matter. 7 (2011) 3607. doi:10.1039/c0sm01326a.

[10] V.M. Boucher, D. Cangialosi, A. Alegría, J. Colmenero, J. González-Irun, L.M. Liz-Marzan, Accelerated physical aging in PMMA/silica nanocomposites, Soft Matter. 6 (2010) 3306. doi:10.1039/c001656j.

[11] D. Cangialosi, M. Wübbenhorst, J. Groenewold, E. Mendes, S.J. Picken, Diffusion mechanism for physical aging of polycarbonate far below the glass transition temperature studied by means of dielectric spectroscopy, J. Non. Cryst. Solids. 351 (2005) 2605–2610. doi:10.1016/j.jnoncrysol.2005.03.070.

[12] D. Cangialosi, M. W??bbenhorst, J. Groenewold, E. Mendes, H. Schut, a. Van Veen, S.J. Picken, Physical aging of polycarbonate far below the glass transition temperature: Evidence for the diffusion mechanism, Phys. Rev. B - Condens. Matter Mater. Phys. 70 (2004) 1–11. doi:10.1103/PhysRevB.70.224213.

[13] S. Gao, S.L. Simon, Measurement of the limiting fictive temperature over five decades of cooling and heating rates, Thermochim. Acta. 603 (2015) 123–127. doi:10.1016/j.tca.2014.08.019.

[14] Y.P. Koh, S. Gao, S.L. Simon, Structural recovery of a single polystyrene thin film using Flash DSC at low aging temperatures, Polym. (United Kingdom). 96 (2016) 182–187. doi:10.1016/j.polymer.2016.04.047.

[15] X. Monnier, A. Saiter, E. Dargent, Physical aging in {PLA} through standard {DSC} and fast scanning calorimetry investigations, Thermochim. Acta. 648 (2016) -. doi:http://dx.doi.org/10.1016/j.tca.2016.12.006.

[16] Y.P. Koh, G.B. McKenna, S.L. Simon, Calorimetric Glass Transition Temperature and Absolute Heat Capacity of Polystyrene Ultrathin Films, J. Polym. Sci. Part B Polym. Phys. 44 (2006) 3518–3527. doi:10.1002/polb.

[17] H. Lu, S. Nutt, Restricted relaxation in polymer nanocomposites near the glass transition, Macromolecules. 36 (2003) 4010–4016. doi:10.1021/ma034049b.

[18] D.S. Langhe, T.M. Murphy, A. Shaver, C. Laporte, B.D. Freeman, D.R. Paul, E. Baer, Structural relaxation of polystyrene in nanolayer confinement, Polymer (Guildf). 53 (2012) 1925–1931. doi:10.1016/j.polymer.2012.02.044.

[19] A.L. Flory, T. Ramanathan, L.C. Brinson, Physical aging of single wall carbon nanotube polymer nanocomposites: Effect of functionalization of the nanotube on the enthalpy relaxation, Macromolecules. 43 (2010) 4247–4252. doi:10.1021/ma901670m.

[20] V.M. Boucher, D. Cangialosi, A. Alegr??a, J. Colmenero, Enthalpy recovery in nanometer to micrometer thick polystyrene films, Macromolecules. 45 (2012) 5296–5306. doi:10.1021/ma300622k.

[21] D. Cangialosi, V.M. Boucher, A. Alegría, J. Colmenero, Enhanced physical aging of polymer nanocomposites: The key role of the area to volume ratio, Polymer (Guildf). 53 (2012) 1362–1372. doi:10.1016/j.polymer.2012.01.033.

[22] E. Verdonck, K. Schaap, L.C. Thomas, A discussion of the principles and applications of Modulated Temperature DSC (MTDSC), Int. J. Pharm. 192 (1999) 3–20. doi:10.1016/S0378-5173(99)00267-7.

[23] a. Celli, M. Scandola, Thermal properties and physical ageing of poly(L-lactic acid), Polymer (Guildf). 33 (1992) 2699–2703. doi:10.1016/0032-3861(92)90440-8.

[24] P. Pan, B. Zhu, Y. Inoue, Enthalpy Relaxation and Embrittlement of Poly (L -lactide) during Physical Aging, Macromolecules. 40 (2007) 9664–9671.

[25] J.A. Forrest, J.R. Dutcher, Interface and chain confinement effects on the glass transition temperature of thin polymer film, Phys. Rev. E. 56 (1997) 5705–5716.

[26] C.J. Ellison, J.M. Torkelson, The distribution of glass-transition temperatures in nanoscopically confined glass formers., Nat. Mater. 2 (2003) 695–700. doi:10.1038/nmat980.

[27] J.E. Pye, C.B. Roth, Physical aging of polymer films quenched and measured free-standing via ellipsometry: Controlling stress imparted by thermal expansion mismatch between film and support, Macromolecules. 46 (2013) 9455–9463. doi:10.1021/ma401872u.

[28] G. Ghazaryan, R. Schaller, K. Feldman, T. a. Tervoort, Rejuvenation of PLLA: Effect of plastic deformation and orientation on physical ageing in poly(l-lactic acid) films, J. Polym. Sci. Part B Polym. Phys. 54 (2016) 2233–2244. doi:10.1002/polb.24133.

[29] N. Delpouve, L. Delbreilh, G. Stoclet, A. Saiter, E. Dargent, Structural dependence of the molecular mobility in the amorphous fractions of polylactide, Macromolecules. 47 (2014) 5186–5197. doi:10.1021/ma500839p.

Conclusion generales et perspectives

Conclusions générales et perspectives

La perméabilité à l'oxygène des polymères a une importance significative dans le domaine des emballages. Afin de maitriser les propriétés barrière des polymères et pouvoir ainsi créer des structures non perméables, la compréhension de la microstructure/morphologie est indispensable. Ces travaux de recherche ont consisté à l'optimisation des conditions de cristallisation du PLA en étudiant l'impact de la structure et de la morphologie cristalline, de ainsi que de la dynamique de la phase amorphe sur les propriétés barrière aux gaz. Ensuite nous nous sommes intéressés à l'impact du confinement du PLLA, obtenu par le procédé de co-extrusion multi-nanocouche, sur la cristallisation, la mobilité macromoléculaire et les propriétés barrières. Le PLLA a été confiné à l'aide de deux polymères amorphes, le polystyrène et le polycarbonate.

Différentes microstructures ont été obtenues par traitement thermique en cristallisant le PLA à partir de l'état vitreux et à partir de l'état fondu à deux températures (85°C et 130°C). Dans un premier temps, nous avons montré que la structure cristalline était guidée par le chemin de cristallisation et que la température de cristallisation n'influençait pas la taille des sphérolites. Nous avons également montré que la température de cristallisation semblait être responsable du remplissage inter-sphérolitique (space-filling). A 85°C, les sphérolites semblent être plus dispersés alors qu'à 130°C ils se touchent, ce qui nous a permis de conclure que les échantillons cristallisés à 130°C avaient un space-filling plus important. L'étude de la morphologie cristalline par SAXS et WAXS a montré que la microstructure des échantillons cristallisés à 130°C était plus organisée que ceux cristallisés à 85°C. Nous avons également montré que les échantillons cristallisés à 85°C présentaient plus de RAF, et donc un couplage entre la phase amorphe et la phase cristalline plus important. Ce couplage dépend de la température de cristallisation mais aussi du temps de cristallisation, vu que les échantillons cristallisés pendant une longue durée possèdent plus de RAF que les échantillons cristallisés rapidement, et ce, même en présence de pre-nucleis. Le PLA cristallisé à des températures élevées permet donc de créer des structures cristallines plus ordonnées avec un meilleur découplage des phases amorphes et cristallines. Nous avons montré que la RAF était responsable de l'accélération de la diffusion d'oxygène car un mauvais découplage entrave la relaxation des chaines polymériques et augmente ainsi le volume libre à l'interface entre les phases amorphes et cristallines.

Apres l'étude du PLA massif, nous nous sommes intéressés au PLLA confiné. La maitrise du procédé de co-extrusion multi-nanocouche a permis de créer des couches de PLLA continues de 30 nanomètres, et donc d'étudier sa cristallisation sous confinement. Grâce à une analyse des images AFM des films, nous avons réussi à montrer que les couches de PLLA étaient continues et homogènes lorsque confinées par le PS. L'analyse s'est révélée plus compliquée par contre pour le couple PLLA et PC, du fait probablement d'une affinité chimique plus importante entre les deux polymères et de l'absence d'une interface franche. . Le confinement du PLLA a ralenti sa cinétique de cristallisation et a changé son orientation cristalline selon le polymère confineur. Le PLLA confiné par le PS et cristallisé à 85°C, possède des lamelles cristallines orientées dans deux directions, « in-plane » et « on-edge » alors que, le PLLA confiné par le PC et cristallisé à 85°C et 120°C, possède des lamelles cristallines dans une seule direction, « in-plane ». Nous avons aussi étudié l'impact du confinement sur la phase amorphe. Le découplage entre la phase amorphe et cristalline dans les films PLLA/PS s'améliore avec la diminution d'épaisseur des couches entraînant une disparition de la RAF pour le film où la couche de PLLA a une épaisseur de 20 nm. L'hypothèse que nous avons donnée à ce résultat met en évidence le fait que, pour le film où la couche de PLLA a une épaisseur de 20 nm il y a seulement de la place pour une ou deux lamelles de PLLA. Ceci entraine un fort découplage entre la phase amorphe et cristalline en empêchant ainsi la formation de la RAF. De même la température de transition dynamique d'un film de 20 nm cristallisé est inchangée par rapport au même échantillon amorphe, confirmant ainsi le fort découplage pour le PLLA confiné dans ces conditions (polymère confineur, température et temps de cristallisation). L'analyse des cinétiques de vieillissement du PLLA confiné a également confirmé ce découplage. Cependant, pour les films PLLA/PC la RAF n'a pas été quantifiable en raison de la présence probable d'une interphase entre les deux polymères. La perméabilité aux gaz a été impactée par la microstructure du PLLA sous confinement. Dans le cas du couple PLLA/PS, la cristallisation du film de PLLA de 20 nm a été améliorée par rapport au film massif cristallisé dans les mêmes conditions. Toutefois, l'amélioration de la perméabilité obtenue pour le PLLA confiné est la même que pour le PLLA mono-matière cristallisé à 120°C. Dans le cas du couple PLLA/PC, la perméabilité n'a pas été améliorée à 85°C, nous supposons, du fait de la présence de l'interphase. L'interphase peut entraver le découplage de la phase amorphe et cristalline, provoquant une augmentation de la perméabilité. Cependant, la cristallisation à 120°C permet l'amélioration de la perméabilité du PLLA au même niveau que la cristallisation à 120 °C du PLLA massif.

Le PLLA étant fortement sensible au vieillissement physique, le comportement des films multicouches PS/PLLA à moyen et long terme a été investigué grâce à la technologie FS-DSC. Il a été montré que la cinétique de relaxation structurale de la phase amorphe peut être fortement ralentie en utilisant le procédé de co-extrusion multi-nanocouche, là où une cristallisation thermique seule a un impact négligeable. Nous avons associé ce résultat à l'orientation des macromolécules durant la mise en forme, générant une contrainte additionnelle au confinement. Sur les couches les plus confinées en revanche les temps de relaxation sont identiques à ceux d'un PLLA massique. Nous en avons déduit qu'à un certain niveau de confinement, un seuil est atteint pour lequel les contraintes structurales disparaissent car la macromolécule est isolée. Ce résultat s'accorde avec l'invariance de la température de transition vitreuse par rapport à un matériau massique et avec la diminution de la coopérativité même en absence de phase cristalline, celle-ci ne pouvant être associée qu'à la réduction purement géométrique du domaine de relaxation.

Malgré ces résultats, il faut continuer l'étude pour améliorer l'interprétation des comportements. Nous proposons ici quelques perspectives de ce travail

- L'optimisation du procédé de co-extrusion multi-nanocouche est nécessaire car son utilisation aujourd'hui est encore trop empirique.
- L'analyse des couches PLLA/PC par AFM doit être améliorée et nécessite une préparation d'échantillon plus minutieuse, afin d'augmenter la qualité de l'image. Une découpe à froid de l'échantillon devrait améliorer la qualité et permettre de mieux sonder l'interface, ainsi que les structures cristallines au sein d'une couche.
- Il a été montré que la perméabilité du polylactide peut être gouvernée par plusieurs facteurs comme la quantité de RAF, l'orientation des lamelles cristallines. D'autres auteurs ont montré que l'orientation « in-plane » des lamelles cristallines améliore énormément la perméabilité d'autres polymères. Dans notre cas avec le PLLA, il serait intéressant de le confiner en utilisant un polymère confineur qui permettrait la formation de lamelles « in-plane », cependant sans la formation d'interphase comme cela semble être le cas du PLLA/PC.
- La discussion concernant l'interphase entre le PLLA et le PC, en particulier l'interprétation du saut de chaleur obtenue par TMDSC et le décalage de la Tg obtenu par DMTA serait enrichie par une analyse de microscopie plus fine comme par exemple, microscopie électronique à transmission (TEM) ou AFM si la qualité de la coupe est

améliorée. La compréhension de l'impact des interactions moléculaires aux interfaces dans différents couples confineur/confiné sur leurs dynamiques de relaxation respectives est une question qui mérite approfondissement. Pour cela, il serait nécessaire d'établir des cartes de relaxation dans les différentes phases amorphes en associant les méthodes d'investigation de la mobilité moléculaire dans l'état vitreux (vieillissement physique), à la transition vitreuse calorimétrique (MT-DSC) et dans l'état liquide (spectroscopie de relaxation diéléctrique). L'exploration de méthodes de simulation par dynamiques moléculaires peut également être envisagée.

- En outre nos analyses ont montré que l'évolution des hétérogénéités dynamiques (CRR) associées à une contrainte structurale pouvait se singulariser de celle des temps de relaxation. La compréhension des phénomènes régissant les variations de ces deux paramètres caractéristiques de la mobilité moléculaire dans la phase amorphe demeure un challenge de premier intérêt.
- Il serait intéressant d'effectuer des analyses en traction sur les échantillons multi-nanocouches afin de relier les propriétés mécaniques à la microstructure et à la dynamique de la phase amorphe du PLLA confiné.

Nous proposons également quelques perspectives à plus long terme pour améliorer la compréhension de l'impact de la structure des multi-nanocouches sur les propriétés barrière des films :

- Il serait intéressant d'analyser plus en détail l'impact de l'épaisseur de la couche confinée sur les propriétés barrière de films recristallisés. Selon des données disponibles dans la littérature, il semblerait qu'une épaisseur de couche limite pour permettre l'amélioration des propriétés barrière puisse exister et qu'elle soit induite par la possibilité des lamelles cristallines de s'orienter dans la couche confinée en se chevauchant.
- L'analyse des paramètres de transport (coefficients de diffusion et de partage) et leur modélisation à l'aide de modèles de tortuosité faisant intervenir des hypothèses géométriques pourraient permettre de mieux comprendre le lien entre structuration des multi-nanocouches et leurs propriétés barrière.

-

Titre : Compréhension de la relation entre la microstructure du polylacide, sa mobilité macromoléculaire et ses propriétés barrières pour la création des emballages issues de ressources renouvelables de demain

Mots clés : Polylactide, cristallisation, mobilité macromoléculaire, confinement, propriétés barrières

Résumé : Ces dernières années, une attention particulière a été portée aux polymères biodégradables et biocompatibles, notamment du point de vue écologique. Le développement de biopolymères pour des applications d'emballage alimentaire implique des exigences industrielles spécifiques telles qu'un bas prix ainsi que de bonnes propriétés mécaniques, thermiques et barrières. Le Polylactide (PLA) a attiré beaucoup d'attention car il est produit à partir de ressources naturelles renouvelables, et en raison de sa capacité de mise en œuvre et de ses bonnes propriétés mécaniques. Pour que le PLA puisse être développé à grande échelle pour des applications industrielles dans le domaine de l'emballage, ses propriétés barrières doivent être améliorées. La cristallisation est une méthode très utilisée pour améliorer les propriétés barrières mais n'est pas suffisante dans le cas du PLA. De nouvelles stratégies sont étudiées pour obtenir des effets plus importants. L'une d'entre elles consiste à confiner géométriquement le polymère jusqu'à l'échelle nano en utilisant le procédé de co-extrusion multicouche combiné éventuellement avec un recuit. Cette technologie respecte l'environnement et a déjà prouvé son efficacité pour améliorer les propriétés barrières aux gaz dans le cas d'autres polymères. Cette étude propose d'abord le développement de films PLA avec des structures cristallines différentes dans le but d'optimiser les conditions de cristallisation pour obtenir de meilleures propriétés barrières à l'oxygène. Parmi les différentes structures cristallines obtenues, la perméabilité est la meilleure lorsque le PLA a été cristallisé rapidement à partir de l'état vitreux pour atteindre un degré de cristallinité élevé et un bon découplage de la phase amorphe et cristalline. Ensuite, le PLLA a été confiné par deux polymères amorphes, le Polystyrène et le Polycarbonate. Nous avons montré que le polymère confineur peut influencer la structure cristalline et la mobilité de la phase amorphe du PLLA, influençant ainsi sa perméabilité.

Title : Understanding structure/function relationships between polylactide microstructure, macromolecular mobility and barrier properties for the creation of tomorrows biobased packaging materials

Keywords : Polylactide, crystallization, molecular mobility, confinement, barrier properties

Abstract : In recent years, much attention has been focused on biodegradable and biocompatible polymers, particularly from an ecological viewpoint. The development of biopolymers for food-packaging applications implies ecofriendly character to specific industrial requirements as low-cost and good mechanical, thermal and barrier properties. Polylactide (PLA) has been attracting great attention, because it can be obtained from renewable sources, and due to its good process ability and mechanical properties. As one of the major challenges for high performance PLA packaging at a large scale is the improvement of its gas barrier properties, the tailoring of the PLA microstructure. Crystallization is a method used to improve barrier properties but is not sufficient in the case of PLA. New strategies are actually studied to obtained stronger effects. One of them consists in the geometrical confinement of the polymer at the molecular scale using the layer-multiplying co-extrusion process combined eventually with annealing processes to create nanometric thickness layers. This technology is environmentally friendly and has already proved its efficiency to improve the gas barrier properties in case of other polymers. This study first proposes the development of PLA films with different structures crystalline with the aim of optimize the crystallization conditions to get better oxygen barrier properties. Among the different crystalline structures obtained, permeability was better when PLA was rapidly crystallized from glass to reach a high crystallinity degree and decoupling of the amorphous and crystalline phase. Then, PLLA was confined by two amorphous polymers, polystyrene and polycarbonate, and its crystals structure and amorphous mobility was changed. We showed that the confiner polymer could influence PLLA confinement, both in the crystalline phase and in the amorphous phase, thus influencing its permeability.